

This work is protected by copyright and other intellectual property rights and duplication or sale of all or part is not permitted, except that material may be duplicated by you for research, private study, criticism/review or educational purposes. Electronic or print copies are for your own personal, non-commercial use and shall not be passed to any other individual. No quotation may be published without proper acknowledgement. For any other use, or to quote extensively from the work, permission must be obtained from the copyright holder/s.



**Faculty of Medicine
and Health Sciences**

Investigating the therapeutic potential of repurposed
drugs that target central nervous system and peripheral
pathologies in cellular and animal models of spinal
muscular atrophy

Özge Çetin

Doctor of Philosophy (Ph.D.) in Pharmacology

June 2024

Keele University

Abstract

Spinal muscular atrophy (SMA) is a neuromuscular disorder caused by the loss-of-function of the survival motor neuron (*SMN*) gene resulting in muscle atrophy and weakness. There are currently 3 gene-based therapies (Spinraza®, Zolgensma® and Evrysdi®) approved for the treatment of SMA. Although these treatments lead to significant life-changing and life-saving improvements, they have limitations.

Moreover, going beyond neuronal pathologies in SMA, developmental and metabolic pathologies in many peripheral tissues have been found in both SMA mouse models and patients. Our previous research has demonstrated that prednisolone, a synthetic glucocorticoid (GC), has been found to alleviate the disease SMA genotype phenotype in *Smn*^{-/-}; *SMN2* and *Smn*^{2B/-} SMA mice. To identify commercially available drugs predicted to ameliorate peripheral pathologies and possess similar effects to prednisolone via RNA sequencing. Combined *in silico* analysis were used to identify commercially available drugs predicted to restore the levels of differentially expressed genes in SMA muscle and similar activity potential with prednisolone. This *comprehensive in silico* approach identified strong pharmacological candidates, pioglitazone, melatonin, and insulin.

Through combined *in silico* analyses, several target genes have been predicted: *Thbs1* and *Ppar-α*, which could be regulated by pioglitazone; *Per1*, *Bcl2*, *Sirt1*, and *Ror-α*, potentially corrected by melatonin; and *Igf1R*, *Rb1*, and *InsR*, which may be regulated via insulin. First, we validated the abnormal expression of these predicted targeted genes in symptomatic skeletal muscle tissue in both SMA mouse models.

Subsequent research has stated the safety and pharmacological impact of pioglitazone, melatonin and insulin on the C2C12s and LCHN-M2 cell line. Importantly, melatonin has been observed to improve weight, lifespan, and RR (righting reflex); pioglitazone has shown positive contributions to weight and survival; and insulin has demonstrated beneficial effects on weight in *Smn*^{2B/-} mouse models. Post-treatment of these candidates caused a change in expression of all these genes compared to untreated counterparts both CNS and periphery. Pioglitazone and melatonin show promise in addressing metabolic disorders by potentially enhancing glucose uptake from circulation into skeletal muscle. They may also shift metabolism towards increased ATP production by supporting

mitochondrial biogenesis and function.

The perspective results highlights the complexity of SMA and the potential multifaceted approach required for effective treatment, underscoring the importance of targeting not just the primary symptoms but also the broader metabolic disturbances associated with the disease aiming to improve overall patient outcomes and quality of life.

Acknowledgement

First and foremost, I want to express my deepest gratitude to my advisor, Dr. Melissa Bowerman. Honestly, I might not have been able to complete my Ph.D. with another supervisor. Not only is she an amazing scientist, but she has also been a role model in many respects, guiding me and always prioritizing making us, good researchers. She taught me wonderful things, I enjoyed doing research with her, and she left a significant mark on one of the most important parts of my life.

In my first year of the Ph.D., I had the opportunity to meet two fantastic scientists, Joe Hoolachan and Emma R Sutton in the lab, who patiently taught me many techniques and they become amazing friends. And my project colleague Eve McCallion, she is wonderful, always complementing me. The calm presence that soothed me when I panicked, and the fun girl I brainstormed with in the lab, I will never forget you. Jess Cook, Yahya Al-Mozani, Ankush Dhoowooah, Maria Susan Varughese, Juanita Koomson, the unsung heroes of the melatonin chapter, learning and teaching with you have been incredible experiences. I sincerely thank each of you, my colleagues, for your support throughout my Ph.D. journey.

A special thanks goes to my partner, Luke Bates, for everything he has contributed to my life. His constant presence by my side, helping to find solutions to every challenge, has been invaluable. He is my beloved, as dear to me as family. I'm so grateful to have met him!

While writing my thesis, since English is my second language, I used the Grammarly AI program to correct my grammatical errors. Additionally, I owe a special thanks to the Turkish Educational Consultancy for sponsoring my doctoral studies.

Table of Contents

Abstract.....	iv
Acknowledgement.....	vi
List of Figure	xiv
List of Tables	xx
List of Abbreviations	xxi
1 INTRODUCTION.....	1
1.1 Spinal muscular atrophy (SMA)	2
1.1.1 <i>Clinical Profile of SMA</i>	4
1.1.2 <i>SMA Mouse Models</i>	6
1.1.3 <i>SMN Has a Housekeeping Role</i>	9
1.1.4 <i>The SMN is Crucial for RNA metabolism.</i>	9
1.1.5 <i>Protein Translation and Related Proteostatic Mechanisms</i>	11
1.2 Neuronal Pathologies in SMA	13
1.2.1 <i>Structural and Functional Abnormalities in CNS</i>	13
<i>Neurons and Astrocytes</i>	13
1.2.2 <i>Cytoskeleton Related Defects</i>	15
1.2.3 <i>Apoptosis</i>	17
1.3 Skeletal Muscle Pathologies in SMA	18
1.3.1 <i>SMA and Myogenesis</i>	19
1.3.2 <i>Metabolism and Contraction of SMA</i>	21
1.3.3 <i>Muscle Weakness and Developmental Changes Occurred Prior to any Neuronal Damage</i>	22
1.4 Neuromuscular junction (NMJ).....	23
1.4.1 <i>NMJ Pathology of SMA</i>	24
1.5 SMA Has a Non-Neuromuscular Multicellular Function	26
1.5.1 <i>Pancreatic Developmental Defects in SMA</i>	26
1.5.2 <i>Liver Developmental Defects in SMA</i>	27
1.5.3 <i>Heart Developmental Defects in SMA</i>	29
1.5.4 <i>SMA Gastrointestinal Dysfunction</i>	30
1.6 Metabolism.....	31
1.6.1 <i>Glucose metabolism</i>	31
1.6.2 <i>Fatty Acid Metabolism</i>	34
1.6.3 <i>Metabolism and Circadian Rhythms</i>	36
1.6.4 <i>Amino Acid Metabolism</i>	37
1.6.5 <i>Mitochondrial Defects in SMA</i>	38

1.7	Therapeutic Developments in SMA	40
1.7.1	<i>Smn-dependent Therapies</i>	40
1.7.2	<i>Smn-Independent Therapies in Clinical Trials</i>	45
1.8	Drug repurposing	47
1.9	Aim and Objective	49
1.9.1	<i>Hypothesis</i>	50
1.9.2	<i>Aim</i>	50
1.9.3	<i>Objectives</i>	50
2	GENERAL METHODS	51
2.1	In Vivo experiment.....	52
2.1.1	<i>Animals</i>	52
2.1.2	<i>Genotyping</i>	52
2.1.3	<i>Phenotypic Analysis on Live Animals</i>	53
2.1.4	<i>Animal Tissue Harvest</i>	54
2.1.5	<i>Immunohistochemistry</i>	54
2.2	In Vitro Experiment.....	56
2.2.1	<i>C2C12s</i>	56
2.2.2	<i>LCHN-M2</i>	58
2.2.3	<i>Deltoid Myoblasts Collected from Type III SMA Patients</i>	59
2.3	Assays	59
2.3.1	<i>Lactate dehydrogenase (LDH)-GloTM cytotoxicity assay</i>	59
2.3.2	<i>BrdU Cell proliferation assay</i>	60
2.4	Molecular Analyses	60
2.4.1	<i>Tissue Lysis and RNA isolation</i>	60
2.4.2	<i>Reverse Transcription (RT)</i>	61
2.4.3	<i>Quantitative PCR (qPCR)</i>	61
	Result of In-silico Analysis.....	64
3	Pioglitazone	68
3.1	Introduction.....	68
3.2	Methods.....	73
3.2.1	<i>In vitro pioglitazone treatment</i>	73
3.2.2	<i>In vivo pioglitazone treatment</i>	73
3.3	Results.....	74
3.3.1	<i>The mRNA expression of Thbs1 and Ppar-α was upregulated in skeletal muscle of symptomatic Smn^{-/-};SMN2 mice</i>	74

3.3.2	<i>The mRNA expression of Thbs1 was increased in skeletal muscle of symptomatic $Smn^{2B/-}$ Mice</i>	75
3.3.3	<i>The predicted targeted gene, PPAR-α, was downregulated in Type III SMA deltoid myoblasts.</i>	73
3.3.4	<i>The mRNA expression of predicted Thbs1 gene was decreased in differentiated Smn-KD C2C12s model.</i>	74
3.3.5	<i>There was no significant change in pioglitazone targeted genes observed in the atrophy-induced D8 C212s.</i>	75
3.3.6	<i>Pioglitazone had dose- and differentiation state-dependent effects on the expression of Thbs1 and Ppar-α genes in C2C12s.</i>	76
3.3.7	<i>Pioglitazone had a toxicity on C2C12s but it caused a negative effect on proliferation of C2C12s.</i>	78
3.3.8	<i>The treatment of the human muscle cell line with 50 μM pioglitazone induced an increase in the level of THBS1 mRNA.</i>	81
3.3.9	<i>There was no negative impact of pioglitazone treatment on proliferation of LCHN-M2.</i>	82
3.3.10	<i>During a 24-hour treatment period, pioglitazone demonstrated no toxic impact on either the proliferating or differentiating states of LCHN-M2 cells.</i>	83
3.3.11	<i>Oral administration of pioglitazone has a positive effect on weight, survival and motor function in $Smn^{2B/-}$ mice.</i>	84
3.3.12	<i>Oral administration of 12.5 mg/kg/day pioglitazone did not lead to any change of hypoglycemia in both non-fasted $Smn^{2B/-}$ and $Smn^{2B/+}$ mice</i>	89
3.3.13	<i>Administering of pioglitazone orally led to an increase in the expression levels of Ppar-α and Ppar-γ in the triceps tissue of symptomatic $Smn^{2B/-}$ SMA mice.</i>	90
3.3.14	<i>The Ide expression had been increased followed by pioglitazone application in $Smn^{2B/-}$ mouse model.</i>	93
3.3.15	<i>Pioglitazone had no impact on muscle atrophy marker gene expression.</i>	94
3.3.16	<i>Pioglitazone induced enhancement of junctional adhesion molecule-A (Jam-A) expression in triceps of mild SMA mouse models.</i>	95
3.3.17	<i>Negative effect of pioglitazone on muscle fiber size was observed in symptomatic TA of $Smn^{2B/-}$, whereas showed opposite pattern in $Smn^{2B/+}$.</i>	96
3.3.18	<i>12.5 mg/kg/day pioglitazone treatment upregulated Ppar-γ expression in spinal cord of $Smn^{2B/-}$.</i>	97
3.3.19	<i>Following the application of pioglitazone, there was an upregulation of Pmaip-1 and Fas mRNA levels in the spinal cord tissues of $Smn^{2B/-}$ mice.</i>	100
3.3.20	<i>Administration of pioglitazone did not change the number of α- motor neurons of symptomatic spinal cord of $Smn^{2B/-}$ and $Smn^{2B/+}$</i>	101
3.3.21	<i>Orally treatment of Pioglitazone led to an upregulation of Thbs1 expression level in symptomatic liver tissue in $Smn^{2B/+}$ SMA mice.</i>	103
3.3.22	<i>There was no change in lipid accumulation in liver of $Smn^{2B/-}$ following pioglitazone treatment.</i>	105

3.3.23 Orally treatment of Pioglitazone downregulated of <i>Thbs1</i> and <i>Ppar-γ</i> mRNA level in symptomatic WAT in both <i>Smn</i> ^{2B/-} and <i>Smn</i> ^{2B/+} mice.....	106
3.3.24 Orally treatment of 12.5 mg/kg/day Pioglitazone downregulated of <i>Thbs1</i> and <i>Ppar-γ</i> mRNA level in symptomatic WAT (white adipose) tissue in both <i>Smn</i> ^{2B/-} and <i>Smn</i> ^{2B/+} SMA mice.	108
3.4 Discussion	110
4 Melatonin	115
4.1 Introduction.....	115
4.2 Methods.....	120
4.2.1 <i>In vitro</i>	120
4.2.2 <i>In Vivo</i>	120
4.3 Results.....	121
4.3.1 There is an observed increase in the mRNA levels of <i>Per-1</i> , <i>Bcl-2</i> , and <i>Sirt-1</i> in skeletal muscle tissue symptomatic <i>Smn</i> ^{-/-} ;SMN2 mice.	121
4.3.2 The expression levels of <i>Per-1</i> and <i>Bcl-2</i> mRNA are elevated in skeletal muscle of symptomatic <i>Smn</i> ^{2B/-} Mice.....	122
4.3.3 The predicted targeted gene, <i>PER-1</i> level is decreased in Type III SMA deltoid myoblasts.....	123
4.3.4 Changes in the Expression Levels of Target Genes Are Independent of <i>Smn</i> Deficiency in C2C12s model.....	125
4.3.5 In D8 C212s, there was no change in the expression levels of melatonin- predicted target genes.....	126
4.3.6 Melatonin's effects on the expression of predicted-targeted genes vary depending on the dosage and the differentiation status of the cells in C2C12s.	127
4.3.7 Melatonin has no negative effect on proliferation of C2C12s.	128
4.3.8 Melatonin shows no toxic effects on the proliferation or differentiation of C2C12 cells over a 24-hour treatment period.....	129
4.3.9 Melatonin treatment increased the expression of <i>PER1</i> in both myoblast and myotube forms of LCHN-M2, while it only increased <i>SIRT1</i> expression in the myoblast form of LCHN-M2.	131
4.3.10 The highest dose of melatonin does not adversely affect myoblast proliferation of LCHN-M2 over 24-hour treatments.	132
4.3.11 Melatonin does not exhibit toxic effects on LCHN-M2 human muscle cells in either proliferated or differentiating stages over a 24-hour treatment duration.	133
4.3.12 Oral administration of melatonin intake leads to an increase in both body weight and survival rate in <i>Smn</i> ^{2B/-} mice.	135
4.3.13 Oral administration of melatonin did not lead to any change of hypoglycaemia both non-fasted <i>Smn</i> ^{2B/-} and <i>Smn</i> ^{2B/+} mice.	140
4.3.14 Melatonin administration led to an increase in the expression in transcriptomic- based targeted genes (<i>Per1</i> , <i>Sirt1</i> , <i>Bcl2</i> and <i>Ror-α</i>) the triceps tissue of symptomatic <i>Smn</i> ^{2B/-} mice.	140

4.3.15 Melatonin administration caused to an elevation in the level of atrophic marker genes in the triceps of <i>Smn</i> ^{2B/-} mice.....	143
4.3.16 Following melatonin treatment, there was an enhancement in the size of muscle fibers in symptomatic tibialis anterior from <i>Smn</i> ^{2B/-} models.....	144
4.3.17 Melatonin application increased the expression of the CAT gene in the symptomatic muscle tissues of <i>Smn</i> ^{2B/-} mice.....	145
4.3.18 Melatonin resulted in elevated expression of the diurnally regulated genes, <i>Clock</i> and <i>Per2</i> , in the triceps tissue of symptomatic <i>Smn</i> ^{2B/-} SMA mice.....	147
4.3.19 Melatonin increased the expression of the <i>Glut4</i> gene, which is responsible for glucose transport, in symptomatic SMA mouse muscle tissue.	149
4.3.20 Daily gavage dosing of 50 mg/kg/day melatonin, there was an upregulation in the expression of predicted target genes (<i>Per1</i> , <i>Bcl2</i> , and <i>Ror-α</i>) in the liver tissues of symptomatic <i>Smn</i> ^{2B/-} mice.....	151
4.3.21 There was a rise in the expression of diurnal genes, <i>Clock</i> and <i>Per2</i> following melatonin within the liver tissue of symptomatic <i>Smn</i> ^{2B/-} mice.	153
4.3.22 Melatonin induced the expression of the CAT gene's mRNA in symptomatic SMA liver tissues.....	155
4.3.23 Melatonin did not result in any change in lipid accumulation in the liver.....	156
4.3.24 Following the melatonin treatment, there was a decrease in the <i>Per1</i> gene expression within the spinal cord tissues in symptomatic <i>Smn</i> ^{2B/-}	158
4.3.25 The level of <i>Pmaip-1</i> and <i>Fas</i> downregulated, following melatonin treatment in <i>Smn</i> ^{2B/-} SMA mice.	160
4.3.26 Melatonin treatment did not alter the count of alpha motor neurons.....	161
4.3.27 Melatonin led to an upregulation of the CAT antioxidant gene in the spinal cord tissues of mice with symptomatic SMA.....	163
4.3.28 Administering melatonin did not alter the mRNA expression of core clock genes in the spinal cord of a milder form of symptomatic SMA mouse model.	164
4.3.29 Melatonin resulted in increased expression levels of <i>Per1</i> , <i>Sirt1</i> , and <i>Bcl2</i> in the symptomatic white adipose tissue of <i>Smn</i> ^{2B/-} mice.....	166
4.3.30 Melatonin may regulate circadian rhythms in the WAT of <i>Smn</i> ^{2B/-} mice through inducing <i>Clock</i> and <i>Per2</i> gene expression.....	168
4.3.31 Melatonin enhanced the defence against oxidative stress in the symptomatic WAT tissue of mice with SMA by increasing the levels of both CAT and SOD.....	170
4.3.32 Melatonin does not to be involved in mediating <i>Glut4</i> -induced glucose uptake in WAT of the SMA mouse model.....	171
4.3.33 Melatonin administration leads to the induction of browning in white adipose tissue in the SMA mouse model.....	172
4.3.34 In the <i>Smn</i> ^{2B/+} mouse, a decrease in the expression of <i>Per1</i> and <i>Bcl2</i> genes within the brown adipose tissue (BAT) is induced by melatonin treatment.....	174
4.3.35 Melatonin administration resulted in the decreased expression of <i>Clock</i> , <i>Bmal1</i> , and <i>Per2</i> genes, potentially influencing the regulation of circadian rhythms in BAT of	

<i>Smn</i> ^{2B/-} mice	176
4.3.36 The mRNA level of CAT mRNA has decreased in symptomatic BAT tissues in <i>Smn</i> ^{2B/+} following melatonin application.	178
4.3.37 Administering of melatonin reduced in mRNA level of Glut4 in the brown adipose tissue of the symptomatic the <i>Smn</i> ^{2B/+} mouse control group	179
4.3.38 Melatonin application downregulated the expression level of Ror- α in the symptomatic pancreas tissues of SMA mice.....	181
4.3.39 Melatonin had no effect on the expression of diurnal genes in the pancreas tissues of SMA mice.	183
4.3.40 After administering melatonin, it was observed that there is no impact on the mRNA expression of the Glut4-glucose transport gene in the symptomatic pancreas tissues of <i>Smn</i> ^{2B/-} SMA mouse.	185
4.3.41 Administering daily melatonin resulted in an upregulation of the CAT gene in the symptomatic pancreas tissues of <i>Smn</i> ^{2B/-} mice.....	186
4.4 Discussion	190
5 Introduction	198
5.1 Insulin	198
5.2 Methods.....	201
5.2.1 In Vitro Insulin Treatment.....	201
5.2.2 In Vivo Insulin Treatment.....	201
5.3 Results.....	202
5.3.1 The expression levels of Rb1 and InsR were observed to increase, whereas the mRNA level of Igf1R was found to be downregulated.....	202
5.3.2 In the skeletal muscle of symptomatic <i>Smn</i> ^{2B/-} mice, there was an elevation in the mRNA level of Rb1.....	203
5.3.3 In Type III SMA deltoid myoblasts, the insulin target genes, IGF1R and INSR, were found to be significantly increased in expression.	204
5.3.4 The level of Igf1R increased in both D0 <i>Smn</i> -KD-C2C12 and D7 <i>Smn</i> -KD- C2C12.	205
5.3.5 Canonical atrophy did not result in alterations of Igf1R, Rb1 and InsR genes in C2C12 cells	206
5.3.6 Upon administering 100nM insulin, an elevation in the expression of the Rb1 target gene was noted in myotubes.	207
5.3.7 At the highest dosage insulin demonstrated neither a negative effect on proliferation nor any toxic impact on the formation of myotubes and myoblasts.	208
5.3.8 The application of insulin at concentrations of 1-10-100nm did not display any effect on predicted insulin target genes in the D0 and D7 LCHN-M2 cell line.	211
5.3.9 Even at the highest dose, insulin did not adversely affect the growth of cells or cause any toxicity in the formation of LCHN-M2 myotubes and myoblasts.....	212
5.3.10 Increasing doses of subcutaneous insulin injections resulted in a body weight increase in <i>Smn</i> ^{2B/-} mice.	214

5.4	Discussion	217
6	General Discussion.....	220
7	Reference.....	225

List of Figure

Figure 1.1 SMN1 and SMN2 expression in SMA patients and healthy control.....	2
Figure 1. 2 SMN protein play a main role in RNA, protein and RNA homeostatic balance...	12
Figure 2.1 C2C12s differentiation process.	57
Figure 2.2 LCHN-M2 differentiation process.	59
Figure 3.1 The heatmap generated from RNA-Seq data indicates that prednisolone re-establishes the expression levels of a wide range of genes in the skeletal muscle of SMA mice. Figure is adapted from (Hoolachan et al., 2023b).....	65
Figure 3. 1 In silico analyses predicted that the expression of the genes Thbs1 and Ppar- α was increased in SMA skeletal muscle and could be downregulated by pioglitazone treatment. ..	68
Figure 3. 2 The mRNA expression of predicted Thbs1 and Ppar- α gene increased in severe (Snm ^{-/-} ;SMN2) SMA mouse models compared to WT mouse models.....	74
Figure 3. 3 The validation study is about predicted candidate genes by restored pioglitazone treatment, Tsbh1 and Ppar- α , in In-Vivo model. The mRNA expression of predicted Thbs1 and Ppar- α gene increased in milder form (Snm ^{2B/-}) of SMA mouse models compared to WT mouse models.....	75
Figure 3. 4 The pioglitazone target gene, PPAR- α , significantly downregulated in Type III SMA deltoid myoblasts.....	73
Figure 3. 5 The mRNA expression of predicted Thbs1 gene is decreased without Smn gene in D7 Smn-KD C2C12s model.	75
Figure 3. 6 Canonical atrophy does not lead to any changes in the level of pioglitazone targeted genes in the serum-starvation-induced atrophy C2C12s.	76
Figure 3. 7 After 200 μ M pioglitazone treatment, a decrease was observed in the predicted candidate Thbs1 target gene in myoblasts. However, for the same target genes, there is an increase in 50 μ M pioglitazone treatment on C2C12 myotubes.....	77
Figure 3. 8 Highest concentration of pioglitazone (200 μ M) has a negative effect on	79
myoblast proliferation during 24H treatments, although it has no toxicity.	79
Figure 3. 9 After 50 μ M pioglitazone treatment on myoblasts form of LCHN-M2, mRNA	

expression of THBS1 target gene increased.	81
Figure 3. 10 Highest concentration of pioglitazone has no negative effect on myoblast proliferation during 24H treatments.....	82
Figure 3. 11 Treating both proliferating and differentiated LCHN-M2 cells with the highest dose of pioglitazone (200µM) or an equivalent volume of the vehicle (DMSO) does not result in toxicity.	83
Figure 3. 12 The effect of 12.5 mg/kg/day oral pioglitazone treatment.....	88
in both $Smn^{2B/-}$ and $Smn^{2B/+}$ SMA mice.....	88
Figure 3. 13 Oral 12.5 mg/kg/day Pioglitazone treatment did not cause any significant change in blood glucose level in symptomatic non-fasting both $Smn^{2B/-}$ and $Smn^{2B/+}$	90
Figure 3. 14 Orally treatment of 12.5 mg/kg/day Pioglitazone caused an upregulation of....	92
Ppar- α and Ppar- γ expression level in symptomatic triceps tissue in $Smn^{2B/-}$ SMA mice.	92
Figure 3. 15 Increases the activity of the Ide gene in the pioglitazone-affected triceps tissues of the $Smn^{2B/-}$ mouse model.....	93
Figure3. 16 12.5 mg/kg/day pioglitazone orally administration has no effect on the atrophic phenotype of triceps of milder form SMA mouse models.....	95
Figure 3. 17 12.5 mg/kg/day pioglitazone application markedly increased the expression of junctional adhesion molecule (JAM-) A gene in triceps of milder form SMA mouse models.	95
Figure 3. 18 Representative images of laminin-stained cross sections of TA muscles from P18 untreated and pioglitazone-treated (12.5 mg/kg/day through gavage)	97
Figure 3. 19 Orally treatment of 12.5 mg/kg/day Pioglitazone causes	99
upregulation of Ppar- γ expression level in symptomatic spinal cord tissue.....	99
in $Smn^{2B/-}$ SMA mice.....	99
Figure 3. 20 12.5 mg/kg/day pioglitazone orally administration had a neuroprotective effect on spinal cord in milder form of SMA mouse, preventing apoptosis.....	100
Figure 3. 21 The number of alpha motor neurons remained steady after 12.5mg/kg/day daily pioglitazone treatment in symptomatic SC in both $Smn^{2B/-}$ and $Smn^{2B/+}$ mouse model.	102
Figure 3. 22 Oral treatment of 12.5 mg/kg/day Pioglitazone lead an upregulation of Thbs1	104

expression level in symptomatic liver tissue in $Smn^{2B/+}$ SMA mice.	104
Figure 3. 23 The administration of pioglitazone at a dosage of 12.5 mg/kg/day does not appear to have a mitigating effect on lipid accumulation in the liver.	106
Figure 3. 24 Orally treatment of 12.5 mg/kg/day Pioglitazone downregulated of Thbs1 and Ppar- γ mRNA level in symptomatic WAT (white adipose) tissue in both $Smn^{2B/-}$ and $Smn^{2B/+}$ SMA mice.	107
Figure 4. 1 In silico analyses predicted that the expression of the genes Per-1, Bcl- 2, Sirt-1 and Ror- α genes was increased in SMA skeletal muscle and could be downregulated by melatonin treatment.	116
Figure 4. 2 The mRNA expression of predicted Per-1, Bcl-2, and Sirt-1 gene increased in severe ($Smn^{-/-}$;SMN2) SMA mouse models compared to WT mouse models.....	121 121
Figure 4. 3 The validation research focuses on examining genes hypothesized to respond to melatonin treatment. In $Smn^{2B/-}$ mice, there was a noticeable elevation in the mRNA expression levels of the anticipated genes, Per-1 and Bcl-2, in comparison to wild-type (WT) mouse models.....	123
Figure 4. 4 The pioglitazone target gene, PER-1, significantly downregulated in Type III SMA deltoid myoblasts.....	124
Figure 4. 5 The mRNA expression changes of Per-1 and Bcl-2 in C2C12 cells are state-dependent and do not rely on Smn deficiency.	125
Figure 4. 6 The expression levels of genes targeted by melatonin does not associate with atrophy in C2C12 cells.....	126
Figure 4. 7 The application of 1mM melatonin has downregulated the Per1 gene level in both myoblast and myotube forms.....	128
Figure 4. 8 The highest dose of melatonin does not negatively impact myoblast proliferation over 24-hour treatment periods.	129
Figure 4. 9 Treatment with the highest dose of melatonin and a comparable volume of vehicle shows no toxicity in both proliferating and differentiated C2C12s cells.....	130
Figure 4. 10 Treatment with melatonin elevated PER1 gene expression in muscle cells across both myoblast and myotube stages, but the enhancement of SIRT1 expression was special to	

the myoblast stage.....	131
Figure 4. 11 The highest dose of melatonin and its vehicle do not adversely affect myoblast growth over 24-hour treatments.....	132
Figure 4. 12 Administering the maximum dosage of melatonin or an equal volume of the vehicle to LCHN-M2 cells, whether in a proliferating or differentiated state, does not lead to toxic effects.....	133
Figure 4. 13 The effect of 50 mg/kg/day oral melatonin treatment in both $Smn^{2B/-}$ and $Smn^{2B/+}$ SMA mice.	139
Figure 4. 14 Oral 50 mg/kg/day Melatonin treatment did not cause any significant change in blood glucose level in symptomatic non-fasting both $Smn^{2B/-}$ and $Smn^{2B/+}$	140
Figure 4. 15 Orally treatment of 50 mg/kg/day Melatonin causes an upregulation of all predicted targeted gene expressions level in symptomatic triceps tissue in $Smn^{2B/-}$ SMA mice.	143
Figure 4. 16 50 mg/kg/day melatonin orally administration cause an increase in the atrophic phenotype of triceps of milder form SMA mouse models.....	144
Figure 4. 17 Representative images of laminin-stained cross sections of TA muscles from P18 untreated and melatonin-treated (50 mg/kg/day through gavage)	145
Figure 4. 18 Treatment of 50 mg/kg/day of melatonin orally increases the expression of the mitochondrial-antioxidant gene, Cat, in P18 SMA triceps muscle tissues in $Smn^{2B/-}$	146
Figure 4. 19 Oral administration of melatonin at a dose of 50 mg/kg/day leads to an increase in the expression of the Clock and Per2 genes in the triceps of milder form SMA mouse models.	148
Figure 4. 20 Treatment of 50 mg/kg/day of melatonin orally increases the expression of the Glut4-glucose transport gene in P18 SMA triceps muscle tissues in $Smn^{2B/-}$	149
Figure 4. 21 Application 50 mg/kg/day of melatonin leads to an increase in the predicted target gene levels of Per1, Bcl2, and Ror-alpha in symptomatic liver tissue in $Smn^{2B/-}$ mice.	153
Figure 4. 22 50 mg/kg/day pioglitazone orally administration induced the mRNA level of Clock and Per2 genes in liver of milder form of symptomatic SMA mouse.	154
Figure 4. 23 The administration of 50 mg/kg/day melatonin increased the	155

expression of the antioxidant CAT gene in symptomatic SMA liver tissues.	155
Figure 4. 24 The daily-gavage administration of 50 mg/kg/day melatonin at does not lead to reduce effect on lipid accumulation in the liver.....	157
Figure 4. 25 After daily oral administration of melatonin at a dose of 50 mg/kg/day, the expression level of the Per1 gene is downregulated in symptomatic spinal cord tissues in both the $Smn^{2B/-}$ and $Smn^{2B/+}$ models.....	160
Figure 4. 26 Melatonin might have a neuroprotective effect on spinal cord in milder form of SMA mouse, preventing apoptosis.	161
Figure 4. 27 The number of alpha motor neurons remain steady after 50 mg/kg/day daily melatonin treatment in symptomatic SC in both $Smn^{2B/-}$ and $Smn^{2B/+}$ mouse model.....	162
Figure 4. 28 The administration of 50 mg/kg/day melatonin increased the expression of the antioxidant CAT gene, in symptomatic SMA spinal cord tissues.	163
Figure 4. 29 Administering melatonin does not alter the mRNA expression of core clock genes in the spinal cord of a milder form of symptomatic SMA mouse model.....	165
Figure 4. 30 Melatonin-induced increase in the expression of anticipated target genes, specifically Per1, Sirt1, and Bcl2, has been observed in the symptomatic white adipose tissue of $Smn^{2B/-}$ mice.	167
Figure 4. 31 Administering melatonin at a dose of 50 mg/kg/day could potentially modulate the circadian rhythms in the white adipose tissue of $Smn^{2B/-}$ mice by enhancing the expression of Clock and Per2 genes.....	169
Figure 4. 32 The administration of 50 mg/kg/day melatonin increased the expression of the antioxidant CAT&SOD gene, in symptomatic SMA WAT.....	170
Figure 4. 33 Treatment of 50 mg/kg/day of melatonin does not regulate Glut-4- induced glucose uptake to WAT in SMA mouse model.	171
Figure 4. 34 The administration of melatonin induces the browning of WAT.....	172
Figure 4. 35 In the $Smn^{2B/+}$ SMA mice, melatonin treatment leads to reduced expression of the Per1 and Bcl2 genes in BAT.	175
Figure 4. 36 Melatonin treatment led to a reduction in the levels of Clock, Bmal1, and Per2 gene expression, which may affect the circadian rhythm control in the BAT of $Smn^{2B/-}$	177

mice.....	177
Figure 4. 37 Following melatonin treatment, there was a reduction in the mRNA levels of CAT in BAT in <i>Smn</i> ^{2B/+}	178
Figure 4. 38 Treatment with 50 mg/kg/day of melatonin decreases glucose uptake from the bloodstream into BAT via the Glut-4 transporter in the <i>Smn</i> ^{2B/+} mouse model.	179
Figure 4. 39 Melatonin application downregulates the expression level of Ror- α	182
in the symptomatic pancreas tissues of SMA mice.	182
Figure 4. 40 Melatonin has no therapeutic effect on the expression of diurnal genes.....	184
in the pancreas tissues of SMA mice.	184
Figure 4. 41 Following melatonin application, there is no effect on the mRNA level of the Glut4-glucose transport gene in symptomatic pancreas tissues.....	185
Figure 4. 42 The treatment with melatonin at a daily rate of 50 mg/kg has been found to enhance the expression of the CAT gene, which acts as a hydrogen peroxide scavenger in mitochondria, specifically in the symptomatic pancreas of <i>Smn</i> ^{2B/-} mice.	187
Figure 5. 1 In silico analyses predicted that the expression of the genes Igf1R, Rb1 and InsR were increased in SMA skeletal muscle and could be downregulated by insulin treatment.	198
Figure 5. 2 In a severe SMA mouse model, it was noted that the expression levels of Rb1 and InsR increased, while the mRNA level of Igf1R exhibited a decrease.	202
Figure 5. 3 The mRNA expression of predicted Rb1 gene increased in milder form <i>Smn</i> ^{2B/-} of SMA mouse models compared to WT mouse models.....	203
Figure 5. 4 The insulin target gene, IGF1R and INSR, significantly upregulated	205
in Type III SMA deltoid myoblasts.	205
Figure 5. 5 The mRNA expression of predicted Igf1R gene is increased in both <i>Smn</i> - KD proliferating and differentiated C2C12s model.	206
Figure 5. 6 Canonical atrophy does not lead to any changes in the level of insulin targeted genes in the serum-starvation-induced atrophy C2C12s.	207
Figure 5. 7 Following 100nM insulin treatment, an upregulation was observed in the predicted candidate Rb1 target gene in myotubes.	208
Figure 5. 8 At its maximum dosage, insulin does not exhibit any adverse effects on the growth	

of cells or any toxic effects on the myotubes and myoblasts C2C12s. 209

Figure 5. 9 Insulin applied at 1-10-100nm concentrations shows no therapeutic effects on the target genes within the D0 and D7 LCHN-M2 cell line. 211

Figure 5. 10 When administered at its highest dose, insulin neither hampers the growth..... 213
of cells nor leads to any toxic effects in the creation of LCHN-M2 myotubes and myoblasts.
..... 213

Figure 5. 11 Elevating the doses of subcutaneous insulin injections leads to a rise..... 216
in body weight in Smn 2B/- mice. 216

List of Tables

Table 1. 1 Clinical types of spinal muscular atrophy (SMA).	5
Table 2. 1 Genotyping primer sequences	53
Table 2. 2 Primers used for quantitative real-time PCR.....	62
Table 2. 3 Human primers used for quantitative real-time PCR.....	63
Table 1. 2 Illustrations of muscle-centric gene ontology (GO) terms linked with differentially expressed genes (DEGs) in SMA mice.....	66
Table 1. 3 Grouping of drug examples predicted to have similarity with	66
Table 3. 1 The overall of pioglitazone results were about validation and in-vitro models.....	84
Table 3. 2 12.5 mg/kg/day Pioglitazone is the most optimal treatment way	86
Table 3. 3 Pioglitazone has a tissue-specific effect in $Smn^{2B/-}$ SMA mice	109
Table 4. 1 Summary of validation of in silico data and in vitro studies.....	134
Table 4. 2 Administering 50 mg/kg/day of Melatonin via daily gavage is the most effective treatment method.	136
Table 4. 3 Summary of melatonin effect on P18 SMA skeletal muscle in $Smn^{2B/-}$	150
Table 4. 4 Summary of melatonin effect on P18 SMA liver in $Smn^{2B/-}$	158
Table 4. 5 Summary of melatonin effect on P18 SMA spinal cord in $Smn^{2B/-}$	166
Table 4. 6 Summary of melatonin effect on P18 SMA WAT in $Smn^{2B/-}$	173
Table 4. 7 Summary of melatonin effect on P18 SMA BAT in $Smn^{2B/-}$	180
Table 4. 8 Summary of melatonin effect on P18 SMA pancreas in $Smn^{2B/-}$	187
Table 5.1 Summary of insulin effect on SMA model.....	210
Table 5.2 Administering 0.2U via subcutaneous injection is the most effective treatment method.....	215

List of Abbreviations

a-C1q anti-C1q antibody

AA Amino Acid

AAG a1-Acid Glycoprotein

AAV Adeno-Associated Virus

AAV8 Adeno-Associated Virus serotype 8

AAV9 Adeno-Associated Viral Vector serotype 9

AAV9-P53shRNA AAV9 and a short hairpin RNA

ACC1 Acetyl-CoA Carboxylase 1

ACC2 Acetyl-CoA Carboxylase 2

Acetyl-CoA Acetyl-coenzyme A

Ach Acetylcholine

ACTH adrenocorticotrophic hormone

AD Alzheimer's Disease

AF Actin Filaments

AK15KO Adipose tissue KLF15 Knockout

ALK7 Activin receptor-like kinase 7

ALS Amyotrophic lateral sclerosis

AMPK AMP-activated protein kinase

ANOVA Analysis of Variance

ANS Autonomic Nervous System

AR Androgen Receptor

Arp213 Actin Related Protein

ARX-2 Actin-related protein 2

ASO Antisense Oligonucleotide

ATP Adenosine Triphosphate

Bac Bacterial Artificial Chromosome

BAT Brown Adipose Tissue

BBB Blood Brain Barrier

BCAA Branched Chain Amino Acid

Bcl2 B-cell lymphoma-2 (BCL-2)

BMP-9/10 Bone Morphogenetic Protein 9

Bota Botulinum neurotoxin type A

BrdU Bromodeoxyuridine

C. elegans *Caenorhabditis elegans*

C1q Complement Component 1q.

C2C12 immortalized mouse myoblast cell line

C3 Complement Component 3

CDK5 Cyclin dependent kinase 5

CHP1 Calcineurin Like EF-Hand protein 1

CMT Charcot-Marie-Tooth disease

CNC Cancer stem cells

CNS Central Nervous System

CORO1C Coronin-1C

COX Cytochrome c Oxidase

CS Cushing's Syndrome

CSF Cerebrospinal Fluid

CYP4 Cytochrome P450 4

D0 Day 0 (zero)

D2 Day 2

D7 Day 7

DamID Dam methylase identification

DD Density Differentiation

Ddit4 DNA-damage-inducible transcript 4

Dex Dexamethasone

DMD Duchenne Muscular Dystrophy

DNA Deoxyribonucleic acid

DRG Dorsal Root Ganglia

ECM Extracellular Matrix

EFAD Essential Fatty Acid Deficiency

ER Endoplasmic reticulum.

ERK Extracellular Signal-Regulated Kinase

ESE Exon Splicing Enhancer

ESS Exon Splicing Silencer

F-Actin Actin Filaments

FADH2 Flavin adenine dinucleotide

FBS Foetal Bovine Serum

FL Full-Length

Fn14 Fibroblast Growth Factor-inducible 14

FoXO Forkhead Box O

G-Actin Globular Actin

GAN Giant Axonal Neuropathy

GAPDH Glyceraldehyde 3-Phosphphate Dehydrogenase

GATA Guanine Adenosine Thymidine Adenosine

GATA4 GATA-binding protein 4

GC Glucocorticoid

GDF-11 Growth Differentiation Factor 11

GDNF Glial Cell-Derived Neurotrophic Factor

GFAP Glial Fibrillary Protein

GLUT4 Glucose Transporter Type 4

GRE Glucocorticoid Elements

GUA Guanabenz

HB9 Homeobox Gene 9

HEK Human Embryonic Kidney

hESC human Embryonic Stem Cells

HD Huntington's Disease

HFMS Hammersmith Functional Motor Scale

HIFs Hypoxia-Inducible Factors

hnRNPs heterogenous nuclear Ribonucleoproteins

HPA Hypothalamic-Pituitary-Adrenal axis

HSC Hematopoietic Stem Cells

IBA1 Ionized calcium Binding Adapter molecule 1

IDT Integrated DNA Technologies

IGF1 Insulin-like Growth Factor

IGF1R Insulin-like growth factor 1 receptor

IkB Inhibitory kB proteins

IKK IkB kinase complex

InsR Insulin Receptor

iPSC induced Pluripotent Stem Cells

IT Intrathecal administration

JAK Janus Kinase

JNK3 c-Jun NH2-Terminal Kinase

KEGG Kyoto Encyclopedia of Genes and Genomes

KLF15 Krüppel-like Factor 15

KO Knock Out

LAL Levator Auris Longus muscle

LAMA2 Laminin alpha 2

LDH Lactate Dehydrogenase

M-Klf15KO Mice KLF15 Knock Out

MAG Myelin-Associated Glycoprotein

MAP Mitogen-Activated Protein

MAPK Mitogen-Activated Protein Kinase

MBP Myelin Basic Protein

MEF2 Myocyte Enhancer Factor 2

MG Medial Gastrocnemius

MHC Myosin Heavy Chain

MLCLF-CRE Myosin Like Chain 1F-CRE

MN Motor Neuron

MND Motor Neuron Disease

MRF Myogenic Regulatory Factors

MS Multiple Sclerosis

MT Microtubules

Myf5 Myogenic Factor 5

MyoD Myoblast Determination protein 1

MyoG Myogenin

nAChR Nicotinic Acetylcholine Receptor

NADH Nicotinamide Adenine Dinucleotide + Hydrogen

NAFLD Non-Alcoholic Fatty Liver Disease

NCALD Neurocalcin Delta

NF Neurofilaments

NFH Neurofilaments Heavy

NF- κ B Nuclear Factor κ enhancer binding protein

NFL Neurofilaments Light

NFM Neurofilaments Medium

NG2 Neuron Glial antigen 2

NMJ Neuromuscular Junction

NRC31 Nuclear Receptor Subfamily 3 Group C member 1

NRF Nuclear Respiratory Factor

ob/ob Obese mouse

OPC Oligodendrocyte Precursor Cell

P21 Cell-Cycle Dependent Kinase Inhibitor 1

P53 Tumor protein

PAX3 Myogenic precursor

p-CREB Phosphorylated- Camp Response Element-Binding protein

PD Parkinson's Disease

Per1 Period Circadian Regulator 1

Per2 Period Circadian Regulator 2

PFT Pifithrin-a

PGC-1a Peroxisome Proliferator-activated receptor Gamma Coactivator

PGK1 Phosphoglycerate Kinase 1

PIK3R3 Phosphoinositide-3-kinase regulatory subunit 3

PLS3 Plastin 3

PolR2J RNA Polymerase II, Subunit J

Ppar- α Peroxisome Proliferator Activated Receptor Alpha

PPMA Post-Polio Muscular Atrophy

PPAR δ Peroxisome Proliferator-Activated Receptor δ

PR Progesterone Receptor

qPCR quantitative Polymerase Chain Reaction

RA Retinoic Acid

RB1 RB Transcriptional Corepressor 1

RBA Relative Binding Affinity

RBP RNA-Binding Proteins

RHS Revised Hammersmith Scale

RNA Ribonucleic Acid

RNAi RNA interference

RNA-Seq RNA sequencing

ROCK Rho-kinase

ROS Reactive Oxygen Species

ROR- α RAR-Related Orphan Receptor A, Paralog A

mRNA Messenger RNA

NRF Nuclear Respiratory Factor

OPC Oligodendrocyte Precursor Cell

PNS Peripheral Nervous System

SAGE Serial analysis of gene expression

scAAV9 Self-Complementary AAV9

SD Standard Deviation

shRNA Short Hairpin RNA

SK-N-SH Human neuroblastoma cell line

Sm Smith Core

SMA Spinal Muscular Atrophy

SMN Survival Motor Neuron

snRNA small nuclear RNA

snRNP small nuclear Ribonucleic Protein

SIRT1 Sirtuin 1

SPI Serratus Posterior Inferior muscle

SPN1 Snurportin-1

STAT Signal Transducer Activator of Transcription

STAT3 Signal Transducer Activator of Transcription 3

STRING Search Tool for the Retrieval of Interacting Gene/Protein

STZ Streptozotocin

TA Tibialis Anterior

TAD Transactivation Domain

TFAM Mitochondrial Transcription Factor A

TFEL Transcription Factor Screening

TGFb Transforming Growth Factor b

THBS1 Thrombospondin 1

TNBC Triple-Negative Breast Cancer

TRAF6 TNF receptor associated factor 6

TSA Trichostatin A

TUNEL Transferase dUTP Nick End Labelling

TWEAK Tumor Necrosis Factor-like Weak Inducer of Apoptosis

UBA1 Ubiquitin-Activating enzyme

UCP1 Uncoupling Protein 1

UPR Unfolded Protein Response

UPS Ubiquitin-Proteasome System

U-SnRNP Uridine-rich snRNPs

WAT White Adipose Tissue

WT Wild Type

WWP1 WW domain containing E3 ubiquitin ligase

XL-SMA X-linked SMA

1 INTRODUCTION

1.1 Spinal muscular atrophy (SMA)

Spinal muscular atrophy (SMA) is an autosomal recessive monogenic neuromuscular disease. Its pathological hallmark is the loss of alpha motor neurons in the spinal cord, progressive muscle weakness and proximal atrophy (Kolb and Kissel, 2011; Baker et al., 2021). SMA arises due to the almost absence of the ubiquitous survival motor neuron (SMN) protein in both the central nervous system (CNS) and the periphery (Chan et al., 2003). It is the second most common autosomal recessive disorder after cystic fibrosis, with an incidence ranging from 1/6000 to 1/10000 and a carrier frequency of 1/40 to 1/50 (Kolb and Kissel, 2015). Molecular Genetics of SMA. The majority of SMA patients (approximately 90-94%) exhibit homozygous deletions in either exon 7 and 8 or exon 7 exclusively within the SMN1 gene on chromosome 5q13 (Crawford, 1996) (Ogino and Wilson, 2004 (Lefebvre et al., 1995)). On the telomeric 5q13 chromosome, there are two copies of the SMN gene: one is the telomeric form, spanning 27 kb in length and composed of 9 exons (SMN1), and the other is the centromeric form known as SMN2 (Bürglen et al., 1996)(Vitte et al., 2007).

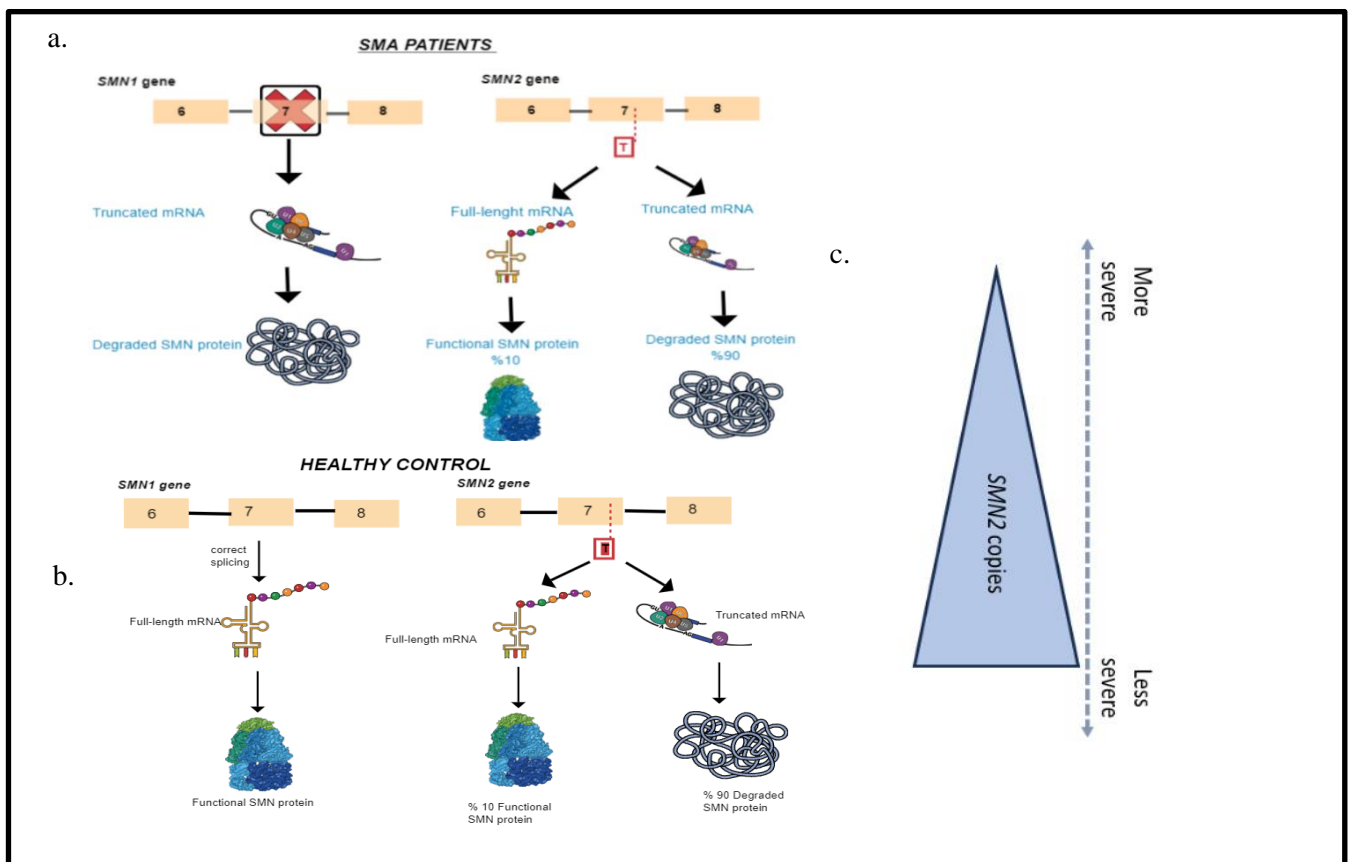


Figure 1.1 SMN1 and SMN2 expression in SMA patients and healthy control

a. In SMA patients, while the deletion of exon 7 in the *SMN1* gene prevents the production of full-length SMN (FL-SMN) protein, a C → T transition in the *SMN2* gene allows for the production of approximately 10% of the full-length SMN protein. b. In healthy individuals, while the *SMN1* gene expresses 100% functional SMN protein, the *SMN2* gene produces 10% functional SMN protein and 90% non-functional SMN protein. c. The quantity of *SMN2* copies directly influences the level of FL-SMN protein production, making SMA a disorder dependent on specific dosage.

These two genes share an almost identical sequence and produce identical proteins (Hahnen et al., 1997; Lorson and Androphy, 1998) (Lorson *et al.*, 1999) (Hahnen *et al.*, 1997). Nonetheless, *SMN2* distinguishes itself from *SMN1* by only five nucleotide differences (Parsons (Lefebvre *et al.*, 1995, p. 4; McAndrew *et al.*, 1997; Parsons *et al.*, 1998). *et al.*, 1998;(McAndrew *et al.*, 1997) Simic, 2008).

Despite the remarkable similarity (99%) between the *SMN1* and *SMN2* genes, a critical cytosine (C) to thymine (T) transition (C → T) in the 6th position of the 7th exon of the *SMN2* gene leads to the formation of an exonic splicing silencer (ESS) sequence by disrupting the exonic splice enhancer (ESE) sequence (Soloviov et al., 2010; Soloviov, Hryshenko, and Livshits, 2013). Consequently, this transition inhibits the binding of serine (S) and arginine (R) amino acid-rich SR proteins to the ESE sequences, causing heteronuclear ribonucleoproteins (hnRNPs) to bind to the newly formed ESS sequences (Bürglen et al., 1996; Monani et al., 1999a). This C to T transition disrupts RNA splicing during post-transcriptional processes (Monani et al., 1999b). As a result, exon 7 is omitted in approximately 90% of transcripts produced by the *SMN2* gene, leading to the generation of a truncated, non-oligomerized and unstable SMN protein, referred to as *SMNΔ7* SMA mouse model (DiDonato et al., 2001).

Although *SMN2* can synthesize around 10% of fully functional full-length (FL) transcripts containing exon 7, this quantity is insufficient to prevent motor neuron loss (Wirth, 2000) (figure 1.1.a). The number of copies of the *SMN2* gene varies among individuals and it is well-established that the levels of FL SMN protein increase in proportion to the number of these gene copies (Wirth et al., 1999). The more copies of *SMN2* there are, the greater the production of FL-SMN protein and so SMA appears as a dosage-specific disorder (figure 1.1.b).

1.1.1 Clinical Profile of SMA

Clinically, SMA is classified into five types (Types 0-IV), taking into account the disease's severity, age of onset, lifespan and motor functions (Pearn, 1980; D'Amico et al., 2011) (Table 1.1). Type 0 represents the most severe and least common form, with a life expectancy of approximately 6 months due to respiratory failure at birth (Dubowitz, 1999) (Table 1.1). Type I SMA, also known as Werdnig-Hoffman disease, is the most prevalent type, with a typical life expectancy of up to 2 years. These individuals display severe hypotonia, symmetrical flaccid paralysis and a complete inability to control head movements. Furthermore, they require external support to sit (Salort-Campana and Quijano-Roy, 2020) (Table 1.1). In contrast, Type II is classified as intermediate (Flunt et al., 2009).

Patients can sit independently without assistance, and some can stand with the aid of leg braces, but none can walk without support. Additionally, fine tremors with finger extension or gripping motions are frequently observed (Lunn and Wang, 2008) (Table 1.1). Type III SMA is considered one of the less severe manifestations of the condition and its symptoms typically become apparent after 18 months. These patients may display some clinical variability. Initially, individuals with Type III SMA can walk without needing assistance, but as they grow older, many of them often find it necessary to rely on a wheelchair for mobility (Lunn and Wang, 2008) (Table 1.1).

Conversely, Type IV SMA, which is the mildest form of the disease, is relatively rare. Symptoms typically arise in adulthood, often in one's thirties, and the disease progresses slowly over time (Baker et al., 2021).

Table 1. 1 Clinical types of spinal muscular atrophy (SMA).

Severity of SMA	Age of Onset	Motor function	Life Span	SMN2 Copy Number
Type 0 (Congenital SMA Prenatal-onset SMA)	Prenatal	- None achieved - Respiratory failure at birth - Neonatal hypotonia	Stillborn to < 6 months	variable
Type I (Werdnig-Hoffman disease)	0-6 months	- No Head control - Sitting with support - Hypotonia, symmetrical flaccid paralysis	< 2 years	Around 2-3 <i>SMN2</i> gene copies; (Calucho et al., 2018; Hadara., 2002)
Type II (Dubowitz disease)	6-18 months	- Sitting but cannot stand - Proximal muscle weakness - Postural tremor of fingers	Adulthood	Around 3 <i>SMN2</i> gene copies (Calucho et al., 2018; Hadara., 2002)
Type III (Kugelberg-Welander disease)	> 18 months	- Able to stand and walk - Loss of motor skills - Postural tremor of fingers	Normal	Around 3-4 <i>SMN2</i> gene copies (Calucho et al., 2018; Hadara., 2002)
Type IV (Adult Late-onset SMA)	Adulthood	- Walk independently - Proximal muscle weakness	Normal	Around 4 or more <i>SMN2</i> copies (Müller-Felber et al., 2020)

1.1.2 SMA Mouse Models

Mice are frequently chosen as model organisms for scientific research for several key reasons. First and foremost, they share a high degree of anatomical and physiological similarity with humans (Perlman, 2016). This includes having tissues that function similarly to human tissues such as the heart, liver, and muscles (Vandenbon and Nakai, 2010; Why are mice considered excellent models for humans? (The Jackson Laboratory, 2023). Building on this, mice also rank just behind humans in terms of the depth of our understanding of their genetic makeup, boasting a wealth of available data (Justice and Dhillon, 2016).

Further strengthening the case for using mice as models, a comparative analysis between mouse and human genomes reveals additional similarities. For example, chromatin domains, which are critical to gene regulation, and ortholog genes have been found to be developmentally stable and conserved in both species (Bryda, 2013).

Diving deeper into genetic similarities, mice possess a homolog of the human *SMN1* gene, which is crucial for understanding conditions like Spinal Muscular Atrophy SMA (Hsieh-Li et al., 2000). Mice are capable of synthesizing the full length of the SMN protein, which closely mimics the human version (Bebee, Dominguez and Chandler, 2012). In a detailed comparison, it was found that the nucleotides in exon 7 of this gene are 81% similar between the two species. Similarly, the amino acid sequences of the SMN proteins share a 75% similarity (DiDonato et al., 1997).

Deletion of the *Smn1* gene in mice has been shown to be embryonically lethal, similar to its effects in humans. To capture the clinical phenotypic diversity created by the human SMN2 gene, various transgenic mouse models have been developed (Monani et al., 2000).

Smn^{-/-}; *SMN2* (Taiwanese mouse model)

Understanding that a complete lack of the *Smn* gene (*Smn*^{-/-}) is embryonically lethal has led researchers to explore ways to partially compensate for this deficiency (Schrank et al., 1997). Building on this, a new SMA mouse model was developed. This model features a null *Smn* background, with two copies of the human *SMN2* BAC transgene but each allele contains two copies of the *SMN2* gene (Hsieh-Li et al., 2000). This configuration enables the model to produce

approximately 15% of the full-length SMN protein, which is sufficient to prevent lethality. However, it still results in a limited lifespan, with the subjects typically dying within the first week after birth. This configuration allows the model to produce about 15% of the full-length SMN protein. These mice have a limited lifespan, typically ranging from 10 to 14 days (Hsieh-Li et al., 2000; Monani, 2005). In this modelling, the investigation of the role of the SMN protein in developmental progression is potentially hindered by short lifespan.

SMN Δ 7 SMA mouse model

It emerged from a crossbreeding strategy where transgenic mice expressing the SMN Δ 7 protein were bred with the *Smn*^{-/-}; *SMN2* background (Le et al., 2005). This model extends the lifespan to up to 14 days, even in cases showing severe phenotypic characteristics (Le et al., 2005). This approach resulted in a new SMA mouse model, providing a more extended period for studying the disease's progression and potential therapeutic interventions.

Smn^{+/-}

The *Smn*^{+/-} mouse model consists of heterozygous mice that have a reduced level of SMN protein, yet do not display a pronounced SMA phenotype (Jablonka et al., 2000). In other words, this suggests that despite the slight alterations in motor neuron characteristics, these changes do not significantly impact the overall longevity of the mice (Jablonka et al., 2000).

Smn^{2B/2B}

Delving into its molecular genetics reveals that the model possesses a mutation in the exonic splice enhancer sequence, which is influenced by the tra2-beta splicing factor, as noted by DiDonato et al. (2001) and Hammond et al. (2010). This specific mutation impedes the inclusion of exon 7. Although this mutation decreases the synthesis of full-length SMN (FL-SMN), it still allows for limited production of FL-SMN protein (Le et al., 2005a). With the thought that exon 7 could be a pathological factor, the *Smn*^{-/-}; *SMN2*; *SMN Δ 7* mice has been merged with the deleted exon-7 (Le et al., 2005). Moving on to the lifespan of these SMN Δ 7 mice, it is notably extended to an average 13.3 days. Importantly, the extended lifespan of the SMN Δ 7 mouse model provides a valuable window for studying severe pathologies, overcoming a limitation commonly encountered in *Smn*^{-/-}; *SMN2* mice (Le et al., 2005).

The limitations of the existing severe mouse models, which have short lifespans, have hindered in-depth research into the long-term pathological effects of Spinal Muscular Atrophy (SMA). Furthermore, these models failed to replicate the phenotypes of patients with milder SMA types, such as Type II, III, and IV. To address these shortcomings, researchers developed a milder SMA mouse model known as *Smn*^{2B/-} (Bowerman et al., 2012).

In the development of the *Smn*^{2B/-} mouse model, a crossbreeding strategy was employed involving the *Smn*^{2B/2B} mouse line and *Smn*^{+/-}. This breeding approach led to the creation of a less severe variant of the model, known as *Smn*^{2B/-} (Bowerman et al., 2012). This process, which resulted in a milder form of the disease phenotype, has been thoroughly detailed in the study by Bowerman et al. This model traces back to the original *Smn*^{2B/2B} mouse line. Delving into its molecular genetics reveals that the model possesses a mutation in the exonic splice enhancer sequence, which is influenced by the tra2-beta splicing factor, as noted by DiDonato et al. (2001) and Hammond et al. (2010). This specific mutation impedes the inclusion of exon 7. The development of the model under discussion, known as *Smn*^{+/-}, was achieved through the interbreeding of mice with one disrupted allele of the *Smn* gene, as documented by Jablonka et al. (2000) and Roy et al. (1995). This *Smn*^{+/-} model was further refined by crossbreeding with the *Smn*^{2B/2B} mouse line, leading to the emergence of a milder *Smn*^{2B/-} variant, a process detailed by Bowerman et al (2012).

Notably, the *Smn*^{2B/-} mice have a lifespan extending from 21 to 30 days, and they begin to display SMA-like symptoms around day 10 (Bowerman et al., 2012). The heterogeneity in human SMA phenotypes has been successfully replicated in mouse models, leading to the development of various strains with varying degrees of severity, including severe and milder forms. These diverse mouse models, each exhibiting a distinct phenotype, have facilitated a detailed examination of SMA pathogenesis with a focus on how severity impacts the disease's progression.

1.1.3 SMN Has a Housekeeping Role

The SMN protein is traditionally regarded as a component of the cell's "housekeeping" system. It is expressed ubiquitously in all tissues (Paushkin et al., 2002) and enables the maintenance of the homeostatic environment of the whole cell and tissue (Coover et al., 1997). The SMN protein plays a role in various housekeeping functions, including small nuclear ribonucleoprotein assembly (snRNP), spliceosome regulation, ubiquitination and mitochondrial homeostasis, contributing to overall cellular integrity (D et al., 2010) (Bachand et al., 2002).

1.1.4 The SMN is Crucial for RNA metabolism.

The SMN protein plays a fundamental role in the biogenesis of ribonucleoproteins (snRNPs) and forms the essential building blocks of spliceosomes, where pre-mRNA splicing occurs (Kolb et al., 2007).

The SMN protein is integral to the biogenesis of snRNP, playing a critical role in the functioning of the spliceosome. Its specific localization and preserved structure are essential aspects as highlighted by Bertrand et al., 1999.

SnRNPs are vital for the maturation of pre-mRNAs, removing introns within the spliceosome structure (Gubitza, Feng and Dreyfuss, 2004). The primary role of the SMN protein in snRNP biogenesis involves mounting Sm proteins onto snRNPs in the cytoplasm (Pellizzoni et al., 2002).

To examine this process step-by-step, in the cytoplasm, seven Sm proteins are initially bound to the chloride conductance regulatory protein (pICln) (Pellizzoni, 2007). This binding process is facilitated by the protein arginine methyltransferases PRMT5 complex and PRMT7, which methylate the SM proteins, enabling their attachment to the SMN complex, which comprises SMN, Gemins2-8, and unrip (Liu et al., 1997). Pre-snRNPs are transcribed in the nucleus and are then transported to the cytoplasm. This transportation is mediated by a complex involving the phosphorylated adaptor for RNA export (PHAX), Cap-binding complex (CBC), exportin (Xpo1) and the ras-related nuclear protein GTP (Ran) (Pellizzoni, 2007). The SMN complex then positions the Sm proteins onto the snRNA (Ogawa et al., 2009). The m7G cap of the snRNA is hypermethylated by trimethyl-guanosine synthetase 1 (TGS), enabling the SMN complex, along with the snRNA, to bind snurportin and importin (Narayanan et

al., 2002). This facilitates the transport of the SMN complex, now equipped with an assembled snRNP, back into the nucleus. Once in the nucleus, the SMN complex and snRNPs localize to the Cajal bodies, where the snRNPs undergo further maturation (Carvalho et al., 1999). Depending on the cell type and developmental stage, SMN can be found as a separate entity adjacent to the Cajal bodies (Carvalho et al., 1999).

Furthermore, the SMN protein is revealed to be an essential component in pre- mRNA splicing, both structurally and functionally, which is governed by two highly conserved regions (Lorson and Androphy, 1998). One of these conserved regions, exon 2, interacts with SIP1 (Gemin2), and this complex plays a pivotal role in the biogenesis of snRNPs, facilitating their transport to the nucleus through snRNP methylation (Fischer et al., 1997). Another conserved region on the SMN protein is located at its C- terminus, housing a tyrosine-glycine-rich motif and a self-oligomerization domain (Plessel et al., 1997; Young et al., 2000) (Plessel, Lührmann, and Kastner, 1997) (Young et al., 2000). This particular region of the SMN protein acts as a scaffold for snRNPs assembly, allowing the formation of a ring-like structure around the SMN protein and facilitating snRNP assembly (Kambach et al., 1999; Massenet et al., 2002) (Kambach et al., 1999) (Massenet et al., 2002).

The hypothesis that Smn depletion can lead to insufficient snRNP formation and consequently cause defects in mRNA processing is supported by various studies. To investigate this hypothesis, the metabolism of snRNPs in the spinal cords of SMA mouse models with varying phenotypic severities was studied. The findings demonstrate that in the spinal cords of SMA mice, there is a proportional decrease in both the expression of Gemin proteins and the activity of snRNP assembly, correlating with the severity of the disease (Gabanella et al., 2007). In parallel studies, research has demonstrated that lowering SMN protein levels in HeLa cells to those seen in SMA patients, leads to a disruption in the assembly of spliceosomal uridine-rich small nuclear ribonucleoproteins (U snRNPs) U snRNPs. When the reduction in SMN was less severe, zebrafish embryos exhibited severe degeneration of motor axons, akin to what is seen in SMA. These findings indicate that the degeneration of motor neurons in SMA is directly linked to the compromised production of U snRNPs (Winkler et al., 2005).

Considering the role played by snRNPs in the spliceosome, questions have been raised about the potential disruption of splicing in SMA disease. This hypothesis is supported by observations of prevalent splicing defects in both pre-symptomatic SMA mice (Bäumer et al., 2009) and fibroblasts from SMA patients (Zhang et al., 2008). The presence of these defects in different models and stages of SMA highlights the critical impact of snRNP function on the splicing process, further emphasizing its importance in the pathology of SMA.

The SMN protein, in addition to its functions in snRNP assembly and mRNA splicing, also interacts with RNA helicase A and RNA polymerase II, which are related to the transcription machinery (Pellizzoni et al., 2001). The SMN protein actively interacts with small nucleolar ribonucleoproteins (snoRNPs) such as GAR1. This interaction results in the accumulation of snoRNPs outside the nucleolus, which are responsible for the processing of ribosomal RNAs (rRNAs) (Girard et al., 1992; Tyc and Steitz, 1989).as identified in the research by Pellizzoni, Baccon, et al., in 2001.

The primary role of the SMN protein in RNA metabolism has been emphasized through its involvement in various stages of this process. This highlights the function of the SMN protein as essential across different tissue types and independent of time. The ubiquity and consistency of SMN's role in RNA metabolism underscore its fundamental importance in cellular processes, regardless of the specific context or timing within the organism.

1.1.5 Protein Translation and Related Proteostatic Mechanisms

Protein degradation plays an equally vital role in maintaining homeostatic balance as protein synthesis, as demonstrated by Kwon et al. (2011). One of the crucial systems responsible for protein degradation is the ubiquitin proteasome system (UPS), wherein ubiquitin-like modifier activating enzyme 1 (UBA1) serves as a key enzyme (Abera et al. 2016). UBA1 activates ubiquitin, facilitating the degradation of specific proteins by introducing them to the 26S proteasome complex (Abera et al., 2016). Notably, this Uba1-based ubiquitin-proteasome pathway can be impaired in cases of SMN protein deficiency (Balak et al. 2017). The reduction in Uba1 enzyme levels observed in the SMA zebrafish model, along with the subsequent improvement in the SMA phenotype upon systemic administration of self-complementary adeno-associated virus (AAV)-

UBA1 to zebrafish, underscores the widespread influence of the SMN protein on ubiquitin homeostasis (Powis et al., 2016).

Once again, the SMN1 gene's inherent housekeeping effect on the ubiquitin proteasome pathway becomes apparent, this time through its interaction with the NF- κ B pathway (Kim and Choi, 2017). NF- κ B resides within the nucleus and initiates pro-inflammatory signaling (Srisankantharajah and Ley, 2010). Its activation relies on the phosphorylation of IKK- γ , a subunit, by the E3 ubiquitin ligase known as TRAF6. The TRAF6-induced-phosphorylated- IKK- γ inhibits the proteasomal pathway (Shifera, 2010). In this context, SMN functions as a natural homeostatic protector by inhibiting TRAF6, thereby preserving the integrity of the proteasomal pathway (Kim and Choi, 2017).

The broad-ranging influence of the SMN gene on protein metabolism, encompassing various tissue types, once again underscores the universal functionality of SMN protein.

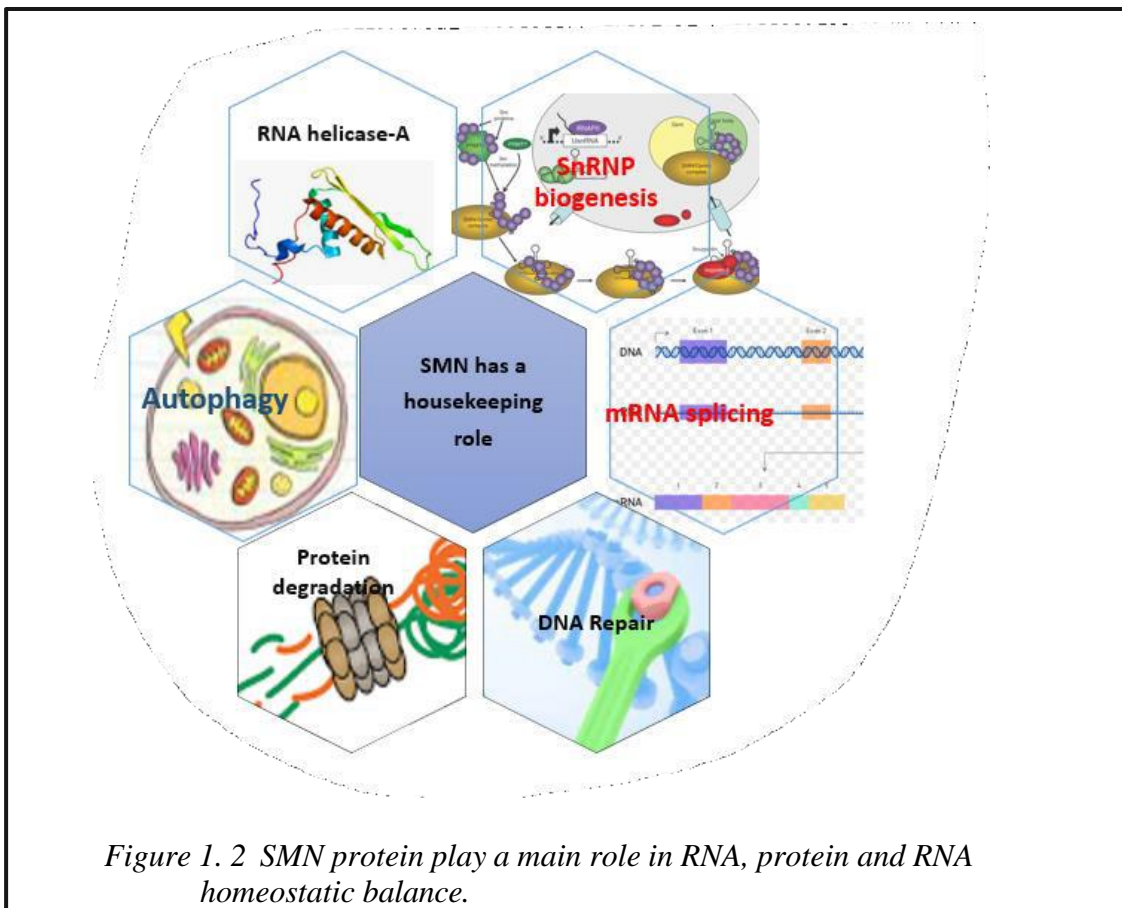


Figure 1. 2 SMN protein play a main role in RNA, protein and RNA homeostatic balance.

1.2 Neuronal Pathologies in SMA

Loss of alpha motor neurons is one of the hallmarks of SMA disease (Battaglia *et al.*, 1997). Even if *SMN* is a housekeeping gene, why motor neurons are most vulnerable to the lack of the SMN protein, has been one of the key questions in research. In general, it was determined that *SMN* loss caused developmental and functional defects in the CNS, involving axonal developmental defects, cytoskeleton components and apoptosis (McWhorter, Monani, Arthur H. M. Burghes, *et al.*, 2003).

1.2.1 Structural and Functional Abnormalities in CNS

Neurons and Astrocytes

In studies conducted using the zebrafish SMA model, researchers observed a decrease in axon length and abnormal branching in axons before the onset of alpha motor neuron death. This observation led to the hypothesis that the *SMN*-dependent axonal defects might be contributing to the loss of motor neurons (McWhorter, Monani, Arthur H.M. Burghes, *et al.*, 2003).

To emphasize the genetic relationship between the SMN protein and axon formation, it is important to note that exon 3 of the *SMN* gene is specifically responsible for axonogenesis and its transcript is referred to as a-SMN (Setola *et al.*, 2007). A-Smn is predominantly expressed in the white matter of the spinal cord and actively participates in the formation of ventral roots (Setola *et al.*, 2007). When we examine the localization of SMN in relation to axons, it is evident that SMN protein is found in axons, axonal branches, growth cones (the areas of axonal growth), and branch points (van Bergeijk *et al.*, 2007). However, it is noteworthy that SMN proteins are particularly concentrated in the growth cone, indicating that Smn serves as a prominent marker for growth cones (Fan and Simard, 2002).

The substantial impact of SMN protein in the central nervous system, primarily localized and expressed in axons and growth cones, becomes evident when considering its role in axon development and other axon components. The deletion of *Smn* gene in the PC12 cell line, originating from sympatho-adrenal pheochromocytoma, serves as an effective model to study neuronal differentiation with nerve growth factor (Greene and Tischler, 1976). In connection with the SMN protein deficiency, the longest neurites in PC12 cells

were morphometrically measured. Observations indicated that the lack of SMN could cause a reduction in neurite lengths. Furthermore, these abnormalities were corrected upon the re-addition of SMN, suggesting that SMN protein plays a role in neurite outgrowth in axons (van Bergeijk et al., 2007). In a parallel study using the same cell line, it was observed that the absence of SMN protein led to neurite swelling and neurogenesis defects. This finding suggests abnormalities in the cytoskeleton and irregularities in axonal transport (Bowerman, Shafey, and Kothary, 2007). Furthermore, reintroducing the *Smn* gene corrected these phenotypes (Bowerman, Shafey, and Kothary, 2007). Consequently, the reversal of the pathology upon *Smn* gene reintroduction implies that this axon-skeleton pathology in neurons is specifically associated with SMN deficiency.

Astrocytes typically serve supportive roles in the central nervous system, including supplying nutrients, releasing trophic factors and recycling neurotransmitters, all of which are essential for neuronal maintenance and homeostasis (Siracusa, Fusco, and Cuzzocrea, 2019).

To investigate its association with SMA disease, SMN was selectively introduced into astrocytes in the *SMN17* mouse model (Rindt et al., 2015). Upon the restoration of astrocytic SMN, it played a role in maintaining the well-being of lumbar motor neurons without increasing their numbers (Rindt et al., 2015). One possible explanation for this positive effect is linked to glial cell line-derived neurotrophic factor (GDNF). Normally, astrocytes secrete GDNF, which promotes the development and proliferation of neuronal cells by preventing apoptosis (Patitucci and Ebert, 2016).

However, in the case of *SMN* deletion, GDNF production is impaired and might be associated with neuronal defects in SMA (McGivern et al., 2013). On the other hand, one of the factors contributing to neuronal maintenance and homeostasis is monocyte chemoattractant protein 1 (MCP1), which has previously been shown to support neuron growth under stress conditions (Stowe et al., 2012). It has been observed that the expression of MCP1 decreases in astrocytes derived from SMA induced pluripotent stem cells (iPSCs) (Martin et al., 2017). Furthermore, to determine whether the effect of MCP1 is directly on motor neurons and, if so, to illustrate the nature of its influence. For this purpose, recombinant MCP1 was administered to cultured neurons. This administration was found to positively regulate neuronal growth, as evidenced in the research the administration of recombinant MCP1 has been shown to positively

regulate neuronal growth (Martin et al., 2017). Therefore, alterations in the level of MCP1 secreted by astrocytes are dependent on SMN related to SMA pathology. levels.

The impacts of astrocytes and astrocytes secreted chemokines on neuronal integrity and survival occurs through neurotrophic factors and MCP1. What's intriguing is that the effects of these factors are dependent on SMN. The mechanisms that affect both astrocytes and neurons are associated with SMA pathology.

1.2.2 Cytoskeleton Related Defects

When examining the structural interaction of the SMN protein, it has been observed that the SMN protein interacts with Gemin2 at a rate of 40% and with Gemin3 at a rate of 48% within neuronal granules, facilitating the formation of snRNP complexes before the bounding of the Sm proteins (Zhang et al., 2006). This complex of SMN and Gemin proteins is present as granules and is transported bidirectionally along the cytoskeleton to reach both dendrites and the growth cone, with their movement being dependent on the cytoskeleton (Zhang et al., 2003).

In the cytoskeleton-dependent neuronal network, communication between neurons occurs through synapses. The branched structure of axons is essential for facilitating the assembly of synapses. Additionally, F-actin plays a crucial role in initiating the formation of axon arbors, which in turn leads to the development of filopodia. A study conducted on F-actin in primary mouse motor cells revealed that α - actin significantly influences filopodia dynamics, while β -actin is primarily involved in growth cone formation (Moradi et al., 2017). Given its widespread functionality, all forms of actin, which are components of the cytoskeleton, play fundamental roles in processes such as synaptogenesis, axon elongation, and innervation of the neuromuscular plate (Chia et al., 2014).

Regarding the interaction of the CNS components mentioned above with the SMN protein, it was observed that the deletion of *Smn* gene in the PC12 cell line, originating from sympatho-adrenal pheochromocytoma, serve as an effective model to study neuronal differentiation with nerve growth factor (Greene and Tischler, 1976). In connection with the SMN protein deficiency, the longest neurites in PC12 cells were morphometrically measured. Observations indicated that the lack of SMN could cause a reduction in neurite lengths and a change in the

ratio. Furthermore, these abnormalities were corrected upon the re-addition of SMN, suggesting that SMN protein plays a role in neurite outgrowth and influences actin dynamics in axons (van Bergeijk et al., 2007).

In a parallel study using the same cell line, it was observed that the absence of SMN protein led to neurite swelling and neurogenesis defects. This finding suggests abnormalities in the cytoskeleton and irregularities in axonal transport (Bowerman, Shafey, and Kothary, 2007). Furthermore, reintroducing the *Smn* gene corrected these phenotypes (Bowerman, Shafey, and Kothary, 2007). Consequently, the reversal of the pathology upon *Smn* gene reintroduction implies that this axon-skeleton pathology in neurons is specifically associated with SMN deficiency.

Profilin, which co-localizes with the SMN protein and regulates actin dynamics by directly binding to actin, has an expressed isoform known as profilin2a in neuronal cells (Giesemann et al., 1999). It has been discovered that the expression of profilin IIa increases in *Smn*- knockdown (KD) KD-PC12 cells (Bowerman, Shafey, and Kothary, 2007). Moreover, profilin's impact on the axonal cytoskeleton stability is mediated through the Rho-Rock pathway, which inhibits neuronal outgrowth and reduces neuronal differentiation (Da Silva et al., 2003). (Bowerman, Shafey, and Kothary, 2007). As a result of its inhibition of Rho-Rock pathway-dependent profilin activity by Y-27632 treatment, ameliorates regulation is observed in the neuronal integrity, and differentiation profile and survival in *Smn*^{2B/-} (Bowerman et al., 2010). The effect of profilin IIa on SMA pathology is also potentially associated to the phosphorylation modification of profilin serine residues (Walter et al., 2020).

Plastin-3 is an actin-binding protein that plays a role in stabilizing the actin cytoskeleton of nerve cells, important for the development and function of the nervous system (Wolff et al., 2021). Its protective effect on neuronal cells has been confirmed in severe SMA mouse models and *Smn*-KD zebrafish models (Oprea et al., 2008). When examined more closely, it has been found that Plastin-3 protein co-localizes with the SMN and F-actin proteins in both axons and growth cones (Oprea et al., 2008). In the *SMN17* mouse model, the overexpression of Plastin-3 has been shown to rescue the phenotypic defects associated with axonal elongation and outgrowth development (Alrafiah et al., 2018).

In detail, the specific type of mRNA being transported along the axons (β -actin), RNA-binding heterogeneous nuclear ribonucleoprotein (hnRNP) and SMN

proteins interact to regulate the cytoskeleton and support the formation of neuronal connections (Jablonka et al., 2007). Furthermore, when primary motor neurons were isolated from *Smn*^{-/-}; *SMN2* SMA mice, it was found that there were reduced levels of β -actin mRNA in the distal axonal region and growth cones, accompanied by a decrease in axonal length (Rossoll et al., 2003). To conduct a more detailed examination of damage in the growth cone, researchers investigated the frequency of calcium transitions in the pre-synaptic active zone, which revealed a decrease in excitability (Jablonka et al., 2007).

The direct interaction between SMN protein and cytoskeletal structures, including their modifications, which play crucial roles in various CNS functions such as the transport of necessary signals-BE SPECIFIC and the formation of synapses- INCOMPLETE. The paramount importance of the SMN protein in both the developmental and functional aspects of the central nervous system has become evident.

1.2.3 Apoptosis

The gene responsible for neuronal apoptosis, known as (neuronal apoptosis inhibitor protein) NAIP, is situated on chromosome 5, in close proximity to the *SMN1* gene location (Roy et al., 1995). Notably, NAIP is mutated in nearly half of SMA patients (Roy et al., 1995). Consequently, it has been hypothesized that the apoptosis mechanism contributes to neuronal loss in SMA.

When *SMN2* copy numbers and NAIP gene expression were jointly evaluated in 42 SMA patients, NAIP deletions were predominantly detected in Type I patients (Watihayati et al., 2009). In simpler terms, SMA patients with the fewest *SMN2* copies also exhibited NAIP mutations (Watihayati et al., 2009). Therefore, it is suggested that NAIP may exacerbate the disease in conjunction with the reduced number of *SMN2* copies.

Furthermore, there was an increase in motor neuron death in *Smn*-KD NSC-34 neuron cells, which was linked to elevated caspase-3 activity, a key player in the process of apoptosis (Parker et al., 2008). In parallel, in iPSCs of SMA patients, the activity of apoptosis-promoting enzymes caspase 3 and caspase 8 increased, resulting in apoptosis to motor neurons. However, this damage could be mitigated by blocking apoptosis by addition of either a Fas blocking antibody, which is ligand of caspase-8, or a caspase-3 inhibitor (Sareen et al., 2012).

Another protein involved in apoptosis is Bcl2-xL, an anti-apoptotic member of the *Bcl2* family that inhibits pro-apoptotic components (Siddiqui, Ahad, and Ahsan, 2015). The neuroprotective effect of Bcl-xL has been validated in primary neuron cultures from ALS rats (embryonic day 15) (Garrity-Moses et al., 2005). In the crossed SMA/Bcl-xL mouse model, the number and size of neurons increased as well as prolonging their life span by decreasing apoptotic activity (Tsai et al., 2008).

1.3 Skeletal Muscle Pathologies in SMA

Muscle atrophy, weakness, and aberrant expression of muscle-specific proteins are hallmarks of SMA pathology (Nicole *et al.*, 2003). The fact that these developmental and functional defects in muscles are observed early, even before CNS abnormalities (J. Boyer et al., 2013), suggests that they may be primary contributing factors in the pathology of SMA.

Transcriptomic analyses conducted in three distinct atrophy models (denervation, immobilization, and hindlimb suspension in rats) led to the identification of muscle ring finger 1 (MuRF1) and muscle atrophy f-box (MAFbx) as prominent ubiquitin ligases associated with atrophy (Bodine et al., 2001). To further investigate the functions of these ligases *in vivo*, studies involving mouse models with deleted *MuRF1* and *MAFbx* genes were conducted, and intriguing findings emerged.

Specifically, mice lacking these genes did not develop an atrophy phenotype (Bodine et al., 2001). In a subsequent study, were targeted for knockdown in the *SMN17* mouse model (Iyer et al., 2014). On the other hand, it was observed that the deletion of the *MuRF1* gene resulted in a shortened lifespan for in in the *SMN17* mouse model this model (Iyer et al., 2014). Conversely, the knockdown of *MAFbx* had no significant impact on weight and lifespan but did lead to an increase in muscle fibers in the same mouse model (Iyer et al., 2014). These results suggest that the deletion of these ligases alone may not be sufficient to reverse atrophy in the context of SMA. Furthermore, it raises the possibility that another gene, involved in the upregulation of these ligases, could potentially contribute to the atrophy observed in SMA cases.

1.3.1 SMA and Myogenesis

Myogenesis is the process of muscle tissue formation during embryonic development (Bentzinger et al., 2012; Davis et al., 1987). This process is carefully orchestrated from myotomes (embryonic progenitors) to development of myofibers (mature muscle cells) (Zammit, 2017). This complex process involves several key factors, including *Pax proteins* and myogenic regulatory factors (*MRFs*) such as myogenin, *MyoD*, *Myf5* and *MRF4*, each playing distinct roles (Zammit, 2017).

To better understand the sequential stages and the factors that influence them, let's break myogenic progression down. The initial stage involves the conversion of somatic mesoderm into nucleated myotomes, driven by the expression of *Pax3* and *Pax7* (Hasty et al., 1993). As we progress to subsequent stages, the roles of *Pax3* and *Pax7* are taken over by *MyoD* and *Myf5*, leading to the formation of myoblasts (precursor cells/proliferation phase) (Mastroiannopoulos et al., 2012). Differentiation begins when myogenin and *MRF4* come into play, resulting in the formation of myocytes. The myocytes are single-nucleus, slender muscle cells, characterized by their inclination towards differentiation and fusion within muscle tissues (Jang, 2013). *MyoD* and myogenin facilitate the fusion of myocytes transforming them into multi-nucleated primary myofibers, which, in turn, express critical proteins like myosin heavy chain and muscle creatine kinase essential for muscle development (Schiaffino et al., 2015). The final stage of myogenesis involves the maturation of myotubes into mature myofibers. It's worth noting that myogenin plays a pivotal role not only in determining the size and number of myofibers but also in the ongoing development of myotubes (Ganassi et al., 2018).

To gain a comprehensive understanding of the interplay between muscle tissue and the SMN protein, researchers have employed a model involving *Smn*-KD C2C12 cells, a mouse muscle cell line, with varying degrees of *Smn* knockdown intensity (Shafey, Côté, and Kothary, 2005). This investigation revealed that as *Smn* depletion increased in C2C12 cells, there was a notable decrease in proliferation, the emergence of abnormal myotubes and impairments in myoblast fusion (Shafey, Côté, and Kothary, 2005). These findings unequivocally establish a direct and substantial correlation between *Smn* loss and muscle defects. Furthermore, to substantiate the connection between the SMN

protein and skeletal muscle, observations from an SMA drosophila models are noteworthy. This model displayed severe atrophic phenotypes such as the inability to fly and jump (Rajendra et al., 2007).

Expanding on muscle development defects of SMA in molecular level, the satellite cell, a pivotal stem cell population within muscle tissue, is commonly assessed through *PAX7* quantification. Remarkably, research has indicated a substantial increase in *PAX7* expression, particularly in atrophic regions during the postnatal phase in prenatal samples of SMA Type I patient, which implies a delay in muscle maturation (Martínez-Hernández et al., 2014). Confirming these findings through histochemistry analyses, it was noted that the levels of *PAX3* and *Ki67*, recognized both as myogenic markers and precursors, exhibited an increase; while the expression of *MYOD* and *MYHIE* decreased in SMA Type I patients (Hellbach et al., 2018). In the context of these factors, it has been shown in the primary myoblasts of *Smn*^{2B/-} mice that the expression of *Pax7*, *MyoD*, *MyoG* and *MHC* is significantly reduced comparing controls (Boyer et al., 2014). This research underscores that the myogenic program is delayed in the context of SMA.

In an examination conducted on *Smn*^{2B/-} and *Smn*^{-/-}; *SMN2* SMA mouse models, a reduction in myogenin was observed alongside a similar decrease in myosin heavy chain, a late marker of myogenic differentiation. These observations suggest the presence of defects in myotube fusion potential and differentiation processes (Boyer et al., 2014). Furthermore, an increase in immature myofibers was detected in the skeletal muscles of SMA mouse models (Boyer et al., 2014). In a parallel study, using a primary muscle cell line derived from the *SMN17* SMA mouse model, it was revealed that the deficiency of *Smn* led to decreased expression of talin, a focal adhesion protein crucial for myoblast fusion. Consequently, myotubes were unable to become polynucleated and transform into myofibers (Bricceno et al., 2014).

In conclusion, a reduction in SMN protein levels has been linked to delays in muscle maturation and impairment myoblast fusion by following abnormalities in the expression of muscle-specific factors.

1.3.2 Metabolism and Contraction of SMA

When exploring the complexities of muscle structure, we encounter the sarcomere, the fundamental unit responsible for muscle contraction (Riddle et al., 1997).

Within the sarcomere, there are bands rich in actin and myosin, as well as structures known as Z-discs that regulate the coordination of sarcomeres and the organization of actin bands (Clark et al., 2002). Notably, in the context of the SMN protein, it is found co-localizing with α -actin at these Z-discs in both SMA *Drosophila* and SMA mouse myofibrils (Da Silva et al., 2003; Rajendra et al., 2007; Walker et al., 2008). Furthermore, the direct interaction of SMN with other sarcomeric proteins like titin and profilin2, as detailed in the cytoskeleton section, defines SMN as a sarcomeric protein itself (Sharma *et al.*, 2005; Berciano *et al.*, 2020). A critical finding is the distinctive localization of the SMN protein in the sarcomeres between skeletal myofibers of SMA Type I patients and those of healthy individuals. In control groups, SMN protein localizes to titin-positive M-bands and actin-positive I-bands. However, in Type I SMA skeletal muscle fibers, its localization shifts to Z-discs (Berciano et al., 2020). These observations suggest that the reduced and altered distribution of SMN protein can impact the sarcomeric architecture, potentially leading to the disruption of myofibrils found in SMA muscle independently of neurogenic myopathy (Berciano et al., 2020).

Turning our attention to the structure of quadriceps in individuals with SMA Type I compared to control muscles; firstly, there's an abundance of fast myosin chains in SMA, while slow myosin chains are less prevalent (Biral et al., 1989). This structural change can impact muscle strength and endurance. Typically, slow myosin chains are found in fibers that are necessary for endurance, possessing the capacity for prolonged contraction. Slow-to-fast fibre-type transitions can lead to muscles tiring more quickly during sustained activities (Putman et al., 2004). Additionally, there's an intriguing structural distinction concerning the proteins desmin and vimentin, which usually decrease as muscles mature (Sarnat, 1992). However, in SMA postnatal muscle fibers, these proteins maintain their levels (Le Verche et al., 2017).

Moving to muscle contraction initiation, it's crucial to emphasize the roles of the Ryr1 receptor, which releases calcium ions, and its counterpart, Serca1, responsible for calcium uptake in the sarcomere. In *Smn*^{2B/-} and *Smn*^{-/-}; *SMN2* SMA mouse models, there is a delay in the transition from neonatal to adult

isoforms of proteins vital for proper muscle contractions, including ryanodine receptors and sodium channels. Thus, factors like *Ryr1* and *Serca1*, might contribute to muscle weakness in SMA due to developmental delays (Boyer et al., 2013).

Let's delve into the realm of muscle catabolism. Two pivotal pathways govern this process: the calcium-dependent calpain system and the ubiquitin proteasome system (explain in the UPS) (Nury, Doucet, and Coux, 2007). Importantly, *Smn* plays a crucial role in regulating proteolysis within catabolic muscle metabolism, primarily through calpain cleavage (Walker et al., 2008). The calpain-proteolysis system contributes to the degradation of proteins at Z-discs, including the SMN protein. Consequently, inhibiting calpain-mediated protein degradation emerges as a critical therapeutic target for SMA muscle development (Walker et al., 2008).

In summary, the SMN protein not only contributes to muscle structure by localizing in the functional unit of muscle, sarcomeres, but also plays a vital role in muscle contraction particularly in the regulation of proteolysis.

1.3.3 Muscle Weakness and Developmental Changes Occurred Prior to any Neuronal Damage

As a well-known, SMA is a neuromuscular disease. In the field of research on this disease, frequently asked questions revolve around what kind of relationship exists between muscles and nerves? Are they interdependent, or do they act dependently of each other? If they are interdependent, which component's pathology influences the other? For addressing this question, the most suitable model area is the neuromuscular junction (NMJ), which is a fundamental structure in the human body where a motor neuron communicates with a muscle fiber, enabling muscle contraction.

Intriguingly, the pivotal role of muscle tissue in the pathophysiology of SMA was initially unveiled through a nerve-muscle co-culture analysis, which involved both SMA patients and a healthy control group back in 1995 (Braun et al., 1995). This enlightening study demonstrated that when satellite cells from SMA patients were incorporated into the culture, it resulted in damaged innervated muscle fibers. In stark contrast, when muscle tissues from the control group were utilized, the NMJ area exhibited a healthy pattern (Braun et al., 1995). Consequently, these findings spurred discussions regarding whether muscle degeneration or motor neuron degeneration serves as the primary driver of the

disease phenotype. Further shedding light on this debate, investigations involving pre-symptomatic *Smn*^{2B/-} and *Smn*^{-/-}; *SMN2* SMA mouse models revealed that muscle weakness and alterations in the expression of muscle-specific contraction proteins occurred even before clinical signs manifested, and prior to any observable neuronal damage (Boyer et al., 2013). This prompted a focused examination into the direct role and potential impact of SMN deficiency within muscle tissue, one of the peripheral tissues affected by SMA.

In a *MyoD-iCre-Smn* SMA mouse model, the SMN protein was selectively deleted within muscle tissues while being retained in spinal cord neurons (Kim et al., 2020). This experiment resulted in the observation of morphological abnormalities in muscle fibers, muscle weakness, impaired muscle function, disruption of the post-synaptic compartment and abnormalities in NMJ morphology—associated with chronic myopathy. Significantly, the reintroduction of SMN protein into the muscle led to the amelioration of these symptoms. In conclusion, it becomes evident that SMN protein deficiency within muscle tissue exerts a direct, independent, and profound influence on the emergence of the SMA phenotype (Kim et al., 2020a).

These collective findings underscore the central role of muscle tissue as a primary target for SMA therapy.

1.4 Neuromuscular junction (NMJ)

The NMJ is a specialized synapse that facilitates the transmission of chemical signals from the nerve terminal to skeletal muscle using the acetylcholine neurotransmitter (Creazzo and Sohal, 1983).

Within the NMJ, three key areas exist: the nerve terminal, synaptic cleft and motor endplate. When the motor neuron undergoes depolarization, voltage-gated calcium channels open. This allows calcium ions to enter, facilitating the interaction of synaptic vesicles with the active zone. Consequently, acetylcholine neurotransmitters are released into the synaptic cleft. Acetylcholine binds to the alpha subunit of ligand-gated channels on the muscle membrane, resulting in the opening of sodium and potassium voltage-gated channels (Liu et al., 2008). These channels permit the entry of sodium ions into the motor endplate area. The increased influx of sodium ions depolarizes the muscle and generates an endplate potential, which serves as the stimulus for muscle contraction (Liu et al., 2008).

A more detailed examination of the skeletal muscles interacting with motor neurons has been conducted. Two different types of skeletal muscles play a role in this synaptic formation. One is called Fast Synapsing – FaSyn (developing within 1 day) and the other is referred to as Delayed Synapsing – DeSyn (developing within several days) in young adult mice (Pun et al., 2002). These two different muscles exhibit varying sensitivity to synaptic stability. Furthermore, their dependence on the agrin protein, released from motor neurons and responsible for inducing acetylcholine receptors differentiation in myotubes, differs (Pun et al., 2002).

As a result, it is evident that skeletal muscles independently initiate the formation of acetylcholine receptors in NMJ formation, and their responses to motor neuron stimuli vary depending on the type of skeletal muscle, contributing a decisive step to NMJ formation (Pun et al., 2002)

1.4.1 NMJ Pathology of SMA

To investigate the direct and clear impact of the SMN protein on NMJ formation and maturation, NMJ-like structures were created using iPSC cells derived from SMA patients. Consequently, it was shown that these SMA iPSC-derived myoblasts had fewer and smaller clusters of AChRs compared to controls (Yoshida et al., 2015). This study has demonstrated a direct pathophysiological relationship between SMN protein and defects in AChR clustering.

Early indicators of SMA pathology are evident at NMJ. Notably, the accumulation of neurofilament (NF) at the endplate serves as an early biomarker, becoming noticeable in the *SMN17* SMA mouse model as early as the first post-natal day (Dale et al., 2011). Upon microscopic examination of NMJ units, a reduced density of synaptic vesicles is apparent in presynaptic terminal of *SMN17* SMA mouse model comparing to control littermates (Kong et al., 2009). There's also a delay in acetylcholine molecules reaching their corresponding acetylcholine receptors, which is linked to an imbalance expression of acetylcholine receptor subunits. These neurotransmitter-related disruptions hinder the effective stimulation required for muscle depolarization, which is crucial for muscle contraction (Kong et al., 2009). Another

factor related to distributed stimulation can be muscle fibre type (Murray et al., 2008). In the *Smn Δ 7* SMA mouse model that fast-twitch myofibers (FaSyn) are more susceptible to nerve connection loss (denervation) compared to slow-twitch fibers (DeSyn) (Murray et al., 2008). Interestingly, the *SMN^{-/-};SMN2* SMA mouse model exhibited both post-synaptic endplate shrinkage and pre-synaptic nerve terminal loss, which occurred independently of each other (Murray et al., 2008). This implies that the post-synaptic changes observed at motor endplates may be part of a more complex pathology that isn't directly a result of pre-synaptic pathology or could even be independent of pre-synaptic issues altogether (Murray et al., 2008).

Studies using primary muscle cells from SMA patients have uncovered myotube fusion defects and differentiation abnormalities, which intriguingly, were linked to a decrease in acetylcholine receptors (AChRs) (Arnold et al., 2004). In the context of postsynaptic development, Z+ agrin, an extracellular matrix protein that aids in the formation and activation of AChR vesicles, has been found to play a significant role in this pathology (Kröger and Pfister, 2009). This was demonstrated in severe and *SMN Δ 7* SMA mouse models, where Z+ agrin's expression levels were notably reduced (Zhang et al., 2013). Offering a glimmer of hope, therapeutic interventions that increase agrin expression have shown promise in enhancing postsynaptic differentiation and improving NMJ defects, particularly in *Smn^{2B/-}* SMA mice (Kaifer et al., 2020). Further expanding on the role of agrin, its regulation through the MuSK receptor tyrosine kinase pathways is of significant importance (Glass and Yancopoulos, 1997). This aspect is especially relevant as *SMN Δ 7* SMA mouse models treated with a MuSK agonist antibody have shown improvements in both innervation and synaptic efficacy, as well as an increase in myofiber numbers (Feng et al., 2021). Thus, within the broader framework of NMJ pathology, both agrin and MuSK are emerging as key factors in its potential improvement. Further emphasizing NMJ dysfunction in SMA, a clinical study involving SMA Type II and type III patients showed repetitive and decremental nerve stimulation compared to control subjects, indicating further impairment of the NMJ (Wadman et al., 2012).

By focusing on these various aspects and models, we can gain a more comprehensive understanding of the complex pathology of SMA, especially as it pertains to NMJ dysfunction.

1.5 SMA Has a Non-Neuromuscular Multicellular Function

Beyond the widely recognized symptoms of muscle atrophy and alpha motor neuron loss in SMA, emerging research is shedding light on a broader scope of issues. These include defects in non-neuromuscular tissues resulting from SMN protein depletion (Poirier et al., 2018). Recent studies in SMA models have demonstrated that SMN protein deficiency leads to developmental issues in various peripheral tissues such as the pancreas (Bowerman et al., 2012), liver (Deguise et al., 2019), adipose tissue (Watson et al., 2021), heart (Palladino et al., 2011) and GI (Sintusek et al., 2016).

To differentiate the effects on the central nervous system (CNS) from those outside of it in SMA, research on SMA mouse models has involved comparing systemic SMN restoration through subcutaneous administration of gene therapy, an antisense oligonucleotide (ASO) that modifies SMN2 pre-mRNA, with CNS-specific SMN restoration achieved by intracerebroventricular ASO administration (Aartsma-Rus, 2017; Passini et al., 2011). Notably, the results showed that subcutaneous SMN administration was significantly more effective, leading to a remarkable 25-fold increase in lifespan (Hua et al., 2011).

This body of research underscores the importance of targeting not just the CNS but also peripheral tissues for effective SMN therapy.

1.5.1 Pancreatic Developmental Defects in SMA

One notable example is the pancreas, a key organ involved in regulating energy balance and glucose homeostasis. In the regulation of glucose metabolism and control of blood sugar levels, the pancreas plays a central role, executing its metabolic and endocrine regulatory functions through its alpha and beta islet cells. Beta islets, by secreting insulin, lower blood sugar levels, while alpha islets release glucagon, a hormone that raises blood sugar, thus creating metabolic balance (Hopcroft, Mason and Scott, 1985).

To delve into the pancreatic changes, immunohistochemical analyses were conducted on the pancreas of the *Smn*^{2B/-} SMA mouse model. These studies specifically assessed the composition and ratio of glucagon-releasing alpha islets to insulin-producing beta islets. The results indicated that SMA mice exhibit a decreased number of beta islets and an increased number of alpha islets

(Bowerman et al., 2012). Notably, these findings were corroborated in human SMA patients, where a similar imbalance between insulin-producing beta islets and glucagon-producing alpha islets was observed (Bowerman et al., 2012).

To further explore whether these pancreatic changes are directly related to the SMN protein, another study re-examined the pancreas in *Smn*^{+/-} mouse models, which are devoid of an overt SMA phenotype, (Bowerman et al., 2014). This subsequent investigation revealed an abnormal composition of both glucagon-producing alpha cells and insulin-releasing α - cells (Bowerman et al., 2014).

Collectively, these studies indicate that the observed pancreatic abnormalities in SMA might develop independent of canonical SMA pathology. Yet, the potential absence of the *SMN1* gene is speculated to make tissues more susceptible to developmental abnormalities, thereby adding another layer of complexity to the disease pathology.

1.5.2 Liver Developmental Defects in SMA

Low levels of SMN protein leads to various systemic pathologies, including those affecting the liver.

In adult human tissue, the liver expresses higher levels of SMN protein compared to some tissues including spinal cord (D. D. Covert et al., 1997). Research on a mouse model with liver-specific deletion of the *Smn* gene has provided significant insights into the pathology of the liver in SMA. This particular model demonstrated notable features such as massive iron overload in the liver and late embryonic lethality, suggesting that the absence of SMN protein impairs the liver's regenerative capacity, leading to liver atrophy (Vitte et al., 2004). Morphologically, when examining the development of the liver in P9 Taiwanese (*Smn*^{+/-} *x* *Smn*^{-/-}; *SMN2*^{tg/tg}) SMA mice, morphological analyses revealed a relative reduction in liver size and a considerably darker colour, which is sign of developmentally immature and congested with blood (Szunyogova et al., 2016). The *Smn*^{2B/-} mice exhibited abnormal features such as paleness, indicative of increased lipid content, which precedes denervation (Deguise et al., 2019). Crucially, in the *Smn*^{2B/-} mouse model, highlights the significant role of the SMN protein in the pathology of SMA, particularly in relation to dyslipidemia and fatty liver diseases (Deguise et al., 2019). These conditions are

particularly noteworthy in pediatric patients. Indeed, liver steatosis has been observed in 37.5% of cases (Schwimmer et al., 2006), and a phenotype indicative of lipid accumulation has been exhibited in 13% of cases (Pacifico et al., 2010), underscoring the increased vulnerability of SMA patients to these liver conditions. Collectively, the evidence of iron and lipid accumulation, along with abnormal morphological indicators, points to a developmental impairment in the liver associated with SMA.

Insulin Growth Factor Binding Protein, Acid Labile Subunit (IGFALS) is primarily produced by the liver. It forms a complex with Insulin-like Growth Factor 1 (IGF1) and Insulin-like Growth Factor Binding Protein 3 (IGFBP3), enhancing the stability and biological life of IGF1 in circulation. A significant reduction in *Igfals* mRNA was observed in the liver of both P1 and P5 Taiwanese SMA mice; furthermore, ASO administration rescued *Igfals* expression, resulting in phenotypic improvement (Hua et al., 2011). Additionally, in Type I SMA patients, the IGF1 receptor and its underlying signaling pathway are disrupted (Millino et al., 2009a). Therefore, the deficiency of *IGF1*, a potent neurotrophic growth factor, has been suggested to contribute to SMA pathogenesis.

Building upon these findings, research on the Taiwanese SMA mouse model focused on the liver's role in erythropoietin and thrombopoietin production during fetal development. These studies revealed that, as an indication of failed liver development in SMA, platelets in these mice aggregate into circulating clot-like accumulations. Additionally, erythropoiesis—the formation of red blood cells—is prolonged, leading to congestion in the liver sinusoids due to the accumulation of erythrocyte precursor cells. This abnormal erythropoiesis alters both the composition and function of blood in the *Smn^{+/-};Smn^{-/-};SMN2^{tg/tg}* mouse model's liver (Szunyogova et al., 2016).

The research underscores the critical role of the SMN protein in liver health, with its deficiency in SMA leading to serious liver pathologies, including atrophy, iron overload, and impaired function. Studies in SMA mouse models reveal liver pathologies such as non-alcoholic fatty liver disease and disrupted erythropoiesis due to SMN protein absence.

1.5.3 Heart Developmental Defects in SMA

In the study of SMA and its impact on cardiovascular health, evidence from both clinical cases and animal models has deepened our understanding of the disease's multi-systemic nature.

Animal models offer crucial insights into the cardiovascular effects of SMA, revealing a range of heart-related issues that manifest before neurological symptoms. For example, severe SMA mouse models showed early onset of cardiac fibrosis, even before neuronal damage could be observed (Shababi et al., 2010). Building on this, subsequent studies using electrocardiogram analysis further discovered signs of cardiac arrhythmia and cardiomyopathy in these models (Heier et al., 2010).

An analysis of pediatric SMA patients, comprising of 37 cases of Type I and 6 of Type II, revealed that 37% experienced right heart ventricular enlargement due to pulmonary hypertension (Distefano et al., 1994). Concurrently, another study examining SMA patients aged between 10 and 79, found myocardial thickening, angina pectoris, and diastolic symptoms following ECG and echocardiographic examinations (Finsterer and Stöllberger, 1999).

To elucidate the ambiguous relationship between SMA and heart diseases, a case study categorized 65 SMA patients based on their *SMN2* copy numbers. Intriguingly, cardiac arterial ventricular septal damage was most frequent in patients with just a single *SMN2* transcript, linking *SMN* gene mutation directly to heart malformations (Rudnik-Schöneborn et al., 2008). Furthermore, congenital heart conditions specific to SMA Type I, such as hypoplastic left heart, were observed (Menke et al., 2008).

In summary, both clinical and pre-clinical studies underline the necessity to consider the cardiovascular system when examining SMA pathology. These findings add another dimension to the understanding of SMA's multi-systemic impact, highlighting the need for treatment approaches that extend beyond targeting the neuromuscular system alone.

1.5.4 SMA Gastrointestinal Dysfunction

According to the 2007 Consensus Statement for Standard of Care in SMA, the initial step in investigating gastrointestinal (GI) defects in SMA patients involves documenting issues such as gastroesophageal reflux and delayed gastric emptying (Wang et al., 2007). This is particularly relevant given that the enteric nervous system, a component of the autonomic nervous system, plays a crucial role in regulating GI functions. The GI system, like the spinal cord, is rich in neurons (Furness, 2000). Additionally, the sedentary lifestyle that many SMA patients lead can exacerbate digestive problems (Yeung and Di Lorenzo, 2012).

Building on this, research using *Smn-KD* mouse models has shown that the loss of *Smn* gene contributes to various GI issues. These include constipation, decreased colonic motility and delayed gastric emptying, all of which occur due to impaired communication between enteric neurons and smooth muscle cells without actual neuron death (Gombash et al., 2015). Notably, treatments involving systemic application of antisense oligonucleotides led to an improvement in GI symptoms. This further supports the notion that GI dysfunction in SMA is linked to *Smn* deficiency, emphasizing the need for therapies that go beyond targeting the central CNS for effective treatment (Sintusek et al., 2016).

Another study by Sintusek et al. found a 65-75% reduction in intestinal blood vessels due to SMN loss. This led to the hypothesis that GI issues could also be a secondary consequence of reduced vascularization, which is linked to low *Smn* levels (Sintusek et al., 2016).

Moreover, a 2018 study connected intestinal damage with systemic inflammation in an SMA mouse model. Through flow cytometric analysis, it was found that elevated levels of pro-cytokines in the intestine triggered inflammation in the bloodstream and liver (Wan et al., 2018).

Research indicates that SMN protein deficiency in SMA leads to gastrointestinal issues due to impaired neuron-muscle communication, exacerbated by patients' sedentary lifestyles. Further studies link these GI dysfunctions to reduced vascularization and systemic inflammation. These insights underscore the need for holistic SMA treatments addressing both central nervous system and gastrointestinal complications.

1.6 Metabolism

As detailed above, it's evident that many peripheral tissues selectively exhibit sensitivity to the SMN protein. The developmental and maintenance defects observed in peripheral organs can easily reflect metabolism, leading to the possibility of multi- metabolic disorders occurring in SMA, either in related or not related to each other. In addition, several studies have shown that reduced SMN protein levels completely associated with certain metabolic processes, including those related to glucose (Bowerman et al., 2012), fatty acid metabolism (Deguise et al., 2021), and circadian rhythms (Lisa M Walter et al., 2018).

These findings suggest a more extensive impact of SMA on overall body physiology and raise questions about whether these effects are organ-specific or occur homogeneously throughout the body.

1.6.1 Glucose metabolism

The pancreas, muscle and liver are the primary peripheral organs responsible for regulating blood glucose levels. The pancreas plays its part by hormonally controlling glucose through the secretion of glucagon and insulin (Nakrani et al., 2023).

Meanwhile, muscle tissue metabolically manages glucose, absorbing up to 80% of it from circulation (Berger et al., 1979). Insulin resistance often arises from muscle tissue losing sensitivity to insulin produced by the pancreas (Minokoshi et al., 2012).

Gluconeogenesis, the process of forming glucose from non-carbohydrate sources, is complemented by the liver's ability to store excess glucose as glycogen (Han et al., 2016). In this context, the pancreas (explained in ‘‘Pancreatic Developmental Defects in SMA ‘‘ section), skeletal muscle and liver serve as pivotal regulators of glucose metabolism circulation. Moreover, adipose tissue can involve indirectly to keep balance in bioenergy due to metabolic crosstalk (Deguise et al., 2021a).

In discussing human cases, a notable example is a 29-year-old male patient with Type II SMA, who was diagnosed with diabetes. This diagnosis was based on elevated blood glucose levels and the presence of beta-hydroxybutyrate and acetone as urinary ketones. The presence of these ketones is indicative of the absence of glucose in tissues, leading to the body using lipids to produce energy

instead of glucose (LaMarca et al., 2013). Further, insulin resistance and urinary ketones were found in 50% of obese pediatric patients with Type II SMA (Davis et al., 2015). Despite having normal glucose levels, 15 out of 35 SMA patients across Types I-III displayed hyperleptinemia, a marker of insulin resistance (Kölbel et al., 2017). In SMA patients, the observed diabetic and glucose resistance symptoms have been studied in detail using the *Smn*^{2B/-} mouse model (Bowerman et al., 2012). This was done by administering an intraperitoneal (IP) glucose tolerance test, which involves an excessive glucose load, to fasting *Smn*^{2B/-} mice. The results of this test revealed that fasting *Smn*^{2B/-} mice had higher blood glucose levels compared to controls, indicating that glucose remained in circulation and was not utilized by the tissues (Bowerman et al., 2012). However, the measurement of fasting blood glucose in SMA Type I patients has not been appropriate due to the pathology of the disease, which includes severely diminished lean body mass and energy reserves (Bowerman et al., 2012).

Thus, various biochemical markers have indicated that glucose metabolism issues are indeed prevalent in SMA patients. These findings highlight the importance of monitoring and managing glucose metabolism in SMA, emphasizing the disease's systemic nature beyond neuromuscular symptoms.

Muscle

In cellular energy production, glucose is the primary fuel and is converted into ATP and NADH through a process known as glycolysis. However, when glucose metabolism is compromised—often due to certain medical conditions—the body can adapt by using alternative substrates like glycerol lactate, and pyruvate to keep the energy production going (Nakrani, Wineland, and Anjum, 2023). Essentially, the body has a fallback mechanism for energy production when glucose is in short supply under glucose metabolism defects.

Transitioning to the specific context of SMA, muscle tissue normally has the capacity to engage in gluconeogenesis using stored biomolecules when blood glucose is unavailable (Jacobsen et al., 1995; Ørngreen et al., 2003). However, the muscle atrophy associated with SMA restricts this ability, leading to reduced gluconeogenesis. This decline may further impair glucose metabolism in SMA patients, potentially causing hypoglycaemia. Supporting this, hypoglycaemia observed in Types I and II SMA patients has been linked to a deficiency in gluconeogenesis (Bowerman et al., 2012a).

Conversely, another hypothesis suggests that muscle tissue, which normally

utilizes about 80% of circulating glucose (da Silva Rosa et al., 2020), may use less due to reduced muscle mass resulting from atrophy. This could lead to increased levels of glucose in circulation, manifesting as hyperglycaemia. Therefore, the complex balance between gluconeogenesis and glucose uptake from circulation due to muscle atrophy in SMA needs to be thoroughly investigated to determine which aspect is more dominant. In the case of SMA, the reduced muscle mass may lead to fewer insulin receptors, resulting in less efficient use of circulating glucose depending on the insulin-insensitive receptors on the skeletal muscle (Turcotte and Fisher, 2008).

Liver

Under normal physiological conditions, when blood glucose levels drop, the body releases glucagon, a hormone that primarily targets the liver. In the liver, glucagon binds to its receptors, activating the cAMP/p-CREB pathway. This leads to increased glucose synthesis in the liver and its release into the bloodstream, thus working to elevate the lowered blood glucose levels (Ramnanan et al., 2011). This process has been investigated in a *Smn*^{+/-} mouse model for better understanding SMA pathology. To assess liver responsiveness to glucagon, researchers measured the levels of phosphorylated-cAMP response element-binding protein (p-CREB), a crucial component in promoting of liver glucagon signaling (Bowerman et al., 2014).

Interestingly, heightened p-CREB levels were noted in the livers of these *Smn*^{+/-} mice (Bowerman et al., 2014). This increase in p-CREB activity implies that hepatic gluconeogenesis is activated, leading to heightened glucose production in the liver.

While the precise underlying mechanisms are still being elucidated, it appears that this increased glucagon sensitivity and subsequent p-CREB activation may be associated with decreased glucose clearance, thus maintaining elevated glucose levels in the bloodstream (Bowerman et al., 2014).

Adipose Tissue

All three types of fat cells—white, beige, and brown—have the shared characteristic of releasing substances, potentially including exosomes, that influence glucose regulation in remote tissues. However, it is worth noting that brown and beige fat cells are proactive in absorbing glucose when stimulated by beta-adrenergic signaling and insulin and they also play a role in increasing energy expenditure (Czech, 2020).

In the context of SMA, it has been proposed that the excessive hyperglucagonemia observed leads to the induction of phosphorylated CREB (p-CREB) activation, which is believed to break down lipids in WAT and subsequently convert them into fatty acids in the liver (Deguise et al., 2021b). Moreover, in the *Smn*^{Δ7/Δ7}; *SMN2*^{+/+} mouse model, an increase in the levels of lipogenic genes in WAT has been observed. Interestingly, this effect can be reversed with exercise (Houdebine et al., 2019a). Another plausible reason for the disruption of metabolism in adipose tissue, which may interact with glucose metabolism through metabolic crosstalk along the pancreas-liver axis, is the observed disruption of circadian rhythm in WAT in the *Smn*^{2B/-} SMA mouse models (Walter, Koch, et al., 2018).

Taking all these into account, it can be hypothesized that due to the SMN protein loss, hyperglucagonemia -induced dysregulation of lipogenesis and circadian genes occurs in WAT tissue.

1.6.2 Fatty Acid Metabolism

Fatty acids serve multiple functions within cells, acting both as sources of energy and as structural components (Wakil and Abu-Elheiga, 2009). They are produced from acetyl-CoA through a complex metabolic process. This begins with the conversion of glucose to pyruvate via glycolysis, which is subsequently funneled into the mitochondria for the Krebs cycle, a process pivotal for generating ATP and other energy molecules (Mao et al., 2006).

In the context of SMA, mouse models have provided deeper insights into fatty acid metabolism, enabling the identification of abnormalities in a comprehensive manner. In the *Smn*^{2B/-} mouse model, researchers first noticed a NAFLD phenotype manifesting before any loss of neurons (Deguise et al., 2019). Significant regulatory changes were identified, including a striking 25-fold increase in triglyceride levels, along with increases in low-density lipoprotein (LDL), very low-density lipoprotein (VLDL), and total cholesterol, which are considered risk factors for hyperlipidaemia and accumulation. Conversely, there was a decrease in high-density lipoprotein (HDL), which is associated with clear cholesterol and preventing accumulation (Deguise et al., 2019). In the muscle tissues of these SMA mice, there was also a noticeable reduction in fatty acid oxidation (Deguise et al., 2019). These abnormalities were confirmed across multiple mouse models, indicating shifts in nine lipid metabolism-specific genes (Deguise et al., 2019). Importantly, these metabolic defects were observed not

just in the liver, but also in muscle, white adipose tissue and the circulatory system.

This focus on lipid metabolism is also supported by findings in SMA patients. One landmark study detected dicarboxylic aciduria, an abnormal condition indicating disrupted lipid metabolism, in the blood tests of SMA patients (Kelley and Sladky, 1986). Another study among paediatric SMA patients found elevated levels of esterified carnitine, essential for fatty acid transport into mitochondria (Tein et al., 1995).

Extending the clinical picture, a detailed study on dyslipidaemia in 72 SMA patients revealed similar trends. Specifically, the paediatric prevalence of LDL was found to be twice the normal rate in their serum (Dathan-Stumpf et al., 2016; Ford et al., 2009). Furthermore, 37% of these patients had at least one indicator of dyslipidaemia, and 20% had at least two (Li et al., 2010). Studies focusing on childhood and adolescent SMA patients have highlighted not just glucose metabolism abnormalities but also a high prevalence of dyslipidaemia, with some patients even exhibiting both hepatic steatosis and glucose metabolism defects (Djordjevic et al., 2021).

Building on this basis, research has shown a link between lipid accumulation in the liver, increased insulin resistance, suggesting an intricate interplay between lipid and glucose metabolism (Mao et al., 2006). In the *Smn*^{2B/-} mouse model, it has been identified that there is an overload of fatty acids coming from the periphery to liver (Deguise et al., 2021b). The causes of this overload fatty acid accumulation could be hyperglucagonemia, breakdown of adipose tissue, and decreased demand from muscle tissue. As a result, there is an accumulation of triglycerides (TG) in the liver, increased oxidative stress, impaired insulin resistance (lowered ability to phosphorylate protein kinase B (Akt)). Moreover, mitochondrial dysfunction and signs of overload in the mitochondria are evidenced by an increase in beta-oxidation, as indicated by elevated levels of reactive ROS and CYP4A, but a decrease in CPT1 (Deguise et al., 2021b).

In summary, the intricate relationship between lipid metabolism and SMA is increasingly clear, highlighting the need for focused metabolic management in all peripheral metabolism for SMA treatment strategies.

1.6.3 Metabolism and Circadian Rhythms

Rhythmicity is an evolutionary trait that is conserved across a broad spectrum of living organisms, from the simplest to the most complex. This rhythmicity operates under the control of a molecular clock situated in the suprachiasmatic nuclei (SCN) of the brain (Mayeux-Louchart, Staels, and Duez, 2015). The molecular clock serves a critical function in the regulation of various physiological processes, including metabolism and energy balance (Dibner, Schibler, and Albrecht, 2010). Recent research has extended our understanding of this system by revealing that, in addition to the central molecular clock in the SCN, each peripheral tissue also has its own self-sustained circadian rhythms. Interestingly, these peripheral clocks have been found to influence each other's rhythmic patterns as well (Yoo et al., 2004).

This rhythmic coordination is controlled by clock genes, specifically *CLOCK* and *BMAL1*. These transcription factors bind to promoter regions of genes essential for circadian rhythm such as *Cry* and *Per* (Menet, Pescatore, and Rosbash, 2014). Importantly, there is a feedback loop between these master regulators and *Cry* and *Per* genes, which can inhibit *CLOCK* and *BMAL1* when overexpressed (Ye et al., 2014). The light-dark cycle orchestrates a rhythm in all physiological processes across various peripheral tissues such as the liver, muscle and pancreas. Specifically, the transcription factor *Klf15*, which maintains metabolic homeostasis in muscle tissues and other peripheral tissues on a diurnal basis, can be considered a biomarker for muscle metabolic and pathological conditions. Observations of diurnal-dependent dysregulation of this factor in SMA mouse models, and the subsequent improvement of SMA mouse phenotypes through the modulation of *Klf15* pathway via GCs, underscore the importance of circadian rhythms and diurnally expressed genes in the pathogenesis of SMA (Lisa M. Walter et al., 2018). To gain a clearer understanding of the relationship between SMA and circadian metabolism, studies have been conducted on *Smn*^{2B/-} SMA mice. These studies found that the *Smn* gene displays a diurnal pattern in both central and peripheral tissues (Lisa M. Walter et al., 2018). Moreover, it was observed that controlled light (CL) treatment alleviated the SMA mouse phenotype.

In human SMA patients, it's clear that the functioning of peripheral tissues under circadian control is compromised. For instance, sleep patterns are disrupted, whereby children with SMA have been found to suffer from nocturnal hypoxemia and hypercapnia (Bersanini et al., 2012). Moreover, SMA Type I patients exhibit extended sleep delays and higher apnea/hypopnea indices (Verrillo et al., 2014).

In conclusion, there's compelling evidence that circadian rhythms play a multifaceted role in the physiology and pathology of SMA. These rhythms not only modulate metabolic processes in affected tissues but may also worsen conditions through a loss of the *Smn* gene, thus underscoring the complexity of SMA and the potential therapeutic avenues that might stem from better understanding these rhythmic patterns.

1.6.4 Amino Acid Metabolism

Branched-Chain Amino Acids (BCAAs), specifically leucine, isoleucine, and valine, are recognized as crucial building blocks for muscle tissue structure (Harper, Miller, and Block, 1984). Initial research on wild-type mouse models indicates that BCAA supplementation can enhance muscle endurance and prolong lifespan by stimulating mitochondrial biogenesis via the activation of the *Sirt1* gene (D'Antona et al., 2010). Importantly, BCAA-dependent mitochondrial biogenesis indirectly supports ATP production, especially in tissues with high energy demands like muscle.

When considering the specific challenges faced by SMA patients, hypoglycaemia is a common issue, as discussed in our earlier section on glucose metabolism. This low blood sugar condition forces the body to utilize amino acids for energy, adding further stress to already weakened muscle tissue (Bruce et al., 1995). Supplementing with BCAAs can mitigate this stress by providing an external source of essential amino acids. In both mouse and human models, BCAAs have been found to enhance mitochondrial biogenesis in skeletal and cardiac muscles. Additionally, they play a role in preventing oxidative damage and boosting physical endurance, particularly in middle-aged mice (D'Antona et al., 2010; Valerio et al., 2011). Based on the these effect of BCAAs on skeletal muscle, administering BCAAs at a dosage of 1.5 mg/kg/day starting from the pre-symptomatic stage (P5) of *Smn*^{-/-}; *SMN2*. Thus, BCAAs lead to significant improvements in both overall weight and lifespan of the mice (Lisa M. Walter et al., 2018). This underlines the potential restorative impact of amino acid metabolism improvement on the SMA phenotype. Promising preliminary results

to have also been documented in children with SMA Type I who were transitioned to a BCAA-based amino acids diet. Importantly, improvements were noted in symptoms like respiratory difficulties and constipation, ameliorating smooth muscle (O'Connor et al., 2023). Looking ahead, further research should aim to identify the specific molecular pathways that could be positively impacted by BCAA supplementation. Such exploratory work could involve utilizing various SMA mouse models for deeper insights.

1.6.5 Mitochondrial Defects in SMA

In SMA, energy regulation is a key issue. Both CNS motor neurons and peripheral skeletal muscles require a high level of energy for proper function. Moreover, evidence of energy-related damage in various peripheral tissues suggests a pathological link between SMA and energy metabolism. One could reasonably speculate that these issues stem from mitochondrial defects, as mitochondria are the primary centers for energy production (James et al., 2021).

Previously, the prevailing thought was that the SMN protein had no location in mitochondria (Acsadi et al., 2009a). Contrary to this traditional view, recent research presents a different perspective. Investigations utilizing the *C. elegans* model for SMA have demonstrated that SMN indeed localizes to mitochondria. This localization is observed in two distinct contexts: transiently under specific cellular conditions and developmental stages, and consistently in proximity to mitochondrial membranes (Schultz et al., 2017; Pagliardini et al., 2000). Furthermore, in the *SMN17* SMA mouse model, mitochondrial morphological abnormalities were observed in motor neuron, including mitochondrial fragmentation, reduced mitochondrial length and mitochondrial swelling (edema) (Miller et al., 2016).

To better elucidate the functional alterations caused by SMA in mitochondria, it's essential to first understand how mitochondria normally operate in energy production. The mitochondria, known as the cell's powerhouse, follow these key steps in their energy-generating process: 1) Electrons are transferred from the electron carriers produced during glycolysis and the Krebs cycle to the electron transport chain (ETC), situated in the mitochondrion's inner membrane (Alberts et al., 2002). 2) Due to the energy derived from these electrons, protons are transported to the outer part of the inner membrane. This movement of electrons plays a critical role in generating a proton gradient across the membrane (Jonckheere et al., 2012) 3) The established proton gradient then activates the

enzyme ATP synthase. This activation leads to the production of ATP, the cell's primary energy currency. The presence and uptake of oxygen is essential for the last step of ATP synthesis (Bertram et al., 2006).

In further investigations, in order to clarify whether there is a specific relationship between mitochondrial defects and SMN protein, the *Smn*-KD NSC-34 cell line was used. These studies revealed that SMN deletion results in increased free radical (ROS) production, leading to mitochondrial oxidative damage (Acsadi et al., 2009). Additionally, there was a noted decrease in mitochondrial membrane potential, which can prevent proton gradient. Additionally, mismatch between energy production (due to reduced mitochondrial ATP synthesis) and energy demand has been observed (Acsadi et al., 2009). Additionally, there was a notable decrease in the basal respiration of *smn* morphant zebrafish, as evidenced by reductions in oxygen consumption rate (OCR) and proton leak (Boyd et al., 2017). Parallel with, reduced oxygen uptake, which in muscle of SMA patients' muscles during exercise is linked to a mitochondrial-based muscle function disorder (Montes et al., 2021). Research on SMA has consistently revealed a pattern of mitochondrial dysfunction. Specifically, studies have identified a reduction in mitochondrial capacity within the spinal cord, which correlates with diminished energy supply (Kirches et al., 1998). This aligns with other research that has reported a significant decrease in mitochondrial DNA levels and compromised activities in the respiratory chain—both in the spinal cord and muscle biopsies from SMA patients (Berger et al., 2003; Ripolone et al., 2015).

In terms of molecular pathway, it's worth noting the role of peroxisome proliferator-activated receptor gamma coactivator 1- α (*PGC1 α*). Studies in post-necrotic mdx mouse skeletal muscle have shown that the upregulation of *PGC1 α* not only augments mitochondrial biomass and calcium ion usability but also enhances the electron transport system (Godin et al., 2012). In symptomatic *Smn*^{2B/-} mice, a decrease in *PGC1- α* levels in muscle tissues has been observed, emphasizing its potential significance as a therapeutic target in mitochondrial in skeletal muscle (Ng, Mikhail and Ljubicic, 2019). Shifting the focus slightly, recent studies have also identified alternative therapeutic strategies. A specific research project found reduced levels of PGK1, a glycolytic enzyme that plays a role in glycolysis, which is linked to the ETC of mitochondria, in the heart muscles and CNS of zebrafish affected by SMA. This opens up the possibility that enhancing PGK1 levels could serve as another mitochondria-targeted treatment

for SMA (Boyd et al., 2017).

The clue of another molecular mechanisms is HuD-mediated transport of mitofusin 2 (Mfn2) transporting in mitochondria (James et al., 2021). HuD is an RNA-binding protein that directly interacts with SMN in hypomorphic *Smn* knockdown MN-1 cell line (Hubers et al., 2011). Besides its role in mRNA transport, the new role of HuD has been defined on mitochondrial dynamics by promoting mitochondrial fusion via Mfn2 (Hong et al., 2020). Mfn2, a protein located on the outer mitochondrial membrane (OMM), is crucial for mitochondrial fusion, particularly in mouse pancreatic β -cells (Hao et al., 2017; James et al., 2021). The detailed investigation of HuD-mediated Mfn2 pathways and their effects on mitochondria in SMA models is important for future studies.

The emerging role of molecular pathways and the potential of novel therapeutic targets underscore the criticality of mitochondrial health in SMA's progression, paving the way for future research and treatment strategies.

1.7 Therapeutic Developments in SMA

There are three gene-based therapies for SMA treatment: nusinersen, onasemnogene, and risdiplam. These treatments are life-changing and life-saving. They achieve this goal either by delivering the *SMN1* gene or by regulating the *SMN2* splicing mechanism. However, these treatments come with disadvantages such as high costs, which limit access for everyone, and reduced therapeutic benefits for older SMA patients.

1.7.1 Smn-dependent Therapies

Nusinersen (Spinraza®)

In 2016, Spinraza made history as the first FDA-approved antisense oligonucleotide for treating children and adults with SMA (Ottesen, 2017). Its primary objective in SMA treatment is to correct the splicing mechanism of *SMN2* by promoting the inclusion of exon 7 into the pre-mRNA transcript, facilitating the production of a functional and stable SMN protein.

Delving into the mechanics of this process, Spinraza accomplishes this correction by targeting the intronic splicing silencer region (ISS-NI) within exon 7 (BORA et al., 2018). It binds to exon 7, preventing the interaction of hnRNP A1/A2, negative splicing regulators, with this region (Singh et al., 2006). Another

crucial aspect of this mechanism involves the activation of the 5' splice region of exon 7 through TIAI, located downstream of ISS-NI (Singh et al., 2015).

In pre-clinical studies, Spinraza has demonstrated excellent tolerance and served as a potent and effective splice-mediated agent, resulting in increased SMN protein levels in model organisms such as transgenic mouse lines and non-human primates (Rigo et al., 2014). In two severe SMA mouse models, CNS-targeted ASO therapy was observed to promote exon 7 exclusion in *SMN2* transcripts. Consequently, higher levels of full-length SMN (FL-SMN) have led to enhancements in muscle and NMJ structures, including larger myofiber sizes, increased motor neuron counts and observed innervated & normal of motor end plates, suggesting that the improvements at these junctions were consistently upheld throughout the observed period. These structural improvements in both muscle and NMJs have translated into functional enhancements, including improved muscle strength and coordination (Berciano et al., 2020; Passini et al., 2011).

Furthermore, during phase 1 studies of Spinraza, involving 28 individuals, the focus was on establishing the safety and efficacy profile of the drug. These studies provided insights into nusinersen's concentration in the blood, along with its corresponding effectiveness and toxicity profiles through pharmacokinetic and pharmacodynamic analyses (Chiriboga et al., 2016). The phase 1 results were consistent with pre-clinical data, affirming that the ASO is well-tolerated and a safe drug (Chiriboga et al., 2016).

In open-label clinical studies involving Type II and Type III SMA patients aged 2 to 14 years, varying concentrations of nusinersen showed a dose-dependent positive effect and the drug was well-tolerated (Chiriboga et al., 2016). During the phase 2 trials, it was observed that 25 children with SMA were able to sit with support and even walk, providing a glimmer of hope for improved quality of life (De Vivo et al., 2019)

Intrathecal the phase 3 study, which administered nusinersen intrathecally to infants with SMA, is demonstrated remarkable improvements in motor functions and an extension of life expectancy (Finkel et al., 2017). On the other hand, Spinraza underwent randomized testing in approximately 121 SMA patients with an average age of around 7 months (Commissioner, 2020). These trials unveiled significant enhancements of motor functions in SMA patients, enabling them to achieve milestones like holding their heads up, sitting, crawling, standing

and walking. However, it is worth noting that a side effect observed during clinical trials was upper respiratory tract infections (De Vivo et al., 2019). The reduced effectiveness of therapy in older SMA patients underscores the critical importance of the therapeutic window in SMA disease. To put it simply, Spinraza treatment is most effective in the early stages when nerve damage remains potentially reversible (Neil and Bisaccia, 2019). Yet another challenge is that Spinraza cannot penetrate the blood-brain barrier when administered systemically (Mercuri et al., 2018).

Consequently, it must be administered intrathecally, limiting its reach to the central nervous system and potentially overlooking peripheral tissue damage in SMA treatment. While this intrathecal delivery method proves effective within the central nervous system, it can be uncomfortable, invasive and carries an increased risk of inflammation (Wurster and Ludolph, 2018). Furthermore, its high-cost places it out of reach for a significant portion of the population (Wurster and Ludolph, 2018).

Onasemnogene Abeparvovec (Zolgensma®)

The blood-brain barrier, which poses a significant challenge in treating neurodegenerative diseases like SMA, has prompted the use of viral vectors to overcome this hurdle. Employing the AAV9 viral vector, the *SMN1* gene can be delivered intravenously, enabling it to reach both the CNS and various peripheral tissues (Foust et al., 2009).

The mechanism of this therapy involves the reintroduction of the *SMN1* gene, responsible for producing FL-SMN protein, using self-complementary adeno-associated viruses. This approach ensures targeted protein expression and distribution, both within the CNS and beyond. Clinical studies have confirmed that intravenous administration of *SMN1*-AAV9 provides sufficient rescue for the disease (Meyer et al., 2015). This gene therapy received FDA approval in 2019.

When assessing the efficacy of recombinant adeno-associated viruses (rAAV), including ssAAV and dsAAV, a notable challenge arises in converting the single-stranded genome into a double-helix structure during transduction, a critical step for accommodating the necessary nucleotides. To tackle this issue, researchers have turned to self-complementary genomes containing inverted repeat sequences. These self-complementary genomes fold during transduction, eliminating the need for DNA synthesis and base pairing, as seen in the gene therapy known as onasemnogene abeparvovec (McCarty, 2008).

In pre-clinical studies involving the *SMN1* mouse model, the re-establishment of the *SMN1* gene using the scAAV9 vector significantly extended

average lifespans, from just 13 days to as long as 199 days. This approach not only prevented motor neuron death but also halted weight loss, demonstrating its potential effectiveness (Dominguez et al., 2011). Furthermore, this treatment prevented the death of neurons and astrocytes while increasing SMN protein levels in peripheral tissues like muscle and liver (Dominguez et al., 2011).

Moving into clinical trials, the administration of gene therapy to 33 SMA Type I patients resulted in the observation of extended lifespans and improvements in muscle physiology milestones (Mendell et al., 2017) ('STRIVE EU Trial Results - SMAUK', 2023). Following this therapy, SMA patients, irrespective of their genetic mutations, gained the ability to stand and walk independently.

Turning the attention to the limitations of this treatment, its side effects arise due to the viral vector used and manifest immunologically. Firstly, it is important to note that the required viral vector dosage is a limiting factor in this therapy. This is because administering the necessary gene therapy dose beyond the age of 12 months in SMA patients may raise concerns related to increased body mass and potential toxicity ('Results Published from STRONG Trial - SMAUK', 2023). Another noteworthy effect is related to the liver. During clinical trials, researchers observed an immunological response and hepatotoxicity linked to the virus capsid carrier. To address this hepatotoxicity, co-administration with prednisolone has been recommended (Chand et al., 2021). Furthermore, it's worth highlighting that the cost of a single course of onasemnogene abeparvovec treatment has been recorded at 19.9 million euros, establishing it as the most expensive drug approved by The National Institute for Health and Care Excellence (NICE) (Nuijten, 2021).

Risdiplam (Evrysdi ©, Roche)

Risdiplam, the first FDA-approved compound offering oral bioavailability for SMA patients aged 2 months and older (Dhillon, 2020), functions by promoting exon 7 inclusion in *SMN2* transcripts during splicing, thus facilitating the production of functional SMN protein (Dhillon, 2020).

This splicing alteration is achieved through three distinct molecular pathways. Firstly, Risdiplam binds to the AG-rich region in exon7 of pre-mRNA

SMN2, inducing a conformational change that creates new functional surfaces for regulatory splicing factors, namely FUBP1/KHSPR, to bind and

ultimately promoting exon 7 inclusion (Wang, Schultz, and Johnson, 2018). Secondly, Risdiplam interacts with the AG-rich region, causing the translocation of hnRNP G and ensuring exon 7 involvement during splicing (Sivaramakrishnan et al., 2017). Lastly, it has been proposed that Risdiplam enhances splicing by restoring the conformation of exon 7's 5' splice site, facilitating accessibility of the U1:C zinc finger and strengthening intron 7-exon 7 connections (Campagne et al., 2019).

In motor neurons derived from SMA patient-derived fibroblasts and SMA Type I-iPSCs, Risdiplam administration promotes exon 7 incorporation into *SMN2* pre-mRNA, resulting in increased levels of functional SMN protein (Ratni et al., 2018).

Even in a severe mouse model, a low dose of 1 mg/kg body weight of Risdiplam administered intraperitoneally robustly enhances SMN protein levels in both the CNS and the periphery (Ratni et al., 2018). Similarly, oral administration of Risdiplam to SMA mouse models significantly increases SMN levels in the periphery (Poirier et al., 2018). In the *SMN Δ 7* mouse model, dose-dependent administration of Risdiplam leads to improvements in NMJ pathology and increased muscle fiber size (Ratni et al., 2018).

Remarkably, 41% of 21 infant SMA patients treated with Risdiplam gained the ability to sit without support, with 81% of them living without the need for a ventilator after a year of use (FDA Press Release, 2020). Clinical studies involving 180 late-onset SMA patients aged 2 to 25 years demonstrated enhanced motor neuroactivity (MDA Conference Abstract, 2023). Notably, the JEWELFISH clinical studies showed that among 45 SMA patients who had previously taken Risdiplam for up to 28.9 months, no adverse effects leading to drug withdrawal were observed, highlighting the safety and tolerability of Risdiplam (MDA Conference Abstract, 2023). As a result, the FDA approved Risdiplam in 2020 (FDA Press Release, 2020).

Despite side effects such as mouth ulcers, joint pain (arthralgia), and diarrhea (Singh, Ottesen, and Singh, 2020), Risdiplam stands as an effective candidate for SMA treatment due to its excellent tolerability, absence of immune responses, oral bioavailability and systemic non-invasive effects.

1.7.2 Smn-Independent Therapies in Clinical Trials

In the treatment of SMA, alongside gene therapies, complementary strategies are necessary to alleviate or correct both the long-term and out-scope of CNS pathologies of the disease. Another reason for this approach is the ineligibility of patients with less severe forms of SMA, such as Type III and IV, for gene therapy, and the presence of candidates with a heterogeneous background that can meet these diverse needs. The text emphasizes the need for a comprehensive approach in SMA treatment that includes both SMN-dependent and SMN-independent strategies, encompassing the central nervous system and the periphery.

Apitegromab (SRK-015)

Myostatin, a member of the TGF β family of growth factors, plays a role in negatively regulating muscle mass by inhibiting satellite cell activity in skeletal muscle (McPherron, Lawler, and Lee, 1997). Inhibiting myostatin has proven successful in increasing muscle mass across various models (Mosher et al., 2007; Schuelke et al., 2004a). Consequently, myostatin inhibition has emerged as a therapeutic target for numerous muscle-related diseases (Lee and McPherron, 2001; Schuelke et al., 2004).

In an SMA mouse model, inhibiting myostatin with follistatin led to improvements in motor function, muscle strength and a 30% increase in life expectancy (Rose et al., 2009). Interestingly, significant changes were observed in motor neurons as well (Rose et al., 2009), indicating that myostatin inhibition is an effective SMN-independent strategy for treating both peripheral and CNS-related aspects of the disease.

However, there is a significant drawback to myostatin inhibition approach. It involves blocking the ActRIIB receptor, which is the receptor for myostatin, with higher affinity to prevent myostatin from binding and triggering the signal cascade (Mendell et al., 2015). This can lead to various side effects because many other growth factors rely on the ActRIIB receptor for signaling (Campbell et al., 2017). Furthermore, the lack of specificity in how this compound targets myostatin is another concern. Due to the high degree of similarity within the TGF family, especially with GDF11, it may lead to unspecific interactions and binding with other growth factors (Lee et al., 2005).

In an effort to address the issue of nonspecific side effects, the SRK-015 molecule was developed by targeting the enzyme involved in the transformation of pro-myostatin into mature, active myostatin (Pirruccello-Straub et al., 2018). As a result, Apitegramab specifically binds to the pro-myostatin form rather than the mature form of myostatin, making it a selective inhibitor of myostatin (Welsh et al., 2021a). Since the pro-domain of myostatin exhibits low similarity to the TGF family, high-specificity antibodies could be produced (Welsh et al., 2021) and the *SMNΔ7* SMA mouse (Kimberly K. Long et al., 2019). These studies demonstrated an increase in muscle mass and strength following treatment with Apitegramab. In preparation for clinical trials involving SMA patients, comprehensive pre-clinical assessments, including the evaluation of pharmacokinetics, pharmacodynamics and toxicity profiles, were performed in cynomolgus monkeys and adult juvenile rats (Welsh et al., 2021b). Results from acute and chronic toxicity analyses, involving a 300 mg/kg/week IV treatment of Apitegramab over 4 weeks and 26 weeks, respectively, indicated that this compound did not exhibit toxic effects and was well-tolerated (Welsh et al., 2021b).

Moving forward, phase 1 studies were conducted in healthy adults using a double-blind, placebo-controlled approach (Barrett et al., 2021). The trial included 58 patients. Over a 12-month treatment period, all patients received apitegromab every four weeks. Notably, 59% of patients showed an increase in HFMSE scores, with 39% achieving a significant 10-point improvement from their baseline, indicating enhanced motor function (*SRK-015 - Therapy for Spinal Muscular Atrophy (SMA)*, 2023).

Apitegramab, has appeared as a novel high-affinity anti-pro-Myostatin monoclonal antibody for treating spinal muscular atrophy SMA.

Moreover, the outcomes of the TOPAZ clinical trial have influenced the design of the upcoming SAPPHERE trial. This trial will explore apitegromab in non-ambulatory patients with Type II and III SMA and is expected to conclude in december 2024 (Clinicaltrials.gov NTC05156320).

GYM329 (RO7204239)

GYM329 is a novel anti-myostatin antibody aimed at promoting skeletal muscle development and strength (Muramatsu et al., 2021). The distinct difference of this compound, GYM329, lies in its ability to specifically bind to the latent form of myostatin, thereby inhibiting its activation. Additionally, through

"sweeping antibody technology," GYM329 effectively reduces or "sweeps away" myostatin in both muscle and plasma (Muramatsu et al., 2021). Currently, the MANATEE study, a global Phase 2/3 trial, is assessing the combined use of GYM329 with risdiplam in ambulant children aged 2-10 years with SMA ('Update on Genentech/Roche Initiation of MANATEE Clinical Study - Cure SMA', December 2023).

Reldesemtiv- (CK-2127107)

Reldesemtiv (CK-2127107) being another promising compound currently undergoing clinical trials. This compound serves as a fast-skeletal muscle troponin activator (FSTA), designed to strengthen muscle contractions and combat muscle weakness fatigue (Gomes, Potter, and Szczesna-Cordary, 2002). Its functional impact on muscle contractions is achieved through its binding to the fast skeletal troponin complex, rendering this complex more sensitive to calcium (Freund, 1983). In the wake of a phase 1 study, it was revealed that CK-107 not only enhances muscle response to nerve stimulation but, notably, it exhibits greater potency than tirasemtiv, achieving the same effect at a lower concentration (Andrews et al., 2018). During phase 2 trials of Reldesemtiv conducted with SMA patients of Types II, III, and IV, assessments included the 6-minute walking test and maximum expiratory pressure, evaluating the compound's impact on muscle function. These evaluations were complemented by an analysis of pharmacokinetic and toxicity data. In addition to the compound's excellent tolerability, significant improvements were observed in both skeletal and posterior muscles compared to placebos (Rudnicki et al., 2021).

Collectively, both pre-clinical and clinical data affirm that targeting skeletal muscle represents a crucial and effective approach in correcting SMA pathology, reaffirming the importance of skeletal muscle-focused therapies for neuromuscular diseases like SMA.

1.8 Drug repurposing

Drug repurposing, also known as drug repositioning, involves identifying new clinical applications for drugs beyond their original medical indications. This approach explores the potential of drugs or compounds, including those that are approved, withdrawn, archived, or in clinical phase studies, to target different diseases (Fetro and Scherman, 2020).

De novo drug development is a costly, risky, and time-consuming process, with an average cost of 2-3 billion US dollars and a duration of 13-15 years. Moreover, the discovery of toxic effects or the ineffectiveness of compounds

developed through this method often leads to low approval rates. In fact, only 10% of compounds in Phase I clinical trials receive approval, while the majority are deemed ineffective or fail due to adverse reactions (Fetro and Scherman, 2020). Furthermore, the cost advantage of drug repositioning becomes evident when pre-clinical and clinical phases I and II are skipped, and the costs of phase III trials are comparable to de novo drug development (Pushpakom et al., 2019). Overall, the drug repositioning approach can reduce costs (Nosengo, 2016). Repositioning drugs offers several advantages over de novo drug development, such as significant time and cost savings, and a higher likelihood of success. These drugs have already been discovered, synthesized, optimized for physicochemical properties, formulated, and undergone phase 1 testing, providing valuable insights into their safety and efficacy profiles. As a result, drug repositioning is increasingly used for both common diseases like cancer, hypertension, and asthma, as well as rare conditions like SMA, leading to the approval of drugs for new indications (Talevi, 2018).

Various computational methodologies, including transcriptomics, molecular docking or AI, can be employed individually or in combination to systematically analyse extensive datasets, providing valuable insights for drug repurposing hypotheses.

SMA treatments, though promising, encounter various limitations (Gidaro and Servais, 2019). To overcome these disadvantages, the drug repurposing approach has emerged as an effective strategy. Additionally, ensuring equitable access to treatments for all SMA patients is crucial. Addressing the issues of cost and accessibility is a vital step towards achieving this objective.

1.9 Aim and Objective

Gene therapies are indeed life-changing and life-saving, but they also come with limitations. The high cost of these therapies can pose accessibility challenges for many individuals. Additionally, the observed reduction in therapeutic benefits among older SMA patients highlights the importance of combination therapies that can complement gene-based treatments. Moreover, to achieve the optimal therapeutic outcome, it's crucial to develop combination treatments that address both the CNS and the peripheral system. This necessity arises from the fact that SMA's pathophysiology involves the SMN protein, which is expressed throughout the body, extending beyond just the neuromuscular system; it serves as a fundamental protein. In other words, numerous non-neuronal tissues are also selectively vulnerable to reduced SMN protein. Considering the wide-ranging pathophysiology of SMA, which involves the SMN protein in various body systems, treatments must target both developmental and functional aspects of peripheral systems for comprehensive disease management, especially addressing the multisystemic nature of SMA (Bowerman et al., 2017). It is essential and urgent to develop alternative therapeutic approaches that specifically target muscle and metabolic functions in SMA. Some of which occur prior to any sign of ND and/or some of them cause extra stress on survival and motor neuron maintenance (J. G. Boyer et al., 2013). The fastest and most successful approach to finding alternative treatments is drug repurposing, which reduces bench-to-bedside time and lowers costs. For this aim we perform transcriptomic analysis, which is one of the drug repurposing methods. To explore the genes expressed differently in the symptomatic skeletal muscle of SMA, we conducted RNA-Seq analysis on the triceps muscle of *Smn*^{-/-}; *SMN2* SMA mice and compared the results with those from their healthy siblings. The DeSeq2 analysis revealed 3,056 genes that were differentially expressed in the SMA mice compared to their untreated peers (Hoolachan et al., 2023a).

Shifting the lens to our transcriptomic research on prednisolone. Since we previously showed that prednisolone, a synthetic glucocorticoid (GC), enhances survival and increases weight pattern in severe *Smn*^{-/-}; *SMN2* and *Smn*^{2B/-} SMA mice (Lisa M. Walter et al., 2018). However, limitation of prolonged use of prednisolone is causing myopathy. Therefore, our aim was to identify the molecular pathways that are affected by prednisolone, with the goal of finding alternative therapeutics that can mimic the short-term effects of prednisolone.

1.9.1 Hypothesis

My hypothesis is that: combining bioinformatic and drug repurposing approaches to identify an alternative therapeutic that mimics prednisolone activity to develop muscle and metabolism targeted therapies for SMA.

1.9.2 Aim

Investigating the therapeutic potential of targeted candidates in molecular, immunohistochemical, and functional terms in both CNS and non-CNS tissues in *In Vivo* and *In Vitro* SMA models

1.9.3 Objectives

- 1- *Validate predicted candidate reporter genes for targeted candidates in SMA patient myoblasts, severe $Smn^{-/-};SMN2$ and milder $Smn^{2B/-}$ SMA mice*
- 2- *Evaluate the pharmacological activities of targeted candidates in both myoblasts and myotubes form of mouse muscle cells (C2C12s) and human muscle cell line (LCHNM2)*
- 3- *Assess therapeutic potential of targeted candidates in SMA animals.*
 - 3.1 *Identify the genes and pathways modulated by targeted candidates in skeletal muscle, spinal cord, liver, white adipose tissue (WAT), brown adipose tissue (BAT) and pancreas of $Smn^{2B/-}$ SMA mice.*
 - 3.2 *Evaluate the histopathological impact of targeted candidates in the spinal cord and skeletal muscle of $Smn^{2B/-}$ SMA mice.*
 - 3.3 *Examine the effects of targeted candidates on survival, weight, and motor function in $Smn^{2B/-}$ SMA mice.*

2 GENERAL METHODS

2.1 In Vivo experiment

2.1.1 Animals

We bred *Smn*^{2B/2B} mice from Charles River with *Smn*^{+/-} mice from Jackson Labs in our animal facility to produce two types of offspring: *Smn*^{2B/-} mice with Spinal Muscular Atrophy (SMA) and *Smn*^{2B/+} healthy littermates.

We originally sourced these mice from two breeding lines:

The *Smn*^{2B/2B} line, which was initially developed by Professor Rashmi Kothary at the University of Ottawa. This line was then transferred to Dr. Lyndsay Murray at the University of Edinburgh, followed by Professor Matthew Wood at the University of Oxford, and finally sent to Charles River for rederivation.

The *Smn*^{+/-} line, identified by stock number 007963, which was obtained from Jackson Labs.

We conducted all experiments involving live animals in the Biomedical Sciences Unit (BSU). Before beginning these experiments, we received the necessary approvals from Keele University's ethics committee and the UK Home Office. We operated under project license P99AB3B95 and personal license I82908187, in compliance with the UK's Animals Scientific Procedures Act of 1986.

2.1.2 Genotyping

To determine the genotypes of *Smn*^{+/-} and *Smn*^{2B/-} mice, we collected ear clips and extracted DNA using the PCR BIO Rapid Extraction PCR Kit from PCR Biosystems. We then prepared a master mix for the PCR reaction, which consisted of 2x PCR BIO Taq Red Mix (containing PCR BIO Taq DNA Polymerase, 6mM MgCl₂, and 2mM dNTPs) and PCR-grade water. To this master mix, we added primers specifically designed for each genotype at a concentration of 500nM, as detailed in the table 2.1.

The PCR protocol for identifying *Smn*^{+/-} and *Smn*^{2B/-} genotypes included these steps: The reaction started with an initial 5-minute denaturation at 94°C. This was followed by 10 cycles of 20 seconds at 94°C, 15 seconds at 65°C (with a 0.5°C decrease in temperature per cycle), and 10 seconds at 68°C. An additional 28 cycles included 15 seconds at 94°C, 15 seconds at 60°C, and 10 seconds at 72°C. The process ended with a 3-minute extension at 72°C, also

using a Techne thermocycler.

Table 2. 1 Genotyping primer sequences

Genotype (Allele)	Forward Primer	Reverse Primer	Size (base pair)
SMN Deletion Mutant KO Single primer pair (Smn-)	GAA CTA GAA GAC AGG TGG AG	GTC TGT CCT AGC TTC CTC ACT G	308

Gel electrophoresis

To analyze the genotypes, we visualized the PCR products for each mouse using gel electrophoresis, specifically with a 10,000X concentration of Gel Red from BIOTIUM. We ran a 1.5% agarose gel at 100 V for 70 minutes on a NanoPac-300p electrophoresis system from Clever Science. After the run, we determined the band sizes and the corresponding genotypes by examining the gel on a ChemiDoc MP Imaging System from BioRad.

2.1.3 Phenotypic Analysis on Live Animals

We conducted daily phenotype analyses by monitoring two key metrics for each mouse: body weight and righting reflex times (capped at a maximum of 30 seconds). If a mouse's weight dropped to less than 80% of its peak body weight, this indicated that the animal had reached a humane endpoint. In such cases, we followed the culling procedures outlined in Schedule 1 and the Home Office Project License (P99AB3B95). In addition to weight monitoring, we assessed the mice's muscle strength and motor function through the righting reflex test. This test measures the time it takes for a mouse, when placed on its back, to turn over

and stand on all four paws again (Hatzipetros et al., 2015). If we observed hindlimb paralysis or immobility in any mouse, we followed the same culling procedures specified in Schedule 1 and the Home Office Project License (P99AB3B95).

2.1.4 Animal Tissue Harvest

We conducted tissue harvesting on P18 or when the SMA mouse models showed symptoms, specifically between 12 PM and 1 PM. Initially, we performed immediate exsanguination to collect blood and measured its glucose level. Following this, we collected various tissues: the triceps muscle, sections of the cervical and thoracic spinal cord, liver, pancreas, and white adipose tissue.

2.1.5 Immunohistochemistry

Laminin Staining

For tissue preparation, we harvested all tibialis anterior (TA) skeletal muscles and fixed them in 4% paraformaldehyde (PFA) overnight. The next day, we replaced the PFA with a 30% sucrose solution. Once the tissues had sunk to the bottom of their tubes, we embedded them in molds filled with a poly freeze solution that also contained 30% sucrose. These samples were then flash-frozen in liquid nitrogen. We used a cryostat machine to cut the frozen samples into 13 μm thick sections.

The slides were then treated with pre-cooled acetone for five minutes, followed by another 30-minute drying phase. To minimize tissue loss, we outlined the tissue area with a PAP PEN. Next, we enhanced the tissue's permeability by incubating the slides in 0.1% Triton-X for 10 minutes at room temperature. We then moved to the blocking stage where the slides were kept at room temperature in a blocking solution (containing 0.3% Triton-X, 10% FBS, and 5% BSA) for two hours. Post-blocking, the slides were incubated with rat anti-laminin primary antibody overnight at 4°C. The following day, we washed the slides thrice in PBS and treated them with Goat-anti-rat IgG 488 secondary antibody for one hour at room temperature. After a final series of PBS washes, we added fluoro-shield with DAPI and affixed a coverslip.

For imaging, we took three photographs of each sample using a fluorescence microscope equipped with a 10x ocular lens. We adjusted light intensity and exposure time for each image to optimize clarity. These images were then saved in the 'tiff' format. In terms of analysis, we used Fiji software to

examine myofiber size in the stained sections.

Oil-red-O Analysis

For tissue preparation, we initially shock-froze the harvested liver tissues from SMA mice and stored them at -80°C. During the preparation phase, these tissues were placed in cryo-molds and filled with a polyfreeze solution that contained 30% glucose. They were then frozen again using liquid nitrogen. Using a cryostat machine, we cut the tissue sections to a thickness of 10 µm. For staining procedure, they were then briefly rinsed with deionized water (ddH₂O). The slides were subsequently incubated in 60% iso-propanol for 2 minutes before treating them with a 0.5% Oil Red O solution for 15 minutes. Following this staining step, we again incubated the slides in 60% iso-propanol for 2 more minutes and then washed them with ddH₂O for 3 minutes. Finally, the slides were mounted using aqueous mounting media containing DAPI. For imaging, 5 photos are taken for each sample with a light microscope (Nikon DS-U2) using a 10x ocular. For each image, the same light intensity and exposure time were maintained.

Nissl spinal cord staining

First, all harvested spinal cord (SC) tissues were fixed in a 4% paraformaldehyde (PFA) solution overnight. The following day, the PFA solution was replaced with a 30% sucrose solution. Afterward, the tissues were positioned in molds filled with a polyfreeze solution that also contained 30% sucrose. These were then rapidly frozen using liquid nitrogen. Sections of the spinal cords were cut to a thickness of 20 µm using a cryostat machine. Upon completing the tissue preparation, outlined with PAP PEN to prevent tissue loss. To rehydrate, the samples were soaked in phosphate-buffered saline (PBS) for 40 minutes. The tissues then underwent a permeabilization step in a 0.1% Triton X solution for 10 minutes. Following three washes in PBS, each lasting 2 minutes, the slides were incubated with Neurotrace 500/525 green, fluorescent Nissl primary antibody (diluted 1:500 in PBS) at room temperature for one hour. After three additional 10-minute washes in PBS, the slides were treated with DAPI and covered with coverslips. They were then briefly stored at -20°C prior to imaging. For the imaging phase, five photographs were taken for each spinal cord sample using a fluorescence microscope. The light intensity and exposure time were individually optimized for each image to capture the most accurate and detailed results. The analysis is conducted in the ventral horn region, which is located between the central canal and the ventral horn. The motor neurons, which are large and

prominent structures, are the main focus within this area. Using the Fiji software, motor neurons are individually counted in each horn area. For each animal, five photographs are taken. The average of these photographs is then used to derive the results for each mouse.

2.2 *In Vitro* Experiment

All cell culture experiments were carried out under Class 2 Biological Safety Cabinet (NUAIRE™).

2.2.1 C2C12s

Murine cell lines were used, C2C12s (Yaffe and Saxel, 1977) (ATCC, USA), which is a murine myoblast cell line originally generated from a thigh muscle of a C3H mouse, the cell line was maintained in growth media, which consisted of high glucose (4.5 g/L) and L-glutamine (0.6 g/L) Dulbecco's Modified Eagle's Media (DMEM) (Lonza), 10% foetal bovine serum (FBS) (Gibco) and 1% Penicillin-Streptomycin (10,000 U/ml) (Lonza). The cells were cultured at 37°C with 5% CO₂ (Heracell 150i CO₂ incubator, ThermoScientific). During passaging, the cell-coated flask, the growth media of which was removed, was washed with PBS (Lonza) and then incubated in the 37°C and 5% CO₂ incubator for 5 minutes with TrpLE-Express Enzyme (Gibco). The detached C2C12s are centrifuged at 500 RMP for 2 minutes to ensure that the cells are collected.

C2C12 cells are managed in two distinct phases: Proliferation and Differentiation. In the proliferation phase, cells are maintained at 60-65% confluency by changing the growth media every two days and are suitable for drug treatment or lysis at a density.

In the differentiation phase, cells at 50-60% density are shifted to a differentiation medium comprising high glucose (4.5% g/2) and L-glutamine (0.6 g/L) DMEM, HS horse serum (HS) (Gibco), 1% Penicillin -Streptomycin (10,000 U/ml) and 0.1% insulin (1 µg/ml) (Sigma). This medium is refreshed every two days up to day 7, with drug treatments typically occurring on day 6 to observe myotube formation on day 7.

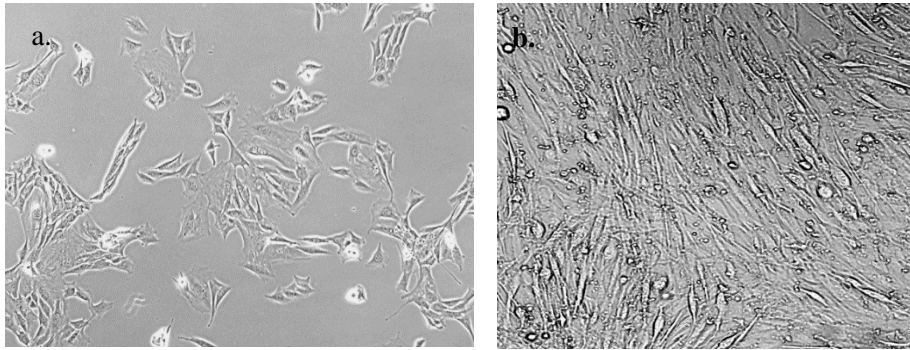


Figure 2.1 C2C12s differentiation process.

a. represents the proliferation, namely the myoblast phase, while b. represents the differentiated myotube phase. As their morphologies differentiate, they elongate and thin out, forming a slender, elongated structure.

Transfection

To investigate the effects of *Smn* gene suppression, we used 10 μM *Smn*-small interfering RNA (siRNA) (also known as miRNASmn1.13.1, IDT). As a negative control, we used a scrambled siRNA (#51-01-19-08, IDT) designed for non-specific suppression. Both the *Smn* and scrambled siRNAs were prepared as lipofectamine complexes using the Lipofectamine® RNAiMAX Reagent from Life Technologies, in accordance with the manufacturer's guidelines. For experiments involving proliferating C2C12 myoblasts with reduced *Smn* levels (*Smn*-KD), the cells were treated with transfection reagents for a 48-hour period. On the other hand, for differentiated C2C12 cells, the transfection was repeated every three days, continuing through the 8th day.

Serum-starvation-induced atrophy model

When cells are serum-starved, they experience nutrient and growth factor deprivation, which mimics the conditions that can lead to muscle atrophy in living organisms. This state triggers a range of cellular processes that are similar to those occurring during muscle wasting conditions in humans, such as those seen in cachexia, sarcopenia, or after prolonged periods of inactivity or bed rest.

For the atrophy protocol, we adapted the methodology from a study by Si

Lei, published in 2019 (Lei et al., 2019). We followed the differentiation protocol up to day 6. On the 6th day, C2C12 cells were subjected to a serum-free medium containing high glucose (4.5 g/L) and L-glutamine (0.6 g/L), along with 1% Penicillin-Streptomycin (10,000 U/ml), for a 24-hour period.

2.2.2 LCHN-M2

LHCN-M2 are a line of human skeletal myoblasts derived from satellite cells from the pectoralis major muscle of a 41-year-old Caucasian male heart transplant donor (Zhu et al., 2007). They are immortalized with lox-hygro-hTERT ("LH"), and Cdk4-neo ("CN") (Zhu et al., 2007).

Gelatinized culture dish protocol

0.1% gelatin solution (ATCC) was dispensed into T-75 flasks (Fisher Sci.) under a Class 2 Biological Safety Cabinet (NUAIRE™). The coated dishes were incubated at 37°C for a minimum of 3 hours. Following incubation, excess gelatin was removed, and the dishes were dried for 30 minutes under a laminar flow hood. The dishes were then sterilized with UV light for 30 minutes. The LCHN-M2 cells were cultivated in a growth medium that has been previously validated by the HudsonAlpha/Caltech ENCODE group, as per their 2011 protocol ('LHCNM2_Wold_protocol.pdf'). This growth medium is a carefully formulated mixture that includes high concentrations of glucose (4.5 g/L) and L-glutamine (0.6 g/L) in Dulbecco's Modified Eagle's Media (DMEM) from Lonza. The media is further enriched with 15% foetal bovine serum (FBS) provided by Gibco, along with a 0.02M hepes buffer by Lonza. Additionally, several other supplements such as 0.03 µg/mL zinc sulphate, 1.4 µg/mL vitamin B12, 0.055 µg/mL dexamethasone (all from Sigma-Aldrich), 2.5ng/mL recombinant hepatocyte growth factor, and 10 ng/mL FGF-2/ basic FGF protein-human recombinant (both from Merck) were included. The media also contained 60 µg/mL Penicillin-Streptomycin (10,000 U/mL) procured from Lonza.

When the focus shifted to the myogenesis differentiation of LCHN-M2 cells, the growth medium was replaced by a differentiation medium, marking this changeover as 'Day Zero'. This differentiation medium is also based on DMEM (Lonza) with high levels of glucose (4.5 g/L) and L-glutamine (0.6 g/L). It includes a 0.02M hepes buffer (Lonza), 0.03 µg/mL zinc sulphate, 1.4 µg/mL vitamin B12, 10 µg/mL insulin, 100 µg/mL apo-transferrin (all from Sigma-Aldrich), and 60 µg/mL of streptomycin- penicillin (Lonza). This medium was refreshed every two days up until the seventh day. If any specific treatment was

planned, it was administered on Day 6, facilitating the study of drug-affected myotube formation in LCHN-M2 cells on Day 7.

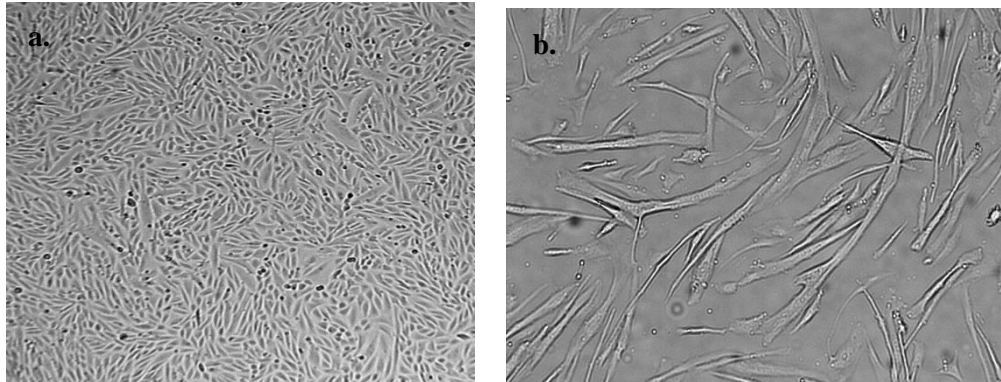


Figure 2.2 LCHN-M2 differentiation process.

a. represents the proliferation, namely the myoblast phase, while b. represents the differentiated myotube phase. As their structures evolve, they become longer and narrower, developing into a slim, extended form.

2.2.3 Deltoid Myoblasts Collected from Type III SMA Patients

Myoblasts are precursor muscle cells that are involved in the growth and repair of skeletal muscle tissue. The deltoid myoblasts specifically come from the deltoid muscle, which is located in the shoulder. The deltoid muscle, located in the shoulder, is relatively easy to access compared to other muscles. This makes the collection of myoblasts less invasive and more practical for both researchers and patients. Biopsies from the deltoid muscle can often be performed with minimal discomfort and risk.

2.3 Assays

2.3.1 Lactate dehydrogenase (LDH)-Glo™ cytotoxicity assay

Cells in either the proliferative or differentiative state were treated with the maximum concentration of the target molecule or an equivalent volume of vehicle for time intervals of 24. Media devoid of cells served as the blank control. Wells containing live cells without any treatment acted as the positive control, while those with cell death induced by Triton X100 served as the negative control. Subsequently the medium was extracted and diluted in a storage buffer composed of 200 mM Tris HCL, 10% glycerol, 1% BSA, and PBS. Assays were conducted

receiving 50 μ L of LDH detection reagent and an equal volume of sample medium (1:1 ratio). Luminescence was measured after a 60-minute incubation using a GloMax Explorer from Promega.

2.3.2 BrdU Cell proliferation assay

To assess the impact of the maximum concentration of the compound and a corresponding volume of the vehicle on cell proliferation, the 5-Bromo-2-deoxyuridine (BrdU) colorimetric system from Merck was employed. Cells were plated with the highest concentration of the drug and an equivalent volume of vehicle for one day during their proliferation phase. A culture medium without cells served as the blank control, while cells without BrdU labeling acted as the positive control. Cells were then subjected to BrdU labeling, followed by exposure to a fluorescently-labeled anti-BrdU antibody. Absorbance levels of BrdU were subsequently recorded at dual wavelengths of 450-600 nm using a GloMax Explorer from Promega.

2.4 Molecular Analyses

2.4.1 Tissue Lysis and RNA isolation

In C2C12 cells was added with 350 μ l of a 1:100 dilution of β -mercaptoethanol (Sigma)/RLT solution and incubated at room temperature. RNA isolation from the resulting cell lysates was carried out using the ISOLATE II RNA Mini Kit (Bioline) according to the manufacturer's instructions.

For LCHN-M2 cells, trizol (SLS) was initially added to the first well, followed by a 5-minute incubation at room temperature. The lysate-trizol mixture was transferred to a second well from the same biological group, and the process was repeated until samples from four wells were pooled. RNA isolation proceeded based on the trizol- plus-columns protocol from Bioline.

Mouse tissues such as spinal cord, triceps, liver, and pancreas were homogenized by adding 350 μ l of a 1:100 dilution of β -mercaptoethanol/RLT solution along with a 7 mm stainless steel ball (Qiagen). For white adipose tissue, Qiazol (Qiagen) was used instead. Mechanical lysis of these tissues was performed for 2 minutes at 60 oscillations/second using the TissueLyser LT (Qiagen), followed by centrifugation at >10,000 RCF (MSE Sanyo Hawk 15/05) for 1 minute. RNA isolation was then conducted using the ISOLATE II RNA Mini Kit (Bioline). For triceps specifically, a mixture of Proteinase K and RNase-

free water (1:60 ratio) was added and incubated at 55°C for 10 minutes, followed by centrifugation at 10,000 g for 3 minutes. RNA isolation began with the supernatant phase.

All samples underwent purity and concentration assessments using a NanoDrop ND 1000 spectrophotometer (Thermo Scientific).

2.4.2 Reverse Transcription (RT)

To synthesize DNA from RNA, reverse transcription (RT) takes place with the enzyme reverse transcriptase. For this reaction, RNA is put into PCR tubes with a maximum concentration of 1000 ng and an exact volume of 15 µl. Then, cDNA mix (mix anchored oligo(dT), random hexamers, 15 mM MgCl₂, 5 mM dNTPs) was prepared in a 4-fold ratio and reverse transcriptase enzyme in a 1-fold ratio, in 5 µl volume per sample (PCR Biosystems). RT reaction is run on the Prime thermal cycler (Techne). Finally, cDNA samples were diluted 1:5 with 80 µl RNase-free water.

2.4.3 Quantitative PCR (qPCR)

The initial product for qPCR per reaction was prepared by adding 200ng cDNA, 1x PCR-BIO Sygreen Blue Mix Hi-ROX (PCR Biosystems), 500nM forward, 500nM reverse primers, and finally up to 50µl RNase-free water. The qPCR reactions were performed in the StepOnePlus™ Real-Time PCR System (ThermoFisher Scientific) with the following programme: initial denaturation at 95oC for 2 minutes followed by 40 cycles of 95oC for 5 seconds and 60oC for 30 seconds and ending with melt curve stage of 95oC for 15 seconds, 60oC for 1 minute and 95oC for 15 seconds. The qPCR data was analysed using the StepOne Software v2.3 (ThermoFisher Scientific) with relative gene expression quantified using the Pfaffl method 673 with *PolJ* (murine) and *POL2RA* (human) housekeeping genes (Table 2.4-5). Primer efficiency for the Pfaffl method was calculated using LinRegPCR V11.0.

Table 2. 2 Primers used for quantitative real-time PCR.

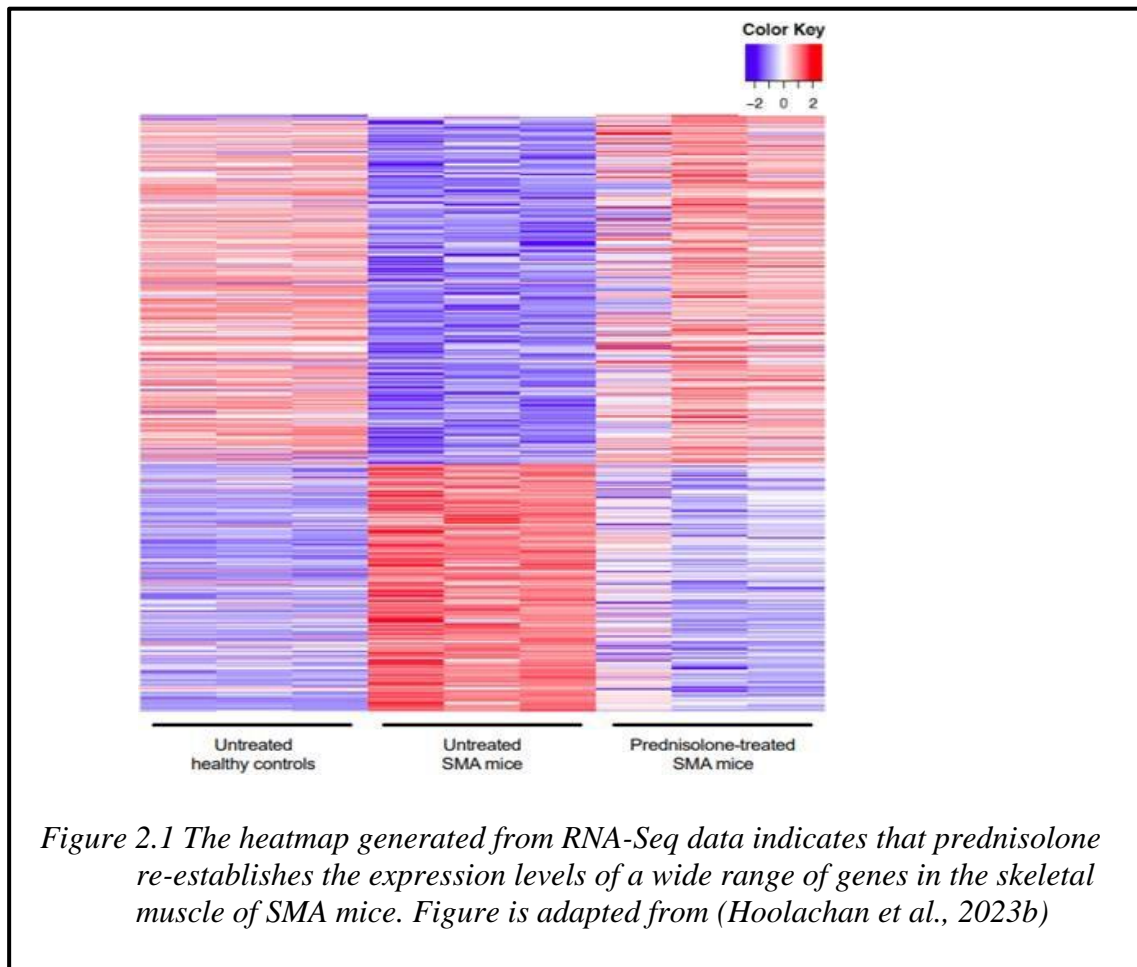
Mouse	Forward (5' – 3')	Reverse(5' – 3')
<i>Igfl1r</i>	AGGAGTGTCCATCAGGCTTCA	CTCGCCGGATGTTAATAAGCA
<i>Rbl1</i>	GTGTAAATTCTGCTGCAAAT	GGTCCAAATGTCGGTCTCTC
<i>Insr</i>	TTCATTCAGGAAGACCTTCGA	AGGCCAGAGATGACAAGTGAC
<i>Sirt1</i>	ACGCTGTGGCAGATTGTTAT	5'-GCAAGGCGAGCATAGATA-3'
<i>Bcl2</i>	CATTGGTACCTGCAGCTTCTTTT	CCCGGTTATCATACCCTGTTCTC
<i>Per1</i>	AGTTCCTGACCAAGCCTCGTTAG	CCTGCCCTCTGCTTGTTCATC
<i>Ror-α</i>	TGCGAGCTCCAGCCGAGGTA	GCCCTTGCAGCCTTCACACGTA
<i>Ppar-α</i>	CCTCAGGGTACCACTACGGAGT	GCCGAATAGTTCGCCGAA
<i>Thbs1</i>	GCCTCTCCTGTGATGAACTATC	CTCTGTTCTCTTCCGTCACTTT
<i>Fas</i>	ATGCACACTCTGCGATGAAG	CAGTGTTACAGCCAGGAGA
<i>P53</i>	GGAAATTTGTATCCCGAGTATCTG	GTCTTCCAGTGTGATGATGGTAA
<i>Pmaip1</i>	5'ATGAGGAGCCCAAGCCCAAC-3'	5'CCATCAACCGGCGGAACTT-3'
<i>Polj</i>	ACCACACTCTGGGGAACATC	CTCGCTGATGAGGTCTGTGA

Table 2. 3 Human primers used for quantitative real-time PCR

Human	Forward (5' – 3')	Reverse (5' – 3')
<i>IGF1R</i>	CGATGTGTGAGAAGACCACCA	ACATTTTCTGGCAGCGGT TT
<i>INSR</i>	TTTGGGAAATCACCAGCTTGGCAGAAC	AAAGCTGGGGTGCAGGTCGTCCTTG
<i>RB1</i>	GACCCAGAAGCCATTGAAATCT	GGTGTGCTGGAAAAGGGTCC
<i>RORA</i>	TCATGGCTGCAAGAAAAGGT	GAGGAAAATGAAGTCGCACAA
<i>BCL2</i>	TTGTGGCCTTCTTTGAGTTCGGTG	GGTGCCGGTTCAGGTA CT CAGTCA
<i>SIRT1</i>	TGACTTCAGGTCAAGGGATGG	GGGAAGTCTACAGCAAGGCG
<i>PER1</i>	CTGCTACAGGCACGTTCAAG	CTCAGGGACCAAGGCTAGTG
<i>THBS1</i>	CAATGCCACAGTTCCTGATG	TGGAGACCAGCCATCGTC
<i>PPARA</i>	CAATGCACTGGA ACTGGATG	TCTTGATGATCTGCACCAGC
<i>POL2AR</i>	CAACGCACACATCCAGAACG	TCCTTGACTCCCTCCACCAC

Result of In-silico Analysis

Subsequent to treating SMA mouse models with prednisolone, we performed transcriptomic analysis on muscle biopsies to discern the gene expression alterations in the muscles of these treated mice (as depicted in figure 2.1)



Following bioinformatics assessments using iPathwayGuide, we identified gene ontology (GO) terms that were statistically significant ($p < 0.05$). These terms pertained to biological processes, molecular functions, and cellular components connected to the metabolism, structure, and function of muscles that had been treated with prednisolone. (Table 2.3).

Table 2. 3 Illustrations of muscle-centric gene ontology (GO) terms linked with differentially expressed genes (DEGs) in SMA mice treated with prednisolone versus those that were not treated.

BIOLOGICAL PROCESSES	MOLECULAR FUNCTIONS	CELLULAR COMPONENTS
Regulation of muscle cell differentiation	Glucose transmembrane transporter activity	Insulin receptor complex
Muscle structure development	Hexose transmembrane transporter activity	Z disc
Regulation of muscle adaptation	MAP kinase phosphatase activity	Voltage-gated potassium channel complex
Regulation of muscle hypertrophy	Insulin receptor substrate binding	Terminal cisterna
Muscle tissue development	Cholesterol transporter activity	Sarcomere

Moreover, we utilized resources like the KEGG DRUG database, iPathwayGuide, and The Drug Gene Interaction Database to compile a list of drugs and pharmacological agents predicted to interact with genes and pathways similar to those affected by prednisolone, as outlined in Table 2.4.

Table 2. 4 Grouping of drug examples predicted to have similarity with prednisolone, according to different databases.

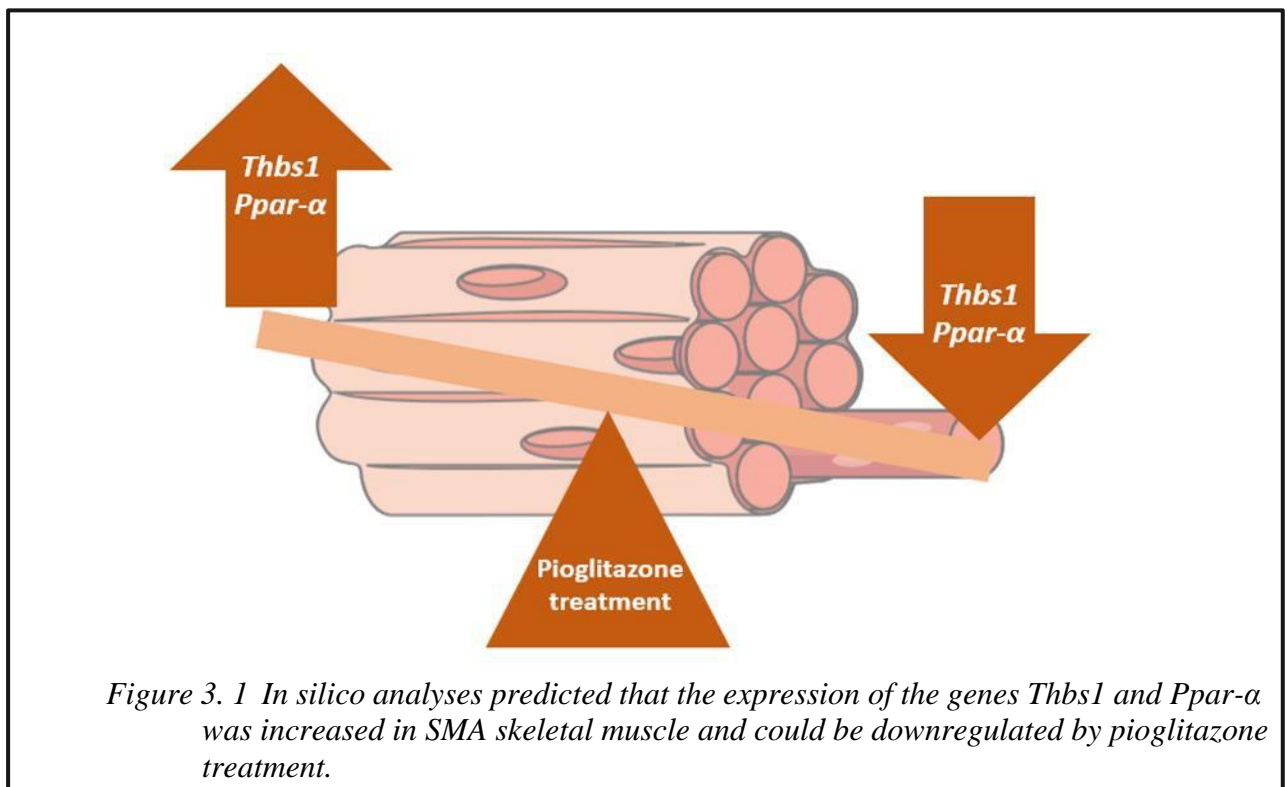
Kegg DRUG Database	iPathwayGuide	The Drug Gene Interaction Database
Buformin	Palm Oil	Celecoxib
Dactolisib	Troglitazone	Dexamethasone
Gedatosilib	Clofibrate	Fasudil
Insulin	Prednisolone	Troglitazone
Pioglitazone	Rosiglitazone	Valproic acid
Melatonin	Valproic acid	Betamethasone
Valproic acid	Dexamethasone	Pioglitazone
Sodium valproate	Fasudil	Insulin
Rosiglitazone	Celecoxib	Prednisolone
Pictilisib	Pioglitazone	Melatonin
Mecasermin	Melatonin	Trichostatin

As a result of combined *in silico* analysis, pioglitazone, melatonin and insulin have been predicted for muscle and metabolic targeted SMA therapy.

3 Pioglitazone

3.1 Introduction

Pioglitazone emerges as a promising therapeutic candidate from combined *in silico* analyses. This compound is predicted to have the potential to correct genes -*Thbs1* and *Ppar-α*- that are dysregulated in SMA. In other words, our findings suggest that Pioglitazone may display activity similar to prednisolone, particularly in the regulatory patterns of the *Thbs1* and *Ppar-α* genes (figure 3.1). Furthermore, the literature has extensively examined pioglitazone's developmental and metabolic effects on various peripheral and central nervous system tissues (Singh et al., 2023). This examination is particularly relevant given SMA's nature as a multi-systemic disease, offering insights into the compound's possible therapeutic impact.



Pioglitazone, classified as a thiazolidinedione, plays a significant role as an anti- hyperglycaemic agent in managing type 2 diabetes, as noted by Al-Majed et al (2016). Its effectiveness primarily lies in diminishing insulin resistance and

facilitating glucose uptake from blood circulation into peripheral tissues (Wilcox, 2005). This process is mediated by the activation of peroxisome proliferator-activated receptors (*PPARs*), as described by Janani and Ranjitha Kumari. These *PPARs* belong to the nuclear hormone receptor (NHR) superfamily and function as ligand-activated transcription factors (d'Angelo et al., 2019). There are three distinct *PPAR* isotypes: *PPAR- α* , *PPAR- δ* , and *PPAR- γ* (d'Angelo et al., 2019). In a nutshell, *PPAR- γ* is primarily expressed in the liver, skeletal muscle, and adipose tissue, where it plays a pivotal role in insulin-dependent glucose uptake (Sakamoto et al., 2000). Considering the presence of fasting hyperglycaemia, hyperglucagonemia and glucose resistance in SMA mouse models (Bowerman et al., 2012a), pioglitazone's potential to counteract the insulin resistance phenotype in SMA is of considerable interest. The simultaneous co-existence of diabetes and non-alcoholic fatty liver disease (NAFLD), marked by an accumulation of lipids in liver and adipose tissue, has led to research into the effects of the antidiabetic drug pioglitazone on lipid metabolism (Kosmalski et al., 2022). Pioglitazone is known for its specific and well-documented.

Initially, the protective role of pioglitazone on pancreas, especially insulin-secreting beta cells has been discovered. This protective role includes increasing the mass of beta cells, boosting their insulin secretion capacity, and safeguarding the existing beta cells, as highlighted in studies by Campbell and Mariz (2007), and Ishida et al. (2004). The action of pioglitazone in enhancing both the functionality and quantity of beta cells is a crucial aspect of its therapeutic effects. This is particularly significant in the context of SMA, where there is a well-documented reduction in beta islets in both human and animal models (Bowerman et al., 2012). On the other hand, *THBS1* might also be involved in hyperglycaemia-induced mitochondrial superoxide production, which affects insulin secretion from pancreatic beta cells. Additionally, some studies, such as those by Wang, Shen, and Kong (2006), suggest that high levels of *THBS1* are associated with the diabetic phenotype and tend to decrease following pioglitazone treatment, thereby alleviating diabetic symptoms. Moreover, the impact of TZD compounds like pioglitazone extends to pancreas, notably through their influence on glucose transport receptors in the periphery, aided by the increased activity of GLUT1 and GLUT4. These transporters are vital for glucose movement in skeletal muscles, the heart, and L6 myocytes, as described by Kim et al. (2000). Additionally, GLUT2, known for its high capacity but low affinity for glucose, plays a role of glucose transporter too. metabolic actions in adipose and liver tissues, including fatty acid

transport, β -oxidation, and storage, as detailed by Peng et al. (2014). Regarding *THBS1*, a glycoprotein in the Thrombospondin family, has been linked to lipid metabolism, as discussed by Gutierrez and Gutierrez (2021). It targets *PPAR- α* , predominantly located in the liver and involves fatty acid breakdown, particularly through the regulation of the β -oxidation enzyme.

Additionally, pioglitazone targets *PPAR- δ* , which is key in activating various polyunsaturated fatty acids, a process outlined by Sakamoto et al. (2000). This aspect is particularly significant in the context of SMA mice, which are known to exhibit reduced β -oxidation capacity, thereby emphasizing the importance of *PPAR- α* in this metabolic process (Deguise et al., 2019). Research on fa/fa Zucker rats and insulin-resistant rhesus monkeys, as documented by de Souza et al. (2001) and Kemnitz et al. (1994), has shown that a 28-day regimen of pioglitazone results in an increase in liver triglycerides and a reduction in hepatic cholesterol. Notably, in the P19 SMA mouse model, levels of triglycerides and total cholesterol were observed to be much higher in the liver compared to control groups (Deguise et al., 2019). This suggests that the impact of pioglitazone on hepatic cholesterol levels in SMA might be a consideration.

Based on results from systematic reviews using data from The Cochrane Central Register of Controlled Trials (CENTRAL), Embase, and Clinical Trials databases, it has been proposed that pioglitazone could significantly improve liver functions and histology. This includes amelioration of steatosis and inflammation (Lian and Fu, 2021). Therefore, pioglitazone is suggested as a primary treatment option for NAFLD, particularly in T2DM patients where FDA-approved pharmacological treatments are currently lacking (Lian and Fu, 2021). The overlap between pioglitazone's therapeutic target of liver steatosis/dyslipidaemia and the SMA phenotype supports further exploration of pioglitazone in subsequent studies.

Ongoing research is exploring the well-established effects of pioglitazone on lipid and glucose metabolism, including its remarkable ability to effectively cross the blood-brain barrier (Alhowail et al., 2022). These studies involve a wide range of neurodegenerative disorders like Alzheimer's, dementia, Parkinson's, and NMD such as ALS due to pioglitazone roles of antioxidant and anti-inflammation (Grommes et al., 2013; Low et al., 2020). The distribution of *PPAR* isotypes within the brain is noteworthy. *PPAR- α* is found across all brain cell types, *PPAR- β* is localized primarily in neurons within gray matter, and *PPAR- γ* is present in astrocytes and microglia. This distribution underscores the potential significance of

PPAR transcription factors in the context of neurodegenerative diseases (Warden et al., 2016).

In the study of SMA, oxidative stress and inflammatory response phenotypes have been observed in microglia, and a direct link with SMN was established through the use of antisense oligonucleotide (SMN-ASO) (Ando et al., 2020). This treatment attenuated phenotypes in SMN Δ 7 model mice and suppressed microglia activation in the spinal cord (Ando et al., 2020). Consequently, there appears to be a suitable match for therapeutic intervention between this SMN-dependent pathology and the effect of pioglitazone, which has been shown to alleviate similar symptoms in other neurodegenerative models.

Studies encompassing both diabetic and healthy individuals have revealed the ability of pioglitazone to enhance mitochondrial DNA and upregulate genes associated with mitochondrial biogenesis in both CNS and periphery (Bogacka et al., 2005). For example, in the NT2 cell line, which serves as a model for human neurons, pioglitazone administration resulted in increased mtDNA content, elevated levels of mtDNA, and higher expression of nuclear-encoded electron transport chain subunit proteins (Ghosh et al., 2007). Additionally, there was an observed increase in oxygen consumption by the neurons. These findings suggest that pioglitazone could be a valuable therapeutic agent in reducing mitochondrial oxidative stress, thereby offering a potential remedy for mitophagy (Ghosh et al., 2007). Further extending its range of beneficial impacts, pioglitazone has demonstrated its ability to strengthen mitochondrial components and functions, offering a safeguard against the impacts of mitochondrial dysfunction and oxidative stress, particularly following CNS injuries (Sauerbeck et al., 2011). The significance of pioglitazone's impact on mitochondria in the context of SMA is particularly relevant due to observed mitochondrial dysfunctions in SMA pathology.

These dysfunctions include disrupted mitochondrial size, altered mitophagy, and variations in the number of mtDNA, all of which are critical aspects of the disease's progression and potential treatment strategies (James et al., 2021). Pioglitazone is employed for its antioxidative effects in conditions such as hypertension, diabetes, and for neuroprotective purposes in neurodegenerative diseases. Oxidative stress caused by ROS released by mitochondria has been shown to reduce SMN protein levels in SMA mouse models (Seo et al., 2016). Additionally, the mitochondrial-targeted compound olesoxime had been included in clinical trials for SMA, highlighting the significance of mitochondrial

biogenesis, oxidative stress, mitophagy, and metabolic functions in improving the SMA phenotype (Pérez and Quintanilla, 2017). Another example can be seen in diabetic mice, where immunohistochemical analysis of oxidative stress markers in pancreatic tissues suggested that pioglitazone reduces these markers, consequently protecting the beta islet cells from damage (Ishida et al., 2004). This suggests that targeting mitochondrial pathways could be a valuable approach in SMA treatment, considering the crucial role these functions play in the disease's progression and management.

The therapeutic targeting of pioglitazone towards liver steatosis/dyslipidaemia, glucose metabolism, pancreas, mitochondrial DNA, and neuroprotective effects, and its join with the SMA phenotype, supports the need for further investigation of pioglitazone in subsequent studies.

3.2 Methods

3.2.1 In vitro pioglitazone treatment

Proliferating C2C12 myoblast cells were plated in 6-well plates (4 wells per group). Once the C2C12 myoblast cells reached 50-60% confluency, and the differentiated C2C12 myotubes were at the D7 stage, they were treated with pioglitazone (Sigma-Aldrich) dissolved in DMSO at concentrations of 50, 100, and 200 micromolar for 24 hours. This procedure was conducted against a control group of DMSO (0.78% v/v). The same concentrations of insulin were also applied to both the 60-70% confluent LHCN-M2 cell line and the D7 LHCN-M2 cells for a duration of 24 hours.

3.2.2 *In vivo* pioglitazone treatment

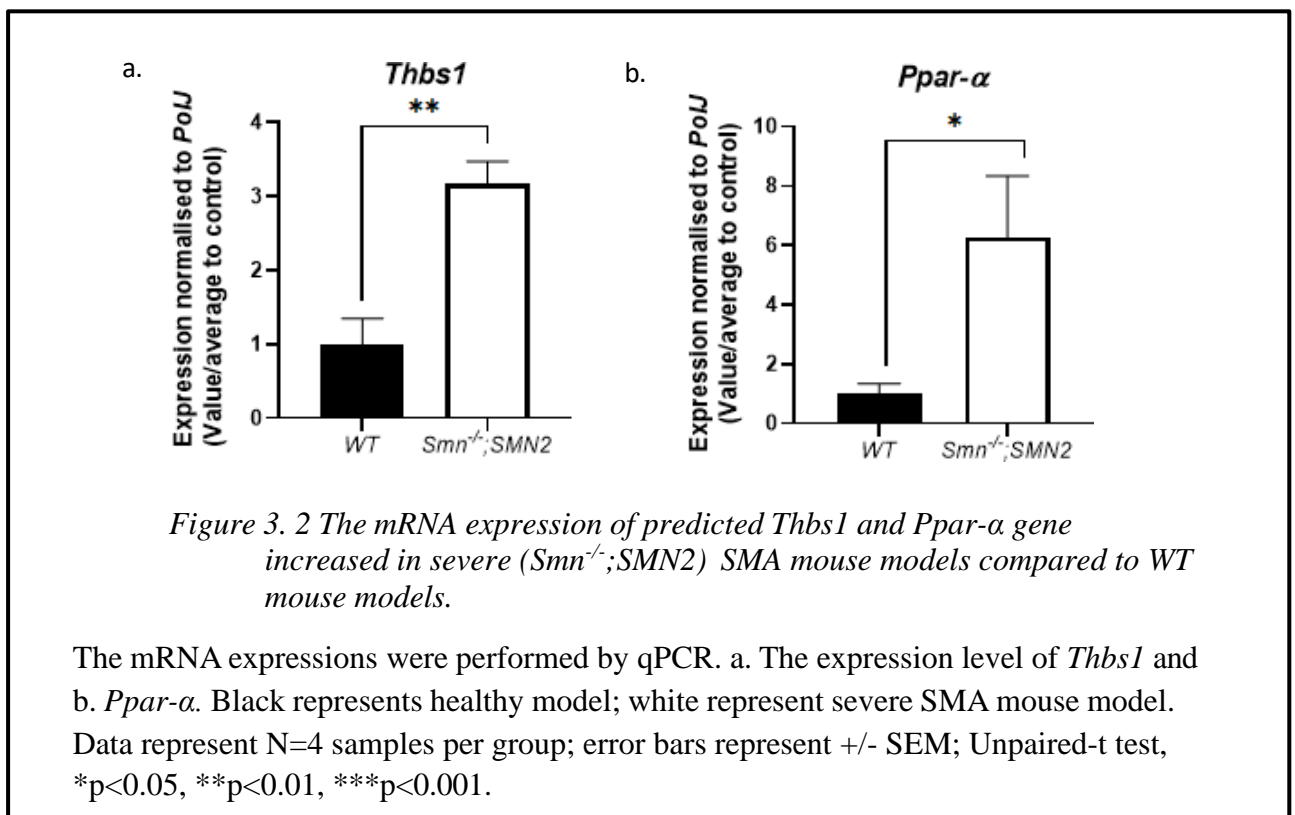
Offspring composed of *Smn*^{2B/-} SMA and *Smn*^{2B/+} healthy mice were phenotypically analysed on a daily basis starting from P0. At P5, the mice were either left untreated, treated with a vehicle (0.5% CMC) or administered pioglitazone (Sigma- Aldrich) at doses of 5, 12.5, and 25 mg/kg per day. The pioglitazone, dissolved in 0.5% CMC, was administered via gavage using a 25 µl syringe (Hamilton) and a 1.25 mm gavage needle (Cadence Science). This procedure continued until the humane endpoint, with more than 10 mice in each group. At P18, skeletal muscles (Triceps brachii and TA), liver, pancreas, white adipose tissue and spinal cord (N > 4) were collected from both untreated and pioglitazone-treated *Smn*^{2B/-} SMA and *Smn*^{2B/+} healthy mice, two hours after the final treatment. Additionally, blood glucose levels (mmol/L) of the non- fasted pups were immediately measured post-euthanasia using the True Metrix Go blood glucose monitoring system (Trividia Health).

3.3 Results

3.3.1 The mRNA expression of *Thbs1* and *Ppar-α* was upregulated in skeletal muscle of symptomatic *Smn*^{-/-};SMN2 mice.

Combined *in silico* analysis has predicted an upregulation of *Thbs1* and *Ppar-α* pathways in symptomatic *Smn*^{-/-};SMN2 mice SMA models, could be downregulated with pioglitazone treatment. In the initial phase of the experiment, we aimed to confirm the expression levels of target genes *Thbs1* and *Ppar-α* in the triceps (skeletal muscle) of symptomatic *Smn*^{-/-};SMN2 SMA mice at P7, using untreated littermates as a comparison group by qPCR. Upon examining the targeted genes for pioglitazone, specifically *Thbs1* and *Ppar-α*, we observed a significant upregulation in the skeletal muscle when compared to WT, as illustrated in figure 3.2.

These validation studies not only corroborate our bioinformatic findings but also reinforce the likelihood that the target genes *Thbs1* and *Ppar-α* may be implicated in muscle pathology.



3.3.2 The mRNA expression of *Thbs1* was increased in skeletal muscle of symptomatic *Smn*^{2B/-} Mice

To further validate our findings, we extended the study to examine the triceps skeletal muscle in *Smn*^{2B/-} at P18. This was considered important because both severe and milder forms of SMA mouse models show pathological defects in muscle.

Upon comparison with untreated littermates, we found an increased expression of *Thbs1* in the triceps of the milder SMA model. However, there was no notable change in the mRNA levels of the predicted target gene *Ppar-α* in these milder SMA models, as shown in figure 3.3. This led us to observe that the expression of *Ppar-α* might be influenced by the severity of the SMA condition. Given that the targeted gene *Ppar-α* showed an increased pattern in the severe SMA mouse model (as illustrated in figure 3.2), whereas no change was observed in the milder form of the SMA mouse model (refer to figure 3.3), this suggests a distinct response in different SMA severity levels.

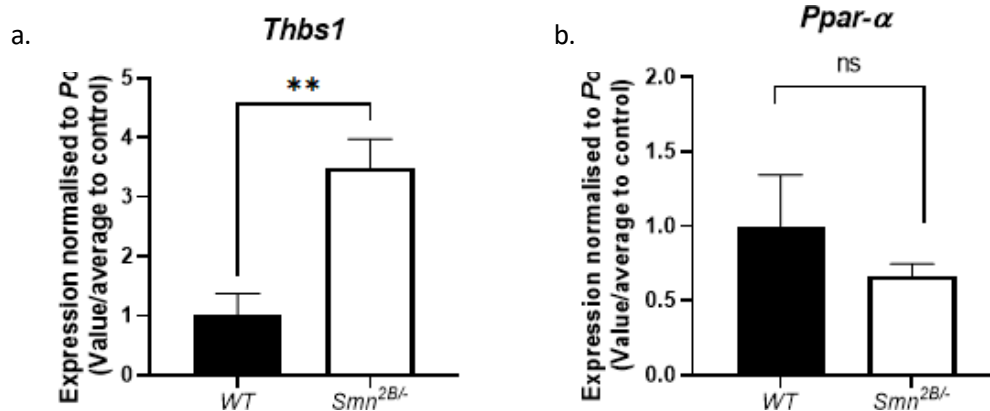


Figure 3. 3 The validation study is about predicted candidate genes by restored pioglitazone treatment, *Tsbh1* and *Ppar-α*, in In-Vivo model. The mRNA expression of predicted *Thbs1* and *Ppar-α* gene increased in milder form (*Smn*^{2B/-}) of SMA mouse models compared to WT mouse models.

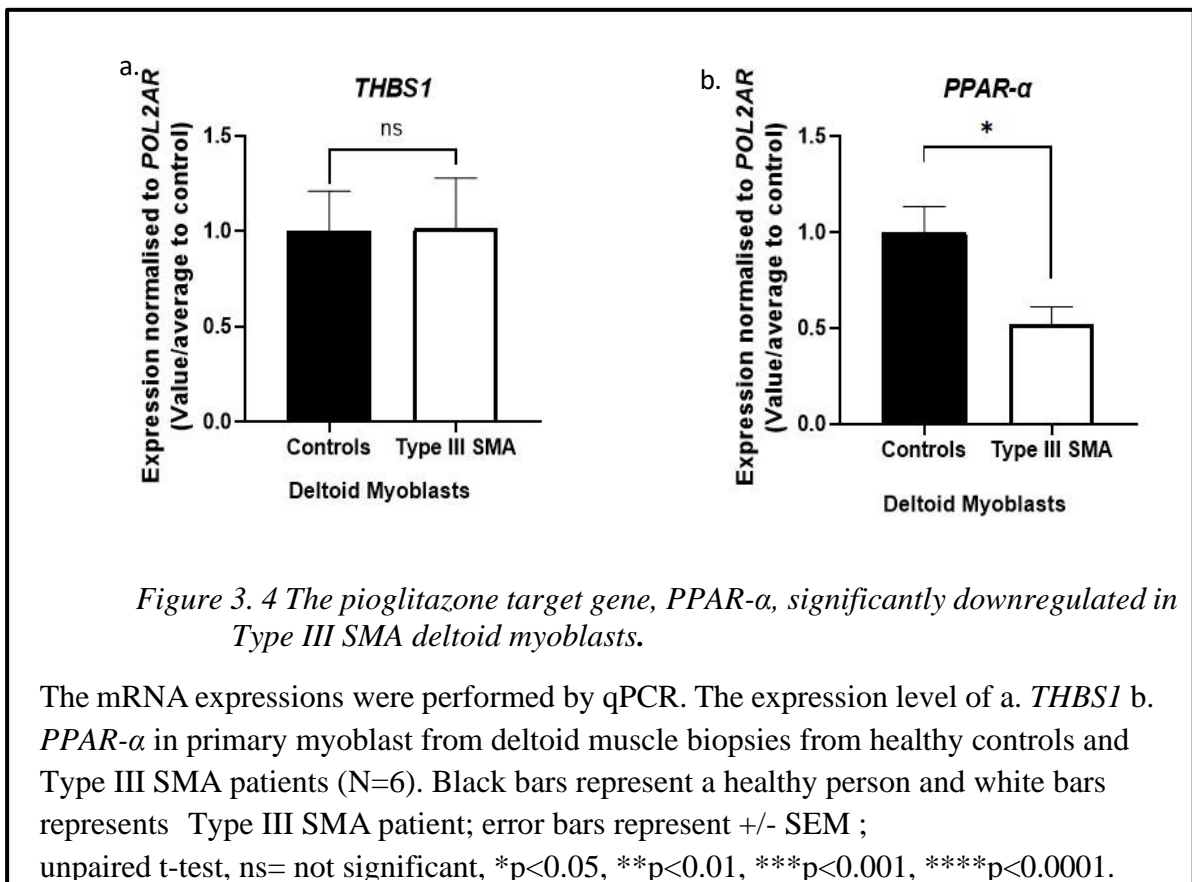
The mRNA expressions were performed by qPCR. a. The mRNA level of *Thbs1* and b. *Ppar-α* are forecasted target gene to be recovery of pioglitazone treatment in milder SMA mouse model (a,b). Black represents healthy model; white represent severe SMA

mouse model. Data represent N=4 samples per group; error bars represent +/- SEM; Unpaired-t test, ns= not significant, *p<0.05, **p<0.01, ***p<0.001, ****p<0.0001.

3.3.3 The predicted targeted gene, *PPAR-α*, was downregulated in Type III SMA deltoid myoblasts.

In our subsequent phase of research, we aimed to explore if the genes we identified as potential targets of pioglitazone—namely *THBS1* and *PPAR-α*—exhibit altered expression in samples from SMA patients. For this purpose, we collaborated with Dr. Stephanie Duguez and utilized primary myoblasts obtained from deltoid biopsies from both healthy controls and Type III SMA patients.

Interestingly, our findings showed a decrease in *PPAR-α* expression levels in Type III SMA myoblasts when compared to healthy controls (fig 3.4.). This trend is notably different from what we observed in the severe SMA mouse model, where *PPAR-α* levels were increased. Additionally, we did not observe any statistically significant differences in the mRNA levels of *THBS1* in Type III SMA deltoid myoblasts, compared to healthy controls (fig 3.4.).



3.3.4 The mRNA expression of predicted *Thbs1* gene was decreased in differentiated *Smn*-KD C2C12s model.

In our combined in silico studies, we validated the dysregulation of predicted target genes in both the SMA mouse model and Type III SMA patients. To further understand whether these changes in gene expression are dependent on the *Smn* gene, we conducted experiments on models with the *Smn*-KD.

To tackle this question, we used *siRNA*-mediated transfection to reduce expression of the *Smn* gene in immortalized murine C2C12s myoblast-like cells. This experimental model allowed us to examine not just whether the dysregulation of these target genes is due to *Smn*, but also how *Smn* deficiency specifically impacts muscle, independent of any nerve degeneration. Since this approach helps to isolate muscle-specific effects from the complex interplay between muscle and nerve tissues.

We carried out the *Smn* gene deletion during two distinct phases of muscle development. First proliferating C2C12s cells, representing the myoblast stage, were exposed to *Smn*-specific *siRNA* for two days (figure 3.5.a). Additionally, differentiated C2C12s cells, representing the myotube stage, were also treated with *Smn*-specific *siRNA* for six days (figure 3.5.b). For the purpose of control, un-transfected C2C12s cells are represented by black bars. To indicate non-specific transfections, we included cells treated with scrambled-RNA, represented by white bars. Finally, for C2C12s cells in which the *Smn* gene was specifically knocked down, grey bars (*Smn*-*siRNA*) were used. Our results revealed that the only significant *Smn*-dependent change was observed in the myotube cells at day 7 (D7), where there was a significant decrease in *Thbs1* expression. Thus, it appears that *Smn* deficiency in D7 C2C12s myotubes contributes to the dysregulation of the *Thbs1* gene.

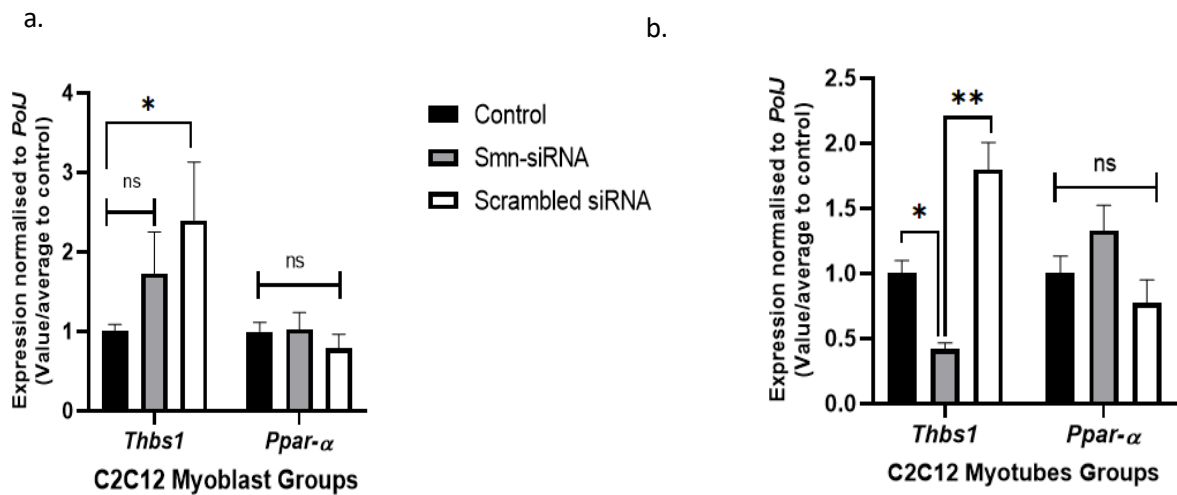


Figure 3. 5 The mRNA expression of predicted *Thbs1* gene is decreased without *Smn* gene in D7 *Smn*-KD C2C12s model.

The mRNA expressions were performed by qPCR. a. The expression level of *Thbs1* and *Ppar-α* in *Smn*-KD myoblast form of C2C12s b. The pattern of target genes show in D7 *Smn*-depleted C2C12S. Black represent positive control, grey represent *Smn*-KD form of C2C12s, white show scrambled-SiRNA in C2C12s. Data represent N=4 samples per group across two-independent experiments; error bars represent +/- SEM; Two-way ANOVA with post-hoc uncorrected Fishers LSD test, ns=not significant, *p<0.05, **p<0.01, ***p<0.001, ****p<0.0001.

3.3.5 There was no significant change in pioglitazone targeted genes observed in the atrophy-induced D8 C212s.

One of the defining characteristics of the SMA disease phenotype is muscle atrophy and weakness. To closely examine the relationship between pioglitazone target genes and this atrophic phenotype, we employed a serum-starvation-induced atrophy model in differentiated C2C12s cells. The central research question in this context is whether atrophy is related to the observed dysregulations in the predicted target genes that we have previously confirmed.

In order to generate a model of serum-deprived C2C12s myotubes, cells were differentiated for up to 7 days and then subjected to 24 hours of starvation in serum-free high glucose DMEM. In the comparison of target gene expression levels between the atrophy-induced C2C12s cells (figure 3.6 / represented by white bars) and the control group (figure 3.6 / indicated by black bars). In

conclusion, no alterations in the genes targeted by pioglitazone were noted in the D8 C2C12s that underwent atrophy induction.

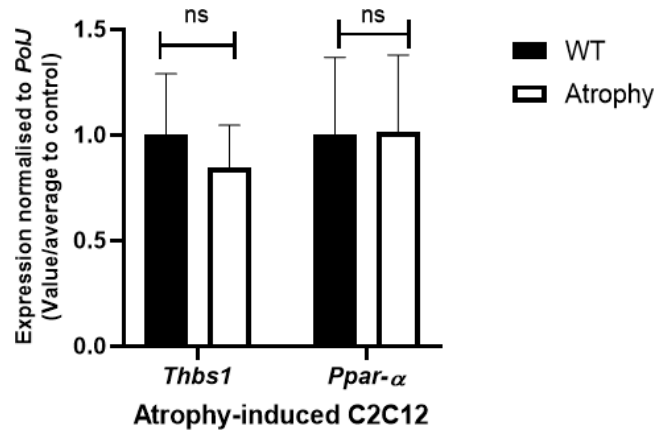


Figure 3. 6 Canonical atrophy does not lead to any changes in the level of pioglitazone targeted genes in the serum-starvation-induced atrophy C2C12s.

The mRNA expressions were performed by qPCR. a. The target genes levels are in atrophy induced C2C12s. Black represents positive control, white shows serum-starvation-induced atrophy C2C12s model. Data represent N=4 samples per group across two-independent experiments; error bars represent +/- SEM; Two-way ANOVA with post-hoc uncorrected Fishers LSD test, ns=not significant. *p<0.05, **p<0.01, ***p<0.001, ****p<0.0001.

3.3.6 Pioglitazone had dose- and differentiation state-dependent effects on the expression of *Thbs1* and *Ppar-α* genes in C2C12s.

In the subsequent stage of our research, our objective is to explore how pioglitazone impacts the expression of *Thbs1* and *Ppar-α* genes in muscle cells. Building upon previous research that showed increased insulin sensitization in C2C12s cells after a 24-hour treatment with 50 μM pioglitazone (Verma, Singh, and Dey, 2004), we chose 50 μM as our starting dose. Initially, we treated proliferating C2C12s cells with varying concentrations of pioglitazone—50 μM (white bars), 100 μM (dark grey bars), and 200 μM (light grey bars)—over a 24-hour period. Notably, we observed a reduction in the expression of the candidate target gene *Thbs1* (the left side) in myoblasts following the 200 μM pioglitazone treatment (figure 3.7.a.). Subsequently, these same pioglitazone concentrations were applied to differentiated C2C12 cells (also

known as D7 myotubes) over an identical incubation period. The outcome was quite revealing; the expression level of *Thbs1* (the left side) notably increased when treated with 50 μ M of pioglitazone (figure 3.7.b.). Thus, the influence of pioglitazone on the expression of *Thbs1* and *Ppar- α* genes in C2C12s varies based on the dosage and the stage of muscle growth stage.

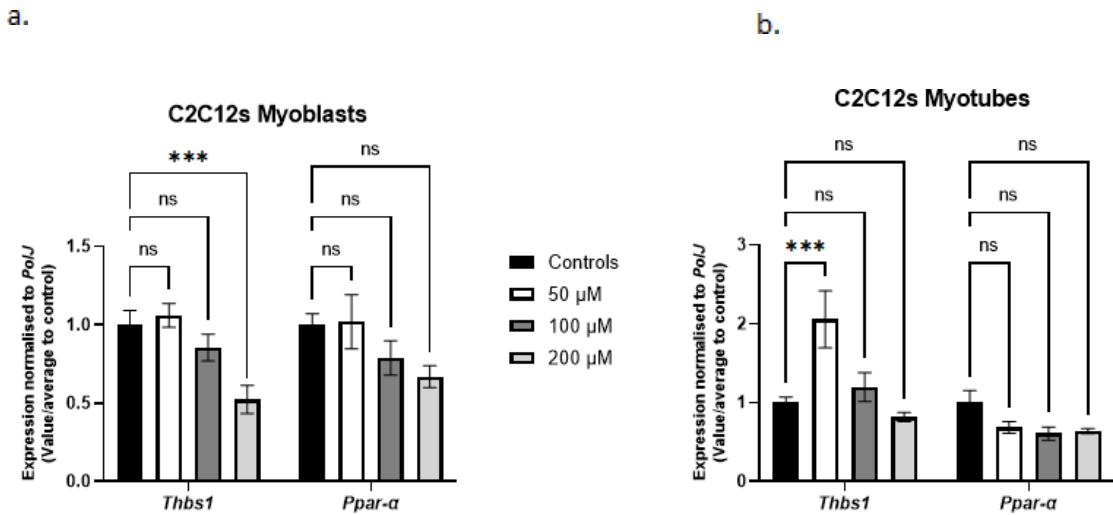


Figure 3. 7 After 200 μ M pioglitazone treatment, a decrease was observed in the predicted candidate *Thbs1* target gene in myoblasts. However, for the same target genes, there is an increase in 50 μ M pioglitazone treatment on C2C12 myotubes.

The mRNA expression of pioglitazone target genes *Thbs1* and *Ppar- α* were performed via qPCR. a. myoblast and b. myotubes form of C2C12s were treated for 24-hours by 50 μ M (white), 100 μ M (dark grey) and 200 μ M (light grey) and without any treatment/control (black). Data represent N=4 samples per group across two-independent experiments; error bars represent +/- SEM; Two-way ANOVA with post-hoc uncorrected Fishers LSD test, ns= not significant, *p<0.05, **p<0.01, ***p<0.001, ****p<0.0001.

3.3.7 Pioglitazone had a toxicity on C2C12s but it caused a negative effect on proliferation of C2C12s.

For our next line of inquiry, we explored whether pioglitazone affects the proliferation of C2C12s cells via BrdU labelling.

In the accompanying graph, the blank (black bar) represents the media components without cells, while the background (medium grey) represents the cell environment without BrdU labelling (figure 3.8.a.) The control, which represents cells labelled with BrdU, is indicated by white bar (figure 3.8.a.). Cells treated with the highest dose of pioglitazone are indicated by light grey bars, and the corresponding an equal volume of vehicle control (DMSO) is depicted in dark grey (figure 3.8.a.).

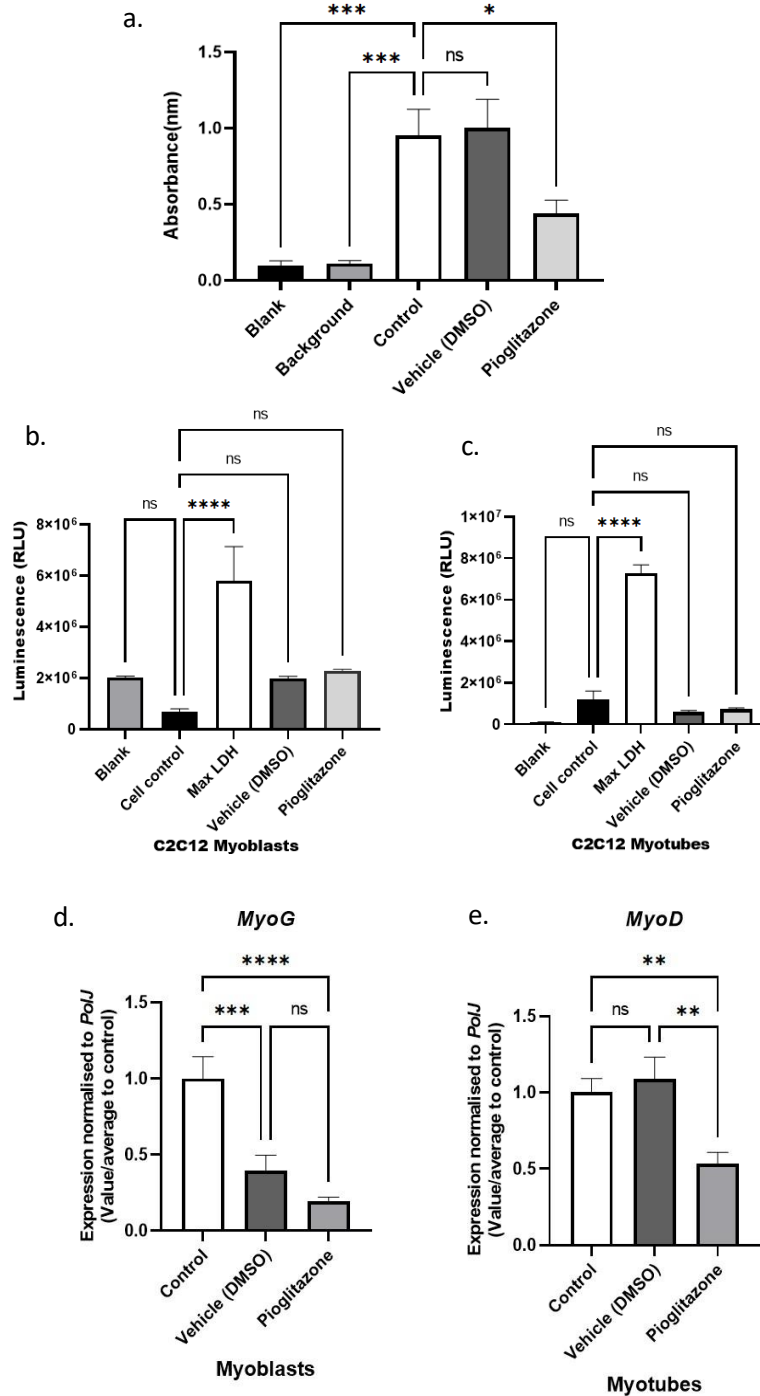


Figure 3. 8 Highest concentration of pioglitazone (200 μ M) has a negative effect on myoblast proliferation during 24H treatments, although it has no toxicity.

We measured the absorbance at various wavelengths (nm) under different conditions: blank (media only), background (cell presence), and C2C12 myoblasts was added with either an anti-BrDU antibody, vehicle (DMSO), or 200 μ M pioglitazone for 24 hours. The results of the BrDU assay are presented in panel a. For the toxicity, LDH assay was performed. Absorbance is readed from lactate dehydrogenase (LDH) level in cell

culture supernatant from b. proliferating C2C12s and c. differentiated C2C12s. Black is untreated, white is negative control (1% Triton-X), dark grey is vehicle (DMSO) control and light grey represent 200 μ M pioglitazone treatment. While *MyoD* expression levels are shown in panel 'd,' and *MyoG* levels are depicted in panel 'e.' Data were obtained from four samples per group, spanning two independent experiments. Error bars represent the standard error of the mean (SEM). Statistical analysis was performed using one-way ANOVA, followed by Dunnett's post-hoc test. Notations for statistical significance are as follows: ns = not significant, * $p < 0.05$, ** $p < 0.01$, *** $p < 0.001$, **** $p < 0.0001$.

According to the results of the BrdU assay, the negative impact of pioglitazone on the growth phase of myoblasts was evident from a significant decrease in absorbance values, which correlate with cell count, when compared to between the control group and pioglitazone treated group.

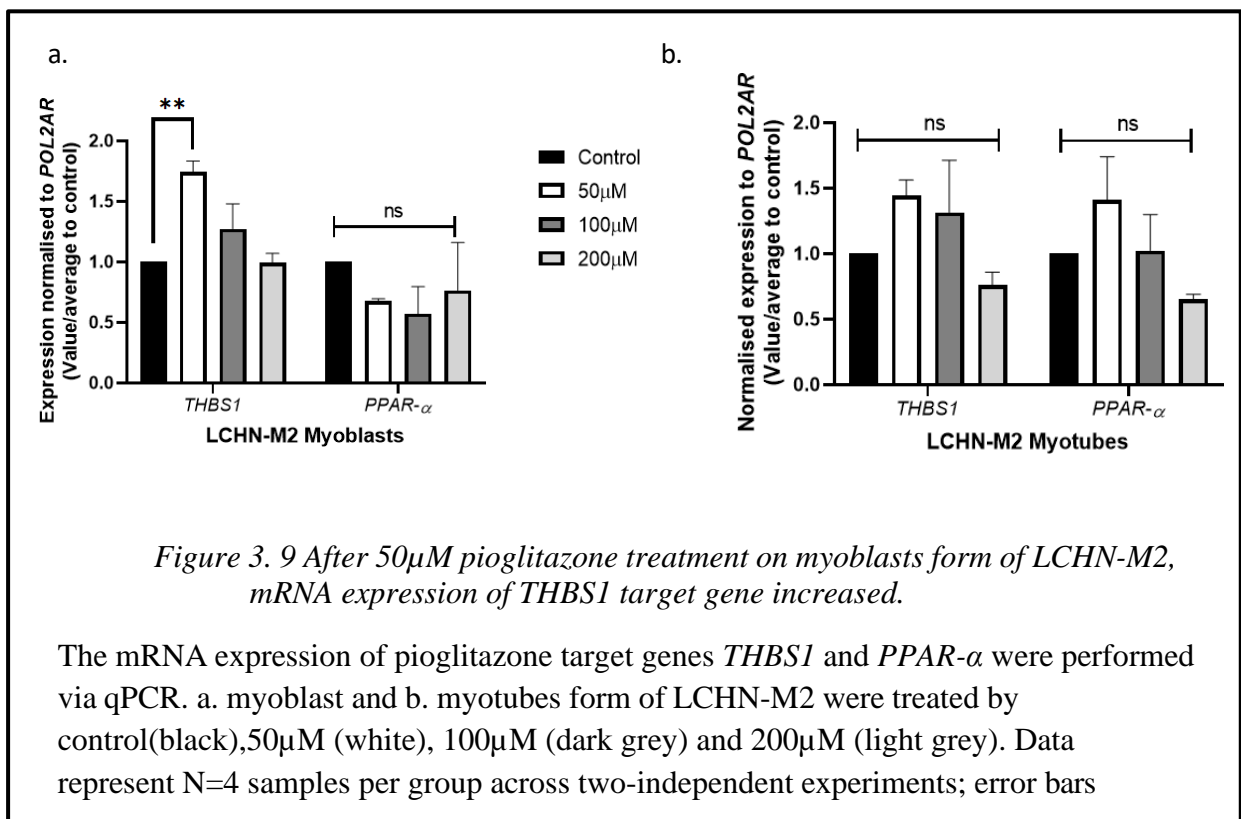
To determine whether decrease in proliferation is associated with toxicity, an LDH assay was conducted to investigate the toxicity of pioglitazone on the myoblast phases (as shown in Figure 3.9.b) as well as myotubes form (figure 3.8.c). We employed various controls for LDH assay: the background control measures the signal originating solely from reagents, without any cells; the cell control serves as a baseline, showing the amount of LDH from healthy cells (represented by the black bar); and the negative control (white bar) is established by killing most cells through the addition of 0.1% Triton-X. Additionally, we used a vehicle control (dark grey bar) and examined the effects of the highest concentration of pioglitazone (light grey bar). Our findings indicate that neither the highest concentration of pioglitazone nor an equal volume of vehicle (DMSO) exhibited toxicity in either the D0 or D7 C2C12s cells. Given the absence of observed toxicity, the question arises whether pioglitazone might be promoting cellular differentiation instead of proliferation. To investigate this, we assessed the expression levels of two key transcription factors critical to muscle biogenesis: *MyoD*, which plays a crucial role in myoblast differentiation, and *MyoG*, which is active in the final stages of muscle cell differentiation. The expression level of *MyoD* (figure 3.8.d.) and *MyoG* (figure 3.8.e.) decreased following the highest concentration of pioglitazone (shown as light grey bars) treatment. Considering the outcomes of all these assays, it appears that pioglitazone does not induce differentiation. Rather, the negative impact on cell proliferation observed might be linked to the use of

DMSO. This association is suggested by the decreased levels of *MyoD* and *MyoG*, which seem to depend on the application of DMSO.

3.3.8 The treatment of the human muscle cell line with 50 μM pioglitazone induced an increase in the level of *THBS1* mRNA.

Another research focus aims to investigate the impact of pioglitazone on the expression of the *THBS1* and *PPAR- α* genes in human muscle cells. Initially, we exposed proliferating LCHN-M2 cells to various concentrations of pioglitazone for a period of 24 hours. These concentrations included 50 μM (represented by white bars), 100 μM (dark grey bars), and 200 μM (light grey bars). Notably, we observed an increase in the expression level of the target gene *THBS1* in myoblasts following the treatment with 50 μM pioglitazone (as shown in figure 3.9.a.).

Subsequently, the same concentrations of pioglitazone were applied to differentiated LCHN-M2 cells, also known as D7 myotubes, over the same incubation period. As a result, no change was observed in the expression levels of the target genes in the differentiated human muscle cells following the pioglitazone treatment (as shown in figure 3.9.b.).



represent +/- SEM; Two-way ANOVA with post-hoc uncorrected Fishers LSD test, * $p < 0.05$ ** $p < 0.01$ *** $p < 0.001$ **** $p < 0.0001$.

3.3.9 There was no negative impact of pioglitazone treatment on proliferation of LCHN-M2.

In the next phase of our research, we aimed to determine the impact of pioglitazone on the proliferation of LCHN-M2 cells. To achieve this, we conducted a comparative analysis between LCHN-M2 cells treated with pioglitazone and those that were not, utilizing the BrdU labelling method. The results are depicted in the accompanying graph (figure 3.10.a.), which includes: a control group of BrdU-labelled, untreated proliferating LCHN-M2 cells (represented by white bars); a vehicle control group with an equal volume of solvent (depicted by dark grey bars); and a group of cells treated with the highest dose of pioglitazone (illustrated with light grey bars). The data from this analysis indicates that pioglitazone does not adversely affect the proliferation of LCHN-M2 cells, suggesting that the drug may not hinder cell growth under these specific conditions.

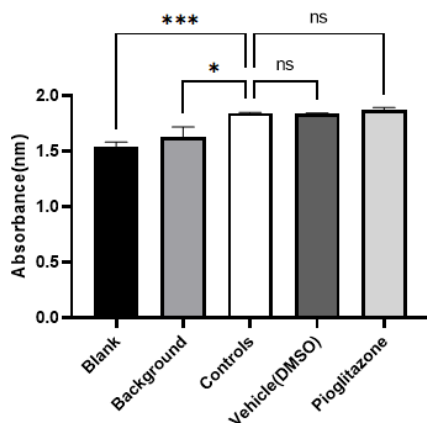


Figure 3. 10 Highest concentration of pioglitazone has no negative effect on myoblast proliferation during 24H treatments.

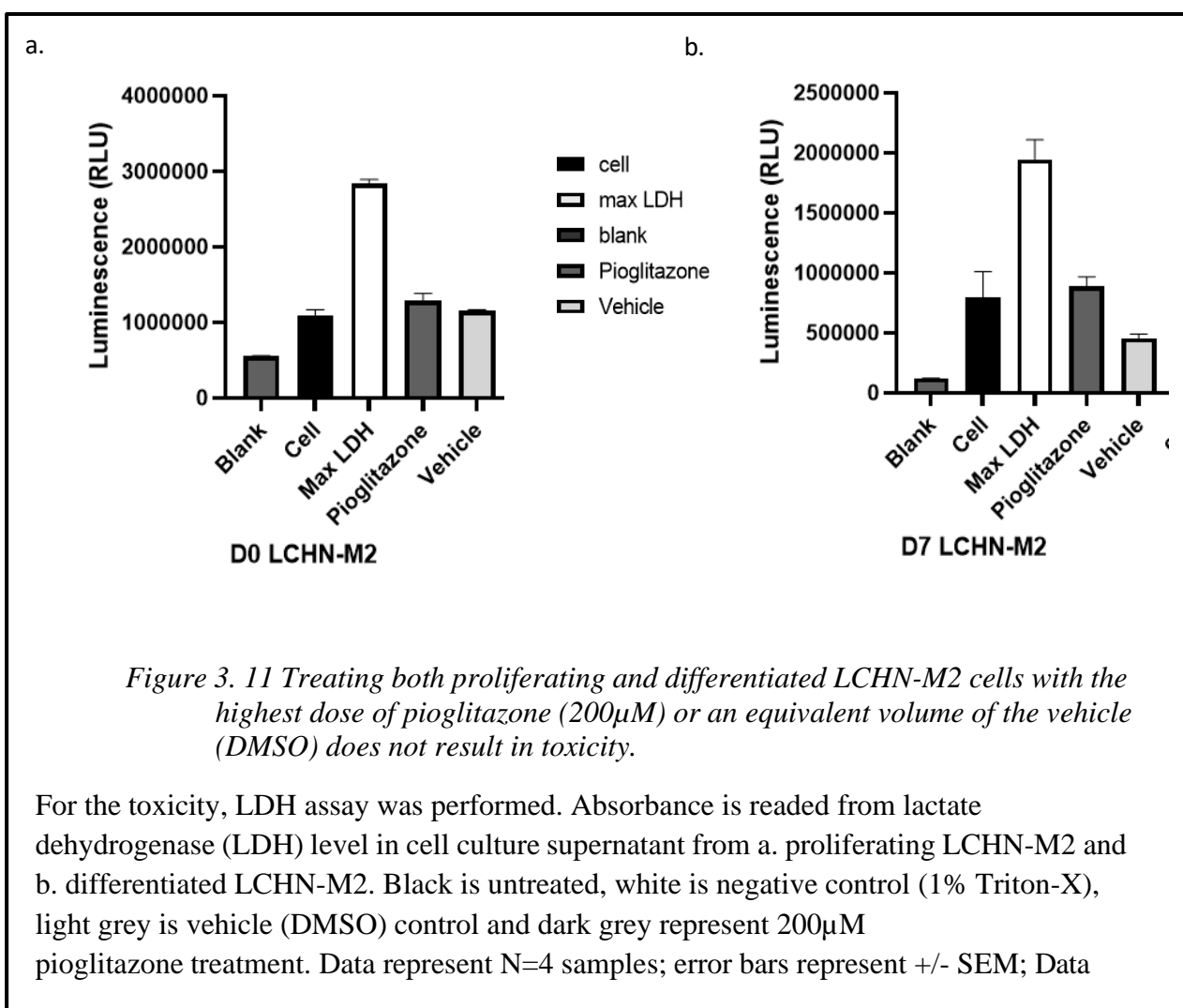
We measured the absorbance wavelengths (nm) for various conditions: blank (media only), background (cell presence), and LCHN-M2 myoblasts treated with either an anti-BrDU antibody, vehicle (DMSO), or 200 μ M pioglitazone for 24 hours. Data were obtained from four samples per group, spanning two independent experiments. Error bars represent the standard error of the mean (SEM). Statistical analysis was performed using one-way ANOVA, followed by Dunnett's post-hoc test. Notations for statistical

significance are as follows: ns = not significant, * $p < 0.05$, ** $p < 0.01$, *** $p < 0.001$, **** $p < 0.0001$.

3.3.10 During a 24-hour treatment period, pioglitazone demonstrated no toxic impact on either the proliferating or differentiating states of LCHN-M2 cells.

In this segment of our research, our goal was to investigate the potential toxic effects of pioglitazone on proliferating LCHN-M2 (human muscle) cells (figure 3.11.a) and cells in the differentiation phase (figure 3.11.b) via LDH assay. Additionally, we incorporated a vehicle control (shown as the light grey bar) and evaluated the impact of pioglitazone at its highest concentration (illustrated by the dark grey bar).

The results of our study revealed that the highest dose of pioglitazone and an equivalent amount of the vehicle (DMSO) did not exhibit any toxic effects on LCHN- M2 cells, whether at the initial stage (D0) or after a week (D7).



represent N=4 samples; error bars represent +/- SEM; One ANOVA with post-hoc Dunnett's multiple comparison test, ns=not significant, *p<0.05
 p<0.01 *p<0.001 ****p<0.0001.

Overall;

Table 3. 1 The overall of pioglitazone results were about validation and in-vitro models

	Model	Tissue/sub-model	Significant difference comparing controls
Validation of <i>in-silico</i> data	<i>Smn</i> ^{-/-} ;SMN2	Triceps Skeletal muscle	Level of <i>Thbs1</i> and <i>Ppar-α</i> increased
	<i>Smn</i> ^{2B/-} Mice		Increased <i>Thbs1</i> gene expression No change in <i>Ppar-α</i>
	Type III SMA patients	Deltoid myoblasts	PPAR-α level decreased.
	Proliferating C2C12s	Smn-KD with <i>Smn</i> -siRNA transfection	<i>Thbs1</i> exp. upregulated with independent of the <i>Smn</i> gene
	Differentiated-C2C12s		<i>Thbs1</i> exp. downregulated with dependent of the <i>Smn</i> gene
	Differentiated-C2C12s	Atrophy-induced	No change
Pioglitazone impact	C2C12s	Myoblast	Downregulation of <i>Thbs1</i> (200μM pioglitazone)
		Myotubes	Upregulation of <i>Thbs1</i> (50μM pioglitazone)
	LCHN-M2	Myoblast	Upregulation of <i>THBS1</i> (50μM pioglitazone)
		Myotubes	No difference

The table depicted in the figure methodically outlines, from left to right, the study plan's objectives, the selected models, the focused tissue/sub-models, and the statistically significant outcomes examined. This format facilitates an understanding of the models employed and their respective outcomes in the context of the *in-silico* validation process. Subsequently, the study investigates the impact of pioglitazone on the expression of certain genes in the C2C12s and LHCN-M2 models after the application of pioglitazone. This method offers a detailed view of how pioglitazone affects gene expression within the *in-vitro* model systems.

3.3.11 Oral administration of pioglitazone has a positive effect on weight, survival and motor function in *Smn*^{2B/-} mice.

The results from in vivo studies indicated that in *Smn*^{-/-};SMN2 and *Smn*^{2B/-} mouse models, the target genes *Thbs1* and *Ppar-α* are affected. Specifically, only *Thbs1* was

observed to be dysregulated in the *Smn*^{2B/-} model. In *Smn*-knockdown C2C12 myotube formations, the dysregulation of the *Thbs1* gene was shown to be directly linked to the *Smn* gene. Ultimately, it has been demonstrated that genes dysregulated in SMA mouse models and in vitro *Smn* models are associated with the pathology of SMA. Importantly, it has been observed that pioglitazone exerts an effect and demonstrates safety in influencing the expression of these specific genes in both C212s and LCHN- M2 cell lines. These findings provide a solid foundation for initiating research using mouse models in the study of SMA.

Initially, we carried out animal studies to identify the most effective dosage and treatment schedule for pioglitazone. We employed the *Smn*^{2B/-} mouse model and initiated testing at either P5 or P8. We tested various dosage levels, ranging from 2 mg/kg/day to 25 mg/kg/day, taking into account findings from previous studies by Drew et al. (2015).

Following this phase of dose optimization, we identified the most effective treatment regimen to be 12.5 mg/kg/day of pioglitazone, starting at day 5 and continuing until the humane endpoint. This specific approach was selected because it showed notable improvements in both the weight pattern and lifespan of the mice (table 3.2).

Table 3. 2 12.5 mg/kg/day Pioglitazone is the most optimal treatment way.

Pioglitazone Concentration	Treatment Starting Day	Effect on Survival	Effect on Weight
2 mg/kg/day	P5	no change	no change
5 mg/kg/day	P5	no change	no change
12.5 mg/kg/day	P5	increase	increase
12.5 mg/kg/day	P8	increase	no change
25 mg/kg/day	P5	no change	no change

This table provides us with the regimen for dosing and timing of pioglitazone in mouse studies. To identify the optimal treatment approach, SMA mice were treated with various concentrations and administration methods of pioglitazone. The therapeutic value of pioglitazone was then assessed over weight and survival patterns.

When comparing the *Smn*^{2B/-} mouse model treated with 12.5 mg/kg/day of pioglitazone to untreated *Smn*^{2B/-} mice, we observed a statistically significant increase in weights at P5 and P6 (figure 3.12.a). Additionally, this upward trend in weight patterns was notable up to P7 and P20 (figure 3.12.a). In a separate comparison involving vehicle-treated and untreated SMA mice, although a positive effect from the vehicle was observed, it was much less substantial than the improvement seen with pioglitazone treatment and lasted only up to 14 days (figure 3.12.d). In conclusion, administering 12.5 mg/kg/day of pioglitazone was found to have a positive impact on weights in pioglitazone treated *Smn*^{2B/-} comparing untreated *Smn*^{2B/-} mouse model (figure 3.12.a)

Our second functional analysis involved the righting reflex (RR) test, aimed at evaluating whether motor functions improved following treatment with pioglitazone (figure 3.12.c). The results of this test showed that administering 12.5 mg/kg/day of pioglitazone had a positive impact on motor function, as evidenced by improved righting reflex times when compared to untreated *Smn*^{2B/-} (figure 3.12.c).

The lifespan results indicated that whereas untreated *Smn*^{2B/-} mice typically have a median lifespan of P20, those treated with pioglitazone showed an extended median lifespan of P22. (figure 3.12.b).

In the *Smn*^{2B/+} mice, however, it was observed that 12.5 mg/kg/day pioglitazone application only had a positive effect on the weight trend (figure 3.12.d). The *Smn*^{2B/+} model contains an adequate amount of the SMN protein necessary for survival, muscle development, and functionality. Consequently, it does not exhibit the disease phenotype, and no differences have been observed in survival and RR reflexes (figure 3.12.f).

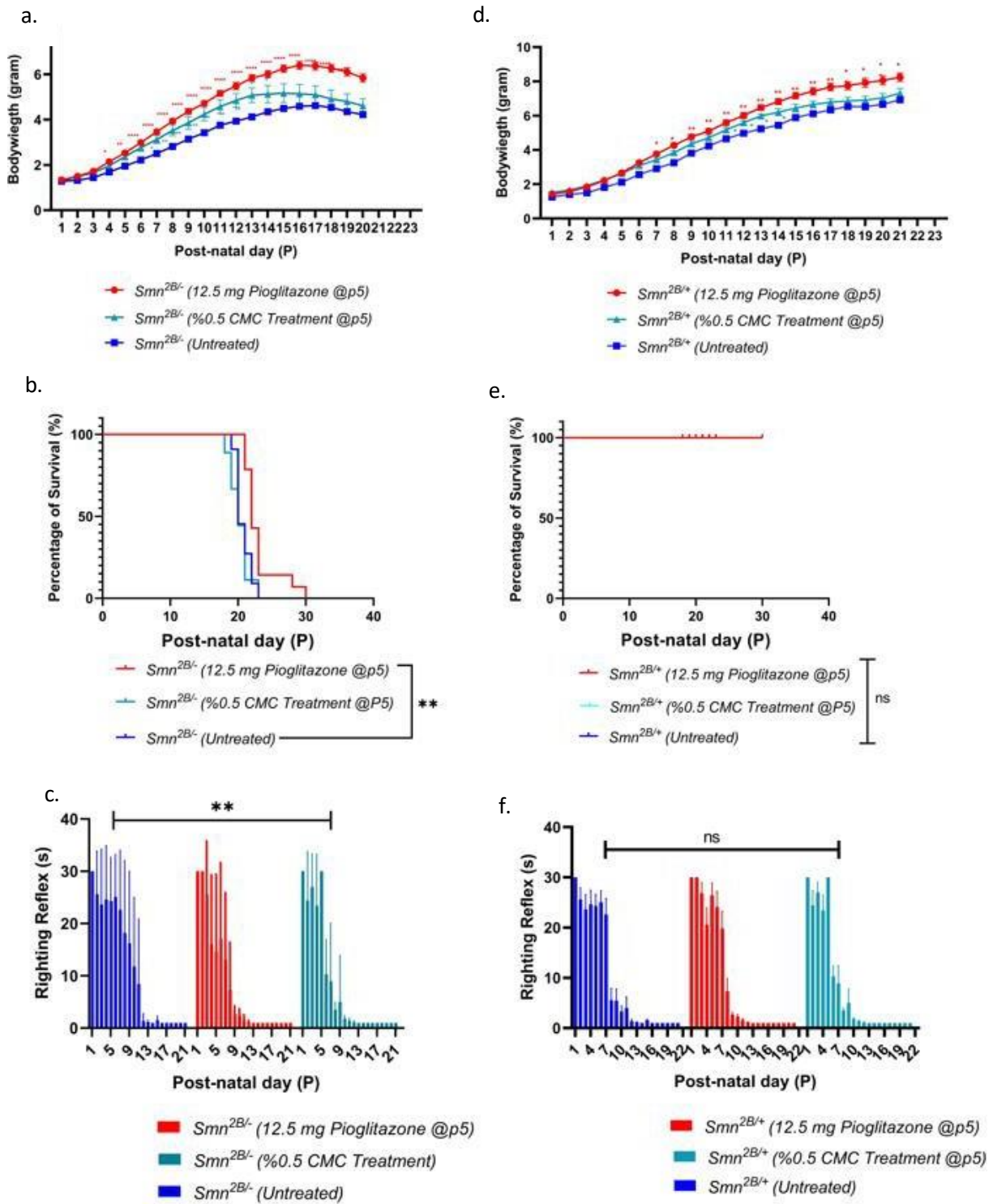


Figure 3.12 The effect of 12.5 mg/kg/day oral pioglitazone treatment in both $Smn^{2B/-}$ and $Smn^{2B/+}$ SMA mice.

All animals were treated with 12.5 mg/kg/day pioglitazone (0.5 % carboxymethylcellulose) via daily gavage starting at P5 on *Smn*^{2B/-} SMA mice. a. Daily weights of pioglitazone-treated (red, n=16), untreated (blue, n=15) and, CMC-treatment (green, n=10) on *Smn*^{2B/-} SMA mice. Error bars represent +/- SEM; Two-way ANOVA with post-hoc Sidak's multiple comparisons test between untreated (blue) and 12.5 mg/kg/day pioglitazone treatment (red), vehicle/0.5 % carboxymethylcellulose treatment (green) *p<0.05, **p<0.01, ***p<0.001, ****p<0.0001. b. Kaplan-Meier survival curves for n=15 untreated (blue, median survival:20 days), n=10 vehicle-treated (green, median survival: 20) and n=16 12.5 mg/kg/day pioglitazone (red, median survival:22 days) on *Smn*^{2B/-} SMA mice, Long-rank (Mantel-Cox) test, **p<0.01, ns= n significant. c. Daily righting reflex test up to a 30 second max time point of drug-treated (red, n=16), vehicle treated (green, n=10) and untreated (blue, n=15) on *Smn*^{2B/-} SMA mice. Data represents mean and +/- SD error bars, One-way ANOVA with post-hoc Turkey's multiple comparisons test. *p<0.05, ns= not significant. d. Daily weights of pioglitazone-treated (red, n=13), untreated (blue, n=13) and, CMC-treatment (green, n=9) on *Smn*^{2B/+} SMA mice. Error bars represent +/- SEM; Two-way ANOVA with post-hoc Sidak's multiple comparisons test between untreated (blue) and 12.5 mg/kg/day pioglitazone treatment (red), vehicle/0.5 % carboxymethylcellulose treatment (green) *p<0.05, **p<0.01, ***p<0.001, ****p<0.0001. e. Kaplan-Meier survival curves for n=13 untreated (blue, median survival:22 days), n=9 vehicle-treated (green, median survival: 22) and n=13 12.5 mg/kg/day pioglitazone (red, median survival:22 days) on *Smn*^{2B/+} SMA mice, Long-rank (Mantel-Cox) test, **p<0.01, ns= n significant. f. Daily righting reflex test up to a 30 second max time point of drug-treated (red, n=13), vehicle treated (green, n=9) and untreated (blue, n=13) on *Smn*^{2B/+} SMA mice. Data represents mean and +/- SD error bars, One-way ANOVA with post-hoc Turkey's multiple comparisons test. *p<0.05, ns= not significant.

3.3.12 Oral administration of 12.5 mg/kg/day pioglitazone did not lead to any change of hypoglycemia in both non-fasted *Smn*^{2B/-} and *Smn*^{2B/+} mice

As our next step, we aim to delve deeper into the pharmacological effects of pioglitazone at both the molecular level and within specific tissues in SMA mice. The goal is to better understand how pioglitazone leads to improved weight gain patterns, enhanced motor function, and extended lifespan in these mice.

We first investigated the impact of pioglitazone treatment on hyperglycaemic blood levels in symptomatic SMA mouse models that were not fasting. Blood glucose levels were measured at P18 two hours after the final dose

of pioglitazone. As a result of that, our measurements revealed no significant effect on blood glucose levels from pioglitazone administration in either the *Smn*^{2B/-} (figure 3.13.a) and *Smn*^{2B/+} (figure 3.13.b.) mice.

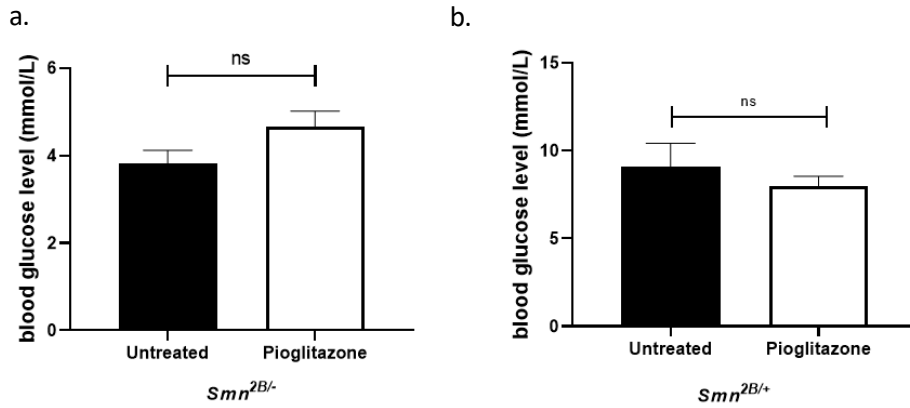


Figure 3. 13 Oral 12.5 mg/kg/day Pioglitazone treatment did not cause any significant change in blood glucose level in symptomatic non-fasting both *Smn*^{2B/-} and *Smn*^{2B/+}.

All animals were treated 12.5 mg/kg/day pioglitazone (diluted in %0.5 CMC) via daily gavage starting at P5 till P18. Blood glucose concentrations (mmol/L) were evaluated after 2 hours final treatment of pioglitazone. Untreated (black bars), and pioglitazone treated (white bars). *Smn*^{2B/-} mouse model result is in the a graph (n=7), b. *Smn*^{2B/+} mouse model result shows in the b graph (n=5). Data represents mean and error bars represent +/- SEM; Unpaired t test, ns=not significant.

3.3.13 Administering of pioglitazone orally led to an increase in the expression levels of *Ppar-α* and *Ppar-γ* in the triceps tissue of symptomatic *Smn*^{2B/-} SMA mice.

To gain a deeper insight into the molecular impact of pioglitazone, our focus was on particular target genes: *Thbs1*, *Ppar-α*, and *Ppar-γ*. The selection of these genes was informed by our bioinformatics data, our previous analyses in cell culture and a review of relevant literature (Bai et al., 2020; Bogacka et al., 2004; Orasanu et al., 2008).

To investigate whether pioglitazone influences the expression of target genes (*Thbs1*, *Ppar-α* and *Ppar-γ*) in the triceps tissue of symptomatic *Smn*^{2B/-} SMA mice, target gene levels were quantified by performing qPCR analyses. Therefore, it was determined that *Ppar-α/γ* expression increased in *Smn*^{2B/-} depending on 12.5 mg/kg/day pioglitazone treatment (figure 3.14.c; e), and there was no change in the *Thbs1* level (figure 3.14.a, b). As for the *Smn*^{2B/+} model, there is no statistically significant change in the levels of target genes in symptomatic pioglitazone treated/untreated triceps tissues (figure 3.14.b; d; f).

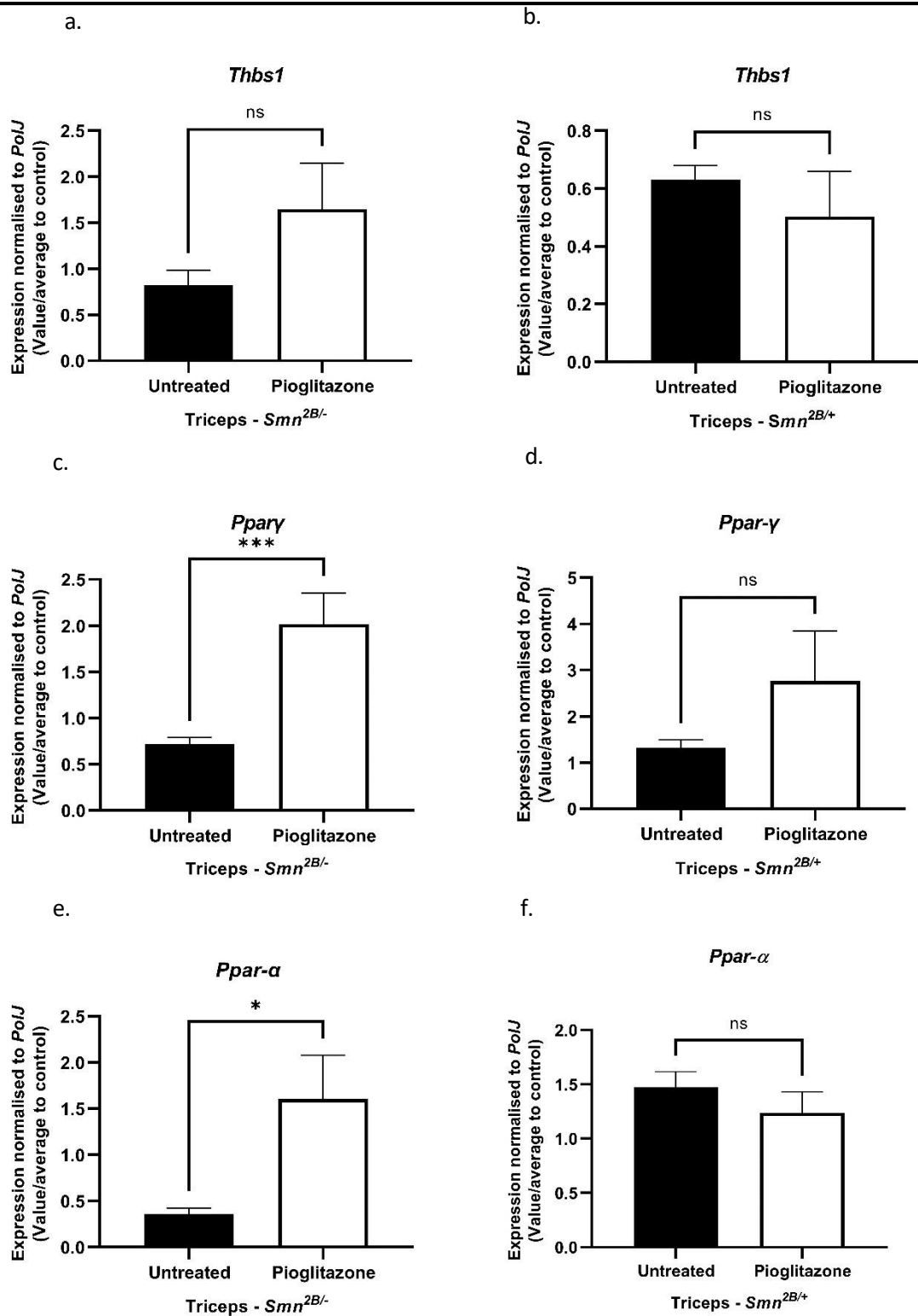
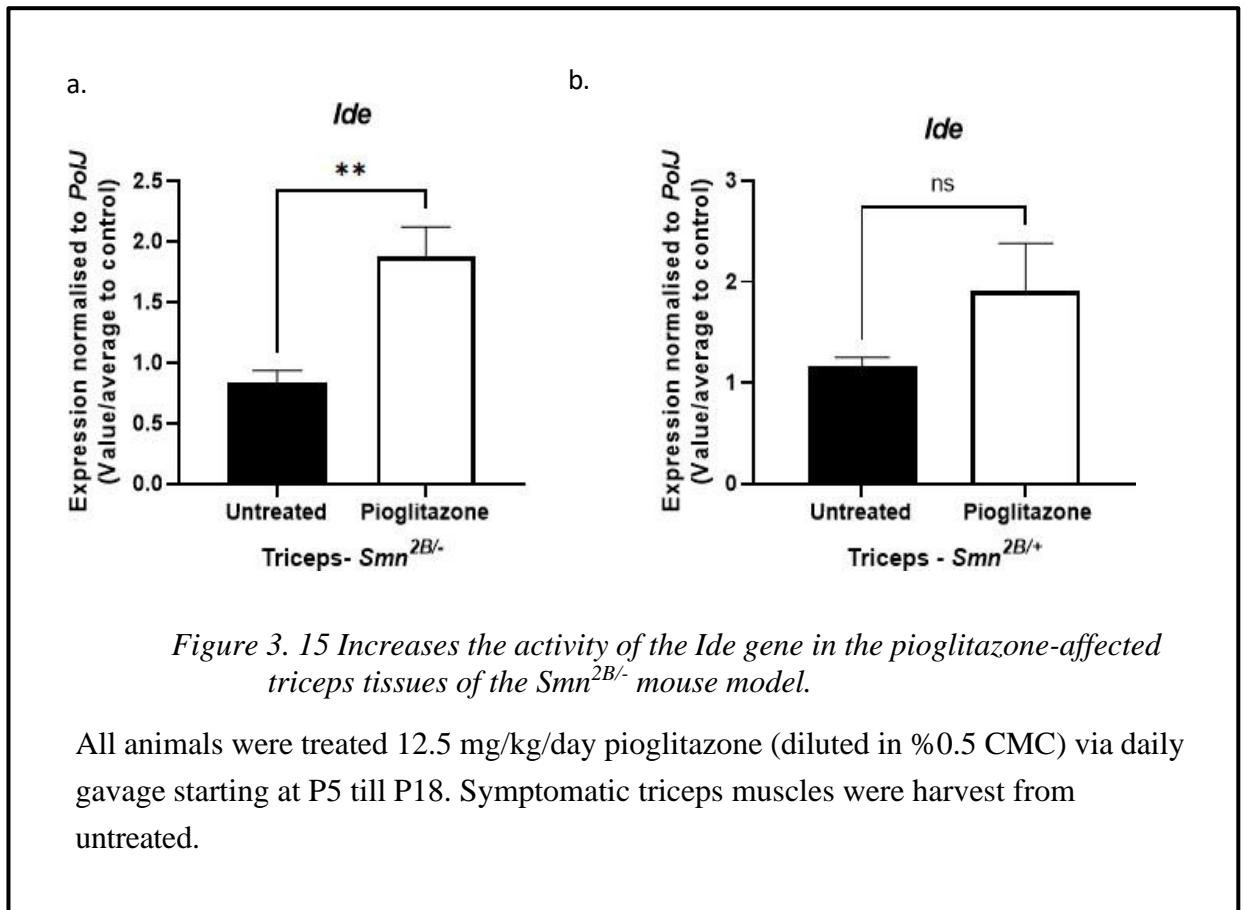


Figure 3. 14 Orally treatment of 12.5 mg/kg/day Pioglitazone caused an upregulation of *Ppar-α* and *Ppar-γ* expression level in symptomatic triceps tissue in *Smn*^{2B/-} SMA mice.

All animals were treated with 12.5 mg/kg/day pioglitazone (diluted in 0.5% CMC) via daily gavage starting at P5 till P18. Symptomatic triceps muscles was harvest from untreated (n=8, black bars) and pioglitazone treated (n=8, white bars) in non-fasted *Smn*^{2B/-} and *Smn*^{2B/+}, after 2hours last pioglitazone treatment. The mRNA levels of *Thbs1* gene are in a. *Smn*^{2B/-} and b. *Smn*^{2B/+} ; these of *Ppar-γ* are in c. *Smn*^{2B/-} and d. *Smn*^{2B/+} and the expressions of *Ppar-a* gene are in e. *Smn*^{2B/-} and f. *Smn*^{2B/+}. Data represents mean and error bars represent +/- SEM; Unpaired t Test, ns=not significant, *p<0.05, ***p<0.001.

3.3.14 The *Ide* expression had been increased followed by pioglitazone application in *Smn*^{2B/-} mouse model.

It has recently been found that pioglitazone enhances mitochondrial function by upregulating *PPAR-γ*, which leads to increased levels of *IDE* proteins (Di Donfrancesco et al., 2023). To understand the specific effects of pioglitazone on mitochondrial function in symptomatic triceps skeletal muscle, a study compared tissues treated with pioglitazone to *Smn*^{2B/-} without treatment. This study revealed that administering pioglitazone at a dosage of 12.5 mg/kg/day elevates the expression of the *Ide* gene in the symptomatic triceps tissues in *Smn*^{2B/-} mouse model (figure 3.15).



(n=8, black bars) and pioglitazone treated (n=8, white bars) in non-fasted *Smn*^{2B/-} a. and *Smn*^{2B/+} b., after 2 hours last pioglitazone treatment.

The mRNA levels of *Ide* gene are in a. *Smn*^{2B/-} and b. *Smn*^{2B/+}. Data represents mean and error bars represent +/- SEM; Unpaired t Test. ns=not significant, **p<0.01.

3.3.15 Pioglitazone had no impact on muscle atrophy marker gene expression.

Next, we examined the effect of pioglitazone on skeletal muscle development through its impact on muscle atrophy, a hallmark of SMA. To investigate this phenotype at the molecular level, our goal was to study the ubiquitin ligases Atrogin-1 and MuRF1, which are upregulated in 13 different skeletal muscle injury (Lecker et al., 1999; Brancaccio, Lippi, and Maffulli, 2010; Foletta et al., 2011). As a result, it was found that 12.5 mg/kg/day pioglitazone treatment had no effect on attenuating the expression of *Atrogin-1* and *MurF1* genes in symptomatic SMA' triceps tissue (as illustrated in figure 3.16).

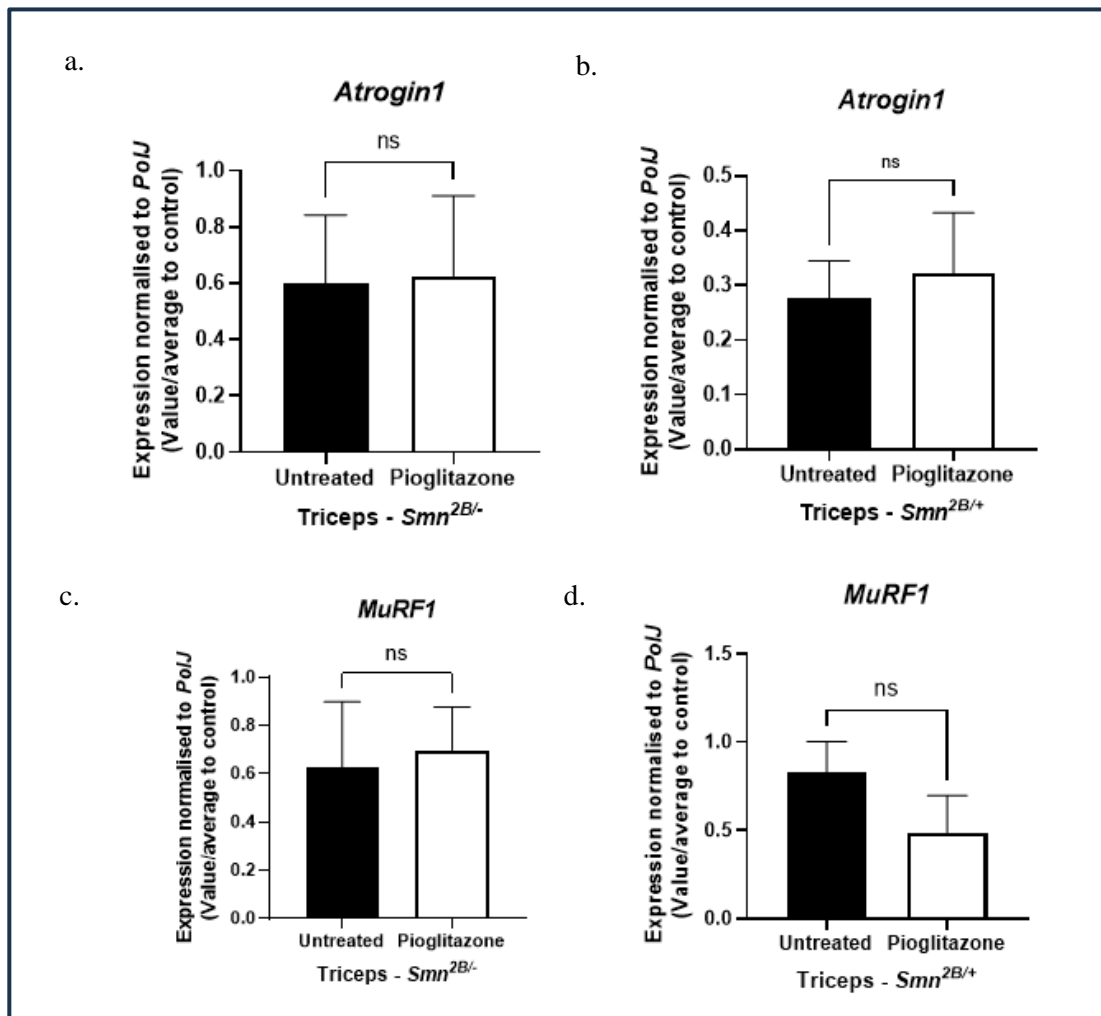


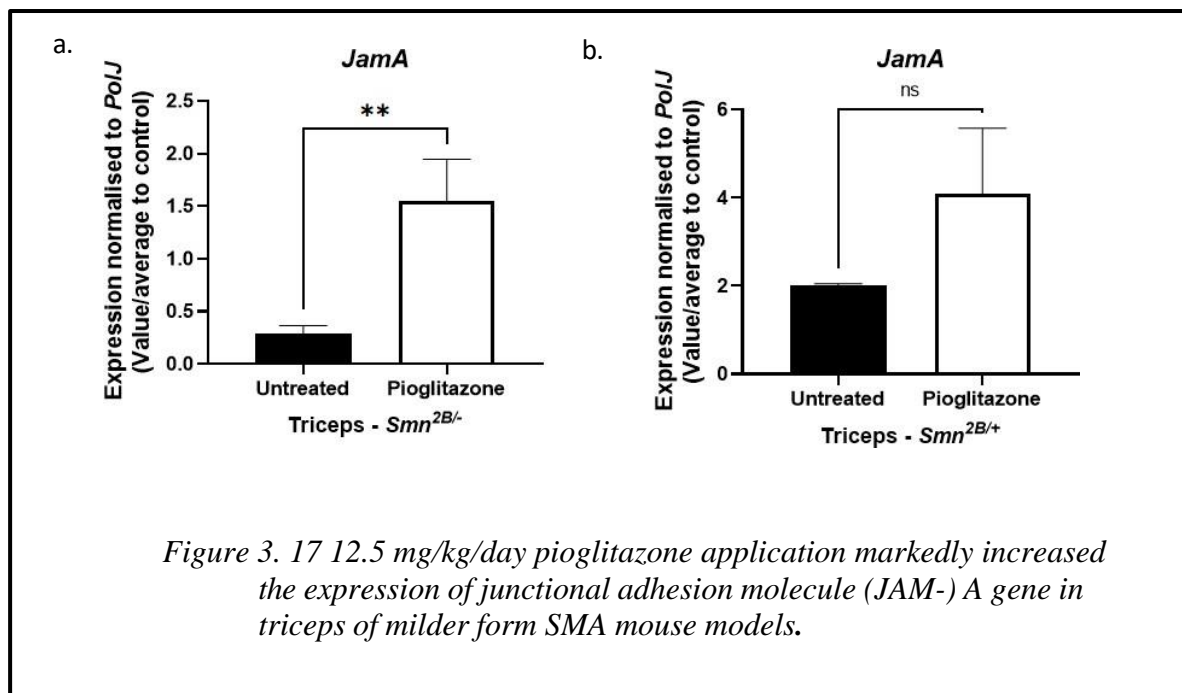
Figure 3. 16 12.5 mg/kg/day pioglitazone orally administration has no effect on the atrophic phenotype of triceps of milder form SMA mouse models

All animals were treated with 12.5 mg/kg/day pioglitazone (diluted in %0.5 CMC) via daily gavage starting at P5 till P18. Symptomatic triceps muscles was harvest from untreated (n=8, black bars) and pioglitazone treated (n=8, white bars) in non-fasted *Smn*^{2B/-} and *Smn*^{2B/+}, after 2hours last pioglitazone treatment. The mRNA levels of *atrogen-1* gene are in a. *Smn*^{2B/-} and b. *Smn*^{2B/+} ; these of *MurF1* are in c. *Smn*^{2B/-} and d. *Smn*^{2B/+}.

Data represents mean and error bars represent +/- SEM; Unpaired t Test, ns=not significant.

3.3.16 Pioglitazone induced enhancement of junctional adhesion molecule-A (*Jam-A*) expression in triceps of mild SMA mouse models.

Junctional adhesion molecule A (JAM-A) is a protein that plays a role in vascular/epithelial permeability and is known to increase the distribution and permeability of leukocytes (Schmitt *et al.*, 2014). Since inflammation is another pathology observed in skeletal muscle of SMA Type 1 and III (Millino *et al.*, 2009b; Papadimitriou *et al.*, 2010). Altogether, the potential effect on the inflammation phenotype in SMA muscle tissue has been investigated through the lens of *Jam-A* expression. As a result, we found that 12.5 mg/kg/day pioglitazone administration caused a significant increase in mRNA level of *JamA* in *Smn*^{2B/-} SMA mice (figure 3.17.a).

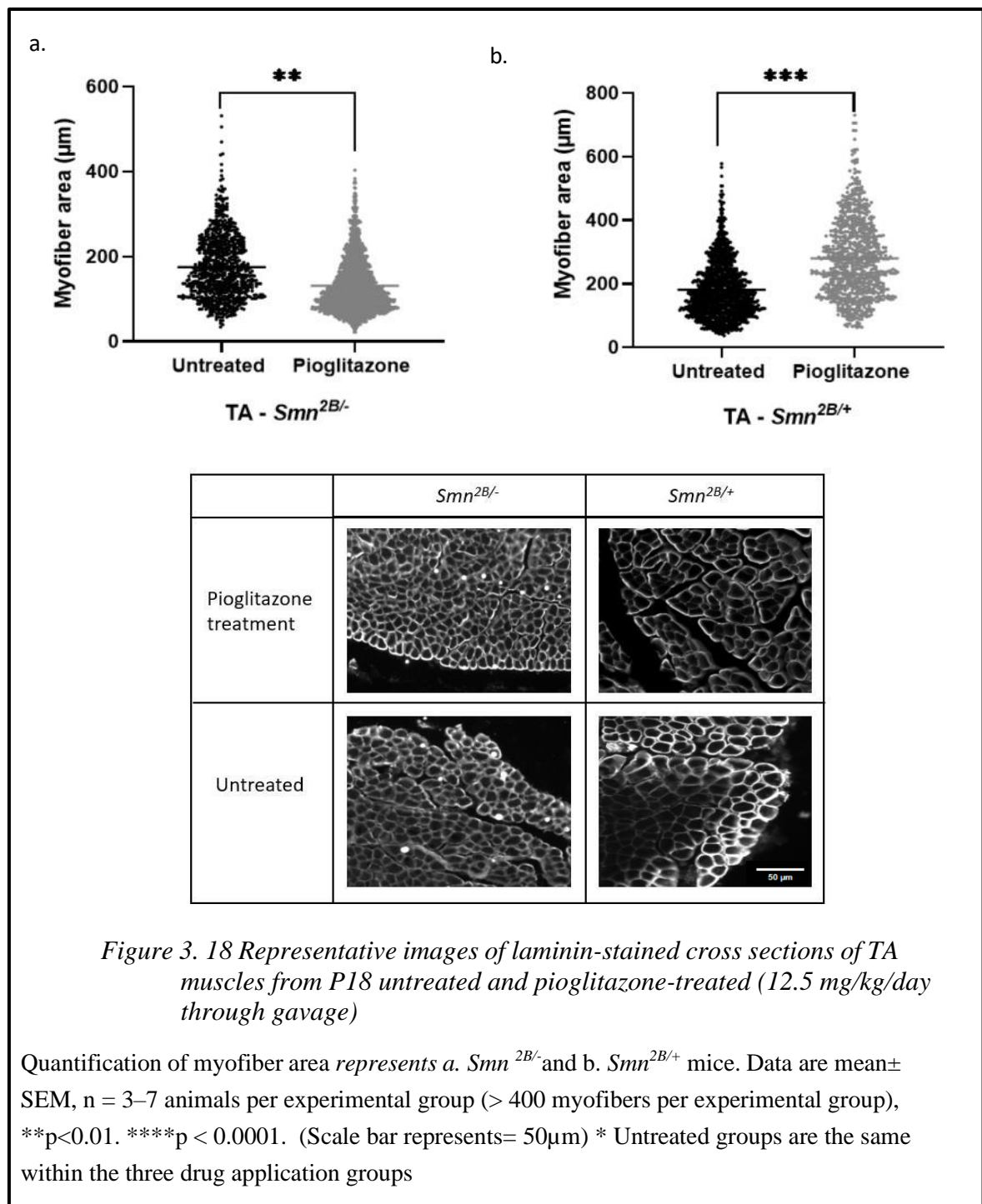


All animals were treated with 12.5 mg/kg/day pioglitazone (diluted in %0.5 CMC) via daily gavage starting at P5 till P18. Symptomatic triceps muscles were harvest from untreated (n=8, black bars) and pioglitazone treated (n=8, white bars) in non-fasted *Smn*^{2B/-} a. and *Smn*^{2B/+} b., after 2hours last pioglitazone treatment. The mRNA levels of *JamA* gene are in a. *Smn*^{2B/-} and b. *Smn*^{2B/+}. Data represents mean and error bars represent +/- SEM; Unpaired t Test. ns=not significant, **p<0.01.

3.3.17 Negative effect of pioglitazone on muscle fiber size was observed in symptomatic TA of *Smn*^{2B/-}, whereas showed opposite pattern in *Smn*^{2B/+}.

The effect of pioglitazone on this morphological phenotype was evaluated by analyzing the cross-sectional area of the muscle fibers, which is commonly associated with enhanced muscle strength and health (Waisman et al., 2021). This aspect has been incorporated into the experimental framework to understand whether pioglitazone can alleviate the muscle weakness observed in SMA pathology (Deymeer et al., 1997).

In both *Smn*^{2B/-} and *Smn*^{2B/+} mouse models, the effects of administering 12.5 mg/kg/day of pioglitazone were evaluated by comparing the size of TA myofibers to untreated controls. The results indicated that in *Smn*^{2B/-}, pioglitazone reduced the fiber size (figure 3.18.a), whereas in the *Smn*^{2B/+} mouse models, it was found to increase the fiber size (figure 3.18.b).



3.3.18 12.5 mg/kg/day pioglitazone treatment upregulated *Ppar- γ* expression in spinal cord of *Smn*^{2B/-}.

Another tissue to be examined for the effects of pioglitazone application is the spinal cord, where the loss of alpha-motor neurons occurs and which is a key area affected by SMA (Daniel D. Covert et al., 1997), potentially providing insights into its overall therapeutic impact on the disease.

Specifically, our analysis involved examining tissue samples from the spinal cord to ascertain if the observed advantages were due to the 12.5 mg/kg/day dosage of pioglitazone treatment. Our results revealed that in the spinal cord tissues of *Smn*^{2B/-} mice treated with pioglitazone, there was a significant upregulation of the *Ppar-γ* gene (figure 3.19.c). However, the expression levels of the other two targeted genes remained unchanged (figure 3.19.a, e.). Interestingly, we found no alterations in the mRNA levels of these genes in the *Smn*^{2B/+} mouse model (figure 3.19.b; d; f.). Therefore, following pioglitazone treatment resulted in enhanced *Ppar-γ* expression in the spinal cords of *Smn*^{2B/-} models.

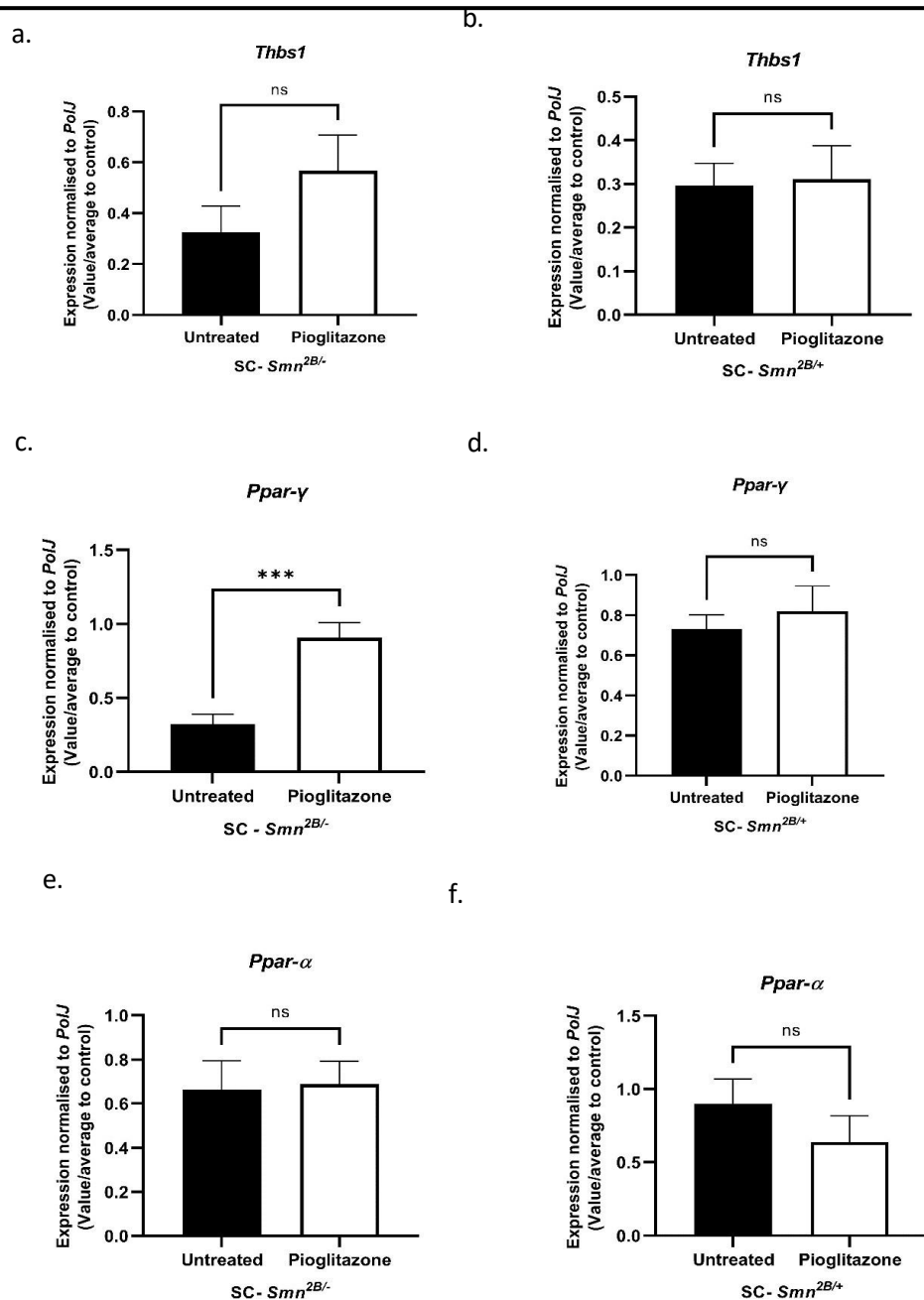


Figure 3. 19 Orally treatment of 12.5 mg/kg/day Pioglitazone causes upregulation of *Ppar-γ* expression level in symptomatic spinal cord tissue in *Snn*^{2B/-} SMA mice.

All animals were treated with 12.5 mg/kg/day pioglitazone (diluted in %0.5 CMC) via daily gavage starting at P5 till P18. Symptomatic spinal cord was harvested from untreated (n=8, black bars) and pioglitazone treated (n=8, white bars) in non-fasted *Snn*^{2B/-} and *Snn*^{2B/+}, after 2hours last pioglitazone treatment. The mRNA levels of *Thbs1* gene are in a. *Snn*^{2B/-} and b. *Snn*^{2B/+}; these of *Ppar-γ* are in c. *Snn*^{2B/-} and d. *Snn*^{2B/+} and the expressions of *Ppar-α* gene are in e. *Snn*^{2B/-} and f. *Snn*^{2B/+}. Data represents mean and error bars represent +/- SEM; Unpaired t Test, ns=not significant, ***p<0.001.

3.3.19 Following the application of pioglitazone, there was an upregulation of *Pmaip-1* and *Fas* mRNA levels in the spinal cord tissues of *Smn*^{2B/-} mice.

To determine whether pioglitazone has a protective effect on the spinal cord, the study focused on the mRNA levels of *Pmaip-1* and *Fas* in SMA SC tissues. These genes, known for their aberrant expression and contribution to pathology in SMA SC (Murray et al., 2015a). As a result of qPCR analyses, it was found that the expression levels of *Pmaip-1* and *Fas*, in SC both in the *Smn*^{2B/-} and *Smn*^{2B/+} were significantly downregulated (figure 3.20.).

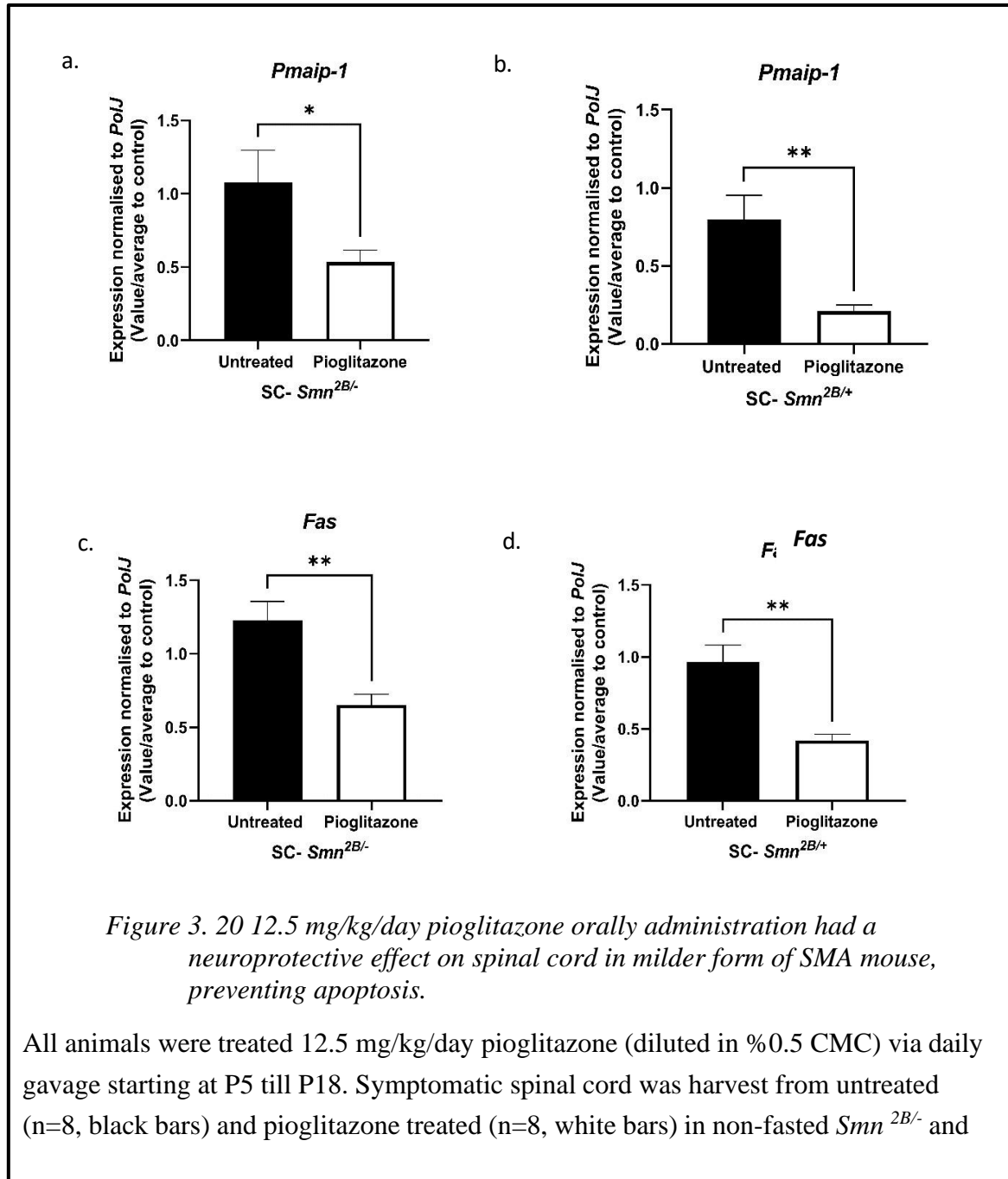


Figure 3. 20 12.5 mg/kg/day pioglitazone orally administration had a neuroprotective effect on spinal cord in milder form of SMA mouse, preventing apoptosis.

All animals were treated 12.5 mg/kg/day pioglitazone (diluted in %0.5 CMC) via daily gavage starting at P5 till P18. Symptomatic spinal cord was harvest from untreated (n=8, black bars) and pioglitazone treated (n=8, white bars) in non-fasted *Smn*^{2B/-} and

Smn^{2B/+}, after 2 hours of last pioglitazone treatment. The mRNA levels of *Pmaip-1* gene are in a. *Smn*^{2B/-} and b. *Smn*^{2B/+}; these of *Fas* are in c. *Smn*^{2B/-} and d. *Smn*^{2B/+}. Data represents mean and error bars represent +/- SEM; Unpaired t Test, *p<0.05, **p<0.01.

3.3.20 Administration of pioglitazone did not change the number of α - motor neurons of symptomatic spinal cord of *Smn*^{2B/-} and *Smn*^{2B/+}

As mentioned earlier, the reduction of *Pmaip-1* and *Fas* expression in symptomatic SC tissues may indicate an alleviation of the SMA-related pathology in the spinal cord. To further investigate this hypothesis, we aimed to perform alpha motor neuron counting in the same tissue. This approach is designed to provide a clearer understanding of pioglitazone's effect on spinal cord pathology, thereby contributing to a more comprehensive picture of its potential therapeutic impact on SMA.

After administering a 12.5 mg/kg/day dose of pioglitazone to both *Smn*^{2B/-} and *Smn*^{2B/+} mouse models, we conducted counts of alpha motor neurons in symptomatic spinal cord cross-sections. These counts were carried out using Nissl staining for both pioglitazone-treated and untreated samples. Given that the depletion of motor neurons is a defining feature of SMA, our objective was to evaluate whether pioglitazone influenced the number of alpha motor neurons in the ventral horn of the spinal cord.

In *Smn*^{2B/-} mice, a comparison between those treated with a 12.5 mg/kg dose of pioglitazone and untreated controls revealed no change in the count of motor neurons, as evidenced by fluorescence microscopy images (figure 3.21.a.). Likewise, in *Smn*^{2B/+} mice, the number of motor neurons was also unaffected following a treatment with 12.5 mg/kg pioglitazone compared to untreated controls, as supported by fluorescence microscopy images (figure 3.21.b.). Given that the motor neuron counts did not change in either the *Smn*^{2B/-} and *Smn*^{2B/+} mice after treatment with pioglitazone, this suggests that pioglitazone does not influence the number of motor neurons in the spinal cord.

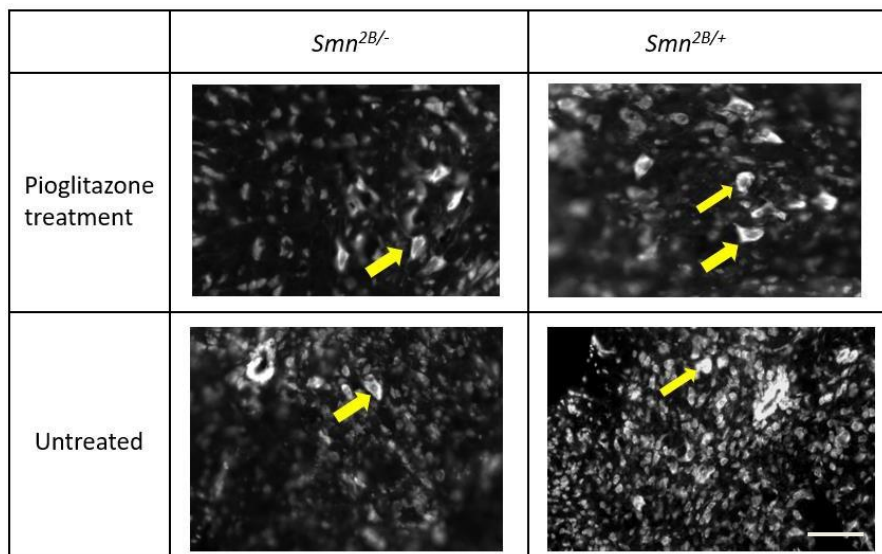
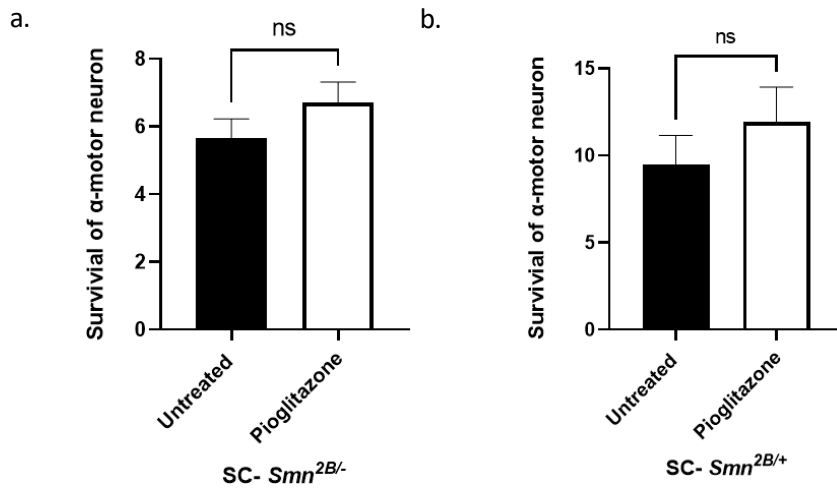


Figure 3. 21 The number of alpha motor neurons remained steady after 12.5mg/kg/day daily pioglitazone treatment in symptomatic SC in both $Smn^{2B/-}$ and $Smn^{2B/+}$ mouse model.

Representative images of Nissl-stained cross sections of SC from P18 untreated and pioglitazone-treated (12.5 mg/kg/day through gavage) a. $Smn^{2B/+}$ and b. $Smn^{2B/-}$ mice (scale bars = 50 μ m) and quantification of horn area. Data are mean \pm SEM, n = 3–7 animals per experimental group, Data represents mean and error bars represent \pm -SEM; Unpaired t Test, ns=not significant. * Untreated groups are the same within the three drug application groups.

3.3.21 Orally treatment of Pioglitazone led to an upregulation of *Thbs1* expression level in symptomatic liver tissue in *Smn*^{2B/+} SMA mice.

Another research question that emerged was whether administering pioglitazone could mitigate the observed abnormalities in fatty acid metabolism in the liver of *Smn*^{2B/-} mice. To delve deeper into this issue, liver tissue samples were collected from two distinct groups of symptomatic *Smn*^{2B/-} mice: one group that had been administered pioglitazone at a dosage of 12.5 mg/kg/day, and another group that had not received any treatment. Subsequent qPCR experiments were conducted to evaluate the effect of pioglitazone on the expression levels of targeted genes in the liver of these SMA mice. The results indicated that oral administration of pioglitazone did not have a significant impact on the expression of *Ppara* α/γ (figure 3.22.c; e.) and *Thsb1* (figure 3.22.a) target genes in the symptomatic liver tissue of *Smn*^{2B/-} mice when compared to healthy littermates. Interestingly, however, there was an observed upregulation in the mRNA levels of *Thbs1* in the symptomatic liver tissue of *Smn*^{2B/+} (figure 3.22.b) mice after pioglitazone treatment.

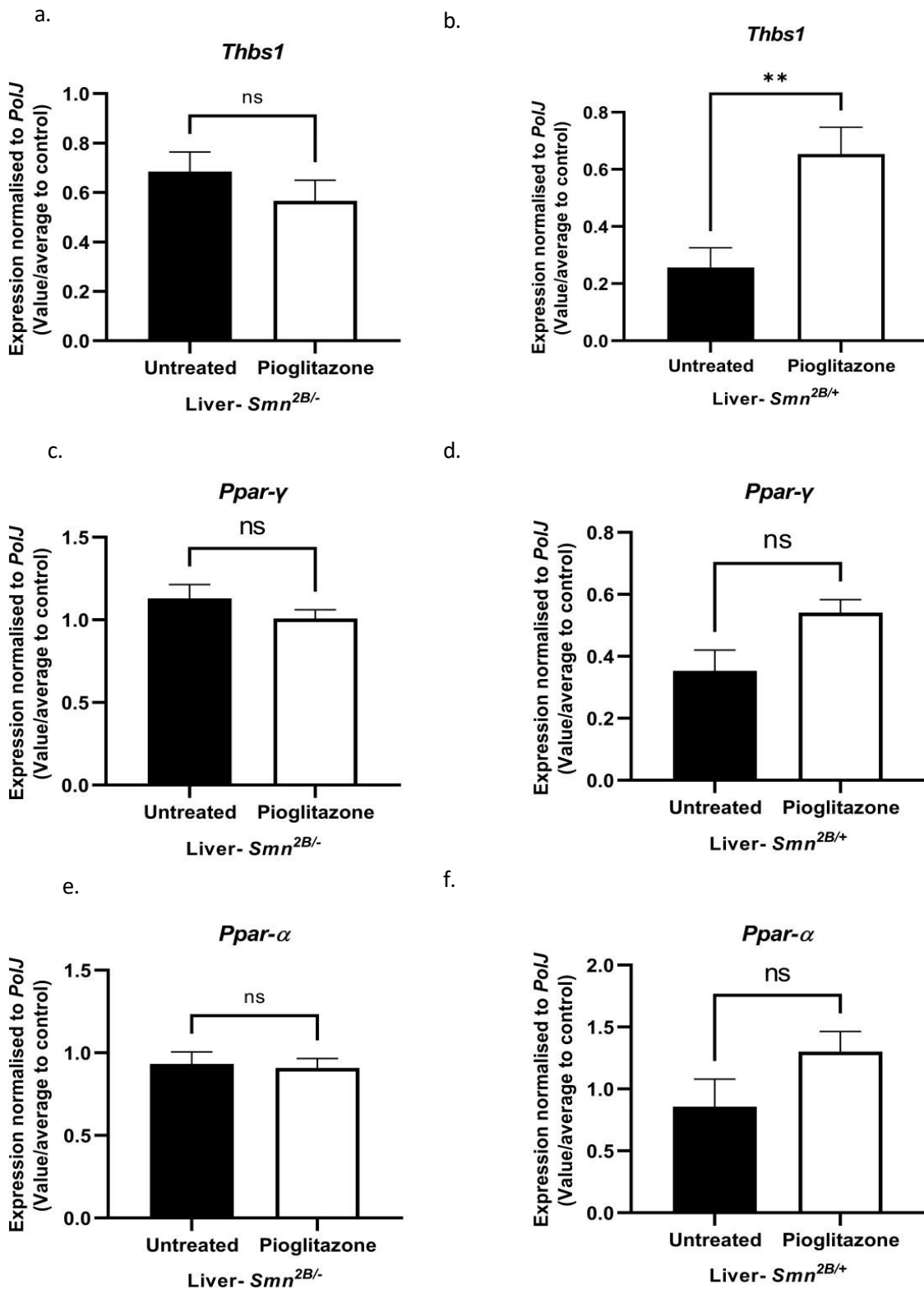
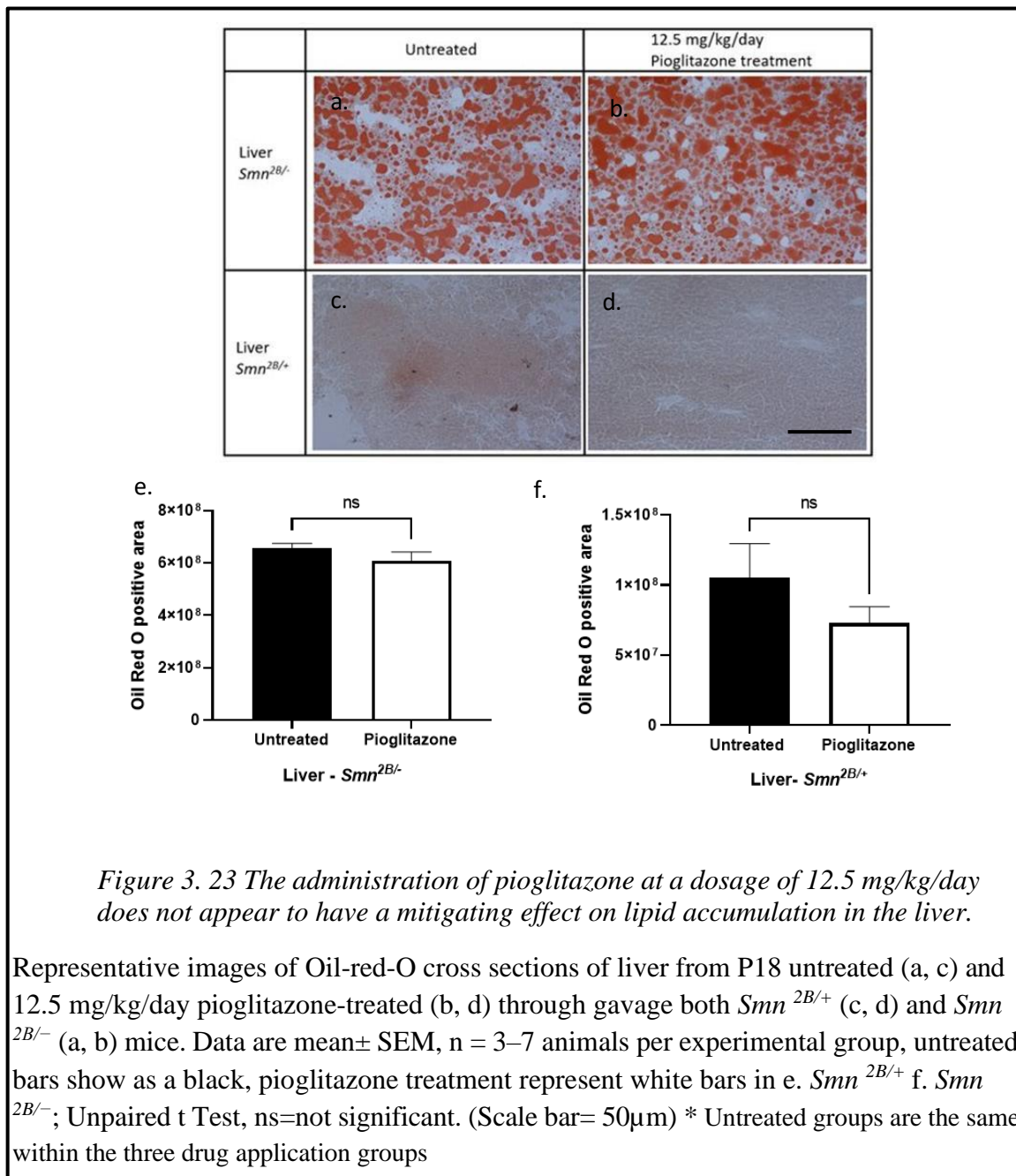


Figure 3. 22 Oral treatment of 12.5 mg/kg/day Pioglitazone lead an upregulation of *Thbs1* expression level in symptomatic liver tissue in *Smn*^{2B/+} SMA mice.

All animals were treated with 12.5 mg/kg/day pioglitazone (diluted in %0.5 CMC) via daily gavage starting at P5 till P18. Symptomatic liver was harvested from untreated (n=8, black bars) and pioglitazone treated (n=8, white bars) in non-fasted *Smn*^{2B/-} and *Smn*^{2B/+}, after 2hours last pioglitazone treatment. The mRNA levels of *Thbs1* gene are in a. *Smn*^{2B/-} and b. *Smn*^{2B/+}; these of *Ppar-γ* are in c. *Smn*^{2B/-} and d. *Smn*^{2B/+} and the expressions of *Ppar-α* gene are in e. *Smn*^{2B/-} and f. *Smn*^{2B/+}. Data represents mean and error bars represent +/- SEM; Unpaired t Test, ns=not significant, **p<0.01.

3.3.22 There was no change in lipid accumulation in liver of *Smn*^{2B/-} following pioglitazone treatment.

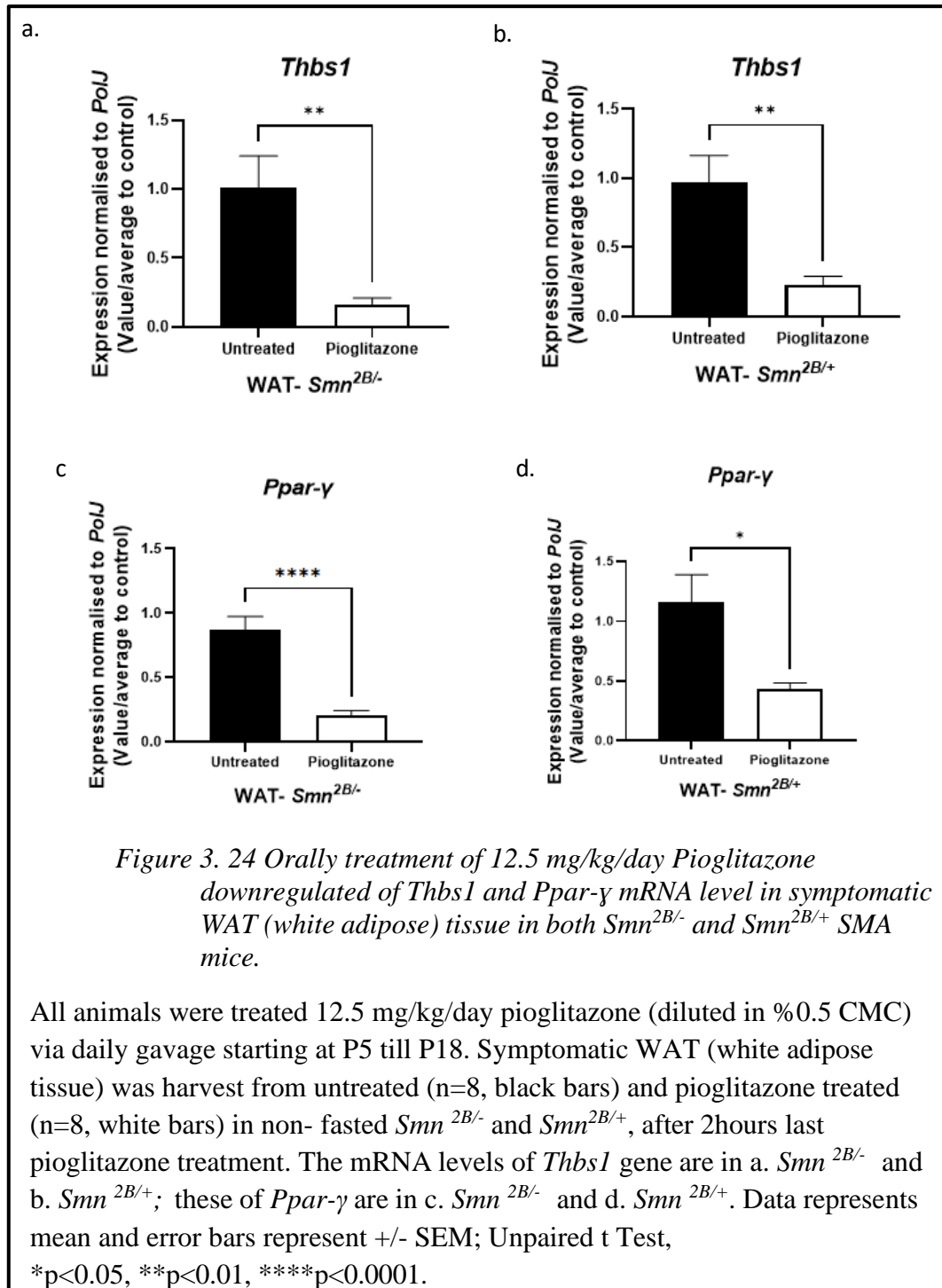
Although no changes were observed in the expression of genes associated with lipid metabolism in diabetic mice (Peng et al., 2014), the characteristics of lipid accumulation, dyslipidemia, and NAFLD-like phenotype in *Smn*^{2B/-} SMA mice (Deguise et al., 2019) were still investigated using the Oil-Red-O assay. This approach was employed to consider the potential influence of different molecular factors in the event of any observed changes in these phenotypes. Oil-red-O is a lipidic dye and diffuses into the lipid region in direct proportion to its lipid density. As seen in the figure below (figure 3.23), a clear lipid accumulation is observed in the *Smn*^{2B/-} (figure 3.23.a; b) mice compared to *Smn*^{2B/+} (figure 3.23.c; d). After administration of 12.5 mg/kg/day pioglitazone, no change was observed in lipid accumulation in *Smn*^{2B/-} (figure 3.23.e.) and *Smn*^{2B/+} (figure 3.23.f.).



3.3.23 Orally treatment of Pioglitazone downregulated of *Thbs1* and *Ppar-γ* mRNA level in symptomatic WAT in both *Smn*^{2B/-} and *Smn*^{2B/+} mice.

The holistic evaluation of fatty acid and energy metabolism, due to the inter- tissue crosstalk, has directed the inclusion of adipose tissue studies in our research (Deguise *et al.*, 2021). This approach recognizes the interconnected nature of metabolic processes across different tissues and the importance of adipose tissue in the broader metabolic context.

In order to analysis pioglitazone effect on lipid and fatty acid metabolism in adipose, symptomatic WAT was collected from SMA mice untreated/ treated with 12.5 mg/kg/day pioglitazone and qPCR experiments were performed to evaluate the effect of pioglitazone on the level of targeted genes in WAT tissue. In conclusion, oral administration of 12.5 mg/kg/day pioglitazone leads to downregulate *Ppar-γ* and *Thsb1* target gene expression in symptomatic WAT tissue comparing untreated symptomatic WAT tissue in ^{-/-} and *Smn*^{2B/+} mouse model (figure 3.24).



3.3.24 Orally treatment of 12.5 mg/kg/day Pioglitazone downregulated of Thbs1 and Ppar- γ mRNA level in symptomatic WAT (white adipose) tissue in both *Smn*^{2B/-} and *Smn*^{2B/+} SMA mice.

In order to analysis pioglitazone effect on lipid and fatty acid metabolism in adipose, symptomatic white adipose tissue (WAT) was collected from SMA mice untreated/ treated with 12.5 mg/kg/day pioglitazone, and qPCR experiments were performed to evaluate the effect of pioglitazone on the level of targeted genes in WAT tissue. In conclusion, oral administration of 12.5 mg/kg/day pioglitazone leads to downregulate Ppar- γ and Thsb1 target gene expression in symptomatic WAT tissue comparing untreated symptomatic WAT tissue in *Smn*2B/- and *Smn*2B/+ mouse model (Fig3.25).

To understand the multisystemic effects of pioglitazone, especially in a multifaceted disease like SMA, it's crucial to study its impact on glucose, lipid, and energy metabolism, recognizing the necessity and significance of inter-tissue crosstalk. This comprehensive approach has led to the preparation of the following Table 3.5, which aims to provide an integrated view of pioglitazone's effects in the context of SMA, highlighting its influence across different metabolic pathways and tissues.

As a general conclusion, we can suggest that in *Smn*^{2B/-} mice, the primary peripheral targets of pioglitazone are skeletal muscle and adipose tissue. The observed increases in lifespan and weight in these mice might be a result of improvements in the metabolism of these two tissues due to pioglitazone's effects.

Table 3. 3 Pioglitazone has a tissue-specific effect in *Smn*^{2B/-} SMA mice

Tissue Type	<i>Thbs1</i>	<i>Ppar-α</i>	<i>Ppar-γ</i>	Lipid accumulation in liver	Myofiber size in TA	α-motor neuron counting in SC
Triceps	↔	↑	↑		↓	
Liver	↔	↔	↔	↔		
WAT	↓		↓			
Spinal Cord	↔	↔	↑			↔

The chart demonstrates the expression of target genes following pioglitazone application in a symptomatic *Smn*^{2B/-} mouse model, specifically within periphery and CNS tissues. The left block denotes the tissue type, and the upper right block presents the target genes. An upward arrow in blue signifies a rise in gene expression, while a green stripe represents stable mRNA levels. A downward arrow in grey indicates a reduction in gene expression following the application of pioglitazone.

3.4 Discussion

One of the *in-silico*-based-alternative therapeutic options for developing muscle and metabolism-targeted therapies for SMA was predicted to be pioglitazone. It can be assumed that pioglitazone could achieve this effect by regulating specific genes, namely *Thbs1* and *Ppar-α*.

The first stage of the experimental plan was the validation phase. During confirmation, it was observed that in the *Smn*^{-/-}; *SMN2* SMA mouse model, both target genes, *Thbs1* and *Ppar-α*, showed increased expression. Furthermore, in the *Smn*^{2B/-} model, only the *Thbs1* gene exhibited this increase. Conversely, in deltoid muscle samples taken from SMA Type III patients, this pattern is reversed. In other words, while *Thbs1* mRNA levels remain unchanged, *Ppar-α* levels decrease. One possible explanation for this inverse pattern of *Ppar-α* could be the use of different muscle groups in humans and mice; deltoid muscles were used for SMA patients, whereas triceps muscles were used for the SMA mouse model (Talbot and Maves, 2016).

Another potential explanation could be the physiological differences between mice and humans, given that they are different species (Bryda, 2013). On the other hand, the expression pattern of *Ppar-α* and *Thbs-1* may depend on the severity of SMA, and this could be related to its metabolic function. In microarray studies conducted on the skeletal muscles of SMA type I and type III patients, it was observed that in SMA Type I, the skeletal muscle phenotype is characterized by prolonged atrophy, where the muscles' capacity to utilize glucose is limited (Millino et al., 2009b). In contrast, SMA type III patients show a unique co-existence of atrophy and hypertrophy, along with metabolic alterations. Specifically, it was found that in SMA type III, the impairment in glucose metabolism occurs primarily in the final stages of glycolysis (Millino et al., 2009b). This distinction between SMA types I and III highlights the potential link between *THBS-1* and *PPAR-α*'s expression and the metabolic differences observed in these forms of SMA.

In *in vivo* studies, we first measured blood glucose levels to examine the effect of pioglitazone, a diabetic agent, on SMA mice known for their glucose intolerance (Bowerman et al., 2012b). After administering pioglitazone, no change was observed in the blood glucose levels of the *Smn*^{2B/-} SMA mouse models. This could be due to the mice not being in a fasting state during the experiment. Previous studies have shown that in WT mice, blood glucose levels decrease, as

expected, after fasting. However, in *Smn*^{2B/-} SMA mice, high blood glucose levels persist even after fasting, revealing their inability to uptake glucose from circulation, indicating glucose intolerance (Bowerman *et al.*, 2012, 2014). This finding underscores the unique metabolic challenges in SMA mice and the need for tailored approaches in their treatment.

Another key peripheral tissue in glucose metabolism is skeletal muscle. This is crucial because skeletal muscle, being the largest peripheral tissue, plays a vital role in energy metabolism and maintaining metabolic homeostasis (Richter and Hargreaves, 2013). In addition to this, skeletal muscle is responsible for approximately 80% of glucose uptake from circulation, a process that significantly contributes to overall glucose regulation. Understanding the role of insulin receptors located in skeletal muscle (Cerf, 2013), which are involved in the development of insulin resistance and the response to insulin released from the pancreas, is also essential (Teranishi *et al.*, 2007). This highlights the multifaceted role of skeletal muscle in glucose metabolism, emphasizing its importance in both energy management and insulin sensitivity. We found that administering pioglitazone caused markedly elevates *Ppar-α* and *Ppar-γ* expression levels in symptomatic triceps tissues of *Smn*^{2B/-} SMA mice, which can cause a decrease in stress on glucose metabolism abnormalities in *Smn*^{2B/-}. This finding aligns with studies on *PPARγ-loxP* mice mouse models (muscle-specific *Ppar-γ* deletion), which have demonstrated glucose intolerance and progressive insulin resistance, highlighting the vital roles of *Ppar-γ* and skeletal muscle in these processes (Norris *et al.*, 2003). Specifically, in muscle tissue, which predominantly undertakes glucose utilization, *PPAR-γ* amplifies the activation of the GLUT4 receptor via the phosphorylated *IRS-1/PI 3-kinase* pathway (Qin *et al.*, 2003). In the triceps tissues of SMA mice, the increase in *Ppar-γ* induced by pioglitazone suggests a link with GLUT4 and glucose uptake. Establishing this connection is recommended for future studies to fully understand the impact on glucose intolerance under SMA pathology.

The effects of pioglitazone on liver dyslipidaemia have been well established, particularly in cases co-existing with diabetes (Shahid *et al.*, 2012). However, the investigation into the influence of pioglitazone on lipid accumulation & dyslipidaemia in the symptomatic liver tissue of the *Smn*^{2B/-} SMA model revealed no significant changes, either through target gene-mediated pathways or via Oil-red-O assay. Using

the SMA mouse model to study liver lipid metabolism has its challenges. A significant concern is that SMA mice do not develop fibrosis, which is a criterion encompassed within the scope of NAFLD (Deguise et al., 2020). SMA is a multifaceted metabolic disease that affects various peripheral tissues, and several elements influence lipid metabolism in the liver such as the increase of lipid droplets in circulation due to muscle atrophy and the lipolysis in WAT induced by hyperglucagonemia (Deguise et al., 2020). This metabolic complexity presents a significant challenge in studying liver pathophysiology within the SMA disease model.

Due to the metabolic crosstalk existing between the liver, skeletal muscle, and adipose tissue in maintaining metabolic homeostasis, our other peripheral target tissue of interest is adipose tissue (Gastaldelli et al., 2009). A significant decrease in the levels of target genes *Thbs1* and *Ppar-γ* has been observed in SMA mouse models treated with pioglitazone-treated WAT. Consequently, it is conceivable that the *Thbs1* gene may be considered a metabolic gene related to fatty acids, potentially leading to abnormalities in lipid metabolism (Ji and Qiu, 2022). Similarly, an elevated *THBS1* gene level has been identified as a serious risk factor in obese children (Li et al., 2023). In these children, applications of metformin, another anti-diabetic agent, were conducted to reduce the *THBS1* gene level. This treatment with metformin has helped lower the gene level and improve the lipid phenotype (Li et al., 2023). Given that metformin and pioglitazone belong to the same chemical class (Pavo et al., 2003), it is plausible to consider that the increased levels of lipogenic genes in sedentary Taiwanese (*Smn*^{Δ7/Δ7}; *SMN2*^{+/+}) mice (Houdebine et al., 2019), could be ameliorated by reducing the *Thbs1* level. On the other hand, it has been observed that the gene *Ppar-γ* is associated with apoptosis, and a reduction in *Ppar-γ* levels has been linked to decreased apoptosis in the lung tissues of hypertensive mice (Ameshima et al., 2003). Given the observed decrease in *Ppar-γ* during the dissociation of WAT, it would be advisable to further investigate whether this reduction is directly related to apoptosis.

So far, we have discussed tissues such as skeletal muscle, liver, and adipose tissue, which have undergone molecular-level changes in the SMA context when treated with pioglitazone. A common characteristic among these tissues is the energy metabolism support, effectively maintaining homeostasis. The key structure responsible for energy metabolism is the mitochondria, often referred to

as the powerhouse of the cell (Cooper, 2000). Furthermore, pioglitazone has been observed to enhance mitochondrial function, indicated by increased *Ide* levels (Di Donfrancesco et al., 2023) in triceps of a symptomatic SMA mouse model. In studies conducted on SMA models, increased ROS production (Ohtaki, 1990), decrease in the number of mitochondrial DNA (Pons et al., 1996) (Keller et al., 2021), and altered morphology have been observed in relation to the reduction of SMN protein (Ripolone et al., 2015a). The effect of pioglitazone on mitochondria should not be limited to the *IDE* level; counting mitochondrial DNA and conducting morphological assessments are recommended. This approach could provide a more comprehensive understanding of pioglitazone's impact on mitochondrial dynamics and function in SMA.

In the context of skeletal muscle structure after pioglitazone treatment, a notable observation was the reduction in myofiber sizes. Furthermore, qPCR assays indicated that there was no significant change in the mRNA levels of the atrogenic markers *Atrogin-1* and *MuRF1* in the skeletal muscle of *Smn*^{2B/-}. In a related vein, research focusing on the *SMNΔ7* SMA mouse model has explored the deletion of muscle atrophic markers like *Atrogin1* or *MuRF1*, aiming to prevent muscle atrophy. While the deletion of *Atrogin-1* did not significantly impact the weight and survival of SMA mice, the deletion of MuRF1 notably reduced their survival rate (Iyer et al., 2014). These findings suggest that in the pathology of SMA atrophy, other muscle ubiquitin ligases, in addition to *Atrogin-1* and *MuRF1*, might play a crucial role. Conversely, pioglitazone has shown promise in preventing muscle atrophy in SBMA by activating *Ppar-γ* and reducing oxidative stress (Iida et al., 2015). Therefore, it is plausible to consider that pioglitazone improves muscle strength by enhancing energy metabolism in muscle tissues instead of preventing atrophy (Yokota et al., 2017), as evidenced by observed increases in muscle strength as a result of RR test (Shea et al., 2011).

Regarding the effects on the SC, pioglitazone stands out as a potential therapeutic agent for SC tissues, particularly due to its capability to penetrate the blood- brain barrier efficiently (Berger and Moller, 2002). Crucially, pioglitazone demonstrates neuroprotective effects, such as reducing neuroinflammation by regulating microglia activity and safeguarding neurons after brain and spinal cord injuries by bolstering mitochondrial bioenergy and integrity (Liu et al., 2017; Patel et al., 2017). In the *Smn*^{2B/-} SMA model, the mRNA level of *Fas* and *Pmaip-1* were downregulated following pioglitazone treatment. The significance of this finding is further highlighted by the understanding that increased expressions of

Fas and *Pmaip-1* genes in SMA spinal cord led to apoptosis (Murray et al., 2015a). The reduction in the levels of these genes following pioglitazone treatment indicates a potential to inhibit apoptosis in SMA spinal cord pathology. Further research on the effects of pioglitazone on health of SC was conducted using Nissl staining, which found that pioglitazone did not induce significant changes in α -motor neurons. Following spinal cord injury, treatment with pioglitazone led to a significant increase in white matter preservation (McTigue et al., 2007). Based on the observed effects, it seems plausible that pioglitazone may prevent apoptosis in various components of the spinal cord, such as astrocytes found in the white matter, rather than exclusively affecting α -motor neurons, which are primarily located in the gray matter. Importantly, it has been found that although *Fas* and *Pmaip-1* genes are modulated, motor neurons continue to undergo apoptosis (Martin et al., 2005). This finding implies that even when genes directly associated with apoptosis are suppressed, MNs can still perish due to other mechanisms. This underlines the multifaceted and complex nature of neurodegenerative processes.

Taking into account these factors, pioglitazone emerges as a promising candidate for a second-generation treatment for SMA, ameliorating the SMA phenotype in *Smn*^{2B/-} mouse model. This was evidenced by improvements in weight, survival rates, RR and regulating genes playing various roles of metabolic homeostasis, along with its protective impact on the integrity of the spinal cord. Altogether, in the case of SMA, which exhibits a multi-systemic phenotype, a therapeutic approach targeting multiple peripheral tissues could yield more promising results in terms of treatment.

4 Melatonin

4.1 Introduction

The enhancement of the *Smn*^{2B/-} phenotype by pioglitazone and its observed impact on the expression of tissue-specific target genes underscores the strength of our comprehensive *in silico* strategy. This strategy, which melds bioinformatics and drug repurposing, is recognized as a formidable approach for anticipating new, advanced treatments targeting the muscular and metabolic defects associated with SMA. Building on this strong *in silico* method, the second phase of our project has identified melatonin as another promising candidate, speculated to have a significant influence on the pathology. Furthermore, melatonin initially identified as a neurohormone secreted by the pineal gland, plays a vital role in regulating circadian rhythms, including the sleep- wake cycle and proves effective in treating sleep disorders (Hardeland et al., 2006), which are already dysregulated in SMA mouse model (Lisa M Walter et al., 2018) and patients, including abnormal sleep (Pera et al., 2017), altered sleep microstructure (Verrillo et al., 2014) and hypercapnia (Bersanini et al., 2012) .

The notable finding from the combine *in silico* analysis was melatonin's recurrent identification across three separate analyses, suggesting its potential to downregulate *Per-1*, *Bcl-2*, *Sirt-1* and *Ror-α* genes, as depicted in figure 4.1. Thus, melatonin stands out as a viable contender for developing second-generation combinatorial therapies aimed at SMA-associated muscular pathologies.

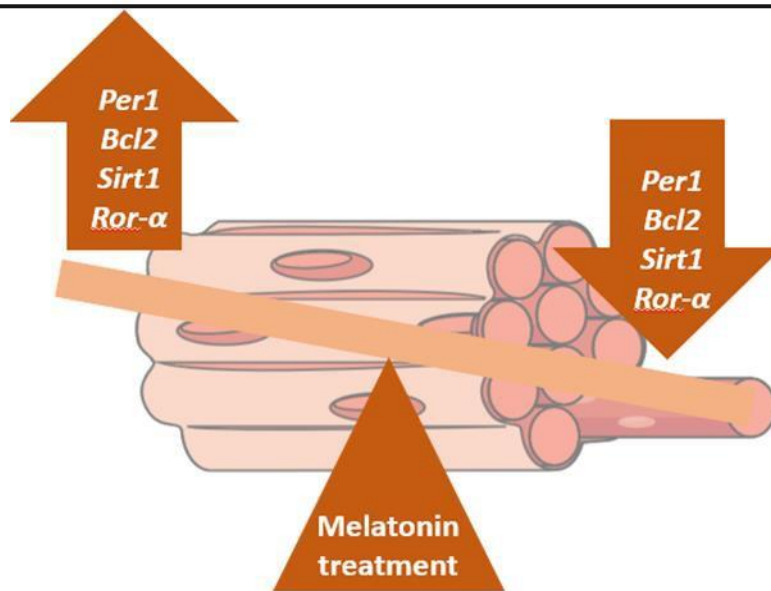


Figure 4. 1 In silico analyses predicted that the expression of the genes Per-1, Bcl- 2, Sirt-1 and Ror- α genes was increased in SMA skeletal muscle and could be downregulated by melatonin treatment.

Recent research has unveiled that not only the pineal gland but also every cell in the body possesses the unique capability to synthesize melatonin at various levels (Rong, Wu and Sun, 2020). Although locally produced, melatonin is underscored for its substantial role in modulating numerous metabolic functions and contributing to the overall physiological equilibrium, it is fundamentally associated with circadian rhythms and antioxidative capacity (Tordjman et al., 2017). This revelation underscores the extensive influence of melatonin across diverse bodily systems, highlighting its significance beyond mere sleep regulation (Samanta, 2022).

The one of the observing the effects of melatonin beyond its primary scope, reveals that melatonin influences liver development and functions through a variety of pathways (Sato et al., 2020). The first of these is related to its antioxidant property. In the liver, pathological fat accumulation leads to increased production of ROS, which in turn causes oxidative stress and liver damage in obese (ob/ob) mice (de Luxán-Delgado et al., 2016). Melatonin can neutralize these ROS types, thereby reducing oxidative stress via activating *Ror- α* in senescence-accelerated mice (SAMP8) (Caballero et al., 2008). The other two pathways focus on inhibiting lipid accumulation. The first one is that suppressing de novo lipogenesis in Syrian hamsters with dyslipidaemia by decreased actions of the hepatic lipogenic enzymes, ACC and FAS (Ou et al., 2019).

The second one is that supporting mitochondrial functions, which promotes the oxidation of free fatty acids in HFD-fed mice via activating *SIRT1* (Das et al., 2017). Regarding why melatonin's effects on the liver are particularly intriguing for SMA: a study identified hyperlipidaemia and liver steatosis in 72 SMA patients (Deguise et al., 2019a). Additionally, *Smn*^{2B/-} mice exhibit a phenotype similar to non-alcoholic fatty liver disease.

Melatonin demonstrates its effects not just limited to the liver, but also in pancreatic tissue. Remarkably, melatonin exhibits its beneficial effects even under conditions of ER stress in insulinoma INS-1 cells (pancreatic β -cells), enhancing insulin release (Yoo, 2013). Moreover, melatonin showcased its protective capabilities by safeguarding beta islet cells from apoptosis, a condition correlated with augmented ROS production in hyperglycaemic condition (Park et al., 2014). This protective effect directly overlaps with studies conducted both on *Smn*^{2B/-} SMA mouse models and SMA patients, which have already established the reduced number of insulin-producing β cells (Bowerman et al., 2012). In addition to triggering insulin release, melatonin indirectly supports pancreatic function by strengthening insulin sensitivity in the liver, adipose tissue, and muscles (She et al., 2009; Zanuto et al., 2013). Furthermore, its potential to correct the pathology in *Smn*^{2B/-} mice and SMA patients with glucose resistance highlights its significant role in addressing this aspect of the disease (Bowerman et al., 2012).

Melatonin's target tissue overlapping with SMA pathology is skeletal muscle, too. Studies conducted on SMA mouse models and patients have identified delays in myogenesis, muscle atrophy, weakness, and aberrant expression of muscle-specific proteins (Deymeer et al., 1997; Kim et al., 2020; Martínez-Hernández et al., 2014; Waisman et al., 2021). Melatonin, by promoting myogenesis and decelerating muscle atrophy in skeletal muscles, becomes a compound worth investigating for SMA. Specifically, Melatonin is suggested to have an impact on skeletal muscle by its ability to alleviate oxidative stress, apoptosis, and inflammation, as demonstrated in research by Ochoa et al. in 2011 and Borges et al. in 2015. To illustrate, melatonin has been shown to suppress pro-inflammatory cytokines like tumor necrosis factor alpha (TNF- α) and interleukin (IL)-6 in skeletal muscles by deactivating NF-kB (Tezze et al., 2017).

When it comes to CNS, melatonin's beneficial role comes from neuroprotection which is gaining significant attention, largely because of its capacity to neutralize free radicals (Lee et al., 2019). The observation that human neuroblastoma cell lines show increased mRNA levels of antioxidant enzymes such as superoxide dismutases (SODs) and glutathione peroxidase (GPx), after treatment with melatonin (Mayo et al., 2002). The retrospective analyses of the PRO-ACT database suggest that melatonin may slow disease progression in patients with ALS (Bald et al., 2021). This potential effect of melatonin in ALS is attributed to its properties as an antioxidant and a scavenger of free radicals (Bald et al., 2021). High-dose melatonin has shown promising results in extending the lifespan of SOD1^{G93A}- ALS transgenic mice (Weishaupt et al., 2006). Additionally, this treatment led to a significant reduction in serum protein carbonyls, which are indicators of oxidative stress and were notably high in a varied group of sporadic ALS patients prior to receiving melatonin (Weishaupt et al., 2006). ALS and SMA, both being motor neuron diseases, have been found to share significant overlaps in their molecular pathologies (Bowerman et al., 2018). Considering the shared molecular characteristics, investigating the efficacy of treatments like melatonin, which have shown promise in improving ALS phenotypes, could be crucial for SMA therapy as well.

In SMA pathology, where mitochondria play a crucial role in both the CNS and periphery, the potential impacts of melatonin on mitochondria become particularly interesting. Melatonin treatment was found to preserve the levels of the *PGC1-α* level, which is downregulated in muscle biopsy samples from SMA patients (Ripolone et al., 2015a). Moreover, the activation of this pathway, as observed in ALS models, led to delayed muscle atrophy and significantly improved muscle endurance (Da Cruz et al., 2012). This observation strongly supports the idea that melatonin could contribute to SMA pathology by promoting mitochondrial biogenesis in skeletal muscle.

In skeletal muscles of SMA patients with Type I, II and III, a reduction in mtDNA (Chemello et al., 2023a; Ripolone et al., 2015b), and impaired oxidative phosphorylation have been observed (Ripolone et al., 2015b). In the context of mitochondrial disorders, melatonin has been shown to play a significant role in activating cell death programs, particularly under conditions of oxidative stress-induced damage, helping in the elimination of impaired cells (Hong et al., 2014). Consequently, an effective approach in treating SMA may involve the use of

melatonin to enhance mitochondrial health and facilitate the mitophagy process, thus addressing these mitochondrial dysfunctions.

Considering the potential effects of melatonin on the development and metabolism of various tissues in periphery and CNS, its examination is crucial for diseases like SMA, which are both multisystemic and neurodegenerative in nature.

4.2 Methods

4.2.1 In vitro

C2C12 myoblast cells in the proliferation phase were evenly distributed across 6-well plates, with four wells allocated for each group. When the C2C12 myoblast cells achieved 50-60% confluency, and the C2C12 myotubes had differentiated to the D7 stage, they underwent treatment. This involved exposure to melatonin (Sigma-Aldrich), which was prepared in 70% ethanol. The cells received varied concentrations of Melatonin, specifically 10, 100, and 1000 μM , and were treated for a duration of 24 hours. A control group was also included, where the cells were treated solely with ethanol at a concentration of 0.32% v/v. The same concentrations of insulin were also applied to both the 60-70% confluent LHCN-M2 cell line and the D7 LHCN-M2 cells for a duration of 24 hours.

4.2.2 In Vivo

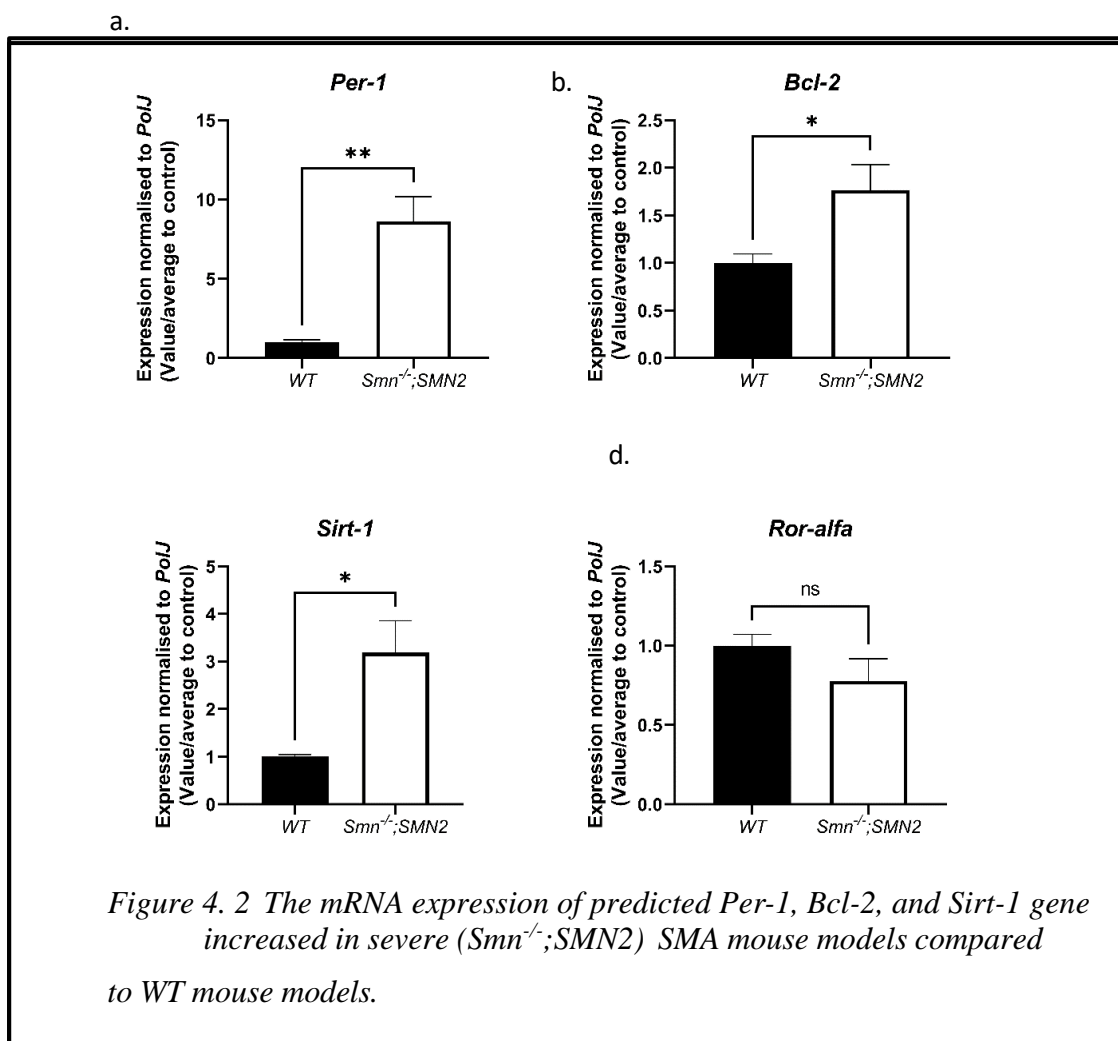
The study extended to *in vivo* experiments, focusing on $Smn^{2B/-}$ SMA and $Smn^{2B/+}$ healthy mice. These mice underwent daily phenotypic assessments starting from the day P0. By P5, the mice were assigned to different treatment groups: untreated, vehicle treatment (0.5% CMC), and melatonin (Sigma-Aldrich) at varied dosages of 25, 50, and 100 mg/kg per day. For the administration of melatonin, dissolved in 0.5% CMC, utilized a 25 μl syringe (by Hamilton) coupled with a 1.25mm gavage needle (from Cadence Science). This treatment regimen was sustained until reaching the humane endpoint, ensuring that each group comprised over 10 mice. On the P18, the skeletal muscles (specifically Triceps brachii and TA), liver, pancreas, white adipose tissue, brown adipose tissue and spinal cord, were collected from both the untreated and melatonin-treated $Smn^{2B/-}$ SMA and $Smn^{2B/+}$ mice, precisely two hours post the final treatment session. In addition to tissue collection, blood glucose levels (measured in mmol/L) of the non-fasted pups were promptly determined after euthanasia, utilizing the True Metrix Go (Trividia Health).

4.3 Results

4.3.1 There is an observed increase in the mRNA levels of *Per-1*, *Bcl-2*, and *Sirt-1* in skeletal muscle tissue symptomatic *Smn*^{-/-};*SMN2* mice.

Our *in silico* analyses predicted that the expression of *Per1*, *Bcl2*, *Sirt1* and *Ror- α* genes is increased in SMA skeletal muscle and can be downregulated by melatonin treatment. In the preliminary stage of our research, we focused on measuring the levels of specific genes, namely *Per-1*, *Bcl-2*, *Sirt-1*, and *Ror- α* , in the triceps muscle of Severe SMA mice exhibiting symptoms on day P7. We compared these levels with those in WT. Our analysis revealed a notable increase in the expression of *Per-1*, *Bcl-2*, and *Sirt-1* in the symptomatic mice's skeletal muscle, as depicted in figure 4.2.

However, no change was detected in the levels of *Ror- α* . These findings confirm our initial bioinformatics predictions and further suggest a potential role for the genes *Per-1*, *Bcl-2*, and *Sirt-1* in the development of muscle-related pathologies.

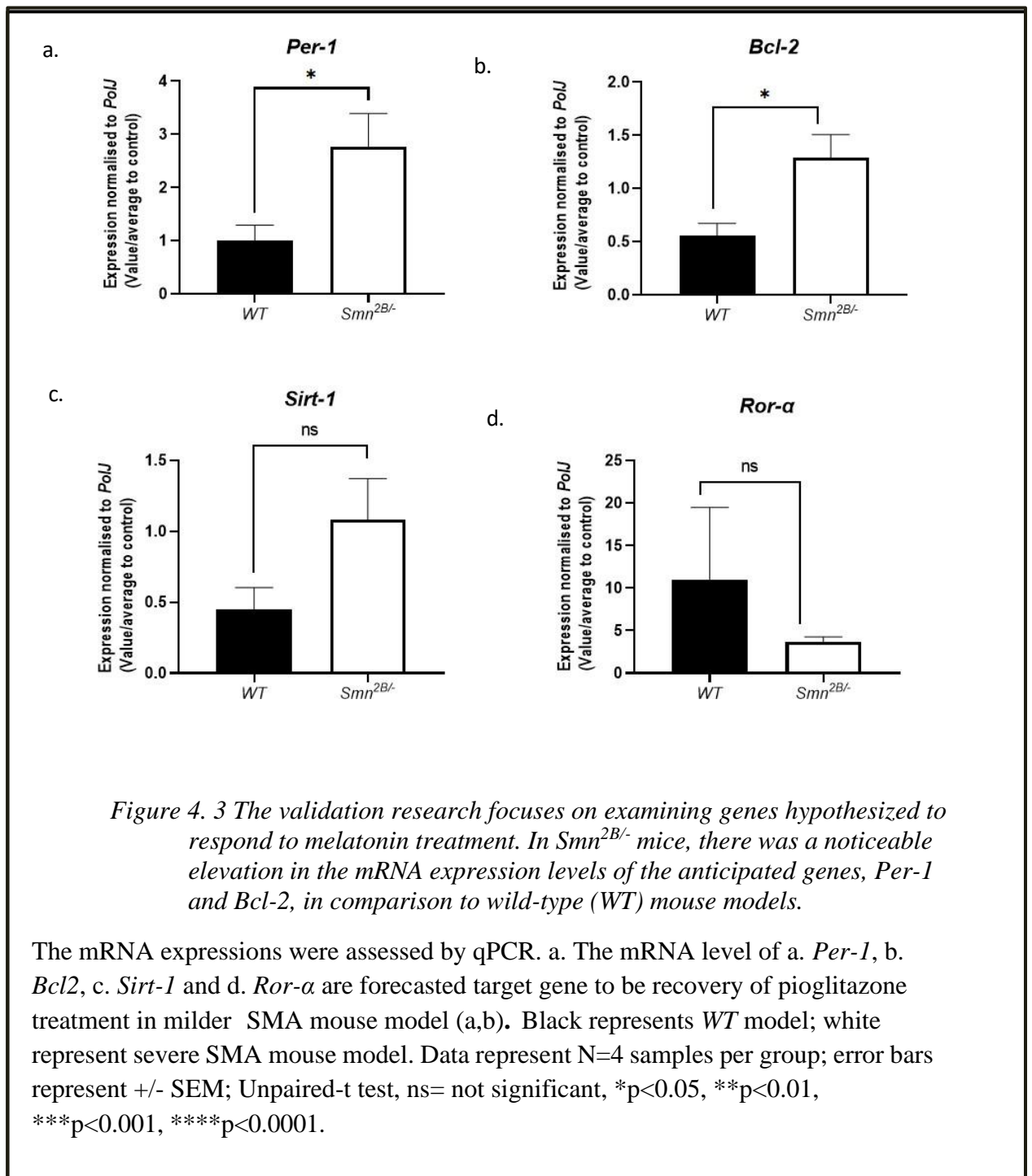


The mRNA expressions were performed by qPCR. a. The expression level of *Per-1*, b. *Bcl-2*, c. *Sirt-1* and d. *Ror-α*. Black represents healthy model; white represents severe SMA mouse model. Data represent N=4 samples per group; error bars represent +/- SEM; Unpaired-t test, *p<0.05, **p<0.01, ***p<0.001.

4.3.2 The expression levels of *Per-1* and *Bcl-2* mRNA are elevated in skeletal muscle of symptomatic *Smn^{2B/-}* Mice

Next validation study was carried out on the triceps muscle of *Smn^{2B/-}* at P18. When we compared these milder SMA models to their WT counterparts, we discovered an enhanced expression of *Per-1* and *Bcl-2* genes. Interestingly, no significant alteration was detected in the mRNA expression levels of *Sirt-1* and *Ror-α*, as detailed in figure 4.3. This pattern suggests that the expression of *Sirt-1* may vary depending on the severity of the SMA phenotype.

To sum up, increased *Per-1* and *Bcl-2* gene expression is noted in milder forms of SMA mouse model, while *Sirt-1* and *Ror-α* levels remain unchanged.



4.3.3 The predicted targeted gene, *PER-1* level is decreased in Type III SMA deltoid myoblasts.

In the next stage of our investigation, we examined whether the genes influenced by melatonin—specifically *PER1*, *BCL2*, *SIRT1*, and *ROR-α*—were also modified in human patients with SMA.

Our data indicated a reduced expression of *PER-1* in the myoblasts from Type III SMA patients relative to those from healthy donors (refer to fig 4.4.a). This observation contrasts with our earlier findings in the severe SMA mouse model, where there was an upregulation of *PER-1*. Furthermore, the expression levels of *BCL2* and *SIRT1* did not show any significant changes in Type III SMA myoblasts in comparison with controls (see Fig 4.4.b; 4.4.c). To sum up, it's observed that the level of the predicted target gene, *PER-1*, is diminished in the deltoid myoblasts of Type III SMA.

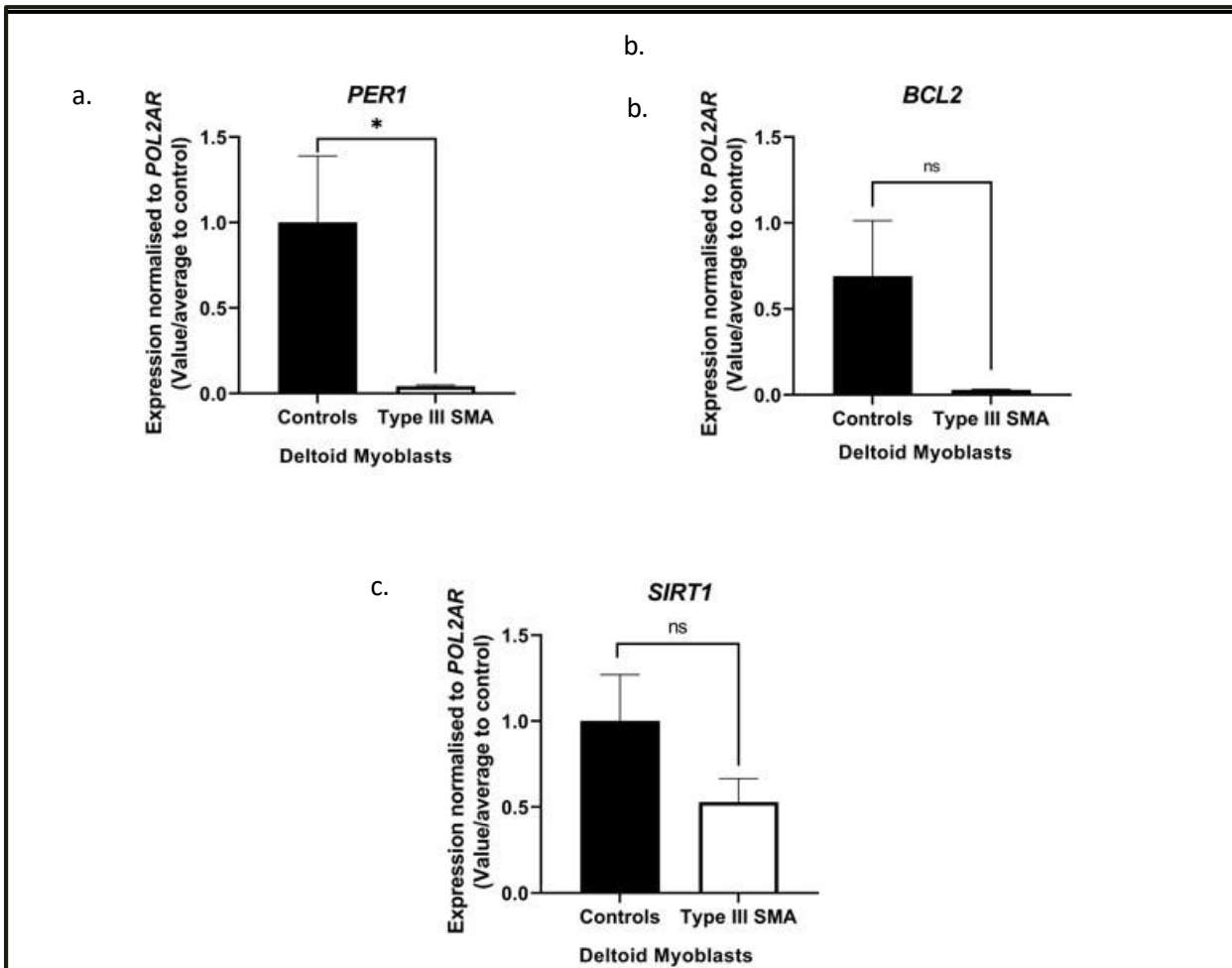


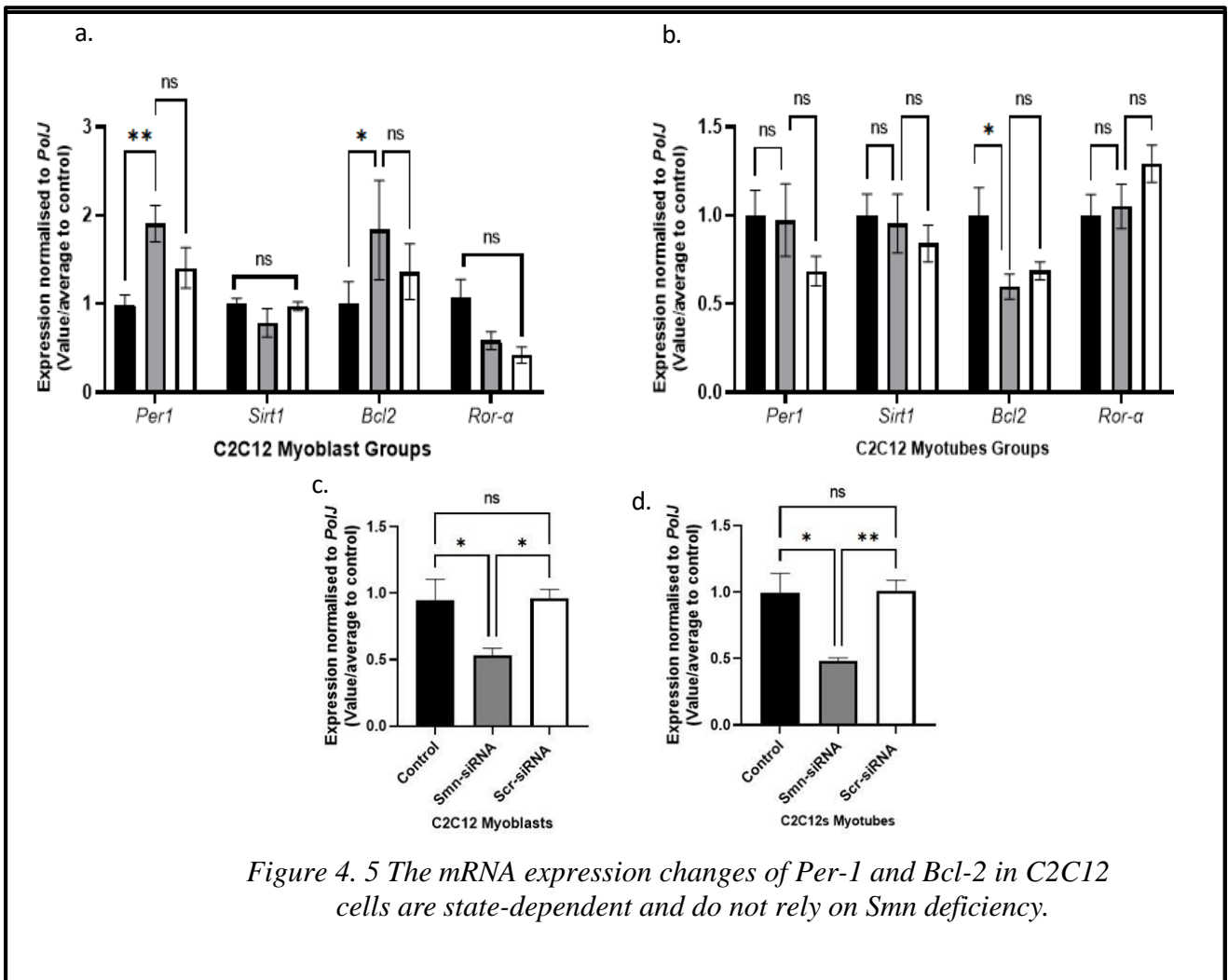
Figure 4. 4 The pioglitazone target gene, *PER-1*, significantly downregulated in Type III SMA deltoid myoblasts.

The mRNA expressions were performed by qPCR. The expression level of a. *PER-1* b. *BCL-2* and c. *SIRT-1* in primary myoblast from deltoid muscle biopsies from controls and Type III SMA patients (N=6). Each black bar represents a healthy person, and each white bar represents Type III SMA patient; error bars represent +/- SEM; unpaired t-test, ns= not significant, *p<0.05, **p<0.01, ***p<0.001, ****p<0.0001.

4.3.4 Changes in the Expression Levels of Target Genes Are Independent of *Smn* Deficiency in C2C12s model.

We expanded our research to detect if these gene expressions were depending upon the *Smn* gene. After confirming the reduction of *SMN* gene expression in both myoblasts (figure 4.5.c.) and myotubes (figure 4.5.d.) our study then focused on examining the expression patterns of target genes.

Black bars depict the baseline control of unaltered C2C12s cells. Cells treated with non-targeting scrambled SiRNA are indicated by white bars as a control for specificity. Grey bars (*Smn*-SiRNA) indicate the C2C12s cells with a targeted knockdown of the *Smn* gene. Our findings indicate that the alterations in the *Per-1* and *Bcl-2* gene expressions are independent of the *Smn* gene, as there is no significant difference in the levels of *targeted genes* between the *Smn*-siRNA and Scrambled siRNA groups of both D0 and D7 C2C12s (shown in figure 4.5.a and 4.5.b).



The mRNA expressions were performed by qPCR. a. The expression level of *Per-1*, *Bcl-2*, *Sirt1* and *Ror- α* in Smn-KD myoblast form of C2C12s b. The pattern of target genes is shown in D7 Smn-depleted C2C12S. c. *Smn* gene level in C2C12s myoblast. d. *Smn* gene level in C2C12s myotubes. Black represents positive control, grey represent Smn-KD form of C2C12s, white show scrambled-SiRNA in C2C12s. Data represent N=4 samples per group across two-independent experiments; error bars represent +/- SEM; Two-way ANOVA with post-hoc uncorrected Fishers LSD test, ns=not significant, *p<0.05, **p<0.01, ***p<0.001, ****p<0.0001.

4.3.5 In D8 C212s, there was no change in the expression levels of melatonin- predicted target genes.

Our next-step aimed to delve into the association between melatonin-targeted genes and muscle atrophy. Upon evaluating gene expression in serum starved, atrophic C2C12 cells (depicted by white bars in figure 4.6) versus non-starved controls (represented by black bars in figure 4.6), we found that the expression levels of our target genes did not significantly alter.

In the C2C12 model, it was determined that melatonin does not have an effect on atrophy through its impact on target genes.

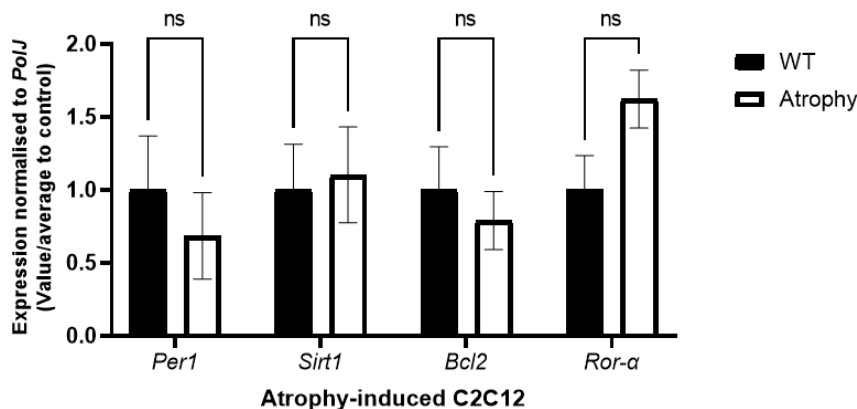


Figure 4. 6 The expression levels of genes targeted by melatonin does not associate with atrophy in C2C12 cells

The mRNA expressions were performed by qPCR. a. The target genes levels are in atrophy induced C2C12s. Black represents positive control, white shows serum-starvation-induced atrophy C2C12s model. Data represent N=4 samples per group across two-independent experiments; error bars represent +/- SEM; Two-way ANOVA with post-hoc uncorrected Fishers LSD test, ns=not significant. *p<0.05, **p<0.01, ***p<0.001, ****p<0.0001.

4.3.6 Melatonin's effects on the expression of predicted-targeted genes vary depending on the dosage and the differentiation status of the cells in C2C12s.

In the next phase of our study, we investigated the potential therapeutic effects of melatonin on its target genes using D0 and D7 C2C12s cells. Previous studies have demonstrated that melatonin shows dose-dependent effects on the C2C12 cell line, with applications of 0.1, 0.2, 0.5, 1, and 2 mM resulting in varied responses after 24 hours (Kim, Kim and Yoo, 2012). Based on this, we applied melatonin in three different concentrations—10, 100, and 1000 micromolar—to the C2C12 cell line over a 24-hour period. We administered melatonin to proliferating C2C12 cells at 10 μ M (represented by white bars), 100 μ M (represented by dark grey bars), and 1000 μ M (represented by light grey bars). We noted a significant decrease in the expression of the candidate gene *Per1* in myoblasts at the highest melatonin concentration (figure 4.7.a). Similarly, both at the same high concentration and at lower concentrations of melatonin, we observed a reduction in the expression level of *Per1* in the myotube form. Furthermore, there was an increase in *Bcl2* levels in D7 C2C12s following the application of 100 micromolar melatonin (figure 4.7.b.).

These changes in expression levels, resulting from the melatonin treatment, suggest that melatonin can influence the expression of its target genes in state- and dose-dependent manner.

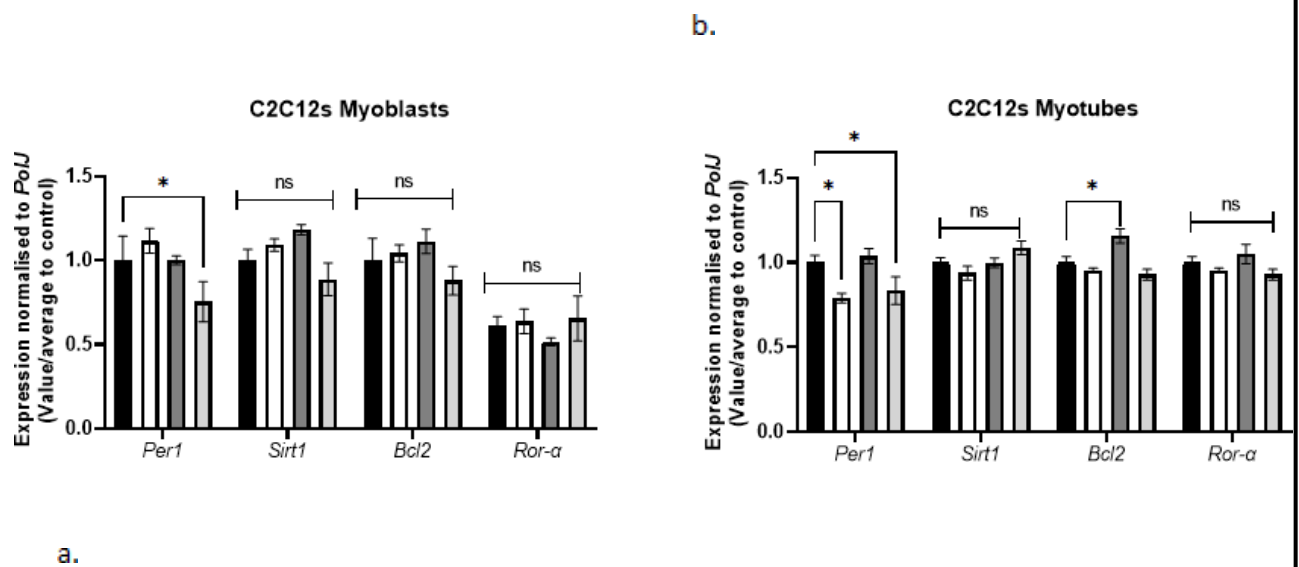


Figure 4. 7 The application of 1mM melatonin has downregulated the Per1 gene level in both myoblast and myotube forms.

The mRNA expression of pioglitazone target genes *Per1*, *Bcl2*, *Sirt1* and *Ror-α* were performed via qPCR. a. myoblast and b. myotubes form of C2C12s were treated for 24-hours by 10μM (white), 100μM (dark grey) and 1000μM (light grey) and without any treatment/control (black). Data represent N=4 samples per group across two-independent experiments; error bars represent +/- SEM; Two-way ANOVA with post-hoc uncorrected Fishers LSD test, ns= not significant, *p<0.05, **p<0.01, ***p<0.001, ****p<0.0001.

4.3.7 Melatonin has no negative effect on proliferation of C2C12s.

Moving forward to determine whether melatonin has a negative effect on the proliferation of C2C12 cells. The corresponding chart illustrates the following groups: control group with BrdU-labelled, untreated proliferating C2C12 cells (represented by white bars); a solvent control group (indicated by dark grey bars); and the group treated with the highest melatonin dose (light grey bars) as shown in figure 4.8. The results demonstrate that neither melatonin nor its carrier (ethanol) adversely affect the proliferation stage of C2C12 cells, as there is no statistically significant difference in proliferation rates between the positive control and the groups treated with the highest dose of melatonin and its equivalent volume carrier.

In the study, it was observed that in C2C12 cells, neither the highest concentration of melatonin nor an equivalent volume of vehicle affects cell proliferation.

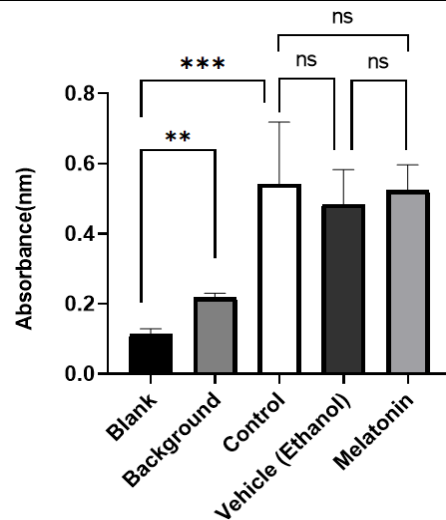


Figure 4. 8 The highest dose of melatonin does not negatively impact myoblast proliferation over 24-hour treatment periods.

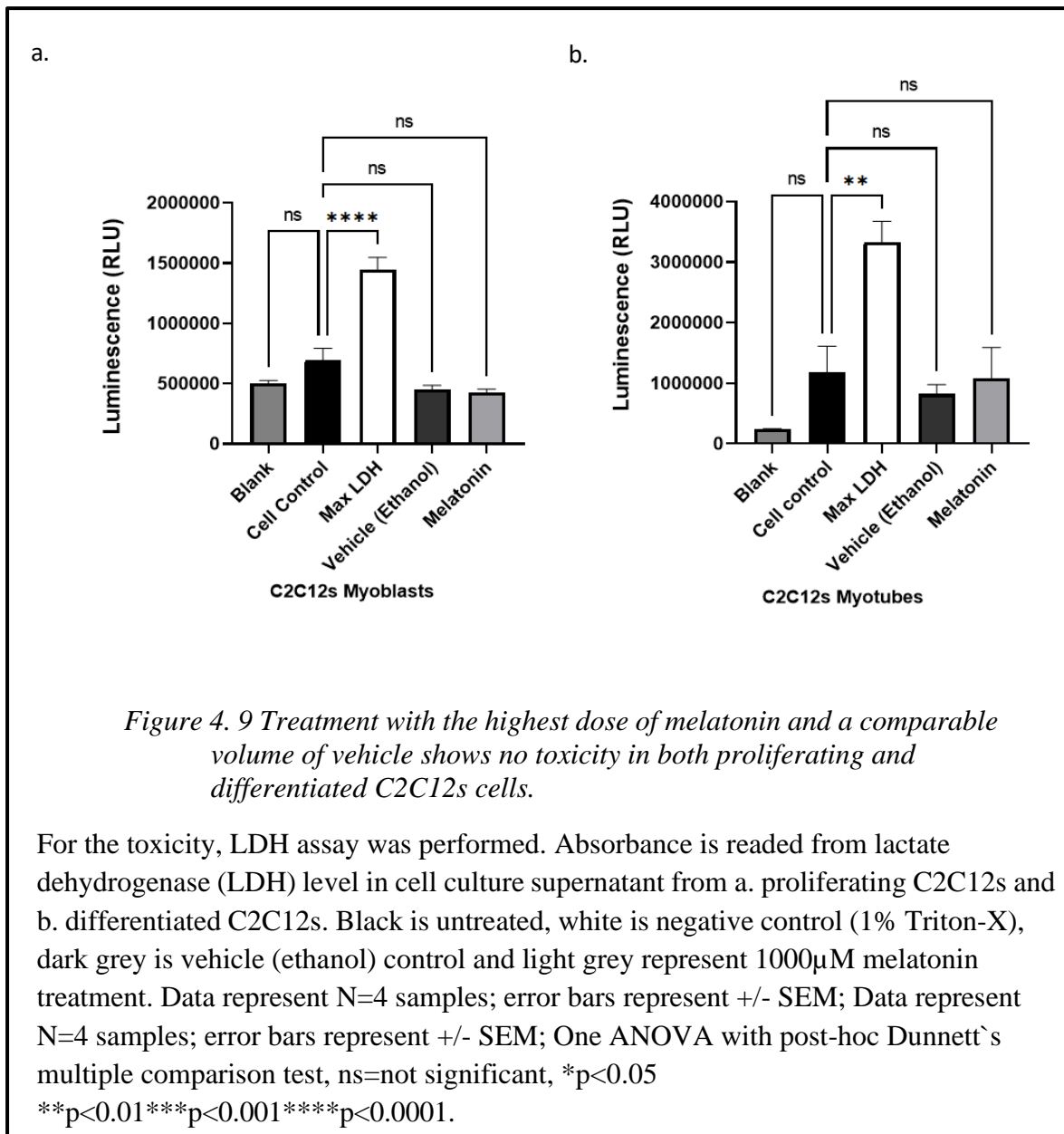
We measured the absorbance wavelengths (nm) for various conditions: blank (media only), background (cell presence), and C2C12 myoblasts treated with either an anti-BrDU antibody, vehicle (Ethanol), or 1000 μ M melatonin for 24 hours. The results of the BrDU assay are presented in panel 'a.' Data were obtained from four samples per group, spanning two independent experiments. Error bars represent the standard error of the mean (SEM). Statistical analysis was performed using one-way ANOVA, followed by Dunnett's post-hoc test. Notations for statistical significance are as follows: ns = not significant, * $p < 0.05$, ** $p < 0.01$, *** $p < 0.001$, **** $p < 0.0001$.

4.3.8 Melatonin shows no toxic effects on the proliferation or differentiation of C2C12 cells over a 24-hour treatment period.

In our examination, we sought to determine the potential toxic effects of melatonin on both proliferating (figure 4.9.a) and differentiating cells (figure 4.9.b). The assay included a background control for signal baseline without cells, a cell control (black bar) representing normal LDH release from healthy cells, and a negative control (white bar) indicating LDH release upon cell death induced by 0.1% Triton-X. A

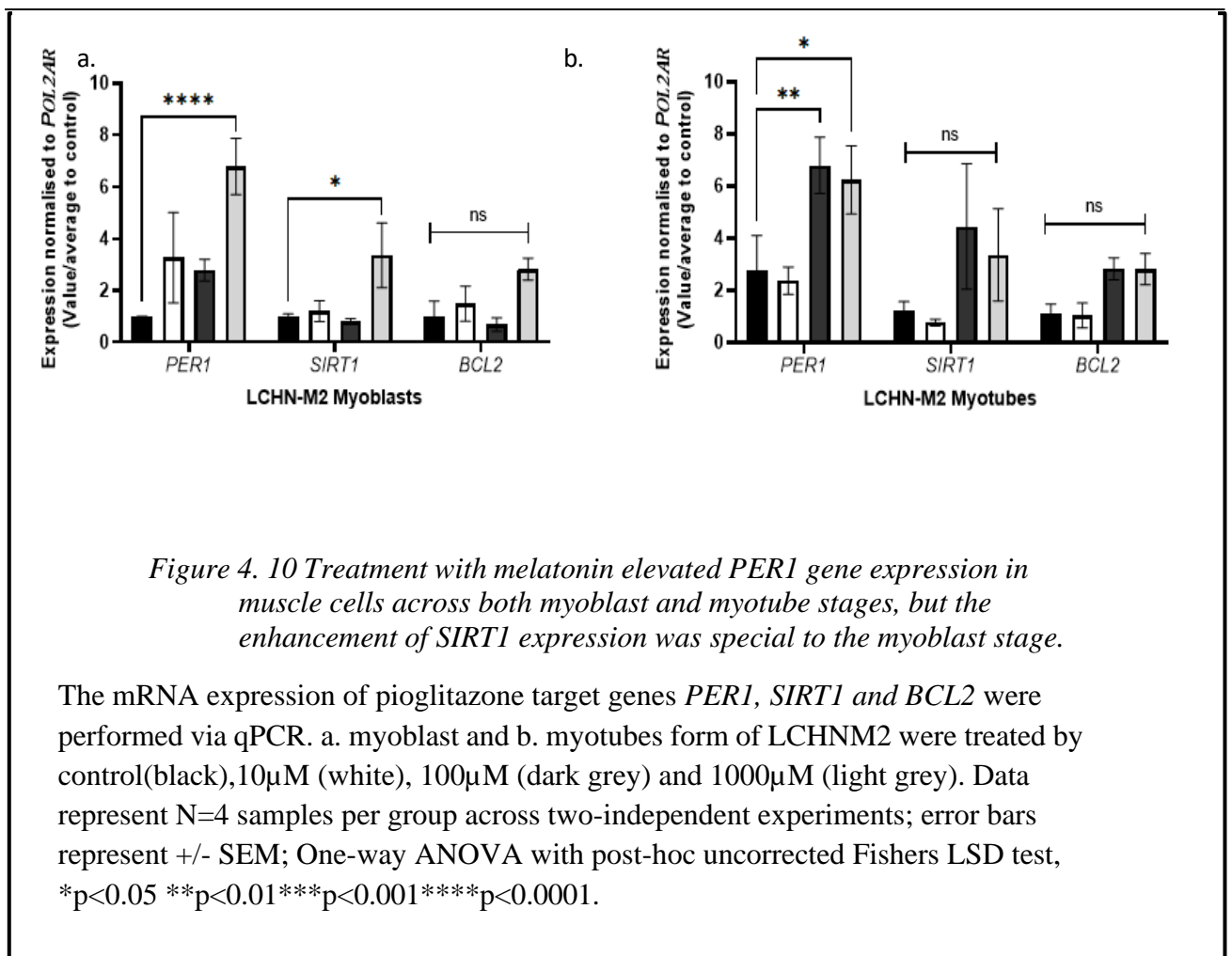
vehicle control (dark grey bar) and the highest dose of melatonin (light grey bar) were also evaluated.

The results demonstrated that the maximum concentration of melatonin, as well as the vehicle (Ethanol), did not cause toxicity in either the initial D0 or D7 stages of C2C12s cell with LDH levels not reaching toxic thresholds when measured against the negative control.



4.3.9 Melatonin treatment increased the expression of *PER1* in both myoblast and myotube forms of LCHN-M2, while it only increased *SIRT1* expression in the myoblast form of LCHN-M2.

Our study also delves into the effects of melatonin on gene expression in human muscle cells, to discern its pharmacological impacts. We treated proliferating LCHN- M2 cells with varying doses of melatonin for a 24-hour duration. The doses were set at 10 μM (indicated by white bars), 100 μM (dark grey bars), and 1000 μM (light grey bars). Notably, after administering 1000 μM of melatonin, we detected an upsurge in the expression levels of the target genes *PER1* and *SIRT1* in the myoblasts (figure 4.10.a). We then subjected differentiated LCHN-M2 cells, or D7 myotubes, to the same range of melatonin concentrations for an equivalent time span. In these differentiated cells, we observed a similar trend in *PER1* gene expression upon exposure to 100 and 1000 μM melatonin treatments, as reflected in figure 4.10.b. Therefore, melatonin exhibits a dose and state-dependent effect on LCHN-M2, as well.



4.3.10 The highest dose of melatonin does not adversely affect myoblast proliferation of LCHN-M2 over 24-hour treatments.

In our continued research, we plan to evaluate the effects of melatonin on the proliferation of LCHN-M2 cells. Through a comparative study using the BrdU labeling technique, we compared the proliferation rates of LCHN-M2 cells with and without melatonin treatment. The findings are represented in figure 4.11., which shows the following groups: the control group of untreated, BrdU-labeled LCHN-M2 cells (white bars), the vehicle control group (dark grey bars) that received the same volume of solvent, and the melatonin-treated cells with the highest dose (light grey bars). Our results suggest that melatonin treatment at the doses tested does not negatively impact the growth of LCHN-M2 cells during the proliferation stage.

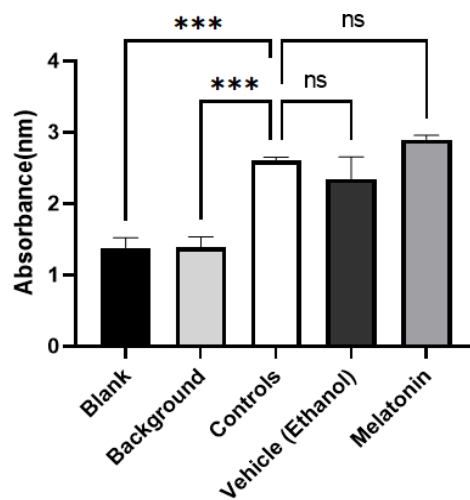
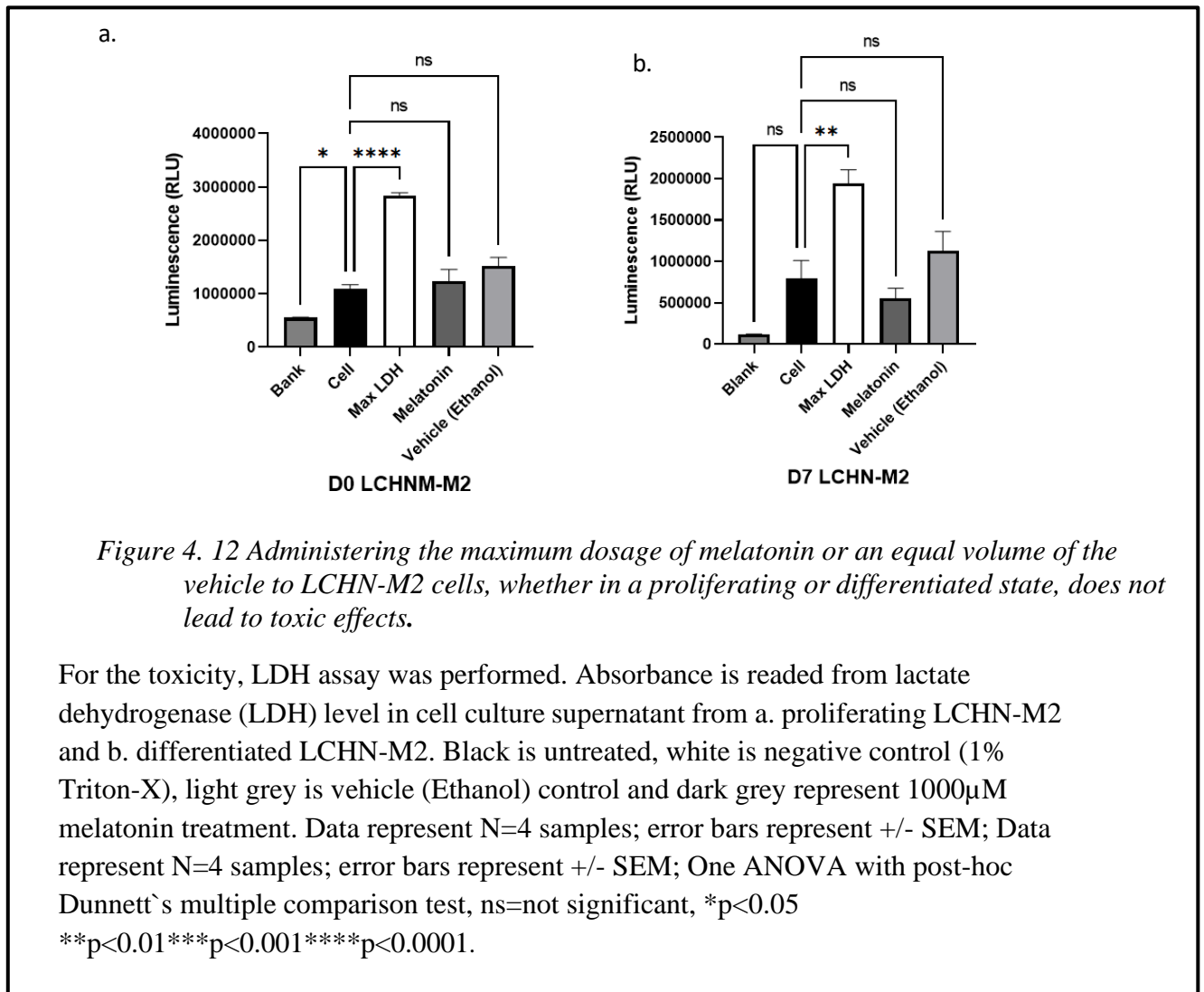


Figure 4. 11 The highest dose of melatonin and its vehicle do not adversely affect myoblast growth over 24-hour treatments.

We measured the absorbance wavelengths (nm) for various conditions: blank (media only), background (cell presence), and LCHN-M2 myoblasts treated with either an anti-BrDU antibody, vehicle (Ethanol), and 1000 μ M melatonin for 24 hours. Data were obtained from four samples per group, spanning two independent experiments. Error bars represent the standard error of the mean (SEM). Statistical analysis was performed using one-way ANOVA, followed by Dunnett's post-hoc test. Notations for statistical significance are as follows: ns = not significant, * $p < 0.05$, ** $p < 0.01$, *** $p < 0.001$, **** $p < 0.0001$.

4.3.11 Melatonin does not exhibit toxic effects on LCHN-M2 human muscle cells in either proliferated or differentiating stages over a 24-hour treatment duration.

In this phase of our study, we aimed to determine if melatonin has any toxicity on LCHN-M2. Our testing protocol included controls: a background control that measures the signal emanating exclusively from the assay reagents in the absence of cells; a cell control that provides a baseline LDH release from healthy, intact cells (black bar); and a positive control (white bar) that measures LDH release following cell lysis induced by 0.1% Triton-X. A vehicle control (light grey bar) was also used, alongside an assessment of the effects from the maximum concentration of melatonin (dark grey bar). Our analysis indicated that neither the highest dose of melatonin nor the corresponding amount of vehicle (Ethanol) caused toxicity in LCHN-M2 cells at either the initial (D0) or advanced (D7) stages of growth.



To sum up:

In the table below, an initial focus was about confirmation the expression patterns of predicted -targeted genes come from combined *in silico* analysis, using both *in vitro* and *in vivo* SMA models. These models included *Smn*^{-/-};SMN2, and *Smn*^{2B/-} mouse models, Type III SMA patient myoblast samples, and myoblast/myotube C212s with *Smn*- siRNA gene transfection to reduce *Smn* gene expression. The final model, atrophy C212, was chosen for its alignment with the canonical SMA phenotype. During the validation studies, we observed both the strengths of the *in-silico* strategy and the dependency of gene patterns on severity and model types (table 4.1). After confirming the dysregulation of these predicted target genes, the study proceeded to examine whether melatonin affects these target genes. To do this, the researchers observed the expression patterns of these genes in both mice (C212s) and human muscle (LCHN- M2) cell lines after administering melatonin (table 4.1). It was observed that the effect of melatonin on the expression of certain target genes is state and dose-dependent (table 4.1).

Table 4. 1 Summary of validation of in silico data and in vitro studies

	Model	Tissue/sub-model	Significant difference comparing controls
Validation of <i>in-silico</i> data	<i>Smn</i> ^{-/-} ;SMN2	Triceps Skeletal muscle	Level of <i>Per-1</i> , <i>Bcl-2</i> , and <i>Sirt-1</i> increased
	<i>Smn</i> ^{2B/-} Mice		Increased <i>Per-1</i> and <i>Bcl-2</i> gene expression
	Type III SMA patients	Deltoid myoblasts	<i>PER-1</i> level is decreased.
	Proliferating C2C12s	Smn-KD with <i>Smn</i> -siRNA transfection	<i>Per1</i> and <i>Bcl2</i> exp. upregulated with independent of the <i>Smn</i> gene
	Differentiated-C2C12s		<i>Bcl2</i> exp. downregulated with independent of the <i>Smn</i> gene
	Differentiated-C2C12s	Atrophy-induced	No change
Melatonin impact	C2C12s	Myoblast	Downregulation of <i>Per1</i> (1mM melatonin)
		Myotubes	Downregulation of <i>Per1</i> (1mM melatonin), upregulation of <i>Bcl2</i> (100µm melatonin)
	LCHN-M2	Myoblast	Upregulation of <i>PER1</i> and <i>SIRT1</i> (1mM melatonin)
		Myotubes	Upregulation of <i>PER1</i> (100µm and 1mM melatonin)

The provided table, as shown in the figure, systematically summarizes from left to right: the objective of the study plan, the chosen model, the targeted tissue/sub-model, the statistically different results result examined. This table allows us to view the models used and their results during the validation process. Following this, the effect of melatonin on the expression of target genes was studied in C2C12s and LHCN-M2

models, post-melatonin application. This approach provides a comprehensive overview of the influence of melatonin on gene expression in these specific model systems.

4.3.12 Oral administration of melatonin intake leads to an increase in both body weight and survival rate in *Smn*^{2B/-} mice.

The dysregulation of target genes identified *in silico* was confirmed in both *in vivo* and *in vitro* SMA models. Subsequently, the observation of melatonin's effect on the expression of these target genes led to a decision to move forward with examining its impact *in vitro*, along with monitoring its safety profile in two different cell lines.

Using the *Smn*^{2B/-} mouse model, we initiated 2 different initiation periods— P5 and P8 and assessed a range of dosages, from 50 mg/kg/day to 100 mg/kg/day, drawing insights from prior research by Drew et al. (2015). In addition to oral administration, we also tested intraperitoneal melatonin delivery (Al Shoyaib, Archie and Karamyan, 2019). When compared to the oral delivery method, intraperitoneal (IP) administration offers a faster and higher absorption pattern (Al Shoyaib, Archie and Karamyan, 2019). It bypasses the acidic pH of the stomach, preventing damage and is directly absorbed by the blood. Although we observed improvements in weight and survival patterns with intraperitoneal administration, it caused additional stress in mice. Since we saw comparable benefits with oral administration and it was presented as a safer and less risky option, we chose to proceed with it.

After this dosage refinement stage, our findings pointed to the most potent treatment protocol being 50 mg/kg/day of melatonin, initiated on day 5 and sustained up to the humane endpoint. We favored this method due to the significant enhancements observed in the mice's weight trend and longevity (table 4.1).

Table 4. 2 Administering 50 mg/kg/day of Melatonin via daily gavage is the most effective treatment method.

Melatonin Concentration	Treatment Starting Day	Administration way	Effect on Survival	Effect on Weight
50 mg/kg/day	P5	oral	increase	increase
50 mg/kg/day	P5	intraperitoneal	increase	increase
50 mg/kg/day	P8	oral	no change	no change
100 mg/kg/day	P5	oral	no change	no change

This table outlines the dosage and schedule of melatonin administration in mouse experiments. To determine the best treatment strategy, SMA mice were exposed to different dosages and delivery techniques of melatonin from 50 mg/kg/day to 100 mg/kg/day. We then evaluated melatonin's efficacy based on weight and survival trends.

In an extensive study, we assessed the effects of administering 50 mg/kg/day of melatonin on *Smn*^{2B/-} mouse models via weight pattern. This dosage was compared against untreated control groups. Remarkably, the melatonin-treated mice exhibited a notable increase in body weight starting from the 7th postnatal day. This upward trend in weight gain was sustained through to the twentieth postnatal days, illustrating a consistent and prolonged beneficial effect of melatonin on physical development (figure 4.13.a.).

Observations from the righting reflex test revealed that *Smn*^{2B/-} mice, when placed on their backs, took less time to return to a normal posture following the administration of melatonin. This is a clear sign of improved motor skills and neuromuscular coordination when compared to their untreated counterparts. This finding suggests that melatonin not only boosts physical growth but also enhances motor abilities in SMA mice models (figure 4.13.c.).

The research revealed a stark contrast of lifespan between the untreated and melatonin-treated groups. Typically, untreated SMA mice had a lifespan of around 18- 20 days. However, the *Smn*^{2B/-} mice treated with melatonin showed a significant extension in lifespan, with some living up to around 35 days. (figure 4.13.b.).

The application of melatonin in the *Smn*^{2B/-} mice mouse model has been shown to improve the SMA phenotype, as evidenced by improvements in weight, survival, and RR outcomes.

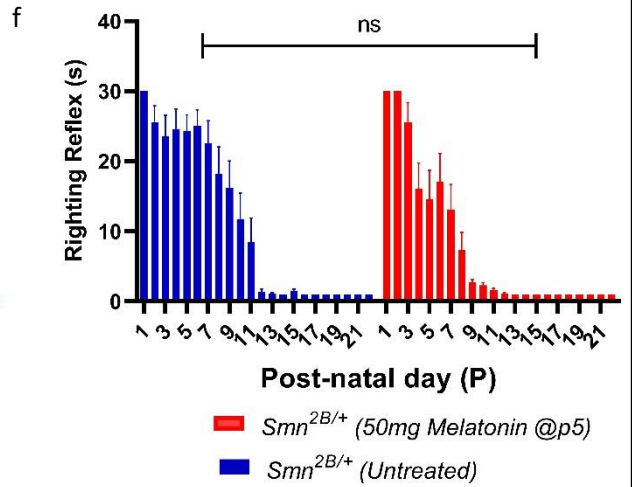
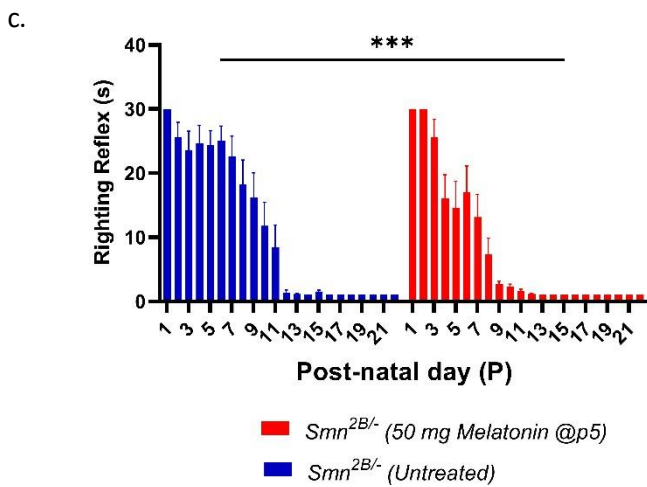
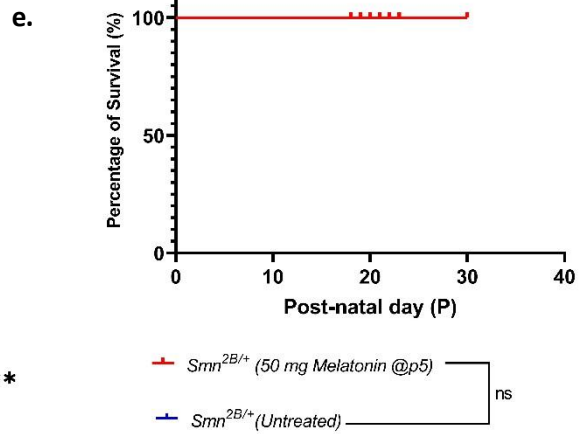
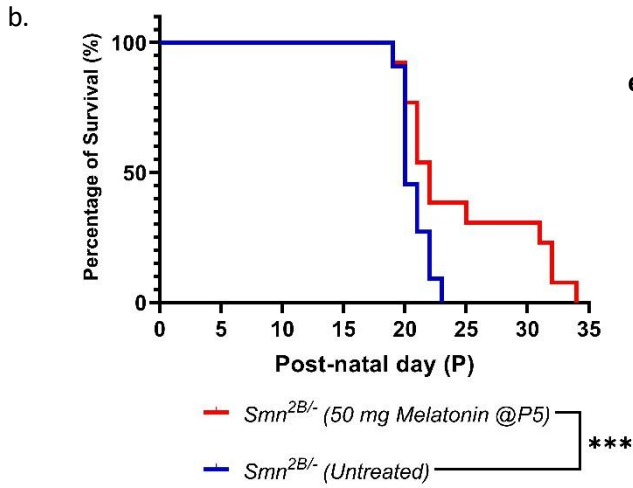
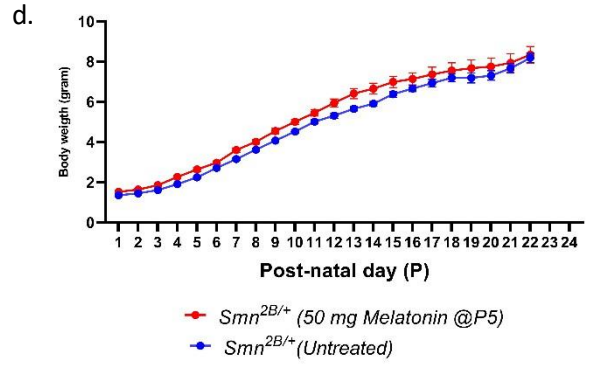
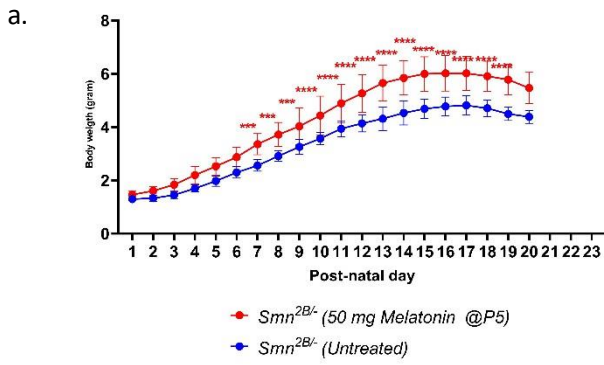


Figure 4. 13 The effect of 50 mg/kg/day oral melatonin treatment in both *Smn*^{2B/-} and *Smn*^{2B/+} SMA mice.

All animals were treated with 50 mg/kg/day oral melatonin (0.5 % carboxymethylcellulose) via daily gavage starting at P5 on *Smn*^{2B/-} SMA mice.

a. Daily weights of melatonin-treated (red, n=16), untreated (blue, n=15) on *Smn*^{2B/-} SMA mice. Error bars represent +/- SEM; Two-way ANOVA with post-hoc Sidak's multiple comparisons test between untreated (blue) and 50 mg/kg/day oral melatonin (red). ns= not significant, *p<0.05, **p<0.01, ***p<0.001, ****p<0.0001. b.

Kaplan-Meier survival curves for n=15 untreated (blue, median survival:20 days) and n=16 50 mg/kg/day melatonin (red, median survival:22 days) on *Smn*^{2B/-} SMA mice, Long-rank (Mantel- Cox) test, **p<0.01, ns= n significant. c. Daily righting reflex test up to a 30 second max time point of drug-treated (red, n=16) and untreated (blue, n=15) on *Smn*^{2B/-} SMA mice. Data represents mean and +/- SD error bars, One-way ANOVA with post-hoc Turkey's multiple comparisons test. ns= not significant, *p<0.05, **p<0.01, ***p<0.001, ****p<0.0001.

d. Daily weights of melatonin-treated (red, n=13), untreated (blue, n=13). Error bars represent +/- SEM; Two-way ANOVA with post-hoc Sidak's multiple comparisons test between untreated (blue) and 50 mg/kg/day melatonin (red). ns= not significant, *p<0.05, **p<0.01, ***p<0.001, ****p<0.0001.

e. Kaplan-Meier survival curves for n=13 untreated (blue, median survival:22 days) and n=13 50 mg/kg/day melatonin (red, median survival:22 days) on *Smn*^{2B/+} SMA mice, Long-rank (Mantel-Cox) test, **p<0.01, ns= n significant.

f. Daily righting reflex test up to a 30 second max time point of drug-treated (red, n=13) and untreated (blue, n=13) on *Smn*^{2B/+} SMA mice. Data represents mean and +/- SD error bars, One-way ANOVA with post-hoc Turkey's multiple comparisons test. ns= not significant, *p<0.05, **p<0.01, ***p<0.001, ****p<0.0001.

4.3.13 Oral administration of melatonin did not lead to any change of hypoglycaemia both non-fasted *Smn*^{2B/-} and *Smn*^{2B/+} mice.

With this in mind, we assessed how melatonin treatment affected the high blood sugar levels in symptomatic non-fasting SMA mouse models. We took the blood sugar measurements on P18, two hours post the last melatonin dosage. Thus, notable changes have not been observed in blood sugar levels after giving melatonin to either the *Smn*^{2B/-} (seen in figure 4.14.a) or *Smn*^{2B/+} mice (seen in figure 4.14.b).

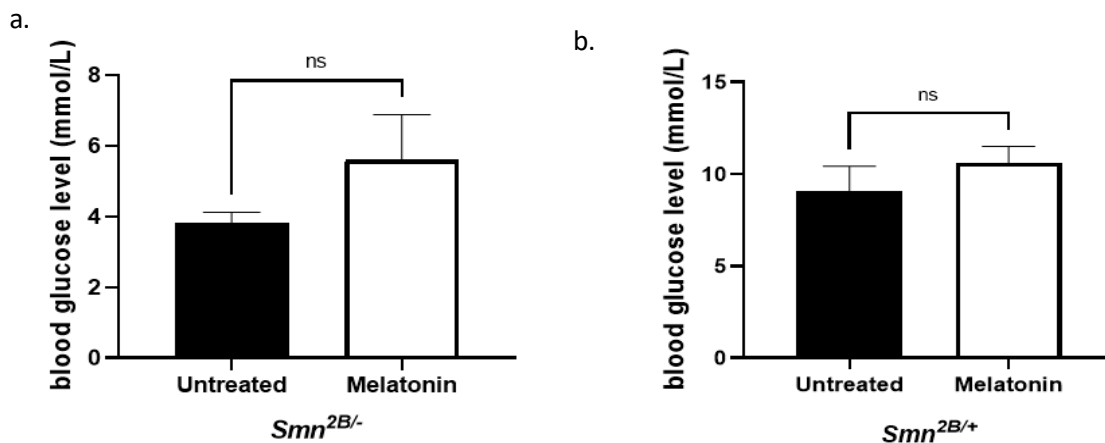


Figure 4. 14 Oral 50 mg/kg/day Melatonin treatment did not cause any significant change in blood glucose level in symptomatic non-fasting both *Smn*^{2B/-} and *Smn*^{2B/+}.

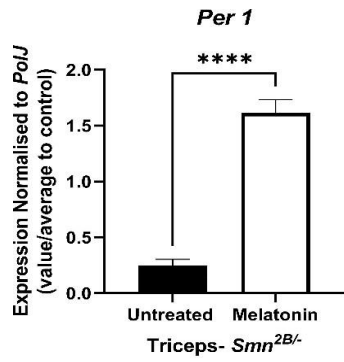
All animals were treated 50 mg/kg/day melatonin (diluted in 0.5% CMC) via daily gavage starting at P5 till P18. Blood glucose concentrations (mmol/L) were evaluated after 2 hours final treatment of melatonin. Untreated (black bars), and melatonin treated (white bars). *Smn*^{2B/-} mouse model result is in a graph (n=7), b. *Smn*^{2B/+} mouse model result shows in the b graph (n=5). Data represents mean and error bars represent +/- SEM; Unpaired t test, ns=not significant.

4.3.14 Melatonin administration led to an increase in the expression in transcriptomic-based targeted genes (*Per1*, *Sirt1*, *Bcl2* and *Ror-a*) the triceps tissue of symptomatic *Smn*^{2B/-} mice.

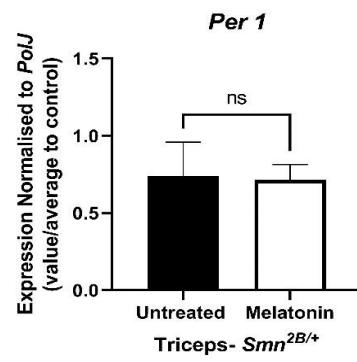
To delve deeper into the molecular implications of melatonin on skeletal muscle, we centered our attention on predicted targeted genes come from *in silico* analysis -*Per1*, *Sirt1*, *Bcl2*, and *Ror*— predicted targeted genes. We administered a daily 50 mg/kg oral dose of melatonin to *Smn*^{2B/-} and *Smn*^{2B/+} mice, from P5 to P18. After two hours of posting the final melatonin dosage on P18, we collected symptomatic triceps samples. For comparison, we also gathered symptomatic

triceps samples from untreated SMA mice during the same timeframe. We carried out qPCR analyses on the symptomatic triceps (both treated and untreated) to determine if melatonin altered the expression of target genes. In *Smn*^{2B/-} mice, an increase in the expression of silico-based predicted target genes was detected in the triceps tissues following melatonin administration (figure 4. 15. a; c; e; g.). Regarding the *Smn*^{2B/+} model, a significant change in the expression levels of the *Sirt1* target genes has been observed between the melatonin treated and untreated symptomatic triceps (figure 4.15.d.).

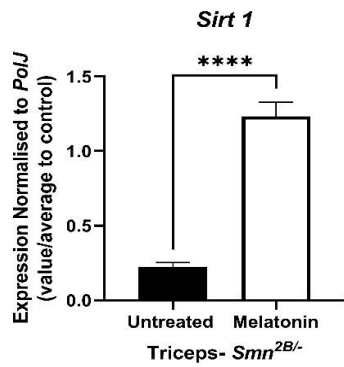
a.



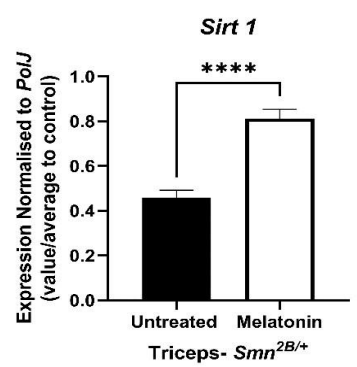
b.



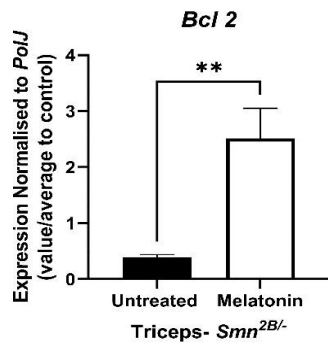
c.



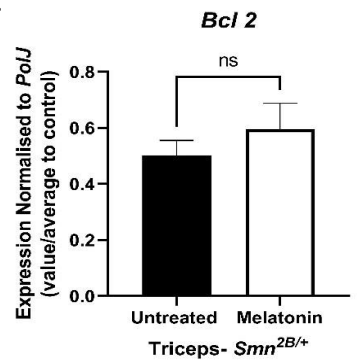
d.



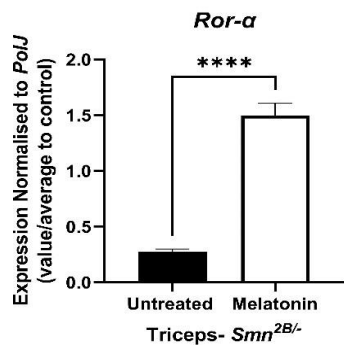
e.



f.



g.



h.

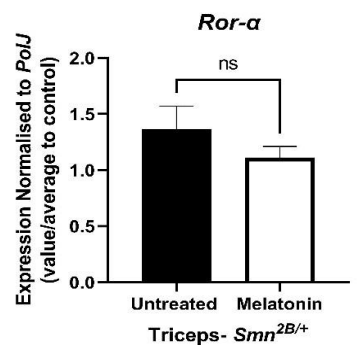


Figure 4. 15 Orally treatment of 50 mg/kg/day Melatonin causes an upregulation of all predicted targeted gene expressions level in symptomatic triceps tissue in *Smn*^{2B/-} SMA mice.

All animals were treated with 50 mg/kg/day melatonin (diluted in %0.5 CMC) via daily gavage starting at P5 till P18. Symptomatic triceps muscles were harvest from untreated (n=8, black bars) and melatonin-treated (n=8, white bars) in non-fasted *Smn*^{2B/-} and *Smn*^{2B/+}, after 2 hours last melatonin treatment. The mRNA levels of *Per1* gene are in

a. *Smn*^{2B/-} and b. *Smn*^{2B/+} ; these of *Sirt1* are in c. *Smn*^{2B/-} and d. *Smn*^{2B/+} , the *Blc2* are in e. *Smn*^{2B/-} and f. *Smn*^{2B/+} and the expressions of *Ror-α* gene are in g. *Smn*^{2B/-} and h. *Smn*^{2B/+} .Data represents mean and error bars represent +/- SEM; Unpaired t Test, ns=not significant, **p*<0.05
p*<0.01*p* <0.001*****p*<0.0001.

4.3.15 Melatonin administration caused to an elevation in the level of atrophic marker genes in the triceps of *Smn*^{2B/-} mice

Given the emerging understanding that melatonin may influence muscle development and function by increasing the expression of *in-silico*-based target genes, there is a targeted objective to conduct a more comprehensive study on the effects of melatonin on muscle health, especially focusing atrophy phenotype. For this aim was studying on the expression of *Atrogin-1* and *MuRF1* genes, which are an atrogenic marker. Consequently, it was determined that a 50 mg/kg/day melatonin treatment led to an increase in the expression of *Atrogin-1* and *MuRF1* genes in the symptomatic triceps tissue *Smn*^{2B/-} mice, as depicted in figure 4.16.a: c. In the *Smn*^{2B/+} model, no change in the expression levels of atrophy marker genes was observed (figure 4.16.b; d.). The administration of melatonin has been found to induce the expression of atrogenic gene markers in the symptomatic skeletal muscle of *Smn*^{2B/-} mice.

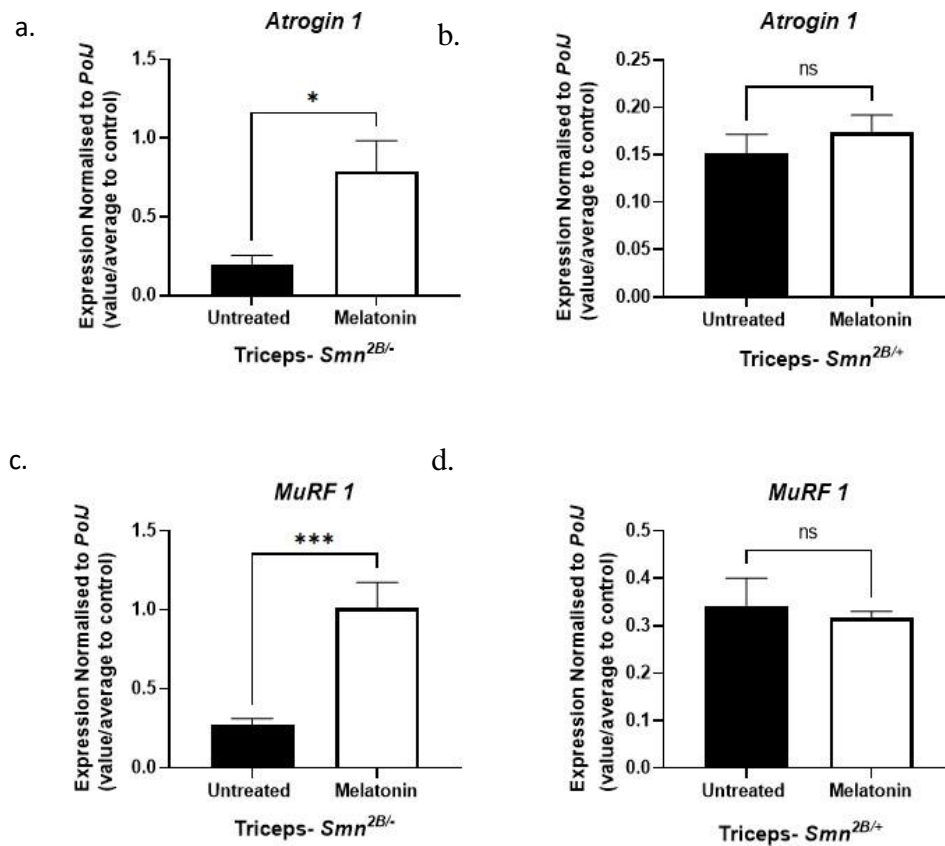


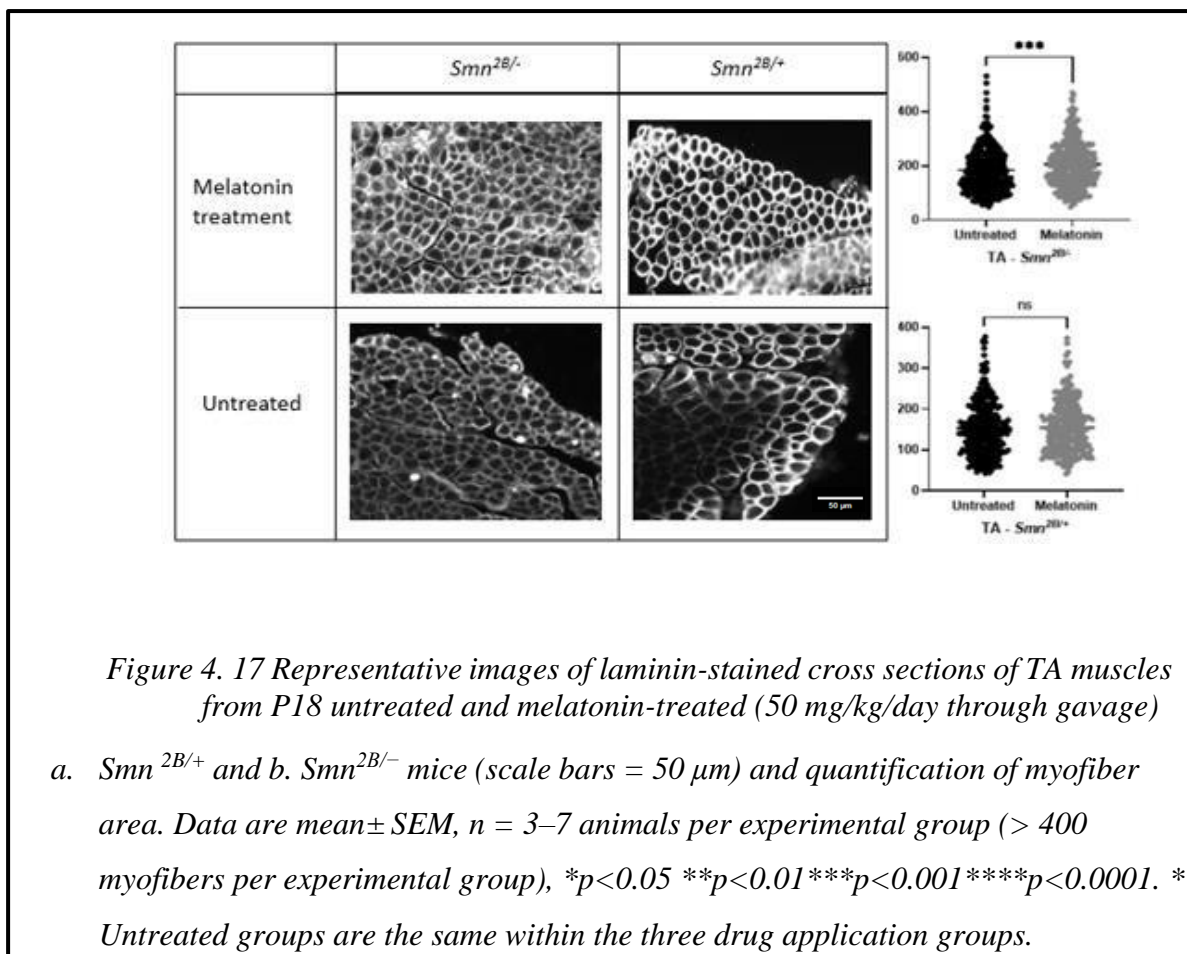
Figure 4. 16 50 mg/kg/day melatonin orally administration cause an increase in the atrophic phenotype of triceps of milder form SMA mouse models.

All animals were treated 50 mg/kg/day melatonin (diluted in 0.5% CMC) via daily gavage starting at P5 till P18. Symptomatic triceps muscles were harvest from untreated (n=8, black bars) and melatonin treated (n=8, white bars) in non-fasted *Smn^{2B/-}* and *Smn^{2B/+}*, after 2hours last melatonin treatment. The mRNA levels of *atrogin-1* gene are in a. *Smn^{2B/-}* and b. *Smn^{2B/+}*; these of *MuRF1* are in c. *Smn^{2B/-}* and d. *Smn^{2B/+}*. Data represents mean and error bars represent \pm SEM; Unpaired t Test, ns=not significant * $p < 0.05$ ** $p < 0.01$ *** $p < 0.001$ **** $p < 0.0001$.

4.3.16 Following melatonin treatment, there was an enhancement in the size of muscle fibers in symptomatic tibialis anterior from *Smn^{2B/-}* models.

Due to the reported involvement of various regulatory mechanisms in the onset of muscle apoptosis, our experimental plan also includes measuring myofiber size to investigate muscle atrophy and health (Deguise et al., 2016). In both *Smn^{2B/-}* models, the consequences of administering melatonin at a dosage of 50 mg/kg/day were assessed by contrasting the TA myofiber dimensions with those of untreated counterparts. The findings revealed that in SMA mouse models, melatonin stimulated an increase in fiber size (figure 4.17.a), whereas in *Smn^{2B/+}* mouse models, there was no alteration (figure 4.17.b).

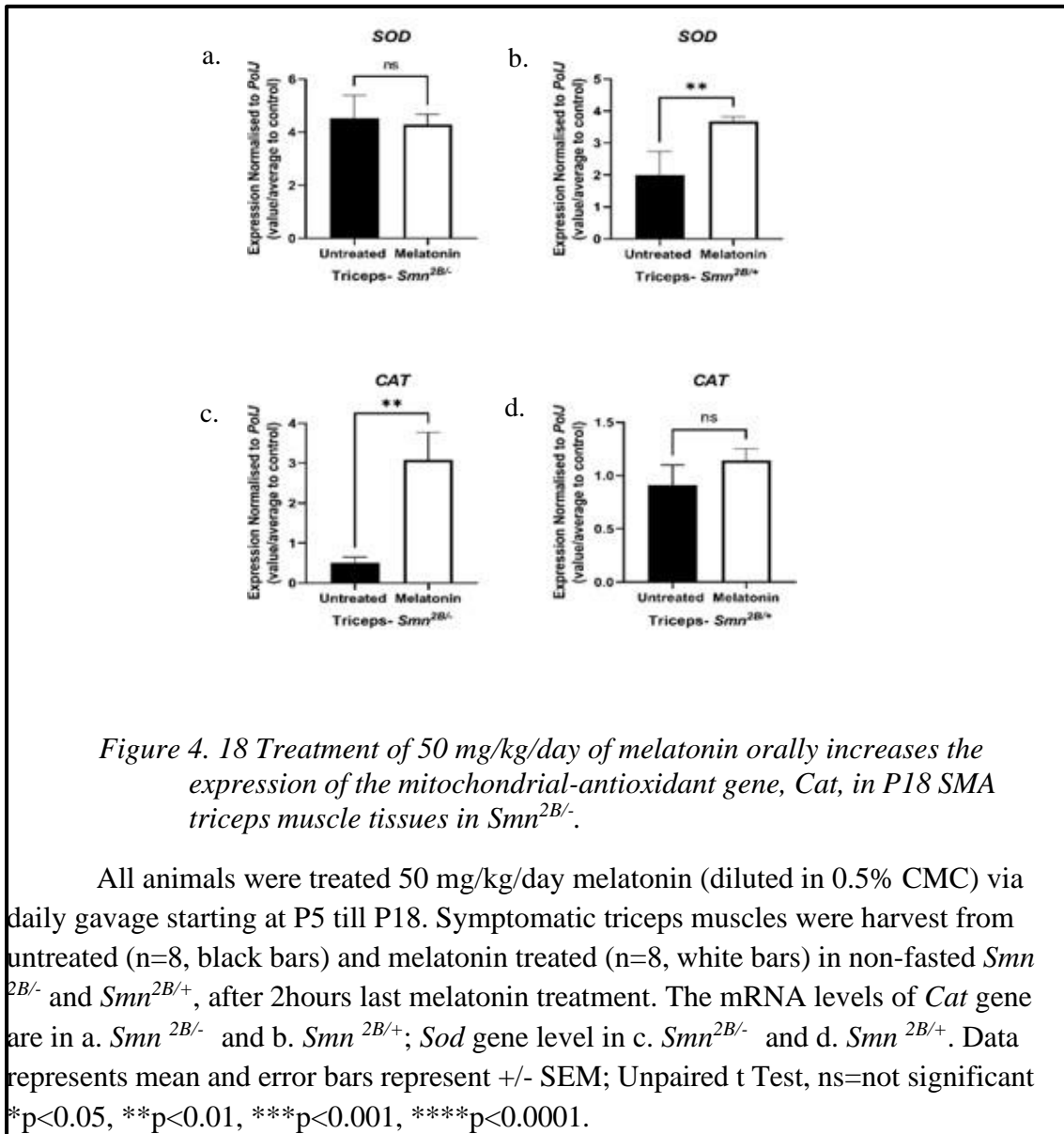
In $Smn^{2B/-}$ mice, an increase in the fiber size of the TA muscle has been observed to be dependent on melatonin treatment. This suggests that melatonin plays a role in influencing muscle size in this specific mouse model.



4.3.17 Melatonin application increased the expression of the *CAT* gene in the symptomatic muscle tissues of $Smn^{2B/-}$ mice.

One of the causes of muscle atrophy is associated with mitochondrial ROS production and the resulting oxidative stress (Powers, Kavazis and McClung, 2007). This oxidative stress disrupts mitochondrial function in muscle tissues, leading to energy imbalance, and subsequent muscle atrophy (Xu et al., 2021). Catalase is an antioxidant enzyme that plays a role in preventing muscle loss by degrading H_2O_2 molecules. Similarly, *SOD* plays a crucial role in protecting the body as part of the antioxidant system (Inal, Kanbak and Sunal, 2001). To better understand the mitochondrial oxidant-antioxidant system, we aimed to conduct qPCR studies on two genes that play a main role as an antioxidant.

When comparing the muscle tissues of melatonin-treated symptomatic SMA mice to those of untreated SMA mice, there was an observed increase in the expression of the *CAT* gene following 50 mg/kg/day melatonin treatment in *Smn*^{2B/-} mouse model (figure 4.18.c.), while the level of *SOD* did not change (figure 4.18.a). In the *Smn*^{2B/+} mice treated with melatonin, there was an increase in the expression of the *SOD* gene when compared to untreated-littermate *Smn*^{2B/+} (figure 4.18.b.), whereas the mRNA of *CAT* did not lead to any change (figure 4.18.d.).



4.3.18 Melatonin resulted in elevated expression of the diurnally regulated genes, *Clock* and *Per2*, in the triceps tissue of symptomatic *Smn*^{2B/-} SMA mice.

Considering the known dysregulation of diurnal expression of core clock genes in the TA muscle of *Smn*^{-/-}; *SMN2* mice (Lisa M Walter et al., 2018), and further taking into account that the circadian rhythm is a key regulator of metabolic balance, we have included the study of core clock gene expressions to fully understand the impact of melatonin on muscle development and metabolism.

To delve deeper into this analysis, qPCR was conducted on symptomatic skeletal muscles that were treated with melatonin, as well as on untreated controls. Our experimental findings showed that the *Clock* and *Per2* genes had a noticeably increased expression in the symptomatic triceps tissues when compared with the untreated symptomatic triceps counterparts in *Smn*^{2B/-} (figure 4.19.a.e). However, in relation to the *Bmal1* gene, we didn't detect any difference in its expression in the *Smn*^{2B/-} mouse models (figure 4.19.c.d.).

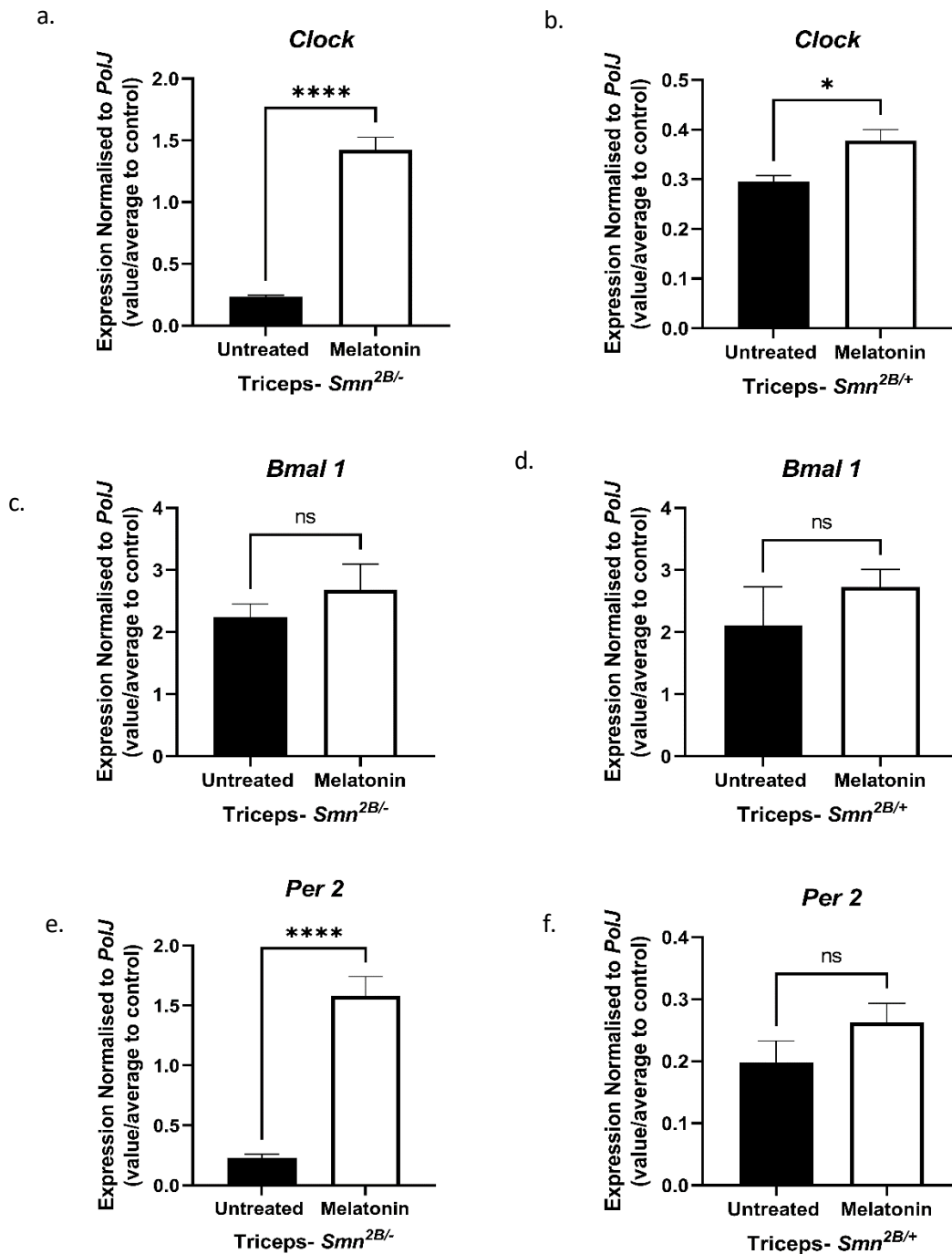


Figure 4. 19 Oral administration of melatonin at a dose of 50 mg/kg/day leads to an increase in the expression of the *Clock* and *Per2* genes in the triceps of milder form SMA mouse models.

All animals were treated with 50 mg/kg/day melatonin (diluted in 0.5% CMC) via daily gavage starting at P5 till P18. Symptomatic triceps muscles was harvest from untreated (n=8, black bars) and melatonin treated (n=8, white bars) in non-fasted *Smn*^{2B/-} and *Smn*^{2B/+}, after 2hours last melatonin treatment. The mRNA levels of *Clock* gene are in

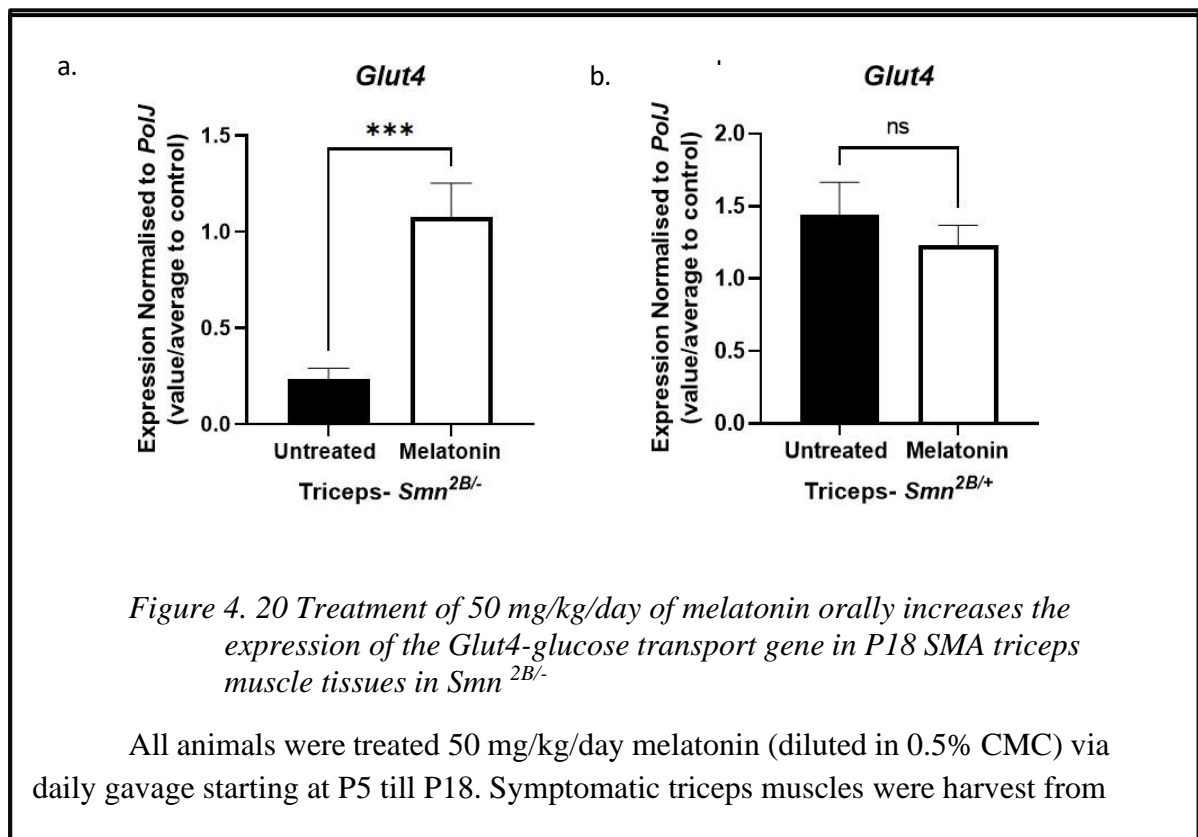
a. *Smn*^{2B/-} and b. *Smn*^{2B/+}; these of *Bmal1* are in c. *Smn*^{2B/-} and d. *Smn*^{2B/+} and *Per2* are in e. *Smn*^{2B/-} and f. *Smn*^{2B/+} Data represents mean and error bars represent +/- SEM; Unpaired t Test, ns=not significant. *p<0.05 **p<0.01 ***p<0.001 ****p<0.0001.

4.3.19 Melatonin increased the expression of the *Glut4* gene, which is responsible for glucose transport, in symptomatic SMA mouse muscle tissue.

In our study system, the non-fasting of SMA mice has masked whether melatonin administration affects blood glucose levels. Therefore, to better understand the effect of melatonin on insulin resistance in SMA mice (reported (Bowerman *et al.*, 2012)), we have included an examination of GLUT receptors, which are responsible for glucose uptake from circulation into muscle tissues.

When comparing melatonin-treated triceps to untreated ones during the symptomatic phase, we noticed a significant increase in *Glut4* gene expression in the treated group in *Smn*^{2B/-} (figure 4.20.a). Whereas there is no change in the mRNA level of *Glut4* gene in *Smn*^{2B/+} (figure 4.20.b).

Overall, melatonin has been shown to induce the expression of the gene responsible for glucose transport in the skeletal muscle of SMA mice.



untreated (n=8, black bars) and melatonin treated (n=8, white bars) in non-fasted *Smn*^{2B/-} and *Smn*^{2B/+}, after 2hours last melatonin treatment. The mRNA levels of *Glut-4* gene are in a. *Smn*^{2B/-} and b. *Smn*^{2B/+}. Data represents mean and error bars represent +/- SEM; Unpaired t Test, ns=not significant. *p<0.05 **p<0.01 ***p<0.001 ****p<0.0001.

Table 4. 3 Summary of melatonin effect on P18 SMA skeletal muscle in *Smn*^{2B/-}

Decipher melatonin effect	Method	Targeted genes/protein	Result	Model	Tissue
Molecular pathway	Quantification of mRNA level via qPCR	<i>In-silico</i> based (<i>Per1, Sirt1, Bcl-2, Ror-α</i>)	Expression of all targeted genes increased	<i>Symptomatic Smn</i> ^{2B/-}	Triceps
Atrophy		Atrogenic markers (<i>Atrogin-1, MuRF</i>)	Both mRNA level upregulated		
Mitochondrial based-oxidative stress		Playing role as anti-oxidant (<i>CAT, SOD</i>)	Down-regulation of <i>CAT</i> ;no change in <i>SOD</i> expression		
Circadian Rhythm		Core clock (<i>Bmal1, Clock, Per2</i>)	<i>Clock</i> and <i>Per2</i> upregulated; <i>Bmal1</i> remained steady		
Glucose intolerance		Responsible of glucose uptake (<i>Glut4</i>)	mRNA level increased		
Complete picture for muscle health	Myofiber size assessment with IHC	Membrane protein (Laminin)	Myofiber size increased		TA

The provided table, as shown in the figure, systematically summarizes from left to right: the objective of the study plan, the chosen method, the targeted gene or protein, the result, the model used, and the type of tissue examined. The targeted genes have been systematically categorized into groups: sequentially, genes predicted through combined *in silico* analyses (*Per1, Sirt1, Bcl-2* and *Ror-α*), genes responsible for atrophy (*Atrogin-1* and *MuRF*), genes playing a role in oxidative stress (*CAT* and *SOD*), core clock genes (*Bmal1, Clock* and *Per2*), and glucose uptake receptor genes (*Glut4*). The levels of these targeted genes have been quantified in triceps tissues following melatonin application using qPCR. Lastly, to complete the overall picture of melatonin's effect on muscle health, a myofiber size assessment was conducted via Laminin assay using the TA muscle. The entire experimental system was carried out on the *Smn*^{2B/-} SMA mouse model.

4.3.20 Daily gavage dosing of 50 mg/kg/day melatonin, there was an upregulation in the expression of predicted target genes (*Per1*, *Bcl2*, and *Ror-α*) in the liver tissues of symptomatic *Smn*^{2B/-} mice.

Continuing our studies with the liver, another peripheral tissue observed to have dysregulations in development and function, we have incorporated a multi-systemic approach of SMA.

Through qPCR analyses, we assessed the symptomatic liver tissues, both with and without melatonin treatment, to see if there were changes in the expression of these selected genes in liver tissue. We observed that in the *Smn*^{2B/-} mice, there was an increase in the expression of all anticipated target genes, except *Sirt1*; following the 50 mg/kg/day melatonin treatment (as shown in figure 4.21.a; e; g.). In the *Smn*^{2B/+} model, no differences were observed in the gene expression between the melatonin-treated and untreated liver (as illustrated in figure 4.21.b; d; f.).

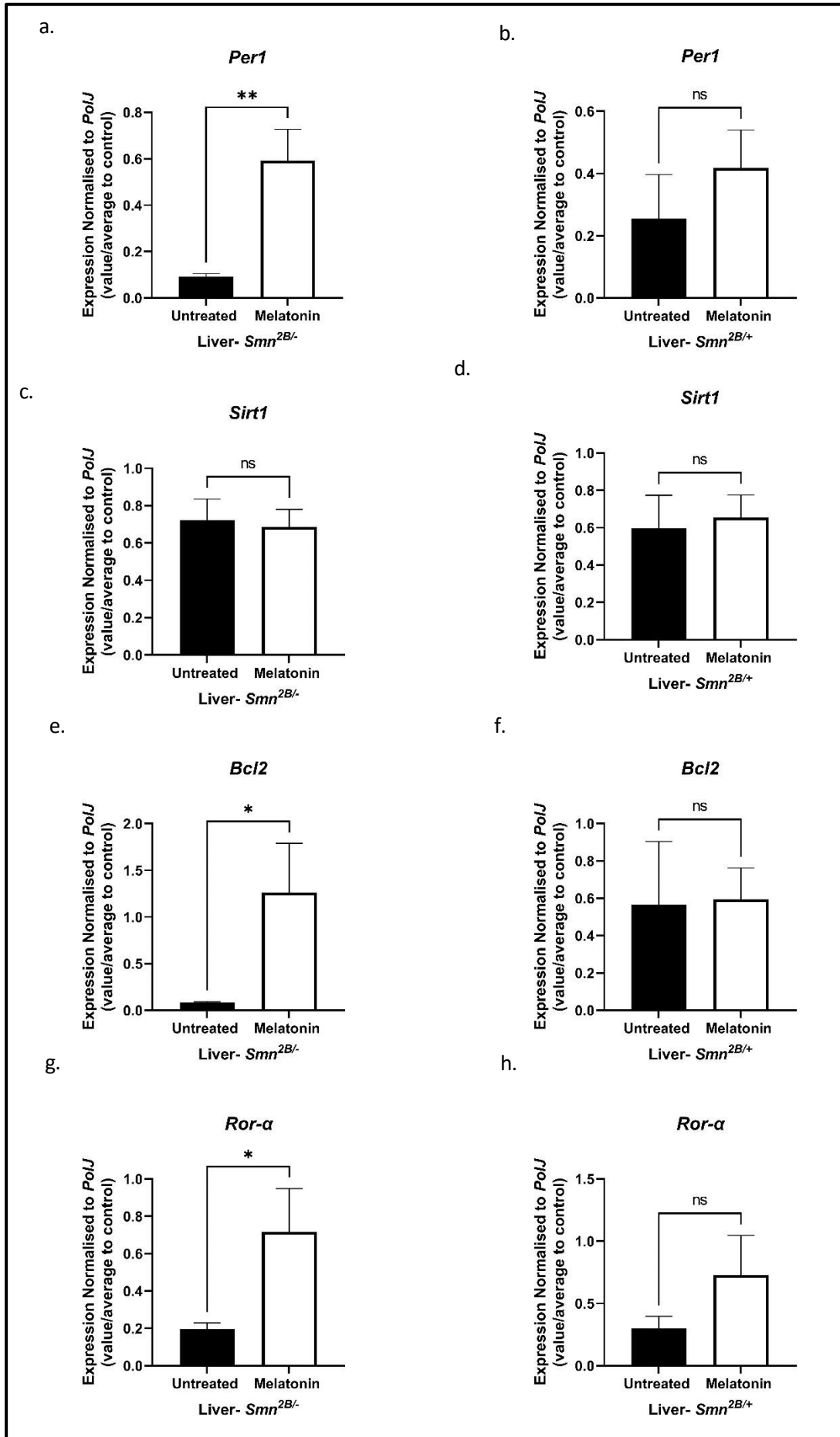


Figure 4. 21 Application 50 mg/kg/day of melatonin leads to an increase in the predicted target gene levels of *Per1*, *Bcl2*, and *Ror-alpha* in symptomatic liver tissue in *Smn*^{2B/-} mice.

All animals were treated with 50 mg/kg/day melatonin (diluted in 0.5% CMC) via daily gavage starting at P5 till P18. Symptomatic liver was harvested from untreated (n=8, black bars) and melatonin treated (n=8, white bars) in non-fasted *Smn*^{2B/-} and *Smn*^{2B/+}, after 2 hours last melatonin treatment. The mRNA levels of *Per1* gene are in a. *Smn*^{2B/-} and b. *Smn*^{2B/+}; these of *Sirt1* are in c. *Smn*^{2B/-} and d. *Smn*^{2B/+}, the *Bcl2* are in e. *Smn*^{2B/-} and f. *Smn*^{2B/+} and the expressions of *Ror-α* gene are in g. *Smn*^{2B/-} and h. *Smn*^{2B/+}.

Data represents mean and error bars represent +/- SEM; Unpaired t Test, ns=not significant, *p<0.05 **p<0.01, ***p<0.001, ****p<0.0001.

4.3.21 There was a rise in the expression of diurnal genes, *Clock* and *Per2* following melatonin within the liver tissue of symptomatic *Smn*^{2B/-} mice.

Since the circadian rhythm functions as the body's central clock for maintaining homeostatic balance (Kim et al., 2015), the study aims to investigate the liver following the application of circadian regulatory agents, melatonin.

There was a noticeable increase in the expression levels of *Clock* and *Per2* genes in the 50 mg/kg/day melatonin-treated symptomatic liver tissues of the *Smn*^{2B/-} mice (figure 4.22.a; e.), in contrast to their untreated counterparts. However, when evaluating the *Smn*^{2B/+} mouse line, there was no statistically significant alteration in the mRNA levels of *Clock* and *Per2* following an orally 50 mg/kg/day melatonin regimen (figure 4.22.b; f.).

On another note, the same melatonin treatment through daily gavage at 50 mg/kg/day, the *Bmal1* gene's expression remained consistent, with no noticeable disparities between the *Smn*^{2B/-} and controls (figure 4.22.c; d.).

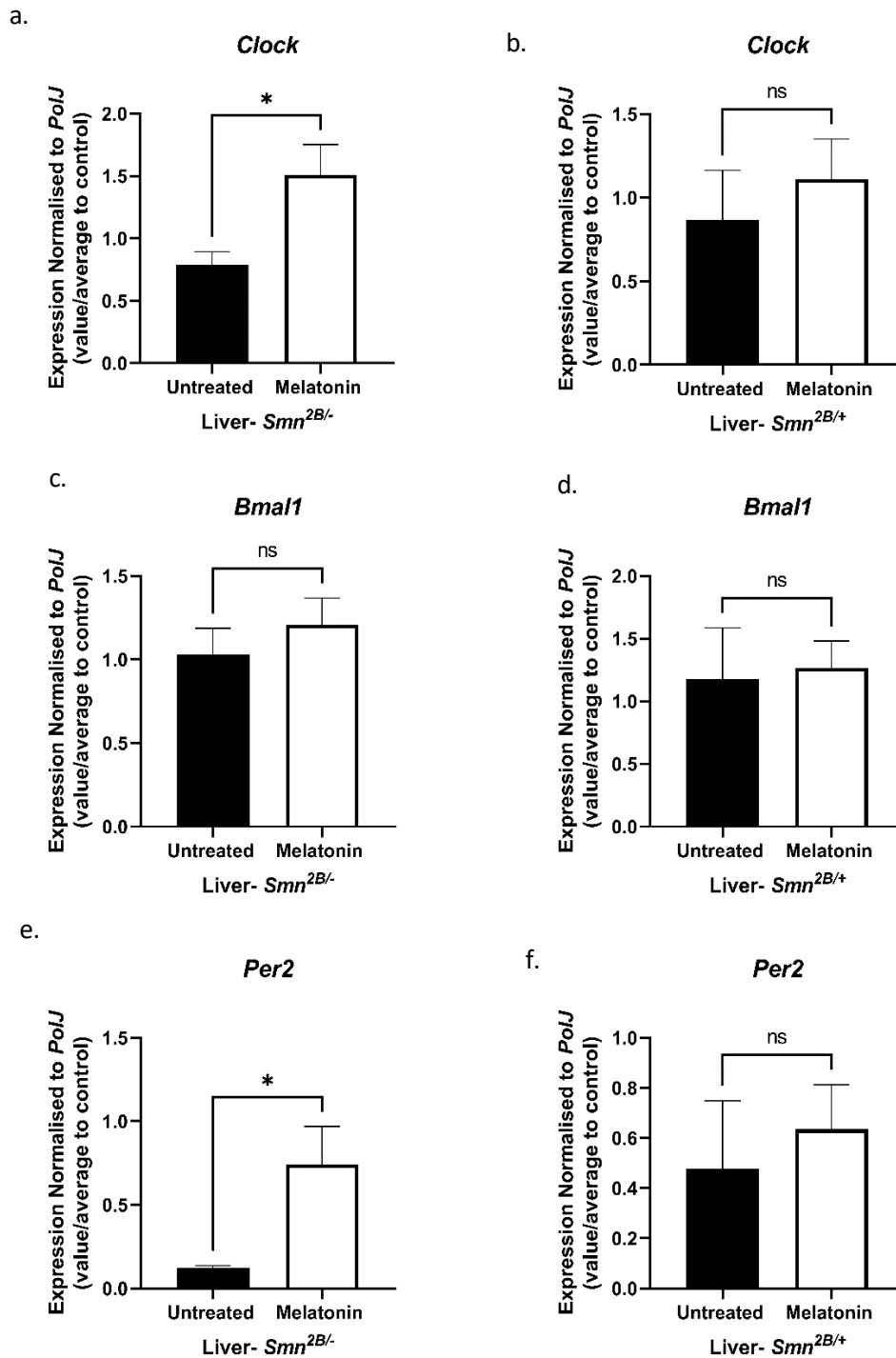


Figure 4. 22 50 mg/kg/day pioglitazone orally administration induced the mRNA level of *Clock* and *Per2* genes in liver of milder form of symptomatic SMA mouse.

All animals were treated with 50 mg/kg/day melatonin (diluted in 0.5% CMC) via daily gavage starting at P5 till P18. Symptomatic liver was harvest from untreated (n=8, black bars) and melatonin treated (n=8, white bars) in non-fasted *Smn^{2B/-}* and *Smn^{2B/+}*, after 2hours last melatonin treatment. The mRNA levels of *Clock* gene are in a. *Smn^{2B/-}*

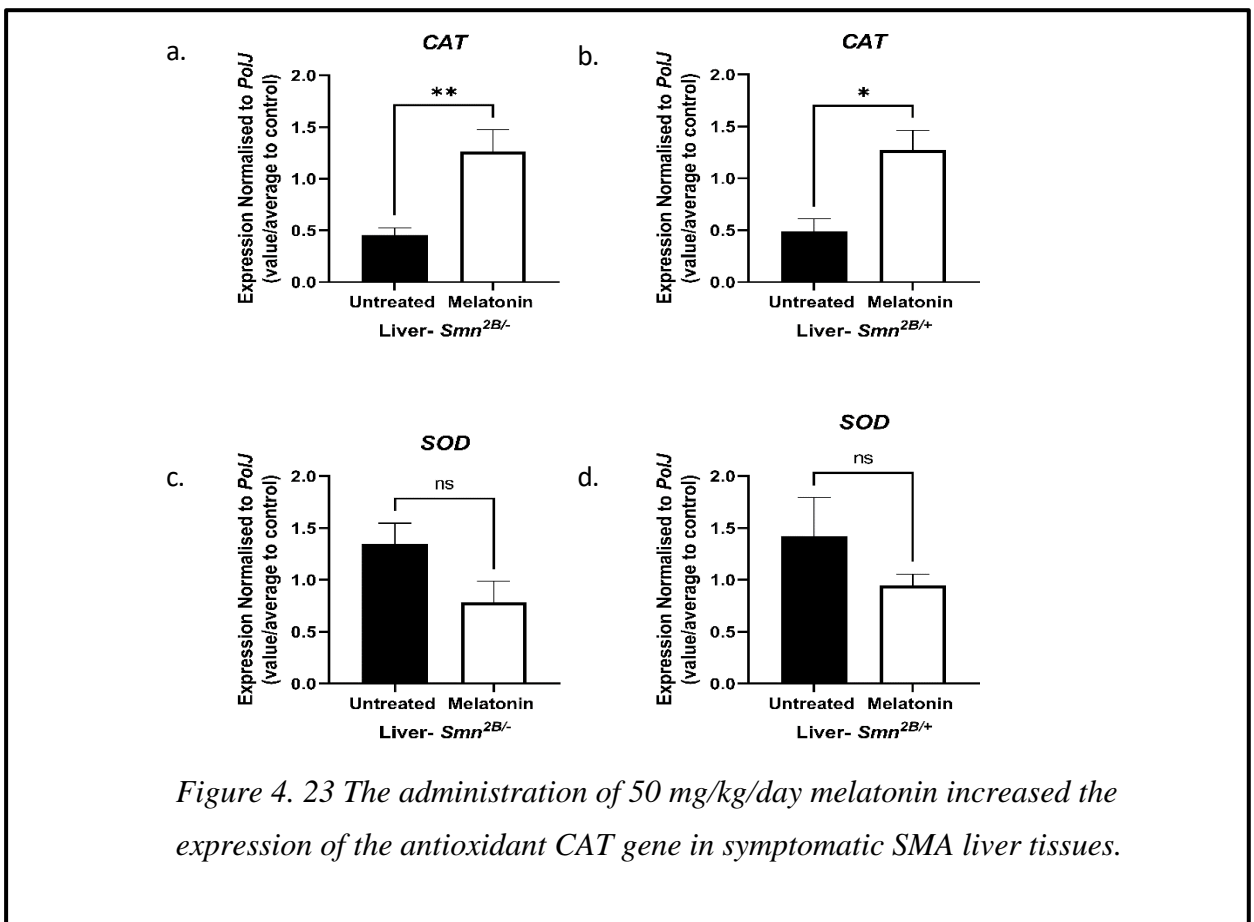
and b. *Smn*^{2B/+}; these of *Bmal1* are in c. *Smn*^{2B/-} and d. *Smn*^{2B/+}. And that of *Per2* are in e. *Smn*^{2B/-} and f. *Smn*^{2B/+}. Data represents mean and error bars represent +/- SEM; Unpaired t Test, *p<0.05 **p<0.01, ***p<0.001, ****p<0.0001.

4.3.22 Melatonin induced the expression of the *CAT* gene's mRNA in symptomatic SMA liver tissues.

Another factor reported to affect the development and function of the liver is the increased production of ROS in *Smn*^{2B/-} mice (Deguise et al., 2021b).

Therefore, it is important to investigate the effect of melatonin administration on oxidative stress of liver. For this aim, analyse the impact of administering 50 mg/kg/day of melatonin on the expression of the *CAT* and *SOD* gene in symptomatic liver tissues was planned.

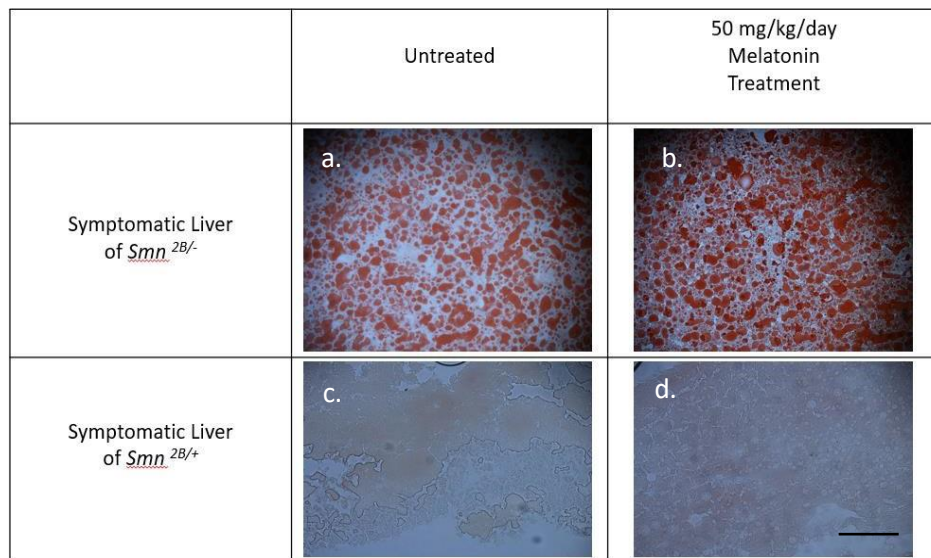
This comparison revealed an increased expression in the *CAT* gene following a treatment regimen of 50 mg/kg/day of melatonin in both the *Smn*^{2B/-} and *Smn*^{2B/+} mouse model (figure 4.23.a; b.). However, there is no change observed in the expressions of *SOD* genes both mouse models (figure 4.23.c; d.).



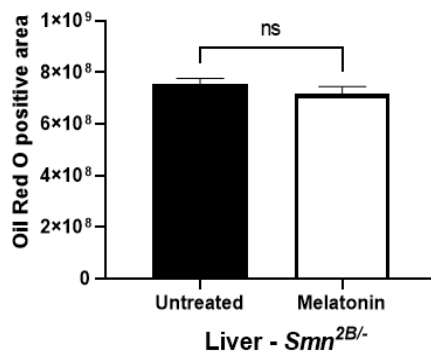
All animals were treated with 50 mg/kg/day melatonin (diluted in 0.5% CMC) via daily gavage starting at P5 till P18. Symptomatic liver was harvest from untreated (n=8, black bars) and melatonin treated (n=8, white bars) in non-fasted *Smn*^{2B/-} and *Smn*^{2B/+}, after 2 hours last melatonin treatment. The mRNA levels of *CAT* gene are in a. *Smn*^{2B/-} and b. *Smn*^{2B/+}; *SOD* gene level in c. *Smn*^{2B/-} and d. *Smn*^{2B/+}. Data represents mean and error bars represent +/- SEM; Unpaired t Test, ns=not significant. *p<0.05 **p<0.01***P<0.001****P<0.0001.

4.3.23 Melatonin did not result in any change in lipid accumulation in the liver

It has been revealed that due to various factors disrupting the metabolism in the liver, fatty acids are not transported to the mitochondria, leading to their accumulation in the liver of *Smn*^{2B/-} mice (Deguise et al., 2021b). A detailed examination of the effects of melatonin application on lipid accumulation could provide more insights into the liver steatosis profile. For this aim, symptomatic liver sections were stained with Oil- red-O. As depicted in the accompanying figure 4.24, a distinct lipid accumulation is visible in the *Smn*^{2B/-} (4.24.a; b.) mice in contrast to the *Smn*^{2B/+} (4.24.c; d.) mouse models. Even after the administration of melatonin at a dosage of 50 mg/kg/day, no alteration in lipid accumulation was noted in either of the mouse models.



e.



f.

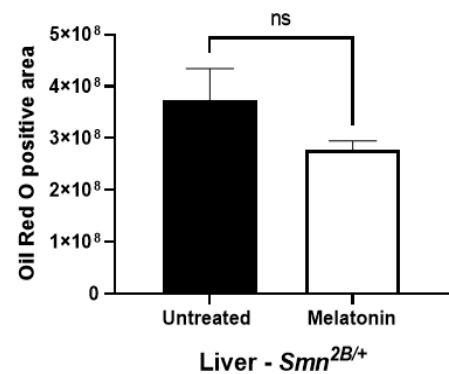


Figure 4. 24 The daily-gavage administration of 50 mg/kg/day melatonin at does not lead to reduce effect on lipid accumulation in the liver.

Representative images of Oil-red-O cross sections of liver from P18 untreated (a, c) and 50 mg/kg/day pioglitazone-treated (b, d) through gavage both *Smn*^{2B/+} (c, d) and *Smn*^{2B/-} (a, b) mice. Data are mean± SEM, n = 3–7 animals per experimental group, untreated bars show as a black, melatonin treatment represent white bars in e. *Smn*^{2B/-} f. *Smn*^{2B/+} ; Unpaired t Test, ns=not significant. (Scale bar= 50µm) *p<0.05 **p<0.01 ***p<0.001 ****p<0.0001. * Untreated groups are the same within the three drug application groups.

Table 4. 4 Summary of melatonin effect on P18 SMA liver in *Smn*^{2B/-}

Decipher melatonin effect	Method	Targeted genes/protein	Result	Model	Tissue
Molecular pathway	Quantification of mRNA level via qPCR	<i>In-silico</i> based (<i>Per1</i> , <i>Sirt1</i> , <i>Bcl-2</i> , <i>Ror-α</i>)	<i>Per1</i> , <i>Bcl-2</i> , <i>Ror-α</i> increased, except <i>Sirt-1</i> (no change)	Symptomatic <i>Smn</i> ^{2B/-}	Liver
Circadian Rhythm		Core clock (<i>Bmal1</i> , <i>Clock</i> , <i>Per2</i>)	<i>Clock</i> and <i>Per2</i> upregulated; <i>Bmal1</i> remained steady		
Mitochondrial based-oxidative stress		Playing role as anti-oxidant (<i>CAT</i> , <i>SOD</i>)	Upregulation of <i>CAT</i> ;no change in <i>SOD</i> expression		
More insights into the liver steatosis profile	Oil-red-O assay	Lipophilic dye	No change in lipid accumulation		

The provided table, as shown in the figure, systematically summarizes from left to right: the objective of the study plan, the chosen method, the targeted gene or protein, the result, the model used, and the type of tissue examined. The targeted genes have been systematically categorized into groups: sequentially, genes predicted through combined *in silico* analyses (*Per1*, *Sirt1*, *Bcl-2* and *Ror-α*), core clock genes (*Bmal1*, *Clock* and *Per2*), genes playing a role in oxidative stress (*CAT* and *SOD*). The levels of these targeted genes have been quantified in liver tissues following melatonin application using qPCR. Lastly, to complete the overall picture of melatonin's effect on liver lipid accumulation (steatosis), Oil-red-O dyeing used. The entire experimental system was carried out on the *Smn*^{2B/-} SMA mouse model.

4.3.24 Following the melatonin treatment, there was a decrease in the *Per1* gene expression within the spinal cord tissues in symptomatic *Smn*^{2B/-}

Further investigates whether the administration of melatonin leads to changes in the expression levels of predicted target genes in symptomatic spinal cord tissues, thereby assessing melatonin's potential therapeutic benefits specifically for spinal cord tissue of

SMA mice. Findings revealed that oral administration of melatonin at a dose of 50 mg/kg/day reduced the expression of the *Per1* gene in both mouse models (figure 4.25.a; b), while the mRNA levels of other targeted genes (*Bcl2*, *Sirt1* and *Ror-α*) did not change in control group (figure 4.25.c; d; e; f; g; h.).

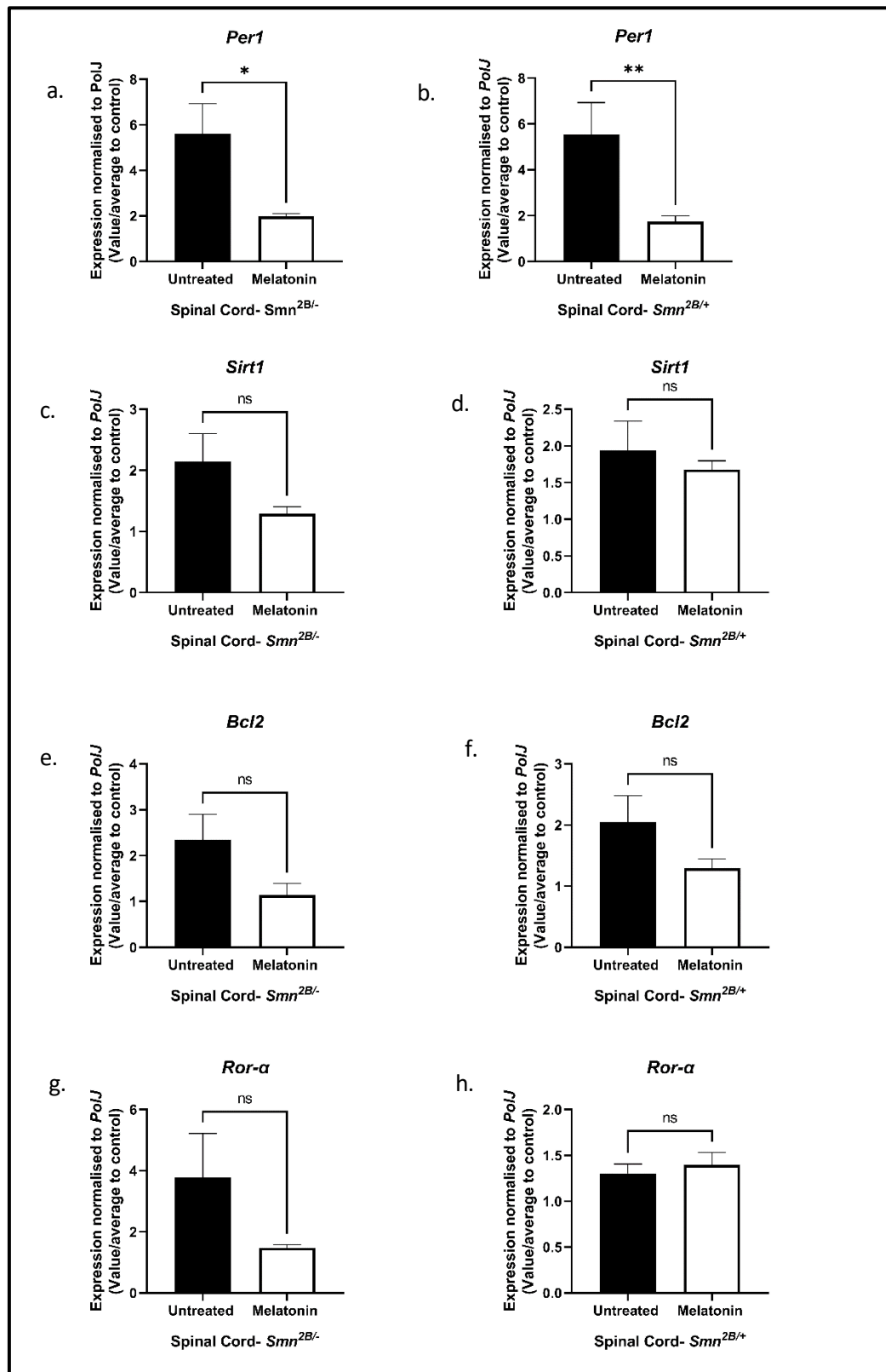


Figure 4. 25 After daily oral administration of melatonin at a dose of 50 mg/kg/day, the expression level of the *Per1* gene is downregulated in symptomatic spinal cord tissues in both the *Smn*^{2B/-} and *Smn*^{2B/+} models.

All animals were treated with 50 mg/kg/day melatonin (diluted in 0.5% CMC) via daily gavage starting at P5 till P18. Symptomatic spinal cord was harvested from untreated (n=8, black bars) and melatonin treated (n=8, white bars) in non-fasted *Smn*^{2B/-} and *Smn*^{2B/+}, after 2 hours last melatonin treatment. The mRNA levels of *Per1* gene are in a. *Smn*^{2B/-} and b. *Smn*^{2B/+}; these of *Sirt1* are in c. *Smn*^{2B/-} and d. *Smn*^{2B/+}, the *Btc2* are in e. *Smn*^{2B/-} and f. *Smn*^{2B/+} and the expressions of *Ror-α* gene are in g. *Smn*^{2B/-} and h. *Smn*^{2B/+}. Data represents mean and error bars represent +/- SEM; *p<0.05 **p<0.01 ***p<0.001 ****p<0.0001.

4.3.25 The level of Pmaip-1 and Fas downregulated, following melatonin treatment in *Smn*^{2B/-} SMA mice.

The next step involves examining *Fas* and *Pmaip-1*, which are pathological markers of SC tissue, to investigate the overall impact of melatonin on the health of SC (Murray et al., 2015b). The qPCR analysis demonstrated a significant reduction in the expression of these two genes that initiate apoptosis in the spinal cord in both *Smn*^{2B/-} and *Smn*^{2B/+} spinal cords.

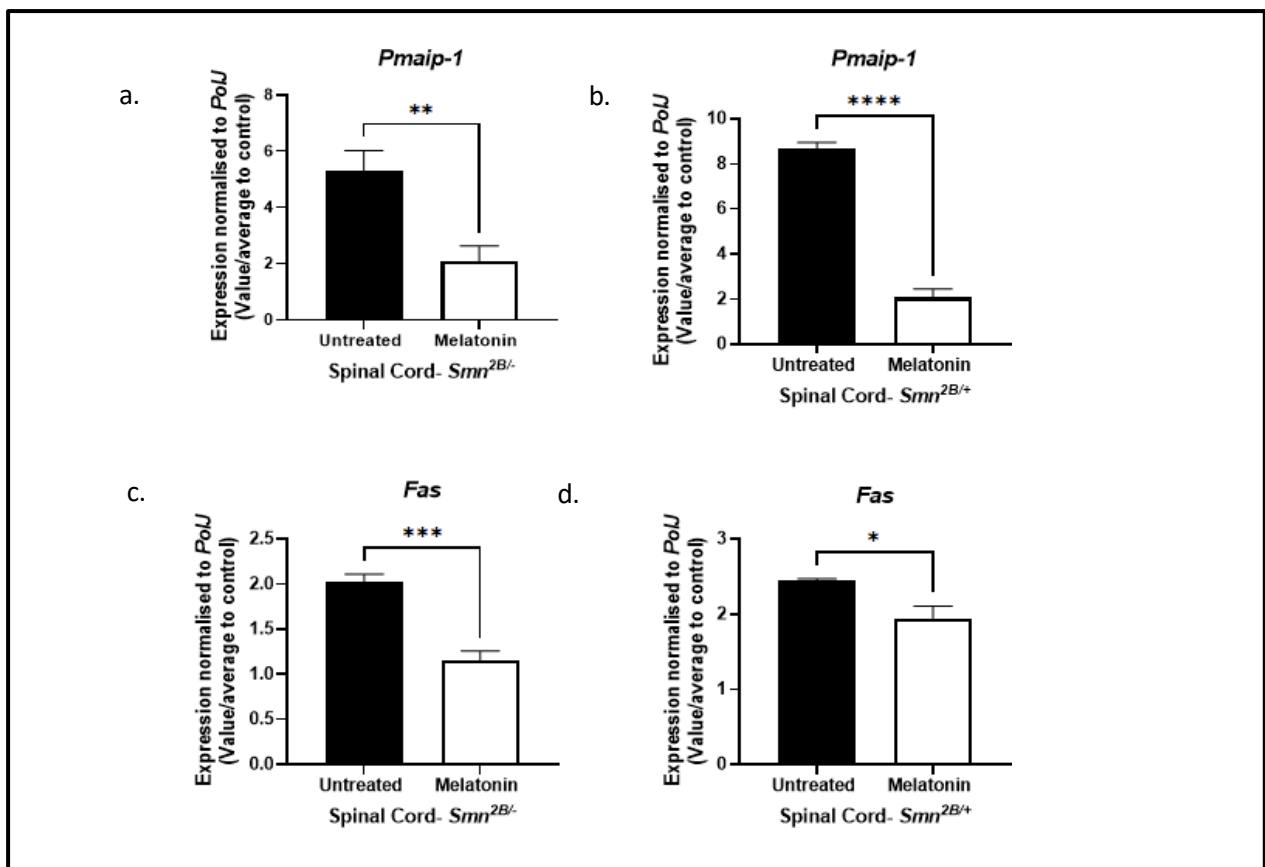


Figure 4. 26 Melatonin might have a neuroprotective effect on spinal cord in milder form of SMA mouse, preventing apoptosis.

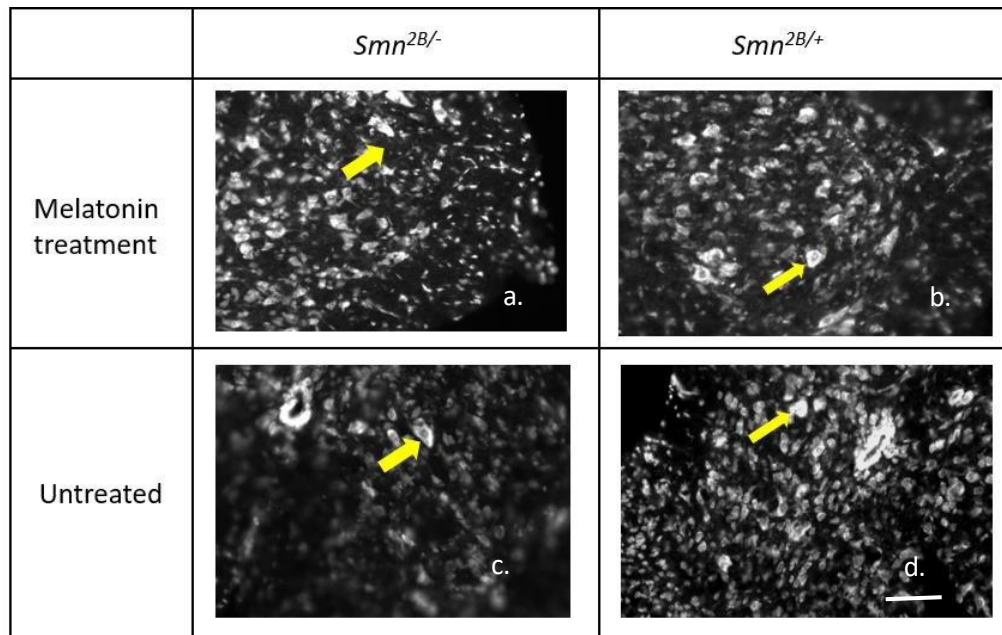
All animals were treated with 50 mg/kg/day melatonin (diluted in 0.5% CMC) via daily gavage starting at P5 till P18. Symptomatic spinal cord was harvest from untreated (n=8, black bars) and melatonin treated (n=8, white bars) in non-fasted *Smn*^{2B/-} and *Smn*^{2B/+}, after 2hours last pioglitazone treatment. The mRNA levels of *Pmaip-1* gene are in a. *Smn*^{2B/-} and b. *Smn*^{2B/+}; these of *Fas* are in c. *Smn*^{2B/-} and d. *Smn*^{2B/+}. Data represents mean and error bars represent +/- SEM; Unpaired t Test, *p<0.05 **p<0.01 ***p<0.001 ****p<0.0001.

4.3.26 Melatonin treatment did not alter the count of alpha motor neurons.

In the previous stage, the decrease in pathological markers of SC suggests that melatonin can have a neuroprotective effect on SC. We aim to investigate whether this protective effect covers alpha motor neurons, which are a hallmark of SMA. To answer this question, counts of alpha motor neurons were performed in symptomatic spinal cord sections, utilizing Nissl staining to analyse following melatonin application.

In the *Smn*^{2B/-} mouse model, our analysis using fluorescence microscopy revealed no significant difference in motor neuron numbers between those treated with melatonin (depicted in figure 4.27.a) and those without treatment (figure 4.27.c).

Similarly, the *Smn*^{2B/+} mice exhibited no change in the number of motor neurons after receiving the same melatonin treatment (figure 4.27.b.) when compared to the controls (figure 4.27.d.), as evidenced by the fluorescence microscopy images Thus, melatonin treatment did not affect motor neuron counts in both the *Smn*^{2B/-} and *Smn*^{2B/+} mice.



e.

f.

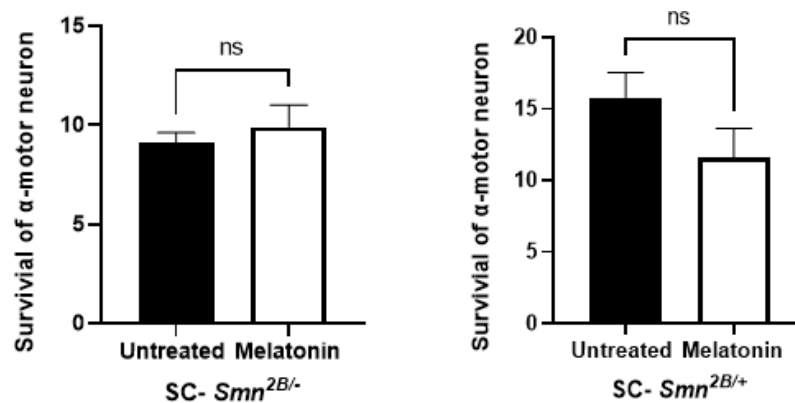


Figure 4. 27 The number of alpha motor neurons remain steady after 50 mg/kg/day daily melatonin treatment in symptomatic SC in both *Smn*^{2B/-} and *Smn*^{2B/+} mouse model.

Representative images of Nissl-stained cross sections of SC from P18 untreated and melatonin-treated (50 mg/kg/day through gavage) a.c. *Smn*^{2B/+} and b.d *Smn*^{2B/-} mice (scale bars = 50 μ m) and quantification of horn area.

Data are mean \pm SEM, n = 3–7 animals per experimental group, Data represents mean and error bars represent +/- SEM; Unpaired t Test, ns=not significant. The arrow points indicate alpha motor neurons for each image.

*p<0.05 **p<0.01 ***p<0.001 ****p<0.0001.* Untreated groups are the same within the three drug application groups.

4.3.27 Melatonin led to an upregulation of the *CAT* antioxidant gene in the spinal cord tissues of mice with symptomatic SMA.

As mentioned above, the observation of melatonin's neuroprotective effect suggests that melatonin could be an antioxidative agent. To examine the effects of melatonin, administered at a dose of 50 mg/kg/day, on the expression of the *CAT/SOD* genes in symptomatic spinal cord tissues. This comparison demonstrated an elevation in *CAT* gene expression as a result of the melatonin treatment at a dose of 50 mg/kg/day in both the *Smn*^{2B/-} and *Smn*^{2B/+} mouse (figure 4.28.a, b). In the case of the *SOD* gene, an increase in expression was noted specifically in the *Smn*^{2B/+} (figure 4.28.d)

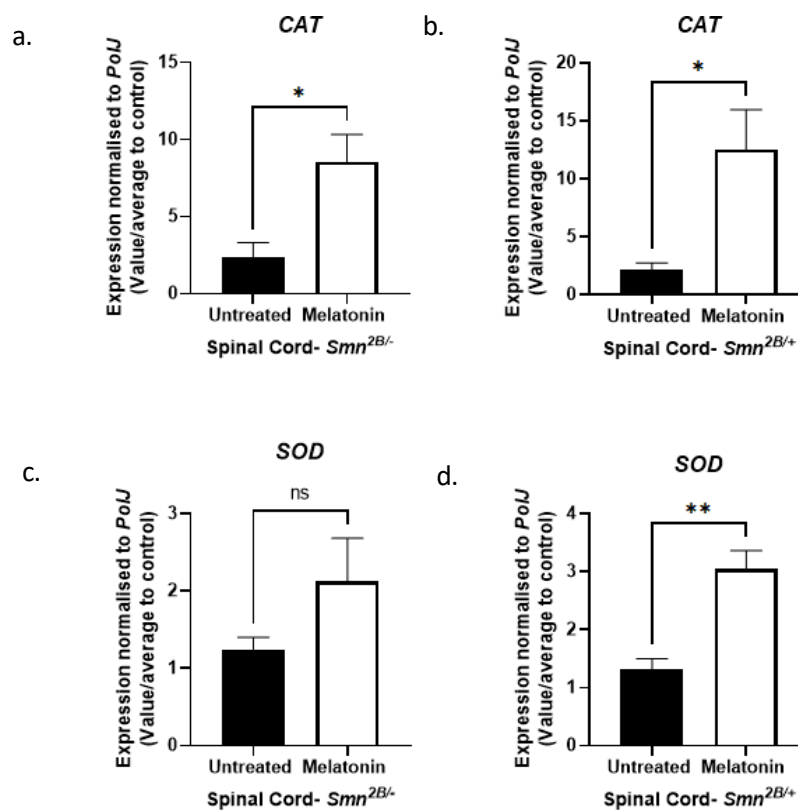


Figure 4. 28 The administration of 50 mg/kg/day melatonin increased the expression of the antioxidant *CAT* gene, in symptomatic SMA spinal cord tissues.

All animals were treated 50 mg/kg/day melatonin (diluted in 0.5% CMC) via daily gavage starting at P5 till P18. Symptomatic spinal cord was harvest from untreated (n=8, black bars) and melatonin treated (n=8, white bars) in non-fasted *Smn*^{2B/-} and *Smn*^{2B/+}, after 2 hours last melatonin treatment. The mRNA levels of *CAT* gene are in a. *Smn*^{2B/-} and b. *Smn*^{2B/+}; *SOD* gene level in c. *Smn*^{2B/-} and d. *Smn*^{2B/+}. Data represents mean and error bars represent +/- SEM; Unpaired t Test, ns=not significant. *p<0.05 **p<0.01***p<0.001****p<0.0001.

4.3.28 Administering melatonin did not alter the mRNA expression of core clock genes in the spinal cord of a milder form of symptomatic SMA mouse model.

To clarify the influence of melatonin on spinal cord development and homeostasis, the regulation of circadian genes, which may act as central controllers, was investigated. To do this, we conducted qPCR analyses to compare gene expression patterns over a daily cycle in spinal cord tissues from P18 symptomatic mice, both with and without melatonin treatment in *Smn*^{2B/-} and *Smn*^{2B/+} mouse. Our findings revealed that melatonin does not affect the expression of genes related to circadian rhythms (*Clock*, *Bmal1* and *Per2*) in the spinal cord tissues of *Smn*^{2B/-} SMA mouse model and control group (figure 4.29).

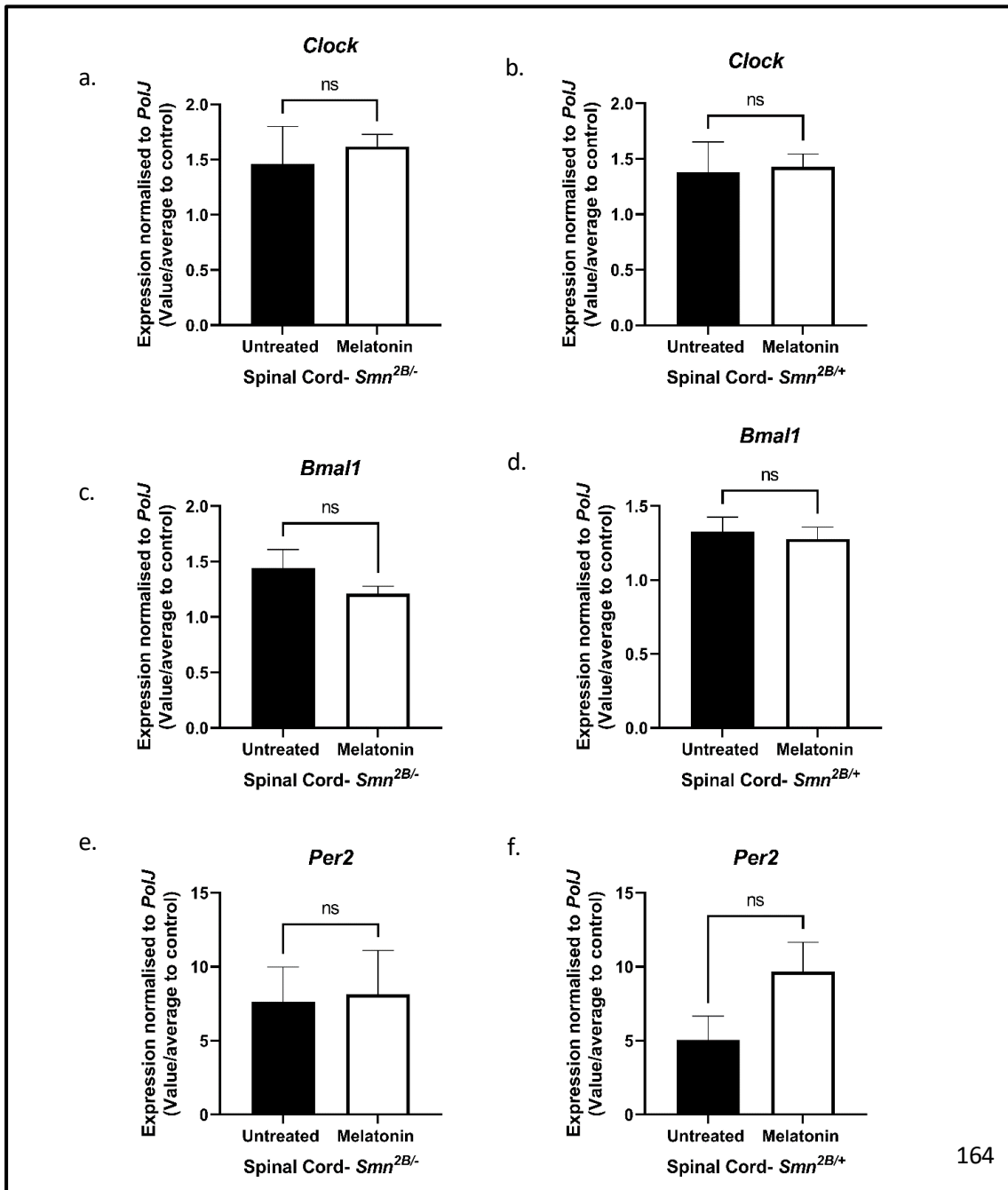


Figure 4. 29 Administering melatonin does not alter the mRNA expression of core clock genes in the spinal cord of a milder form of symptomatic SMA mouse model.

All animals were treated with 50 mg/kg/day melatonin (diluted in 0.5% CMC) via daily gavage starting at P5 till P18. Symptomatic spinal cord was harvested from untreated (n=8, black bars) and melatonin treated (n=8, white bars) in non-fasted *Smn*^{2B/-} and *Smn*^{2B/+}, after 2hours last melatonin treatment. The mRNA levels of *Clock* gene are in a. *Smn*^{2B/-} and b. *Smn*^{2B/+}; these of *Bmal1* are in c. *Smn*^{2B/-} and d. *Smn*^{2B/+}. And that of *Per2* are in e. *Smn*^{2B/-} and f. *Smn*^{2B/+}. Data represents mean and error bars represent +/- SEM; Unpaired t Test, *p<0.05 **p<0.01 ***p<0.001 ****p<0.0001.

Table 4. 5 Summary of melatonin effect on P18 SMA spinal cord in *Smn*^{2B/-}

Decipher melatonin effect	Method	Targeted genes/protein	Result	Model	Tissue
Molecular pathway	Quantification of mRNA level via qPCR	<i>In-silico</i> based (<i>Per1</i> , <i>Sirt1</i> , <i>Bcl-2</i> , <i>Ror-α</i>)	<i>Per1</i> level decreased; rest of them did not change	Symptomatic <i>Smn</i> ^{2B/-}	Spinal Cord
SC-specific pathologic marker for SMA		<i>Fas</i> , <i>Pmaip-1</i>	Both were downregulated		
Mitochondrial based-oxidative stress		Playing role as anti-oxidant (<i>CAT</i> , <i>SOD</i>)	Upregulation of <i>CAT</i> ; no change in <i>SOD</i> expression		
The counting of α- motor neurons	Nissl- Staining	Targets the Nissl bodies in the cell bodies and dendrites of neurons.	No alternation in the number of α- motor neurons		
Circadian Rhythm	Quantification of mRNA level via qPCR	Clock genes (<i>Clock</i> , <i>Bmal1</i> , <i>Per2</i>)	There was no change in core clock genes		

The provided table, as shown in the figure, systematically summarizes from left to right: the objective of the study plan, the chosen method, the targeted gene or protein, the result, the model used, and the type of tissue examined. The targeted genes have been systematically categorized into groups: sequentially, genes predicted through combined *in silico* analyses (*Per1*, *Sirt1*, *Bcl-2* and *Ror-α*), SC-specific pathologic marker (*Fas* and *Pmaip-1*), genes playing a role in oxidative stress (*CAT* and *SOD*), IHC technique for alpha motor neuron counting, core clock genes (*Bmal1*, *Clock* and *Per2*), The levels of these targeted genes have been quantified in spinal cord tissues following melatonin application using qPCR. The entire experimental system was carried out on the *Smn*^{2B/-} SMA mouse model.

4.3.29 Melatonin resulted in increased expression levels of *Per1*, *Sirt1*, and *Bcl2* in the symptomatic white adipose tissue of *Smn*^{2B/-} mice.

Since adipose tissue interacts with the liver, skeletal muscle, and pancreas to maintain metabolic balance, it should be studied in the context of SMA, which possesses a multifunctional pathology. Initially, symptomatic WAT tissues, both treated with melatonin and untreated, were harvested and subjected to qPCR analyses. Upon comparing the untreated *Smn*^{2B/-} model to the melatonin-treated *Smn*^{2B/-} mice, an increase in the mRNA levels of *Per1*, *Sirt1*, and *Bcl2* was observed (figure 4.30.a; c; e).

However, in the $Smn^{2B/+}$ mouse, a comparison between melatonin-treated and untreated WAT tissues showed no change in the levels of the transcriptomic-based target genes (figure 4.30.b; d; f).

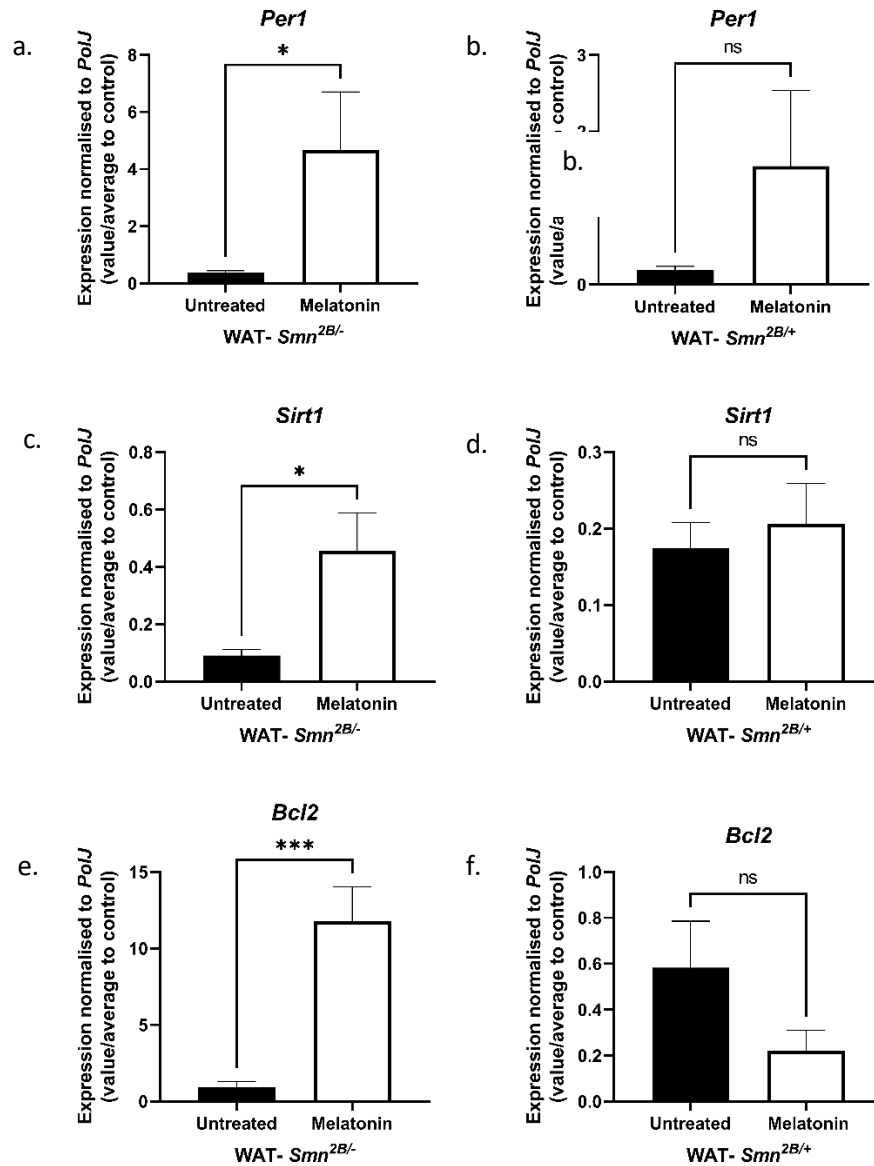


Figure 4. 30 Melatonin-induced increase in the expression of anticipated target genes, specifically *Per1*, *Sirt1*, and *Bcl2*, has been observed in the symptomatic white adipose tissue of $Smn^{2B/-}$ mice.

All animals were treated 50 mg/kg/day melatonin (diluted in 0.5% CMC) via daily gavage starting at P5 till P18. Symptomatic WAT tissue was harvest from untreated (n=8, black bars) and melatonin treated (n=8, white bars) in non-fasted $Smn^{2B/-}$ and $Smn^{2B/+}$, after 2 hours last melatonin treatment. The mRNA levels of *Per1* gene are in a. $Smn^{2B/-}$ and b. $Smn^{2B/+}$; these of *Sirt1* are in c. $Smn^{2B/-}$ and d. $Smn^{2B/+}$, the *Bcl2*

in e. *Smn*^{2B/-} and f. *Smn*^{2B/+}. Data represents mean and error bars represent +/- SEM; Unpaired t Test, ns=not significant, *p<0.05
p<0.01*p<0.001***p<0.0001.

4.3.30 Melatonin may regulate circadian rhythms in the WAT of *Smn*^{2B/-} mice through inducing *Clock* and *Per2* gene expression.

Next step, we aimed to determine the effects of melatonin on genes associated with circadian rhythms in symptomatic WAT of SMA mouse model via qPCR. Our findings revealed a marked upregulation of *Clock* and *Per2* gene expression in the WAT tissues of symptomatic *Smn*^{2B/-} mice treated with melatonin at a dose of 50 mg/kg/day, compared to the untreated littermate (figure 4.31.a; e). In the case of the *Smn*^{2B/+} mice, a downregulation of both *Clock* and *Bmal1* mRNA levels was observed following the same dosage of melatonin administered orally comparing untreated WAT tissue from *Smn*^{2B/+} mice (figure 4.31.b; d).

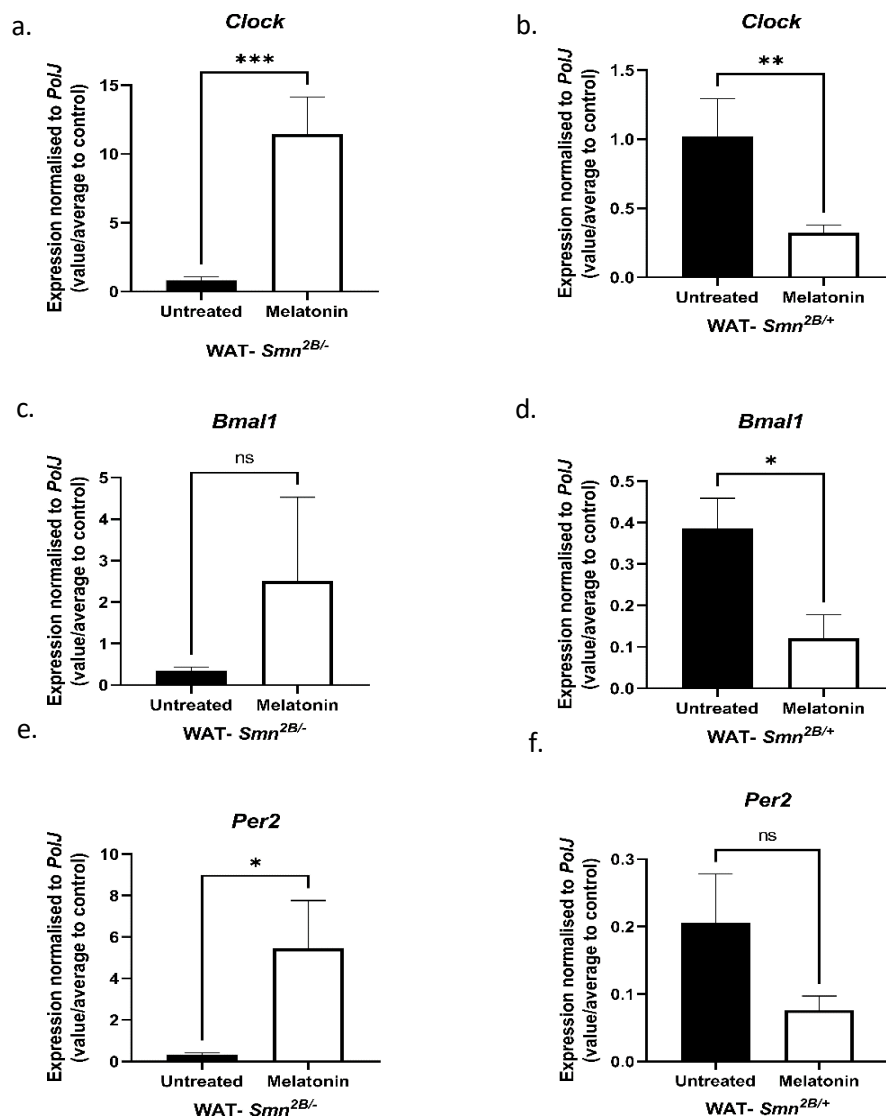


Figure 4. 31 Administering melatonin at a dose of 50 mg/kg/day could potentially modulate the circadian rhythms in the white adipose tissue of *Smn*^{2B/-} mice by enhancing the expression of *Clock* and *Per2* genes.

All animals were treated with 50 mg/kg/day melatonin (diluted in 0.5% CMC) via daily gavage starting at P5 till P18. Symptomatic WAT was harvest from untreated (n=8, black bars) and melatonin treated (n=8, white bars) in non-fasted *Smn*^{2B/-} and *Smn*^{2B/+}, after 2hours last melatonin treatment. The mRNA levels of *Clock* gene are in a. *Smn*^{2B/-} and b. *Smn*^{2B/+}; these of *Bmal1* are in c. *Smn*^{2B/-} and d. *Smn*^{2B/+}. And that of *Per2* are in e. *Smn*^{2B/-} and f. *Smn*^{2B/+} Data represents mean and error bars represent \pm SEM; Unpaired t Test, ns= not significant, *p<0.05 **p<0.01 ***p<0.001 ****p<0.0001.

4.3.31 Melatonin enhanced the defence against oxidative stress in the symptomatic WAT tissue of mice with SMA by increasing the levels of both *CAT* and *SOD*.

To maintain a balance in lipid and glucose metabolism, the relationship between adipose tissue and oxidative stress is complex and bidirectional (Fischer et al., 2013). To elucidate this interaction, the expression levels of the *SOD* and *CAT* genes in WAT were examined following melatonin treatment. When the harvested WAT tissues from the melatonin-treated mice were compared with untreated WAT, it was observed that *CAT* expression increased only in the *Smn*^{2B/-} mouse model (as shown in figure 4.32.a); meanwhile, *SOD* gene levels rose in the WAT tissues of both *Smn*^{2B/-} and *Smn*^{2B/+} mice (as indicated in figure 4.32.c; d), suggesting a potential antioxidative effect.

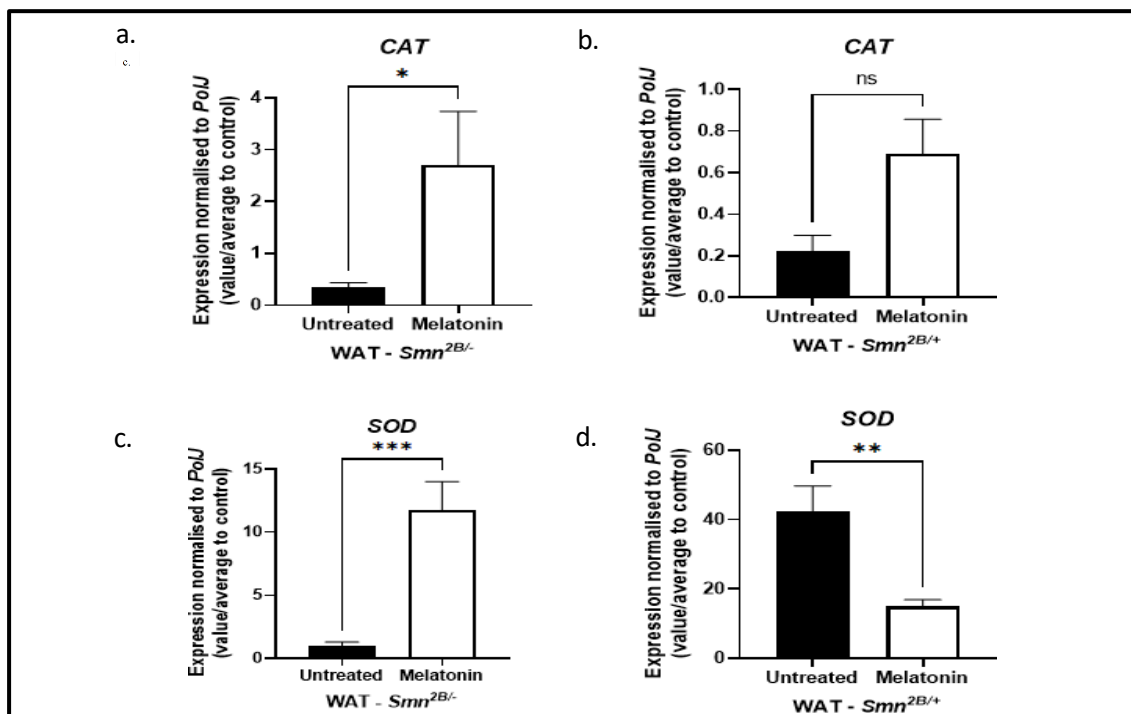


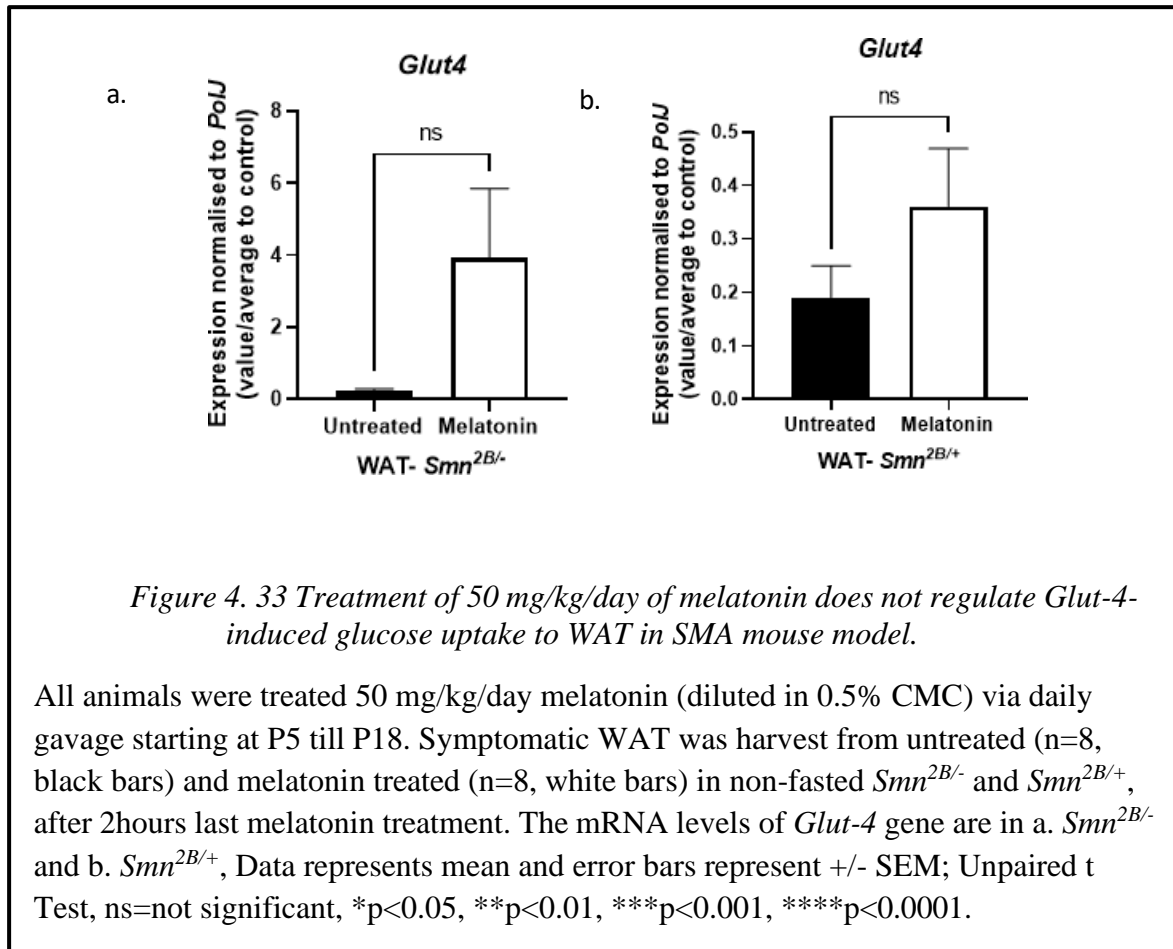
Figure 4. 32 The administration of 50 mg/kg/day melatonin increased the expression of the antioxidant *CAT*&*SOD* gene, in symptomatic SMA WAT.

All animals were treated 50 mg/kg/day melatonin (diluted in 0.5% CMC) via daily gavage starting at P5 till P18. Symptomatic spinal cord was harvested from untreated (n=8, black bars) and melatonin treated (n=8, white bars) in non-fasted *Smn*^{2B/-} and *Smn*^{2B/+}, after 2 hours last melatonin treatment. The mRNA levels of *CAT* gene are in

a. *Smn*^{2B/-} and b. *Smn*^{2B/+}; *SOD* gene level in c. *Smn*^{2B/-} and d. *Smn*^{2B/+}. Data represents mean and error bars represent +/- SEM; Unpaired t Test, ns=not significant. *p<0.05 **p<0.01 ***p<0.001 ****p<0.0001.

4.3.32 Melatonin does not to be involved in mediating Glut4-induced glucose uptake in WAT of the SMA mouse model.

To clarify the relationship insulin resistance and WAT tissue; the change in *Glut4* gene expression in symptomatic WAT of SMA mouse models was searched following melatonin treatment. Upon comparing WAT from melatonin-treated mice with that from untreated controls during the symptomatic phase, it was observed that there were no changes in *Glut4* gene expression in the treatment group for both *Smn*^{2B/-} (as illustrated in figure 4.33.a) and *Smn*^{2B/+} (as depicted in figure 4.33.b) mice.



4.3.33 Melatonin administration leads to the induction of browning in white adipose tissue in the SMA mouse model.

Melatonin is known to increase the mitochondrial content in WAT, from energy storage to energy burning, a process referred to as browning (Xu *et al.*, 2020).

The experiment revealed that, in the *Smn*^{2B/-} mouse model, there was a significant increase in *UCP-1* gene, marker for BAT, expression following administration of melatonin at 50 mg/kg/day (figure 4.34.a) (Jespersen *et al.*, 2013). There was also an observed increase in *ASC-1*, marker for WAT, expression in the symptomatic WAT of the *Smn*^{2B/-} mice (figure 4.34.c) (Ussar *et al.*, 2014). In the *Smn*^{2B/+}, there was no change in the mRNA levels of both genes following the administration of melatonin (figure 4.34.b; d.).

Melatonin administration in the SMA mouse model leads to the induction of browning in white adipose tissue.

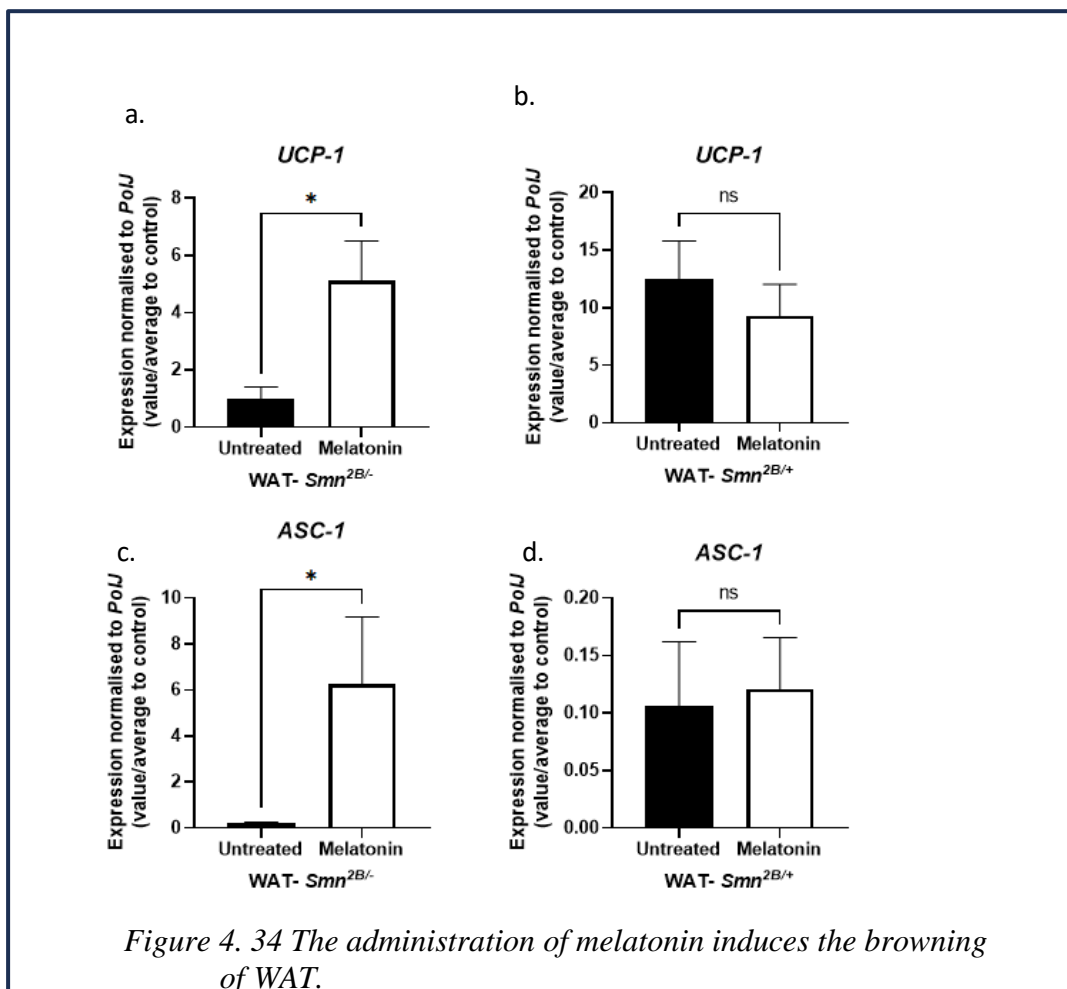


Figure 4. 34 The administration of melatonin induces the browning of WAT.

All animals were treated with 50 mg/kg/day melatonin (diluted in 0.5% CMC) via daily gavage starting at P5 till P18. Symptomatic WAT was harvest from untreated (n=8, black bars) and melatonin treated (n=8, white bars) in non-fasted *Smn*^{2B/-} and *Smn*^{2B/+}, after 2hours last melatonin treatment. The mRNA levels of UCP-1 gene are in a. *Smn*^{2B/-} and b. *Smn*^{2B/+}; these of ASC-1 are in c. *Smn*^{2B/-} and d. *Smn*^{2B/+}. Data represents mean and error bars represent +/- SEM; Unpaired t Test, ns=not significant. *p<0.05 **p<0.01***p<0.001****p<0.0001.

Table 4. 6 Summary of melatonin effect on P18 SMA WAT in *Smn*^{2B/-}

Decipher melatonin effect	Method	Targeted genes/protein	Result	Model	Tissue
Molecular pathway	Quantification of mRNA level via qPCR	<i>In-silico</i> based (<i>Per1</i> , <i>Sirt1</i> , <i>Bcl-2</i>)	mRNA level of all were upregulated	<i>Symptomatic Smn</i> ^{2B/-}	WAT
Shifting WAT' function (browning)		<i>UCP-1</i> and <i>ASC-1</i>	Both were increased		
Mitochondrial based-oxidative stress		Playing role as anti-oxidant (<i>CAT</i> , <i>SOD</i>)	Upregulation of <i>CAT</i> and <i>SOD</i> expression		
Glucose Uptake		<i>Glut4</i>	No alternation		
Circadian Rhythm		Clock genes (<i>Clock</i> , <i>Bmal1</i> , <i>Per2</i>)	There was an increase in <i>Clock</i> and <i>Per2</i> <i>Bmal1</i> → no change		

The provided table, as shown in the figure, systematically summarizes from left to right: the objective of the study plan, the chosen method, the targeted gene or protein, the result, the model used, and the type of tissue examined. The targeted genes have been systematically categorized into groups: sequentially, genes predicted through combined *in silico* analyses (*Per1*, *Sirt1*, *Bcl-2* and *Ror-α*), shifting WAT function marker (browning), genes playing a role in oxidative stress (*CAT* and *SOD*), gene involving glucose uptake from circulation (*Glut4*), core clock genes (*Bmal1*, *Clock* and *Per2*), The levels of these targeted genes have been quantified in WAT tissues following melatonin application using qPCR. The entire experimental system was carried out on the *Smn*^{2B/-} SMA mouse model.

4.3.34 In the *Smn*^{2B/+} mouse, a decrease in the expression of *Per1* and *Bcl2* genes within the brown adipose tissue (BAT) is induced by melatonin treatment.

In addition to its role in energy metabolism, the dysregulation of pathways like *Klf15* associated with SMA pathology (Lisa M. Walter et al., 2018) makes BAT a target for inclusion in the study of peripheral perspective of SMA. To examine the molecular effects of melatonin on symptomatic BAT, qPCR experiments were conducted to assess melatonin's impact on the expression of *in silico*-based-targeted genes within the BAT. The findings indicate that oral administration of 50 mg/kg/day of melatonin resulted in the downregulation of *Per1* and *Bcl2* gene expression in the symptomatic BAT tissue of the *Smn*^{2B/+} mouse model, as shown in figure 4.35.b; f. In contrast, no melatonin-related changes in the mRNA levels of genes identified through transcriptomic analysis were observed in the symptomatic BAT tissues of the *Smn*^{2B/-} control group (figure 4.35.a; c; e).

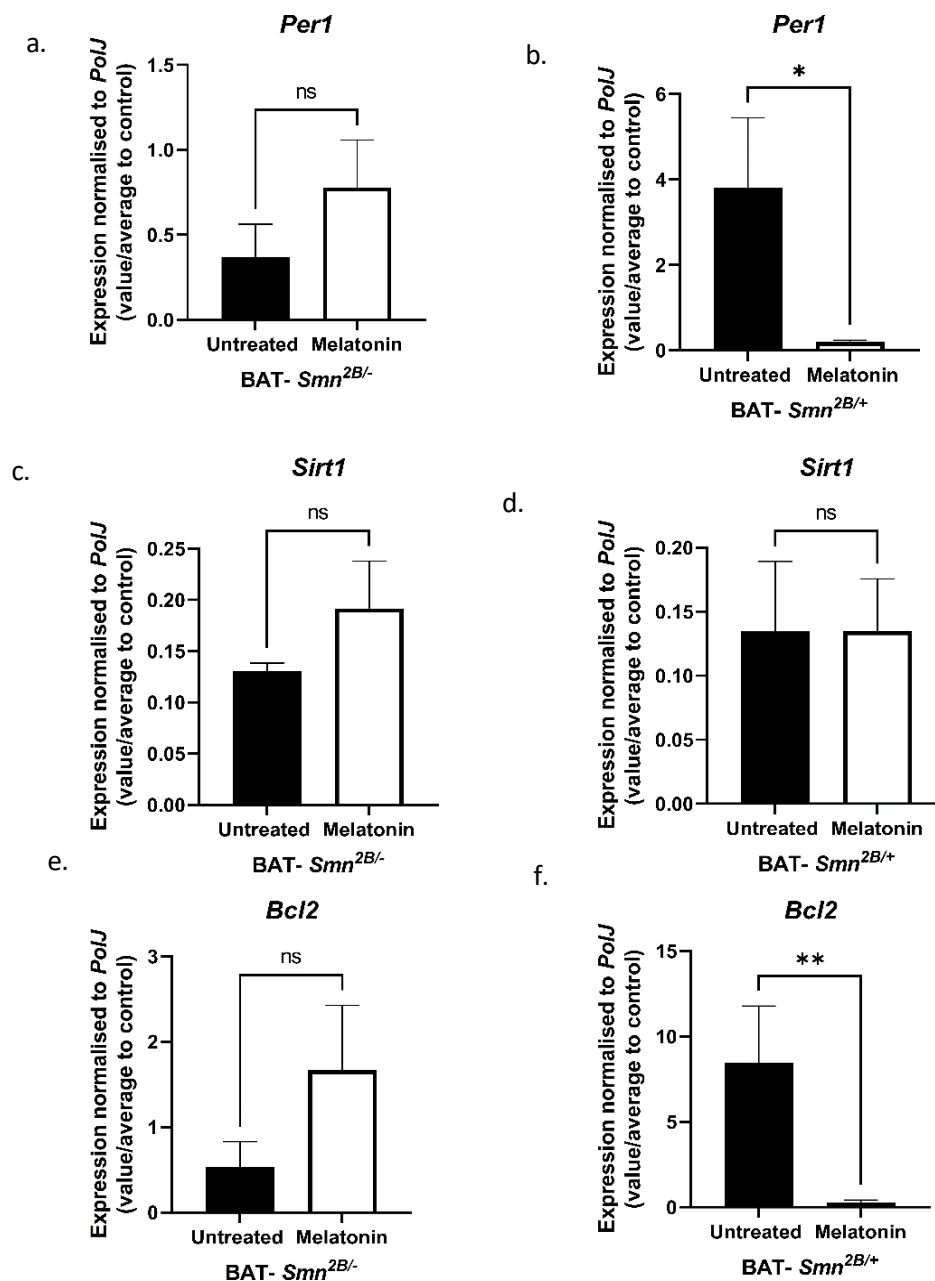


Figure 4.35 In the *Smn*^{2B/+} SMA mice, melatonin treatment leads to reduced expression of the *Per1* and *Bcl2* genes in BAT.

All animals were treated with 50 mg/kg/day melatonin (diluted in 0.5% CMC) via daily gavage starting at P5 till P18. Symptomatic BAT was harvested from untreated (n=8, black bars) and melatonin treated (n=8, white bars) in non-fasted *Smn*^{2B/-} and *Smn*^{2B/+}, after 2 hours last melatonin treatment. The mRNA levels of *Per1* gene are in a. *Smn*^{2B/-} and b. *Smn*^{2B/+}; these of *Sirt1* are in c. *Smn*^{2B/-} and d. *Smn*^{2B/+}, the *Bcl2* are in e. *Smn*^{2B/-} and f. *Smn*^{2B/+}. Data represents mean and error bars represent +/- SEM; Unpaired t Test, ns=not significant, *p<0.05 **p<0.01 ***p<0.001 **p<0.0001.

4.3.35 Melatonin administration resulted in the decreased expression of *Clock*, *Bmal1*, and *Per2* genes, potentially influencing the regulation of circadian rhythms in BAT of *Smn*^{2B/-} mice.

Given that the diurnal dysregulation of BAT in the Taiwanese *Smn*^{-/-}; *SMN2* model is known, the study aims to investigate the effect of melatonin, a circadian rhythm regulator, on this dysregulation (Lisa M Walter et al., 2018). The data indicated a significant downregulation in the expression of genes *Clock*, *Bmal1*, and *Per2* in the BAT of *Smn*^{2B/-} mice administered with a melatonin when contrasted with their untreated counterparts (figure 4.36.a; c; e). On the other hand, the *Smn*^{2B/+} mice showed no notable change in mRNA levels following the melatonin treatment (figure 4.36.b; d; f.).

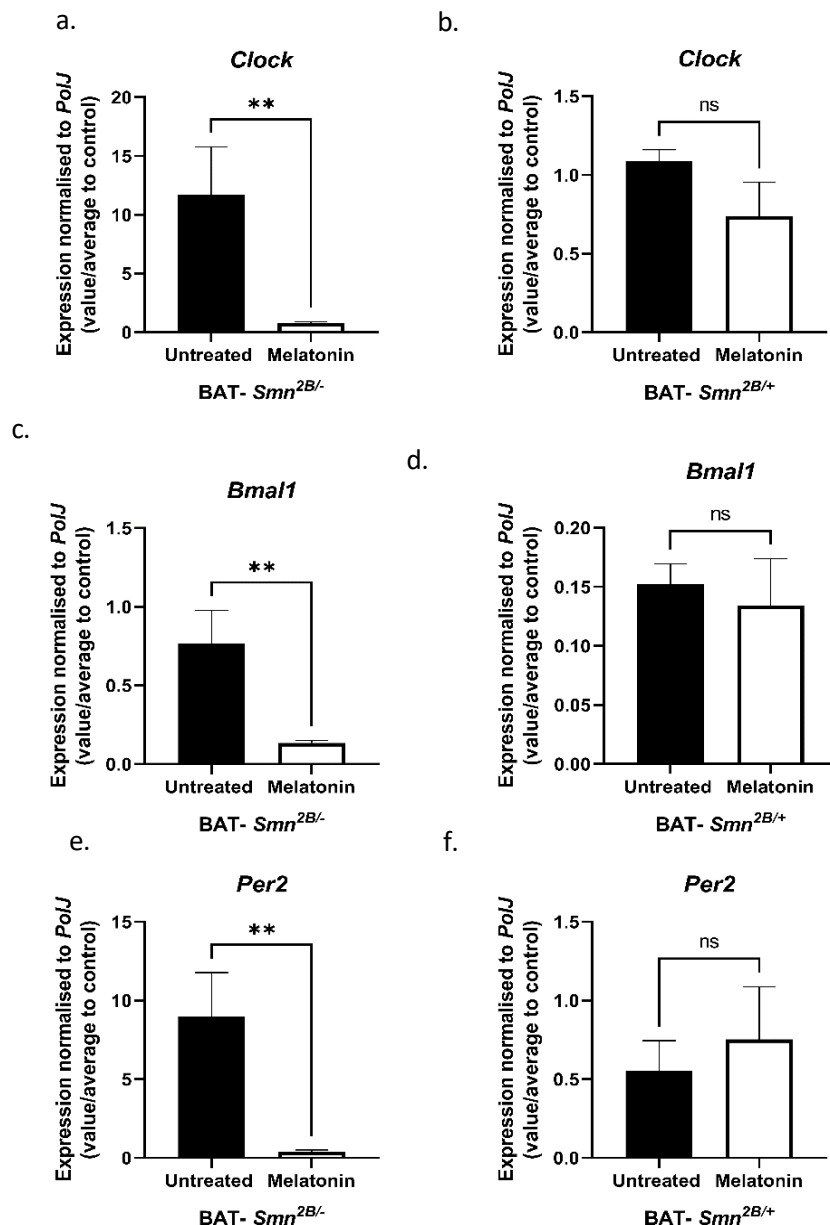


Figure 4. 36 Melatonin treatment led to a reduction in the levels of *Clock*, *Bmal1*, and *Per2* gene expression, which may affect the circadian rhythm control in the BAT of *Snn2B*^{-/-} mice.

All animals were treated with 50 mg/kg/day melatonin (diluted in 0.5% CMC) via daily gavage starting at P5 till P18. Symptomatic BAT was harvest from untreated (n=8, black bars) and melatonin treated (n=8, white bars) in non-fasted *Snn*^{2B/-} and *Snn*^{2B/+}, after 2hours last melatonin treatment. The mRNA levels of *Clock* gene are in a. *Snn*^{2B/-} and b. *Snn*^{2B/+}; these of *Bmal1* are in c. *Snn*^{2B/-} and d. *Snn*^{2B/+}. And that of *Per2* are in e. *Snn*^{2B/-} and f. *Snn*^{2B/+} Data represents mean and error bars represent \pm SEM; Unpaired t Test, * $p < 0.05$ ** $p < 0.01$ *** $p < 0.001$ **** $p < 0.0001$.

4.3.36 The mRNA level of CAT mRNA has decreased in symptomatic BAT tissues in $Smn^{2B/+}$ following melatonin application.

The efficacy of melatonin in reducing oxidative stress was evaluated in the symptomatic BAT of SMA mice by measuring the expression of *SOD* and *CAT* genes. A comparative analysis of BAT tissue from melatonin-treated and untreated mice revealed a specific decline in *CAT* gene expression within the $Smn^{2B/+}$ mouse strain (illustrated in figure.4.37. a.). In contrast, the levels of the *SOD* gene remained unchanged in both $Smn^{2B/-}$ and $Smn^{2B/+}$ mouse (as detailed in figure 4.37.c; d).

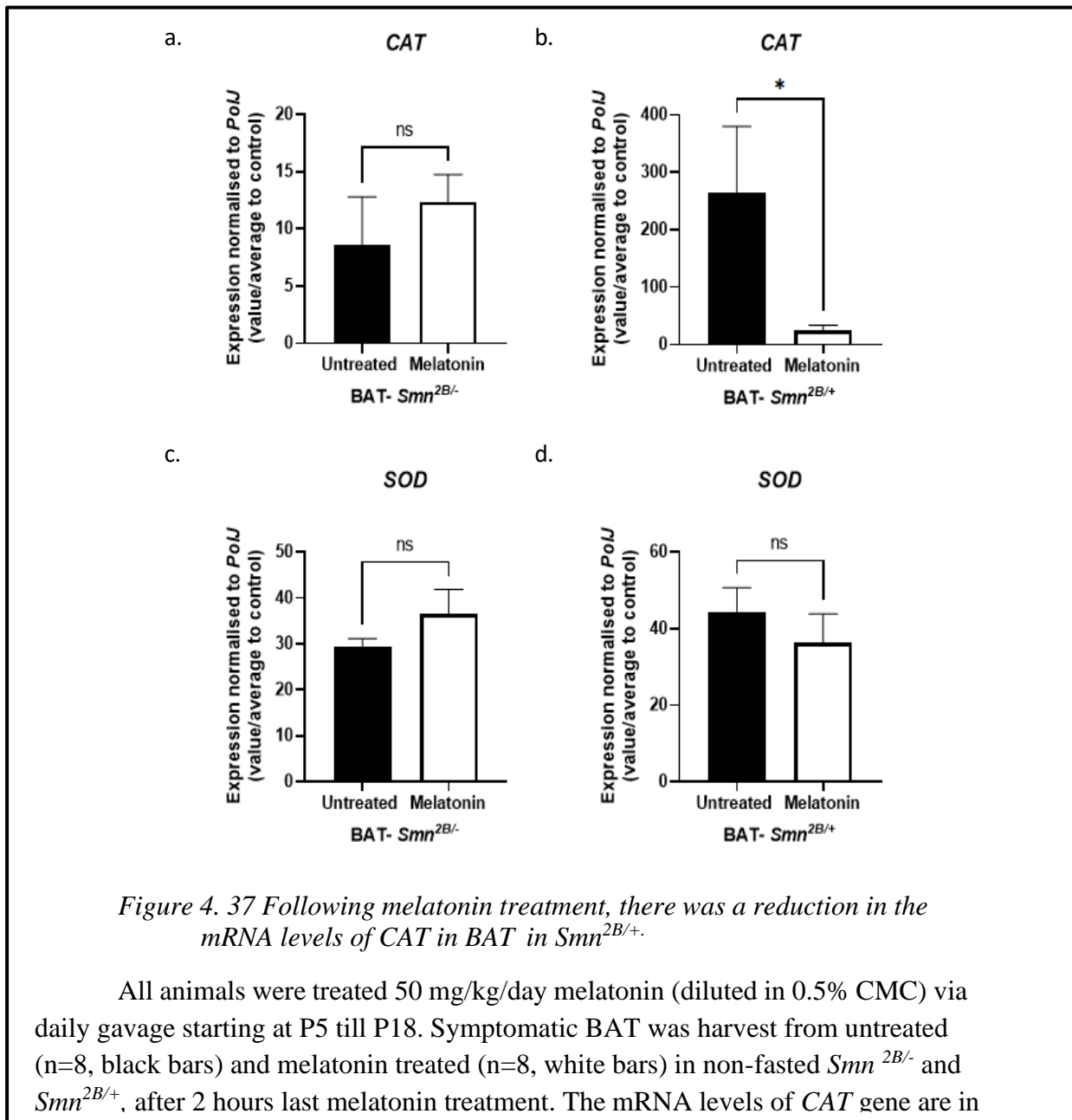


Figure 4. 37 Following melatonin treatment, there was a reduction in the mRNA levels of CAT in BAT in $Smn^{2B/+}$.

All animals were treated 50 mg/kg/day melatonin (diluted in 0.5% CMC) via daily gavage starting at P5 till P18. Symptomatic BAT was harvest from untreated (n=8, black bars) and melatonin treated (n=8, white bars) in non-fasted $Smn^{2B/-}$ and $Smn^{2B/+}$, after 2 hours last melatonin treatment. The mRNA levels of *CAT* gene are in

- a. $Smn^{2B/-}$ and b. $Smn^{2B/+}$; *SOD* gene level in c. $Smn^{2B/-}$ and d. $Smn^{2B/+}$.
Data represents mean and error bars represent +/- SEM; Unpaired t Test, ns=not significant. * $p < 0.05$ ** $p < 0.01$, *** $p < 0.001$, **** $p < 0.0001$.

4.3.37 Administering of melatonin reduced in mRNA level of *Glut4* in the brown adipose tissue of the symptomatic the $Smn^{2B/+}$ mouse control group

We tested whether melatonin administration alters *Glut4* expression in the brown adipose tissue of symptomatic SMA mice., we found no alteration in *Glut4* expression within the $Smn^{2B/-}$ mice (as shown in figure 4.38.a). However, in the $Smn^{2B/+}$, *Glut4* expression decreased in the BAT following melatonin application (as indicated in figure 4.38.b).

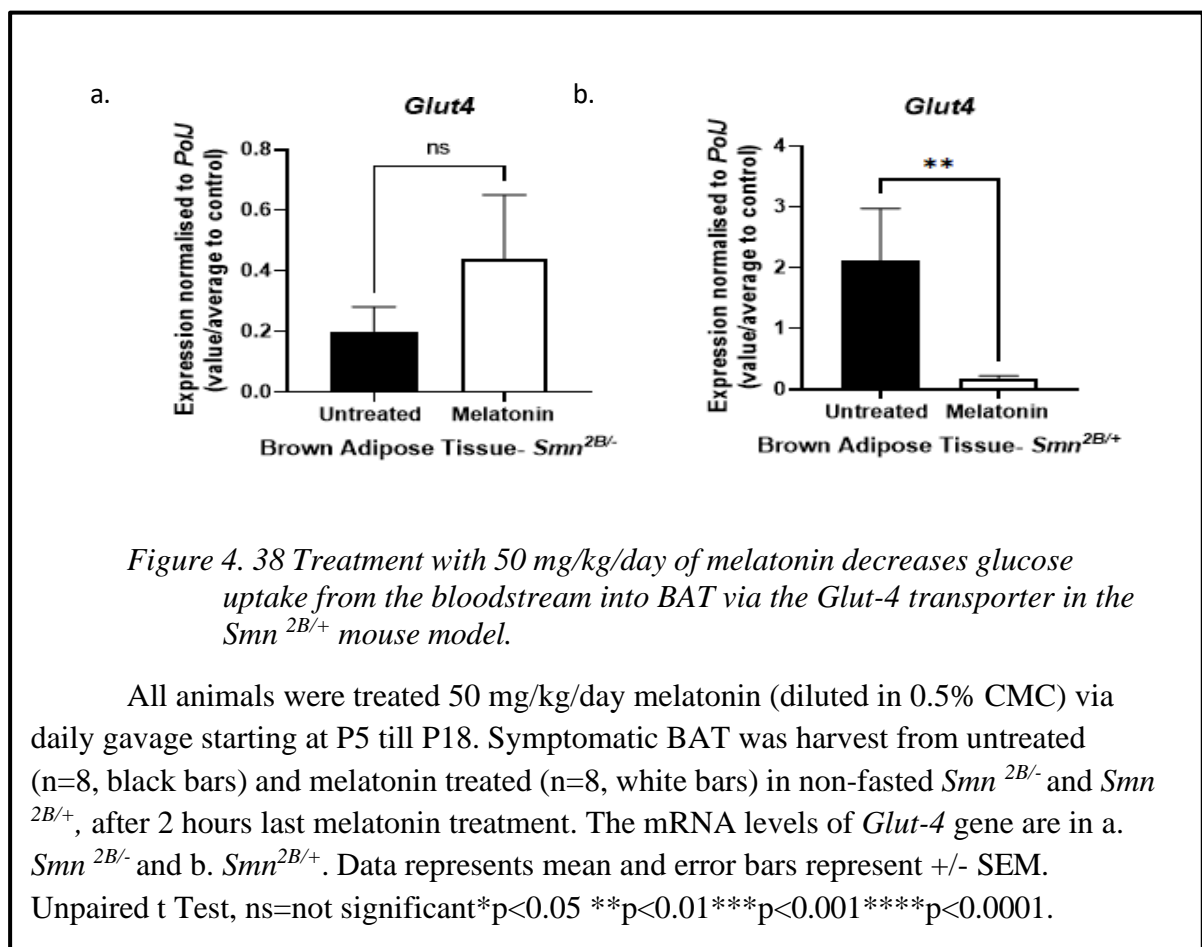


Table 4. 7 Summary of melatonin effect on P18 SMA BAT in *Smn*^{2B/-}

Decipher melatonin effect	Method	Targeted genes/protein	Result	Model	Tissue
Molecular pathway	Quantification of mRNA level via qPCR	<i>In-silico</i> based (<i>Per1, Sirt1, Bcl-2</i>)	No alternation	<i>Symptomatic Smn</i> ^{2B/-}	BAT
Mitochondrial based-oxidative stress		Playing role as anti-oxidant (<i>CAT, SOD</i>)	No change		
Glucose Uptake		<i>Glut4</i>	No difference		
Circadian Rhythm		<i>Clock genes</i> (<i>Clock, Bmal1, Per2</i>)	Level of all were downregulated		

The provided table, as shown in the figure, systematically summarizes from left to right: the objective of the study plan, the chosen method, the targeted gene or protein, the result, the model used, and the type of tissue examined. The targeted genes have been systematically categorized into groups: sequentially, genes predicted through combined *in silico* analyses (*Per1, Sirt1, Bcl-2*), genes playing a role in oxidative stress (*CAT* and *SOD*), gene involving glucose uptake from circulation (*Glut4*), core clock genes (*Bmal1, Clock* and *Per2*), The levels of these targeted genes have been quantified in BAT tissues following melatonin application using qPCR. The entire experimental system was carried out on the *Smn*^{2B/-} SMA mouse model.

4.3.38 Melatonin application downregulated the expression level of *Ror-α* in the symptomatic pancreas tissues of SMA mice.

The protective effect of melatonin on pancreatic tissue, as reported in the literature (Abdulwahab et al., 2021), and its potential influence on the developmental defects of the pancreas observed in the SMA model (Bowerman et al., 2014), warrant further investigation for comprehensive understanding of peripheral pathology. Our research aimed to understand the effect of melatonin on the pancreas tissue, focusing on the *Per1*, *Bcl2*, and *Ror-α* genes. Our results showed a decrease in *Ror-α* expression in *Smn^{2B/-}* mice treated with melatonin at a dose of 50 mg/kg/day (see figure 4. 39. e). In the *Smn^{2B/+}*, we observed no significant changes in the expression levels of all the targeted genes between the melatonin-treated and untreated symptomatic pancreas (refer to figure 4.39.b; d; f.).

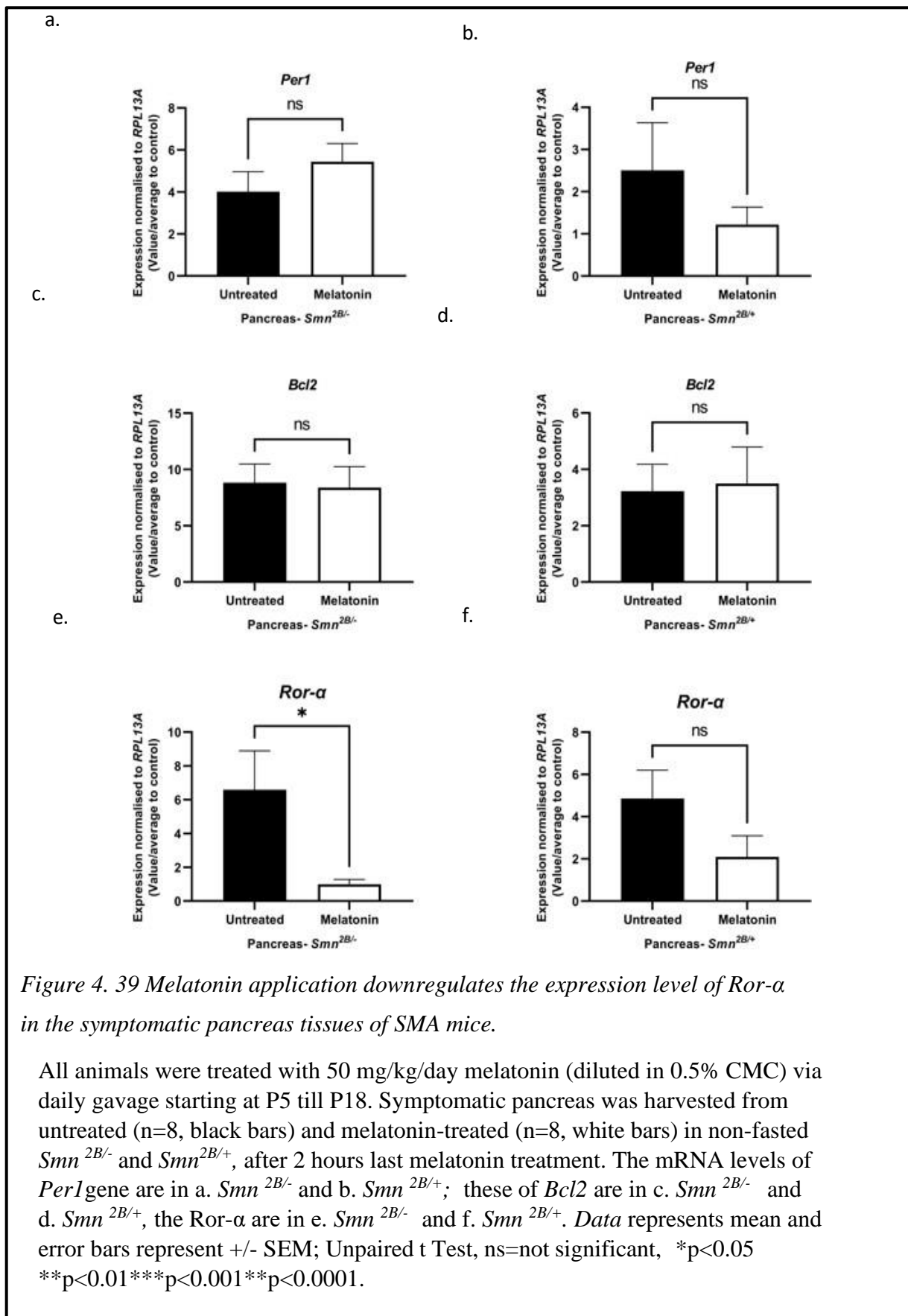


Figure 4. 39 Melatonin application downregulates the expression level of *Ror-α* in the symptomatic pancreas tissues of SMA mice.

All animals were treated with 50 mg/kg/day melatonin (diluted in 0.5% CMC) via daily gavage starting at P5 till P18. Symptomatic pancreas was harvested from untreated (n=8, black bars) and melatonin-treated (n=8, white bars) in non-fasted *Smn^{2B/-}* and *Smn^{2B/+}*, after 2 hours last melatonin treatment. The mRNA levels of *Per1* gene are in a. *Smn^{2B/-}* and b. *Smn^{2B/+}*; these of *Bcl2* are in c. *Smn^{2B/-}* and d. *Smn^{2B/+}*, the *Ror-α* are in e. *Smn^{2B/-}* and f. *Smn^{2B/+}*. Data represents mean and error bars represent +/- SEM; Unpaired t Test, ns=not significant, *p<0.05 **p<0.01 ***p<0.001 **p<0.0001.

4.3.39 Melatonin had no effect on the expression of diurnal genes in the pancreas tissues of SMA mice.

Disruptions in circadian rhythms are linked to metabolic syndrome, affecting pancreatic functions and increasing the risk of T2DM (Corella et al., 2016); a condition already associated with SMA (Bowerman et al., 2012a). Researching the impact of circadian molecular stabilizers, such as melatonin, on the pancreas in *Smn^{2B/-}* mouse models, could yield significant insights into the comprehensive pathology of SMA. In our study, we also examined the possible therapeutic impact of melatonin on the expression of genes associated with circadian rhythms, specifically *Clock*, *Bmal1*, and *Per2*, in the symptomatic pancreas tissues of SMA mouse models. The results of our experiments indicated that melatonin did not affect the regulation of diurnal gene mRNA levels in *Smn^{2B/-}* SMA models of symptomatic pancreas tissue, as compared to control group (refer to figure 4.40.).

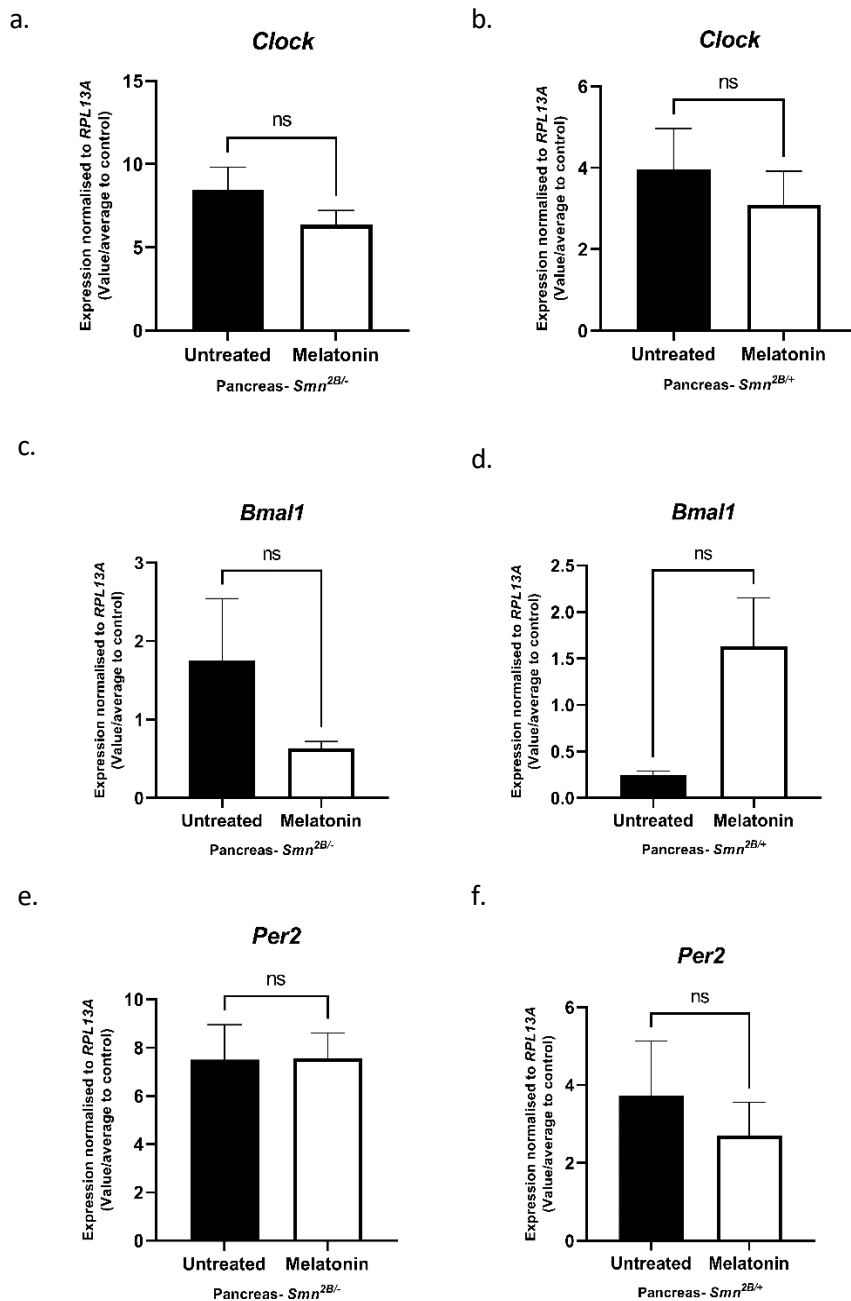


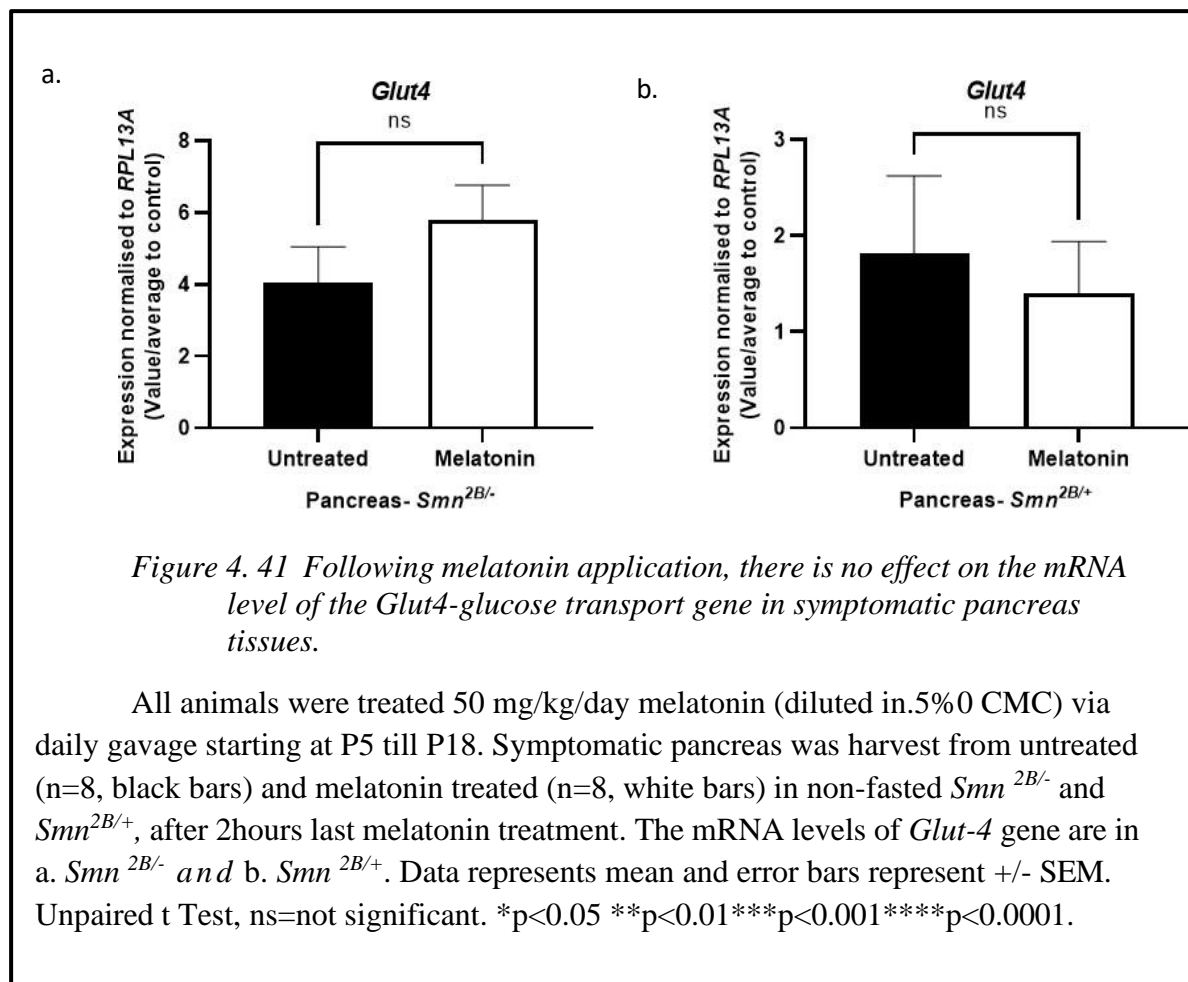
Figure 4. 40 Melatonin has no therapeutic effect on the expression of diurnal genes in the pancreas tissues of SMA mice.

All animals were treated with 50 mg/kg/day melatonin (diluted in 0.5% CMC) via daily gavage starting at P5 till P18. Symptomatic pancreas was harvest from untreated (n=8, black bars) and melatonin treated (n=8, white bars) in non-fasted *Smn*^{2B/-} and *Smn*^{2B/+}, after 2hours last melatonin treatment. The mRNA levels of *Clock* gene are in a. *Smn*^{2B/-} and b. *Smn*^{2B/+}; these of *Bmal1* are in c. *Smn*^{2B/-} and d. *Smn*^{2B/+}. And that of *Per2* are in e. *Smn*^{2B/-} and f. *Smn*^{2B/+} Data represents mean and error bars represent +/- SEM; Unpaired t Test, *p<0.05 **p<0.01 ***p<0.001 ***p<0.0001.

4.3.40 After administering melatonin, it was observed that there is no impact on the mRNA expression of the *Glut4*-glucose transport gene in the symptomatic pancreas tissues of *Smn*^{2B/-} SMA mouse.

Our study delved into the potential effects of melatonin on glucose metabolism, an important aspect of pancreatic function. The aim was to assess whether a dosage of 50 mg/kg/day of melatonin could alter the expression of the *Glut4* gene in the symptomatic pancreas of SMA mice, in comparison with triceps tissues from age matched SMA mice not treated with melatonin.

Upon comparing the triceps tissues of melatonin-treated mice to those of untreated mice during the symptomatic phase, we observed no notable increase in the expression of the *Glut4* gene in either the *Smn*^{2B/-} or *Smn*^{2B/+} mouse, as indicated in figure 4.41.



4.3.41 Administering daily melatonin resulted in an upregulation of the *CAT* gene in the symptomatic pancreas tissues of *Smn*^{2B/-} mice.

Melatonin is known to reduce lipid peroxidation and help revert the activity of antioxidant enzymes in the pancreas (Carrasco et al., 2014). Therefore, it is of interest to research whether melatonin could impact pancreatic pathologies seen in SMA through its influence on oxidative stress.

Our findings revealed that in the pancreas tissues of melatonin-treated symptomatic *Smn*^{2B/-} mouse model, there was a noticeable increase in *CAT* gene expression following the 50 mg/kg/day melatonin treatment, as shown in figure 4.42.a. However, for the *SOD* gene, there was no significant difference in expression observed between the melatonin-treated and untreated SMA mice, as depicted in figures 4.42.c and 4.42.d.

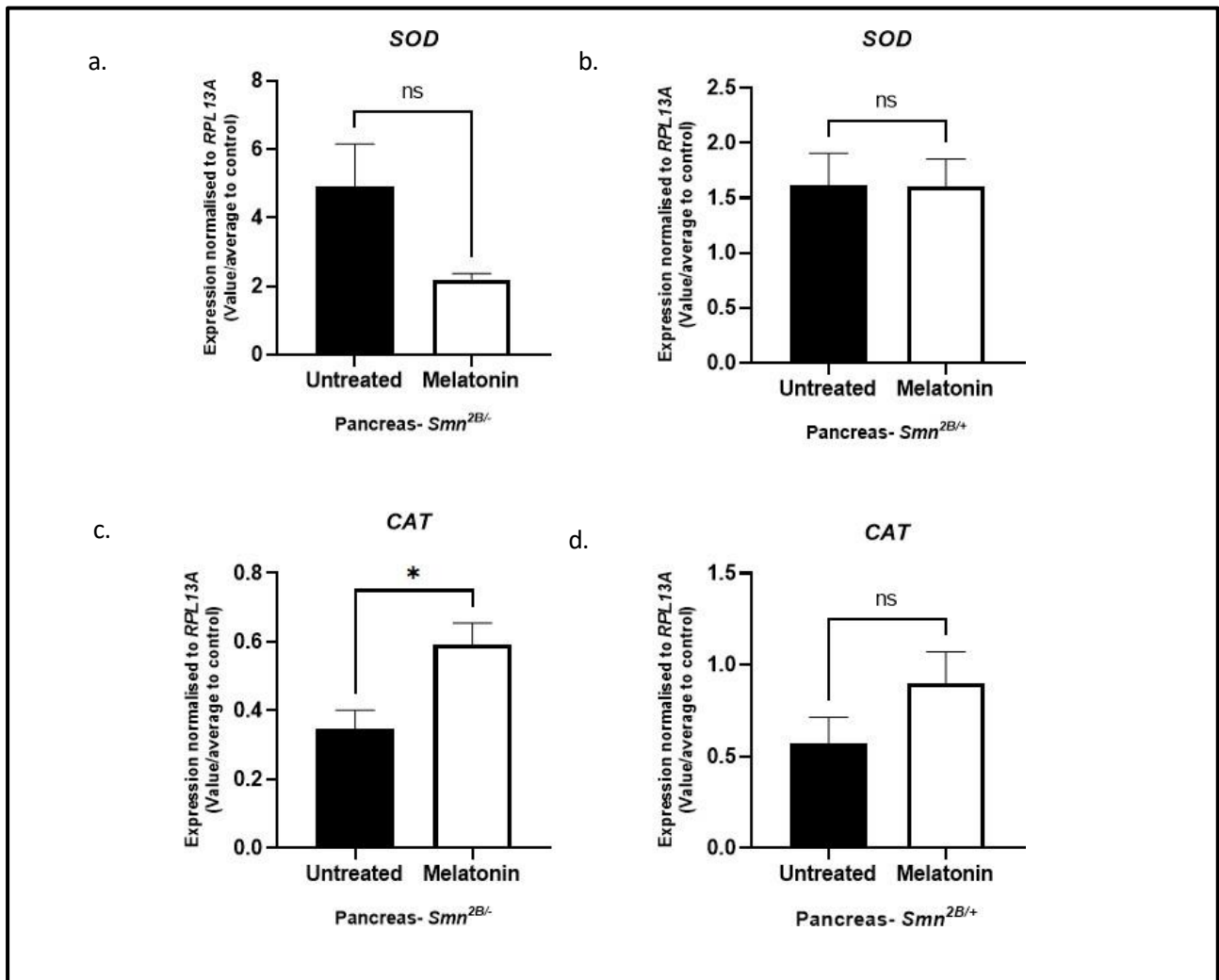


Figure 4. 42 The treatment with melatonin at a daily rate of 50 mg/kg has been found to enhance the expression of the CAT gene, which acts as a hydrogen peroxide scavenger in mitochondria, specifically in the symptomatic pancreas of *Smn*^{2B/-} mice.

All animals were treated with 50 mg/kg/day melatonin (diluted in 0.5% CMC) via daily gavage starting at P5 till P18. Symptomatic pancreas were harvested from untreated (n=8, black bars) and melatonin treated (n=8, white bars) in non-fasted *Smn*^{2B/-} and *Smn*^{2B/+}, after 2hours last melatonin treatment. The mRNA levels of CAT gene are in a. *Smn*^{2B/-} and b. *Smn*^{2B/+}; SOD gene level in c. *Smn*^{2B/-} and d. *Smn*^{2B/+}. Data represents mean and error bars represent +/- SEM; Unpaired t Test, ns=not significant *p<0.05, **p<0.01, ***p<0.001, ****p<0.0001.

Table 4. 8 Summary of melatonin effect on P18 SMA pancreas in *Smn*^{2B/-}

Decipher melatonin effect	Method	Targeted genes/protein	Result	Model	Tissue
Molecular pathway	Quantification of mRNA level via qPCR	<i>In-silico</i> based (<i>Per1</i> , <i>Sirt1</i> , <i>Bcl-2</i> , <i>Ror-α</i>)	<i>Ror-α</i> mRNA level increased	<i>Symptomatic Smn</i> ^{2B/-}	Pancreas
Mitochondrial based-oxidative stress		Playing role as anti-oxidant (<i>CAT</i> , <i>SOD</i>)	<i>CAT</i> expression induced		
Glucose Uptake		<i>Glut4</i>	No difference		
Circadian Rhythm		Clock genes (<i>Clock</i> , <i>Bmal1</i> , <i>Per2</i>)	No alternation		

The provided table, as shown in the figure, systematically summarizes from left to right: the objective of the study plan, the chosen method, the targeted gene or protein, the result, the model used, and the type of tissue examined. The targeted genes have been systematically categorized into groups: sequentially, genes predicted through combined *in silico* analyses (*Per1*, *Sirt1*, *Bcl-2*), genes playing a role in oxidative stress (*CAT* and *SOD*), gene involving glucose uptake from circulation (*Glut4*), core clock genes (*Bmal1*, *Clock* and *Per2*), The levels of these targeted genes have been quantified in pancreas tissues following melatonin application using qPCR. The entire experimental system was carried out on the *Smn*^{2B/-} SMA mouse model.

To sum up:

In summary, melatonin emerges as a promising candidate for treating SMA, a multifaceted multisystemic condition. Its therapeutic potential is rooted in improving metabolism in both the central nervous system and peripheral tissues. Additionally, melatonin offers protection by influencing and reducing processes related to apoptosis, glucose metabolism and oxidative stress. This comprehensive approach, tackling various aspects of SMA pathology, highlights melatonin's potential to significantly improve the overall characteristics of SMA, which is beyond the NMD. In detail, this study examines melatonin-treated tissues from mice with symptomatic SMA, focusing on both central nervous system regions such as the spinal cord and non-central areas including skeletal muscle, pancreas, liver, and adipose tissue. A comprehensive molecular analysis was conducted, exploring a range of genes involved in various metabolic processes and circadian rhythm regulation. The image features a green square representing the role of melatonin in controlling diurnal genes, crucial for maintaining circadian rhythm, metabolism, and overall body homeostasis (figure 4.43). Melatonin's ability to cross the BBB is shown to reduce the expression of apoptotic markers like *Fas* and *Pmaip1* in the SC. The interconnected dark blue lines among four peripheral tissues illustrate the metabolic interactions in these organs, which exhibit specific abnormalities in SMA pathology. This interconnection suggests the potential role of melatonin in regulating metabolic balance by influencing various genes. Notably, in the upper left corner of the image, there is a noted increase in *GLUT4* levels, essential for glucose uptake, particularly in skeletal muscle tissue. Moreover, melatonin is also observed to enhance muscle fiber size. The orange arrows in the image emphasize melatonin's anti-apoptotic impact in muscle and adipose tissues, which correlates with an increase in the *Bcl-2* gene (figure 4.43). Furthermore, melatonin is implicated in promoting mitochondrial biogenesis, linked with *Sirt1*, in both adipose and islet muscle tissues. A common feature across these tissues is the effect of mitochondrial oxidative stress and subsequent ROS, impacting genes such as *CAT* and *SOD*. Additionally, melatonin's role in elevating UCP-1 levels in WAT suggests a shift in its function towards that of brown tissue (figure 4.43). As a result of these analyses, it has been observed that melatonin has tissue-specific metabolic and circadian effects. The analyses revealed that melatonin exhibits distinct metabolic and circadian effects in different tissues.

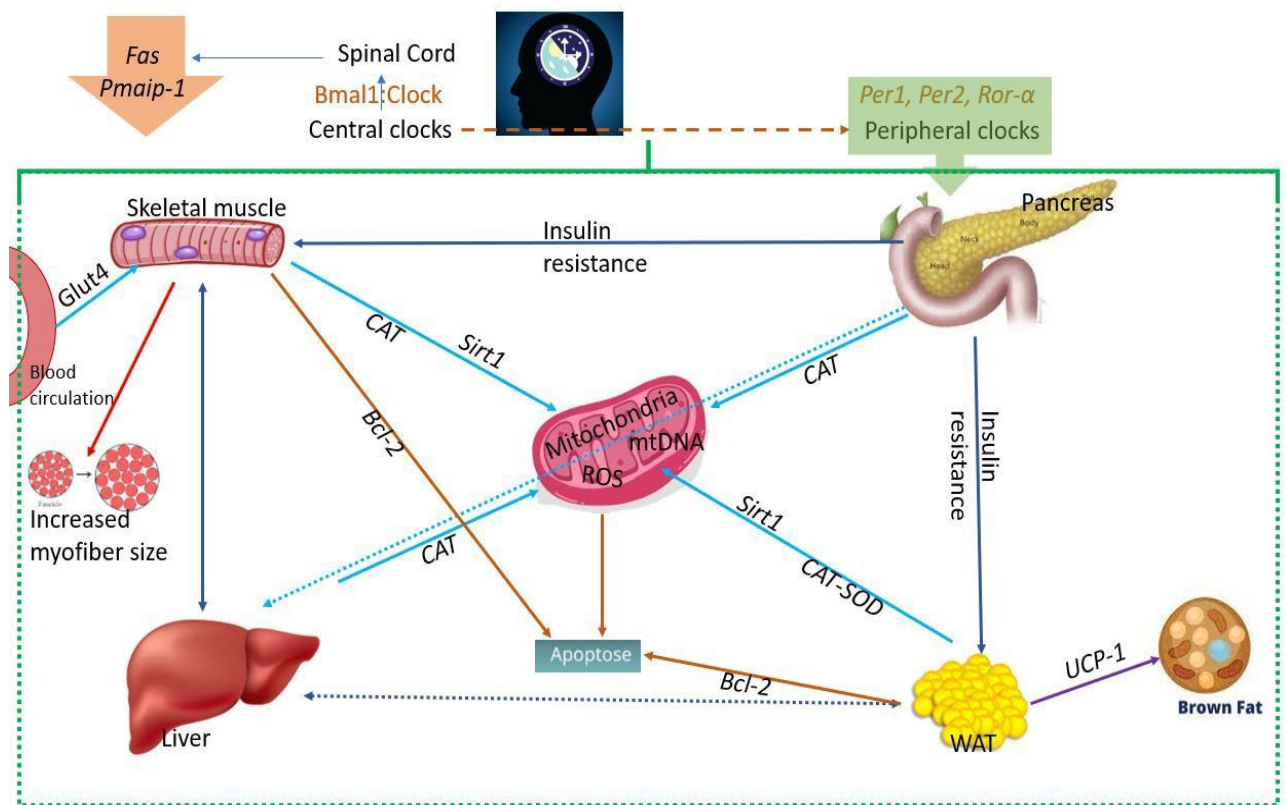


Figure 4. 43 Result of melatonin-induced genes, which play different roles of metabolic balance.

This assessment encompasses tissues treated with melatonin from symptomatic SMA mice, covering both central nervous system areas like the spinal cord and non-central nervous system tissues such as skeletal muscle, pancreas, liver, and adipose tissue. The image illustrates the green square, symbolizing melatonin-mediated diurnal genes that affect circadian rhythm.

Melatonin decreased expression of apoptotic markers such as *Fas* and *Pmaip1* in the SC. The dark blue lines connecting four peripheral tissues demonstrate the metabolic interplay among these organs, which display abnormalities in SMA pathology. In the upper left corner, as depicted, there is an elevation in *GLUT4* levels especially in skeletal muscle tissue.

Additionally, melatonin has been shown to increase muscle fibre size. The orange arrows highlight melatonin's anti-apoptotic effects in muscle and adipose tissue, leading to the upregulation of the *Bcl-2* gene. Melatonin may also enhance *Sirt1* expression, in adipose and islet muscle tissues. A shared characteristic in these four tissues is associated with *CAT* and *SOD*. Moreover, melatonin increases *UCP-1* levels in WAT, transitioning its function towards that of brown tissue.

4.4 Discussion

Considering the multi-systemic peripheral pathologies of SMA, a second compound, melatonin, is anticipated to improve the SMA phenotype. Our *in silico* analyses predicted that the expression of *Per1*, *Bcl2*, *Sirt1* and *Ror- α* genes is increased in SMA skeletal muscle and can be downregulated by melatonin treatment. First, we validated the abnormal expression of *Per1*, *Bcl2*, *Sirt1* and *Ror- α* in symptomatic skeletal muscle tissue in both SMA mouse models. Subsequent research has stated the safety and pharmacological impact of melatonin on the C2C12s and LCHN-M2 cell line, uncovering a dose-dependent alteration in the expression levels of the target genes. The administration of 50 mg/kg/day melatonin on *Smn*^{2B/-} mice led to notable improvements in weight, survival and RR patterns. The potential molecular impacts of a melatonin treatment were assessed in relation to the expression levels of genes, which are playing role in glucose uptake, mitochondrial biogenesis, anti-oxidative stress, apoptosis and circadian rhythm in *Smn*^{2B/-} mice. Post-treatment of melatonin, both the symptomatic skeletal muscle, liver, WAT, BAT and spinal cord tissue has a tissue-specific effect on metabolic and circadian functions.

In the *Smn*^{-/-}; *SMN2* SMA mouse model, we observed that the genes *Per1*, *Sirt1*, and *Bcl2* were upregulated, whereas in the *Smn*^{2B/-} SMA mouse model, an increase in the expression of *Per1* and *Bcl2* genes was noted. Based on these findings, it can be inferred that the expression of the *Sirt1* gene is influenced by the severity of SMA. In 2009, Millino and colleagues conducted studies on the skeletal muscles of patients with SMA types I and III, revealing that the severity of SMA is correlated with two distinct gene expression signatures in muscle tissues. The muscles from SMA type I patients showed that dysregulated genes primarily play roles in energy metabolism and muscle physiology (Millino et al., 2009b). In parallel, we found that an increase in *Sirt1* expression was found in the severe mouse model, aligning with its known role in mitochondrial biogenesis (Yuan et al., 2016). Another role of the *Sirt1* gene is its involvement in atrophy through the activation of *Foxo* and *Atrogen*, where are placed in downstream of *Sirt1* (Lee and Goldberg, 2013). Furthermore, overexpression of *Sirt1* has been shown to potentially reverse the atrophic phenotype (Lee and Goldberg, 2013). Thus, *Sirt1* plays a significant role in muscle atrophy, positioning it as a new therapeutic target. Importantly, we found that melatonin application caused increased level of *Sirt1* and enhancement of myofiber size. In future studies, it is

suggested to explore the direct relationship of *Sirt1* gene activation on atrophy in SMA muscles, such as, through vector-mediated specific activation. This approach is recommended as a focus for upcoming research.

In the deltoid muscle samples from SMA Type III patients, a decrease in *PER1* mRNA levels was observed, which contrasts with the increased level of *Per1* in SMA mouse studies. This inverse pattern could be attributed to several factors. One reason might be the use of different muscle groups in humans and mice; deltoid muscles were analysed in SMA patients, whereas triceps muscles were used in the SMA mouse model (Fridén and Lieber, 2001). Another contributing factor could be the physiological differences between the two species, considering the inherent variations between mice and humans (Suetterlin et al., 2022). Lastly, it's also plausible that the Type III SMA patient group, which generally exhibits a less severe phenotype, might show variations in gene expression related to the disease's severity (Lefebvre et al., 1997).

In C2C12 cells, the application of melatonin leads to varying effects on the expression of *Per1* target genes, and these effects depend on both the dosage of melatonin and the differentiation state of the cells. Similarly, in the LCHN-M2 model, the application of 1mM melatonin increasing the level of *Per1* suggests that melatonin might promote the transition from myoblast form to myotubes. Turning to the changes in skeletal muscle from *Smn*^{2B/-}, upregulated level of *Per1* and *Per2* gene level as found. Therefore, it's important to consider the role of circadian rhythm in regulating peripheral tissue development and maintenance when studying the impact of circadian genes on muscle development, which is found that differentiated-induce role of *Per1* in muscle development (Katoku-Kikyo et al., 2021). The study in the Per KO model has revealed that *Per1* and *Per2* are initiating and decisive genes in the differentiation of myoblasts in circadian rhythm (Katoku-Kikyo et al., 2021). The significant roles of the *Per1/2* gene in muscle regeneration and the negative effects of the absence of these genes on the size of muscle fibers, the exit from the cell cycle, and the regeneration process have been revealed in *Per1/2* KO mouse models through the monitoring of *MHC* and *MyoD* levels over time and the results of IHC assays (Katoku-Kikyo et al., 2021) (Small et al., 2020). To provide a definitive answer, it is recommended to compare the differentiation states by looking at the levels of *MyoD*, *MyoG* and *MHC* in further studies. As for the melatonin effect on muscle contraction, the effect of muscle contraction on the calcium-dependent pathways in human muscle samples has been shown to be directly related to the increased

expression of *Per2*, as evidenced by calcium imaging and *ex vivo* muscle contraction experiments (Small *et al.*, 2020). Consequently, this finding prompts an important question: could the elevation of *Per2* levels in the triceps of SMA mice (we found melatonin increased *Per2* gene in SMA' triceps), enhance muscle contraction? Further adding to the significance of these findings, Small *et al.* (2020) have also uncovered that the role of *Per2* in these promoted-calcium-dependent pathways is facilitated by the phosphorylated form of CREB (p-CREB). This insight positions the CREB protein as a critical subject for future research, particularly in the study of SMA and its associated phenotypes.

Another important finding related to muscle structure is that the application of melatonin increases the expression of genes *Atrogin1* and *MuRF1*, which are considered markers of muscle atrophy. Based on laminin assay investigating the overall impact of melatonin on muscle health, it was found that melatonin increases muscle fibre size.

This finding in the context of SMA pathology suggests that different pathways or unidentified muscle ubiquitin ligases may play a role in the atrophy seen in SMA (Iyer *et al.*, 2014; McElhinny *et al.*, 2002). Additionally, this enlargement may be attributed to melatonin's supportive role in muscle metabolism, as it seems to promote mitochondrial activity (increased the *Sirt1* level), mitigate oxidative stress (increased the *CAT* level) and enhance glucose uptake via inducing *Glut4* (increased *Glut4* in melatonin-induced triceps of SMA), all of which are vital for muscle structure development in melatonin induced *Smn*^{2B/-} mouse model. This insight contributes to a more comprehensive understanding of the mechanisms by which melatonin affects muscle health. Extending these findings to porcine studies, melatonin has also been demonstrated to augment myofiber size, with a notable upregulation of molecular markers such as paired PAX7, myogenin (MYOG), myosin heavy chain (MYHC) IIA, and MYHC IIB, presenting a consistent pattern of melatonin's positive impact on muscle development (Chen *et al.*, 2023). For the first time, we have demonstrated using IHC methods that melatonin increases muscle fibre size in symptomatic *Smn*^{2B/-} mouse models. This result suggests that factors involved in muscle development and differentiation, such as *Pax7*, *MyoD*, *MyoG*, myosin heavy chain (*MYHC*) IIA, and *MYHC* IIB, should be examined to evaluate melatonin-induced-myogenesis under SMA condition.

Following the application of melatonin, we observed an increase in the expression of core clock genes *Per1*, *Per2*, and *Clock* in the liver tissues of symptomatic *Smn*^{2B/-} mice. Literature indicates that the circadian rhythm influences metabolic homeostasis in the liver-pancreas axis, particularly by suppressing gluconeogenesis (Faria *et al.*, 2013). Moreover, melatonin emerges as a potential hypoglycaemic agent-insulin similar activity-(Watanabe *et al.*, 2023). In the *Smn*^{2B/-} mice, hyperglucagonemia (Bowerman *et al.*, 2012a), hyperglucagonemia-induced hepatic glycogen breakdown has been reported (Deguise *et al.*, 2021b). In other words, under SMA conditions, the liver responds to hyperglucagonemia by breaking down glycogen to produce and release more glucose into circulation. Melatonin, acting through circadian genes, could potentially reverse this mechanism, similar to the action of insulin, thus alleviating the condition. This suggests the importance of further detailed studies on melatonin's impact on the liver- pancreas axis, hepatic glycogen levels and liver enzyme activities. Metabolic crosstalk exists between the liver, pancreas, skeletal muscle, and adipose tissue (Chan *et al.*, 2022). In other words, a compensatory response to a changing condition in one tissue can come from other tissues. Turning to the topic of adipose tissue in *Smn*^{2B/-} involves increased adipocyte lipolysis in response to hyperglucagonemia, leading to the release of fat droplets into circulation and subsequent TG accumulation in the liver (Deguise *et al.*, 2021c).

In our project, in adipose tissue, post-melatonin application in *Smn*^{2B/-} mice, an increase in *Per1*, *Per2*, and *Clock* gene expression was observed in WAT tissue. We asked the question whether there is a change in lipid accumulation in the liver as a result of the decrease in lipolysis in adipose tissue due to the effect of melatonin. To answer this question, oil-red-O assay has been carried. We found that there was no difference in lipid accumulation of liver of *Smn*^{2B/-}. This could be due to the hallmark feature of SMA muscle atrophy, leading to the hypothesis that lipids from the breakdown of atrophied muscles might still be accumulating in the liver (Pasmans *et al.*, 2021). Strikingly, due to significant muscle loss, the required amount of energy in SMA patients cannot be met (Sproule *et al.*, 2009). One of the melatonin-mediated compensatory mechanisms in this context could be the transformation of WAT into brown adipose tissue BAT following melatonin application (Xu *et al.*, 2020). For the first time, we discovered that melatonin application in *Smn*^{2B/-} mice functionally shifts WAT towards BAT characteristics. This shift was observed through a significantly increase in *UCP-1* (BAT tissue

biomarker) in WAT (Xu et al., 2020).

This finding suggests that in SMA mice, melatonin-induced-WAT might be used for energy production rather than merely storing fats, to try to meet energy demand.

It would be advisable to perform mitochondrial biogenesis and functional tests in these tissues to potentially confirm this energy metabolism process (Suliman and Piantadosi, 2014). *Sirt1* contributes to mitochondrial biogenesis and maintenance by promoting the activity of *PGC-1 α* , positioned upstream (Zhou et al., 2018). Based on these, the aim was to examine the *Sirt1* mRNA in *Smn*^{2B/-}. We found that upregulation of *Sirt1* gene had been observed in triceps and wat from symptomatic *Smn*^{2B/-}. It is suggested that in SMA mice, the application of melatonin might supports mitochondrial biogenesis, which has already decrease the number of mtDNA, increased mitophagy under SMA pathology (Xu et al., 2016). To clarify the impact of melatonin on mitochondria in an SMA model, it is recommended to carry out the future studies, including mitochondrial DNA quantity and quality, citrate synthase activity (proxy for mitochondrial content), and measurements of oxygen consumption rate or ATP production. Another effect of melatonin on mitochondria is its association with anti-oxidative pathways. Melatonin scavenges free radicals produced as a byproduct of mitochondrial oxidative metabolism, thus preventing damage to mtDNA and supporting mitochondrial functions (Melhuish Beaupre et al., 2021; Ramis et al., 2015). Building on this, our project included experiments to examine the expression of antioxidant enzymes responsible genes, *CAT* and *SOD*. We observed in *Smn*^{2B/-} mouse models that *CAT* levels increased in triceps, liver and spinal cord whereas, in the liver, both *CAT* and *SOD* expression levels upregulated. In the literature, increased production of ROS has been observed in the heart (Shababi et al., 2012) and spinal cord (Patitucci and Ebert, 2016) in the *Smn* Δ 7 SMA mouse model, the liver tissue in the *Smn*^{2B/-} mouse model (Deguise et al., 2021d), and finally, in the skeletal muscle in a muscle-specific *Smn1* knockout mouse model (Chemello et al., 2023b).

Another point to highlight is melatonin's potential to enhance *CAT* expression in the pancreas tissues of *Smn*^{2B/-} mice, thereby can support antioxidation. A literature review, including research by Park et al., 2014, suggests that melatonin may help reduce oxidative stress in pancreatic tissues, which could stimulate insulin secretion. Given the insulin resistance observed in SMA mouse and human models, and the disorganization of β -islets, future studies should focus on a

detailed examination of melatonin's effects on the pancreas. To investigate if this effect is also present in the pancreas of SMA mouse models, it is recommended to measure insulin protein levels, possibly through techniques like ELISA /Western blotting or dynamic measurement of insulin and glucagon secretion via radioimmunoassay.

To highlight the significance of understanding how melatonin mitigates oxidative stress in various tissues affected by SMA, it is recommended to conduct extensive studies on its effect on glutathione peroxidase enzyme activity, particularly in the liver, skeletal muscle, spinal cord, and adipose tissues.

Another focus in SMA mouse models is on the effect of melatonin on insulin resistance observed in SMA mice and patients (Bowerman *et al.*, 2012). Following melatonin administration, non-fasting blood glucose levels were measured, and no significant difference was found compared to control groups. This could be related to the non-fasting state (Bowerman *et al.*, 2014), as discussed in the pioglitazone section. To understand the overall picture of glucose intolerance, we examined the expression pattern of the Glut4 receptor protein, responsible for glucose uptake from blood, following melatonin administration. Our results indicated that melatonin increased *Glut4* expression in the skeletal muscle of *Smn*^{2B/-} mice. Although the increase in expression may help mitigate glucose intolerance, further experiments are necessary to establish this connection. Specifically, assessing glucose uptake using radio-labeled glucose analogs in future studies will provide a more comprehensive understanding of this relationship. On the other hand, when examining *Glut4* downregulation, a direct interaction between *Akt* and *Glut4* has been observed (Faria *et al.*, 2013). In detail, p- Akt2 significantly enhances the translocation of Glut4 receptors to the plasma membrane, a process almost comparable to the effect of insulin (Ng *et al.*, 2008).

Additionally, melatonin is known to activate the PI3K-AKT pathway through phosphorylation, impacting downstream targets including mTOR and PTEN (Beker *et al.*, 2019). Studies on SMA mouse models have shown that phosphorylated PTEN increases SMN protein stability, thus alleviating the SMA phenotype (Rademacher *et al.*, 2020). Based on these findings, while it's known that melatonin initiates the PI3K/AKT pathway and elevates GLUT4 level, further research is needed to determine whether its interaction with the SMN protein is direct or indirect and if it's tissue- specific to comprehensive glucose tolerance phenotype of *Smn*^{2B/-}. Controversially, it has been observed that

melatonin activates the PI3K/AKT pathway by increasing *Bmal1* levels (Beker et al., 2019). In the SMA mouse model, when melatonin was applied to triceps, WAT, and liver tissues, *Bmal1* levels located in the suprachiasmatic nucleus remained unchanged (Beker et al., 2019). This suggests that in addition to the influence of the central clock within the suprachiasmatic nucleus, melatonin also affects peripheral tissue-specific circadian rhythms, and the impact of melatonin might be even more pronounced through the peripheral clock, an aspect that should not be overlooked.

Melatonin's potential anti-apoptotic effect is well-recognized (Kim et al., 2011). In investigating its connection with SMA pathology, we focused on the expression levels of *Bcl2*, an anti-apoptotic marker (Gao and Wang, 2009). Our results indicated that 100 μ M melatonin increases *Bcl2* levels in C2C12 myotubes. In *Smn*^{2B/-} mouse models treated with melatonin, a significant increase in *Bcl2* expression was observed in symptomatic skeletal muscle, liver, and WAT tissues. This rise in *Bcl-2* levels, stimulated by melatonin, counteracts the pro-apoptotic Bax protein at the mitochondrial level, effectively inhibiting apoptosis in the hippocampus, as shown in studies by Radogna et al., 2008, and Keskin-Aktan et al., 2018. To further explore this anti-apoptotic effect, additional studies in specific SMA mouse tissues, including caspase activity assays and apoptosis quantification using Hoechst DNA staining, are suggested. Future research should focus on the direct interaction between *Bcl2* and *Bax* in SMA mouse tissues, employing small molecular inhibitors, such as si-RNA targeted at *Bax* or *Bcl2*.

Considering melatonin's antioxidative and anti-apoptotic properties, it has been defined as neuroprotective in CNS tissues, as noted by Alghamdi in 2018. Melatonin significantly supports spinal cord tissue survival by downregulating *Pmaip1* and *Fas*, which are apoptosis-inducing factors of SC. Despite this, melatonin did not alter motor neuron count, suggesting other pathways might be involved in motor neuron death in the spinal cord (explained in pioglitazone discussion chapter). On the other hand, another possible hypothesis involves the NF- κ B pathway, which modulates apoptosis by melatonin in neuronal cells (Tiong et al., 2019). Importantly, studies conducted on primary cultures established from the spinal cords of SMA mice have shown that the activation of the NF- κ B pathway regulates the SMN protein levels (Israël, 2010). This activation typically occurs through the canonical pathway, involving the phosphorylation of IKK α /IKK β and the translocation of RelA to the cell nucleus

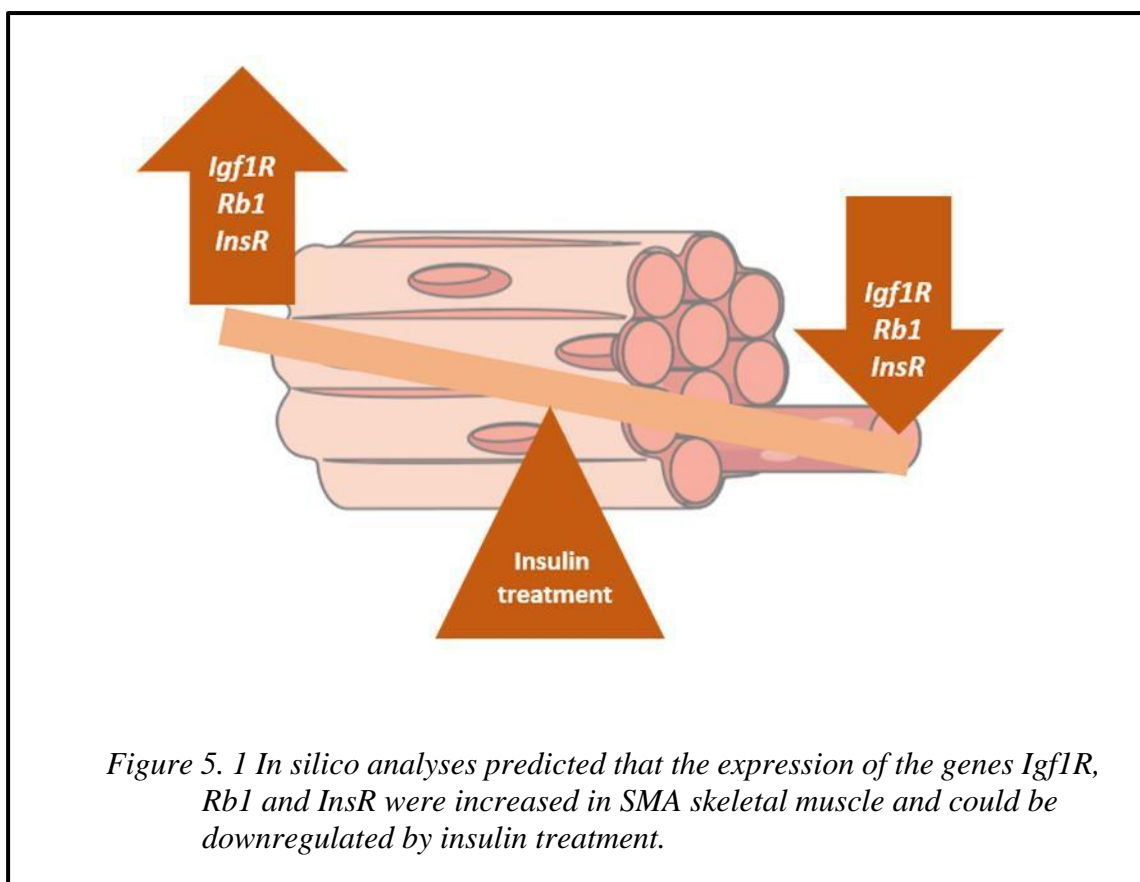
(Israël, 2010). Additionally, exploring the potential role of melatonin in the downregulation of NF- κ B pathway and its interaction with related proteins (RelA and Bax) could provide deeper insights. This line of research could be particularly valuable in understanding the mechanisms of SMA and developing potential therapeutic strategies that target these molecular interactions.

To sum up, melatonin shows promise as a potential therapeutic agent for SMA, a complex multisystemic disorder. Furthermore, melatonin demonstrates protective capabilities by targeting and mitigating processes involved in apoptosis and oxidative stress. This holistic strategy, which addresses multiple facets of SMA pathology, underscores the versatile role of melatonin in potentially improving the overall phenotype of SMA.

5 Introduction

5.1 Insulin

Similar to melatonin and pioglitazone, three candidate compounds have been proposed as a result of combine *in silico* approaches, third of which is insulin with similar transcriptomic pattern to prednisolone. Our findings anticipated that in the skeletal muscle of symptomatic SMA mouse models, genes such as *Igfr1*, *Rb1*, and *InsR* were upregulated, which would be downregulated by insulin application.



Insulin, an FDA-approved treatment for hyperglycaemia, is produced through recombinant DNA technology. This peptide hormone, secreted by the beta cells of the pancreas, plays a pivotal role in regulating blood glucose levels. Notably, insulin also has multiple metabolic functions, including boosts protein synthesis, and prevents lipolysis and proteolysis. These diverse actions of insulin underscore its critical role in maintaining glucose homeostasis and overall metabolic balance (*Insulin human*, 2023).

Insulin-like growth factor 1 (*IGF-1*) is an anabolic hormone with significant impacts on metabolism and is closely associated with metabolic syndrome (Holt et al., 2003), particularly affecting lipid and glucose metabolism (Saukkonen et al., 2006). Regarding the role of *IGF* in SMA pathology, it has been found that *Igf* levels are reduced in liver and blood of *Smn Δ 7* SMA model (Murdocca et al., 2012). Meanwhile, in both Type I SMA patients (Millino et al., 2009c) and mouse models, an increase in *IGF* receptor levels in skeletal muscle has been observed (Bosch-Marcé et al., 2011). Additionally, elevated levels of *Igf1R* have been noted in the spinal cord tissues of SMA-like mouse models (Biondi et al., 2015). Reducing expression levels in the *Smn Δ 7/+;SMN2;Igf-1r $^{+/-}$* SMA-like mouse model has led to significant improvements in lifespan and motor behaviour, as well as protection of motor neurons and increased SMN expression in spinal cord and skeletal muscles (Biondi et al., 2015). This phenotypic improvement is attributed to the robust activation of the neuroprotective AKT/CREB pathway, while concurrently suppressing the ERK and JAK pathways' activity (Biondi et al., 2015). Focusing on IGF highlights the interconnectedness of metabolic processes in SMA and underscores the importance of exploring its potential neuroprotective effects.

The research suggests that *Rb1*, another predicted targeted gene of insulin, offers a protective shield against diabetes and related complications, thanks to its ability to regulate mitochondrial energy metabolism, improve insulin resistance, and reduce the risk of ensuing complications (Zhou et al., 2019). A detailed examination of the underlying mechanisms has revealed that in the C2C12 cell line, an increase in glucose uptake is associated with the induced levels of *Rb1*. This uptake is connected to the phosphorylation of *Irs1* and protein kinase B (PKB), which in turn stimulates the translocation of GLUT1 and GLUT4 to the cell surface (Shang et al., 2008).

Furthermore, in an obese rat model, it has been observed that *Rb1* activate the PI3k/Akt signalling pathway in dose-dependent manner, thereby encouraging energy expenditure and leading to a decrease in body fat content (Xiong et al., 2010). Observing the age-related dysregulation of GLUT4 in the skeletal muscles of SMA mice (Meijboom et al., 2022), especially considering the known glucose abnormalities (Bowerman et al., 2012a), underscores the importance of investigating the relationship between *Rb1* and SMA.

Turning to the literature studies related to the last predicted target gene of

insulin, *InsR* (insulin receptor), playing a significant role of insulin resistance, and *InsR*-KD-mouse show extreme susceptibility to overt hyperglycaemia when subjected to a HFD (Lee et al., 2015). Delving into the molecular mechanism, an excessive amount of glycerol from WAT leads to an increased expression of the *G6pc* (glucose-6-phosphatase) gene in the liver in this mouse model (Lee et al., 2015). *Insr* plays a crucial role in balancing the increased gluconeogenesis from glycerol in the liver and the exacerbated lipolysis in WAT (Lee et al., 2015). In the pathology of SMA, irregularities in the metabolism of liver (Deguise et al., 2019a) and WAT (Feng et al., 2023) are playing a significant role. Therefore, investigating the role of INSR in the metabolism of peripheral tissues in SMA and examining whether insulin treatment could potentially exacerbate or alleviate the pathology becomes crucial.

In conclusion, the role of targeted genes playing a role of peripheral metabolism and development in SMA pathology, potentially regulated by insulin, has been predicted through *in silico* analyses and supported by literature studies. Therefore, examining insulin and its target genes under the umbrella of SMA pathology is significant to explain multi-systemic profile of SMA.

5.2 Methods

5.2.1 *In Vitro* Insulin Treatment

C2C12 myoblast cells were seeded in 6-well plates (4 wells per group). When the C2C12 myoblast cells reached 50-60% confluency, and the differentiated C2C12 myotubes were at the D7 stage, they were treated for 24 hours with Insulin Human Recombinant (Sigma-Aldrich) dissolved in dH₂O at concentrations of 1nM, 10nM, and 100nM. The same concentrations of insulin were also applied to both the 60-70% confluent LHCN-M2 cell line and the D7 LHCN-M2 cells for a duration of 24 hours.

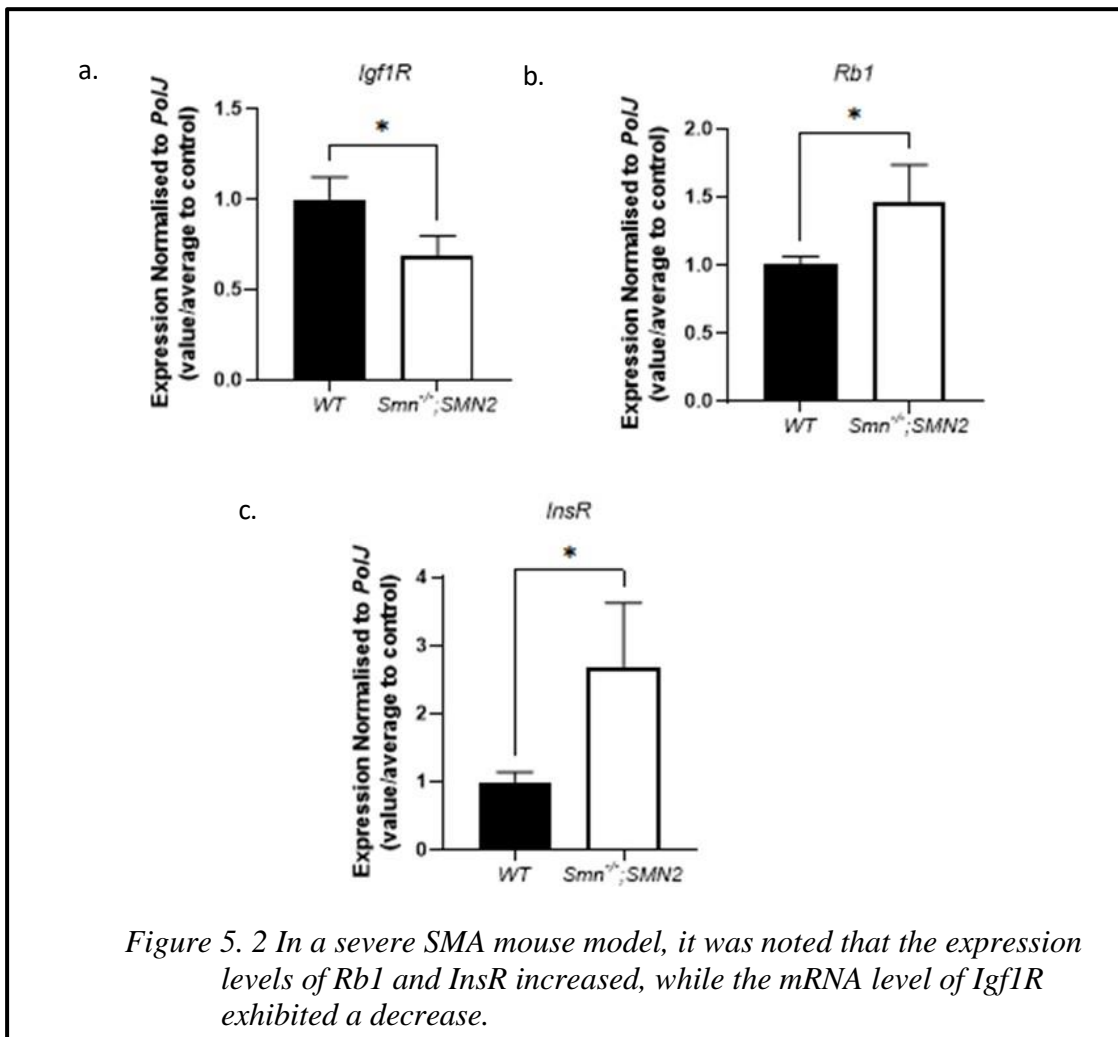
5.2.2 *In Vivo* Insulin Treatment

Beginning from day P0, offspring with *Smn*^{2B/-} SMA and *Smn*^{2B/+} healthy mice underwent daily phenotypic analysis. On P8, the mice either received no treatment, were given a vehicle (Sterile Molecular Biology Grade Water), or were administered insulin in an escalating dose regimen, starting at 0.2U and increasing by 0.5U every 5 days. The insulin was administered through 50 µl subcutaneous injections using BD Micro-fine 0.5ml/8mm/30g Insulin Syringes (SLS). This treatment continued until the humane endpoint was reached, with each group containing more than 10 mice. By P18, tissue samples from skeletal muscles (Triceps brachii and TA), liver, pancreas, white adipose tissue, and spinal cord (N > 4) were collected from both the untreated and insulin-treated *Smn*^{2B/-} SMA and *Smn*^{2B/+} healthy mice, two hours after their final treatment. Additionally, blood glucose levels (mmol/L) of the non-fasted pups were immediately measured post-euthanasia using the True Metrix Go blood glucose monitoring system (Trividia Health).

5.3 Results

5.3.1 The expression levels of *Rb1* and *InsR* were observed to increase, whereas the mRNA level of *Igf1R* was found to be downregulated.

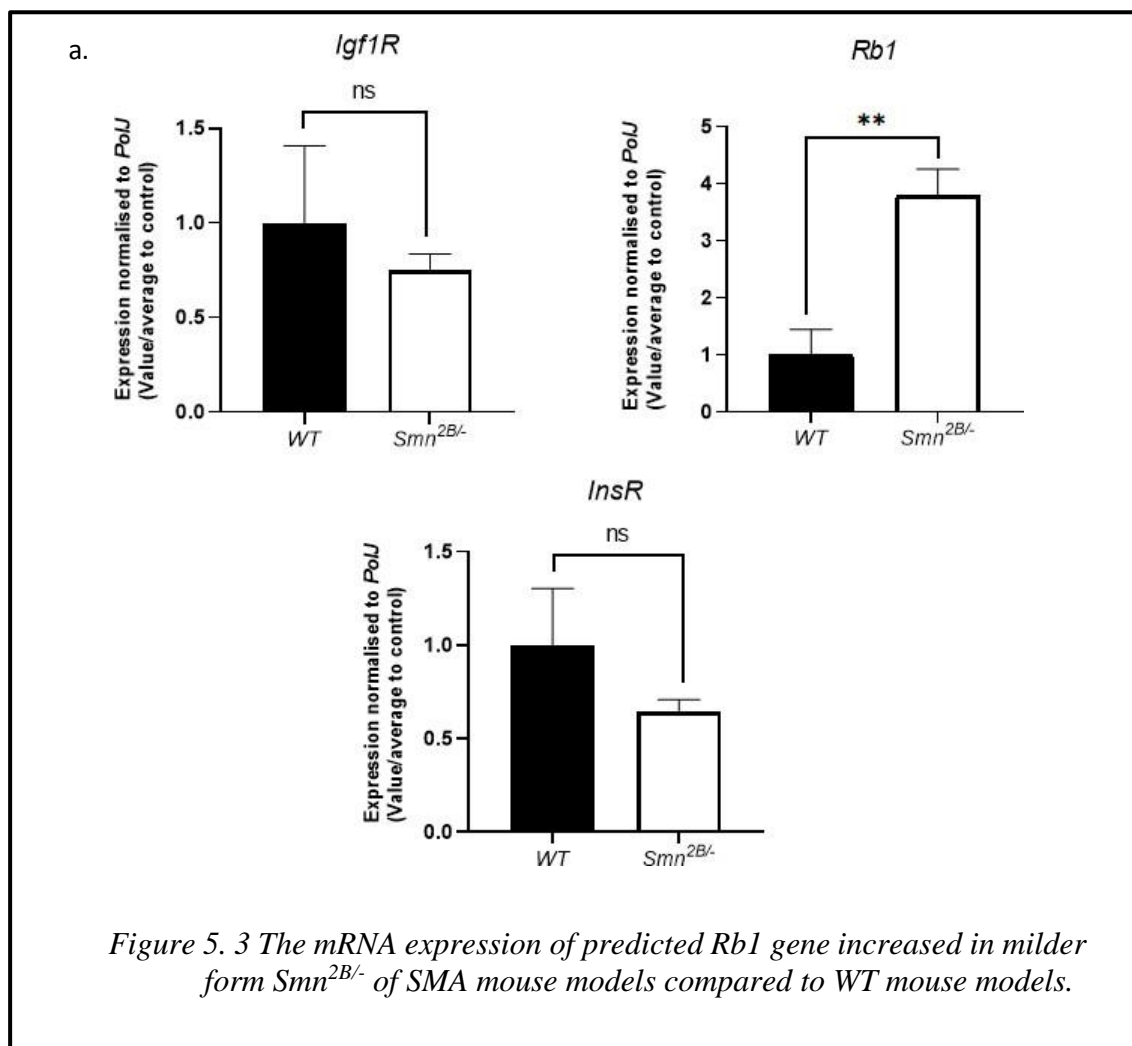
At the onset of our experiment, our focus was on assessing the expression levels of *Igf1R*, *Rb1* and *InsR* in the triceps (skeletal muscle) of symptomatic *Smn*^{-/-}; *SMN2* SMA mice at P7. In our targeted examination of predicted genes targeted by insulin, specifically *Rb1* and *InsR*, we observed a significant upregulation in their expression in the skeletal muscle relative to WT, as shown in figure 5.2.b; c. Interestingly, an increase in the expression level of *Igf1R* was also noted (figure 5.2.a). Thus, in the symptomatic *Smn*^{-/-}; *SMN2* mice's skeletal muscle, an increase in the expression levels of *Rb1* and *InsR* was noted, while the mRNA level of *Igf1R* showed a decrease.



The mRNA expressions were performed by qPCR. a. The expression level of *Igf1R*, b. *Rb1* and c. *InsR*. Black represents healthy model; white represents severe SMA mouse model. Data represent N=4 samples per group; error bars represent +/- SEM; Unpaired-t test, *p<0.05, **p<0.01, ***p<0.001

5.3.2 In the skeletal muscle of symptomatic *Smn*^{2B/-} mice, there was an elevation in the mRNA level of *Rb1*.

To substantiate our results, we expanded the research to include an analysis of the skeletal muscle (triceps) in *Smn*^{2B/-} at P18. In this phase, when compared with WT, an increase in the expression of *Rb1* was detected in the triceps of the milder SMA model. However, there were no significant changes in the mRNA levels of the anticipated target genes *Igf1R* and *InsR*, as depicted in figure 5.3. As a result, there is an upregulation in the expression of *Rb1* in skeletal muscle of symptomatic *Smn*^{2B/-} mice.



The mRNA expressions were performed by qPCR. a. The expression level of *Igf1R*, b. *Rb1* and c. *InsR* are forecasted target gene to be recovery of insulin treatment in milder SMA mouse model (a,b). Black represents healthy model; white represents severe SMA mouse model. Data represent N=4 samples per group; error bars represent +/- SEM; Unpaired-t test, ns= not significant, *p<0.05, **p<0.01, ***p<0.001, ****p<0.0001.

5.3.3 In Type III SMA deltoid myoblasts, the insulin target genes, *IGF1R* and *INSR*, were found to be significantly increased in expression.

In the next stage of our research, we focused on determining whether the genes we identified as potential insulin targets—specifically *IGF1R*, *RBI*, and *INSR*—showed different expression patterns in primary myoblasts from SMA patients.

Our analysis revealed an increase in the expression levels of *IGF1R* and *INSR* in Type III SMA myoblasts compared to those from healthy controls, as illustrated in figure 5.4.a.c. However, in Type III SMA myoblasts, there were no statistically significant differences in the mRNA levels of *RBI* when compared to healthy controls, as shown in figure 5.4.b.

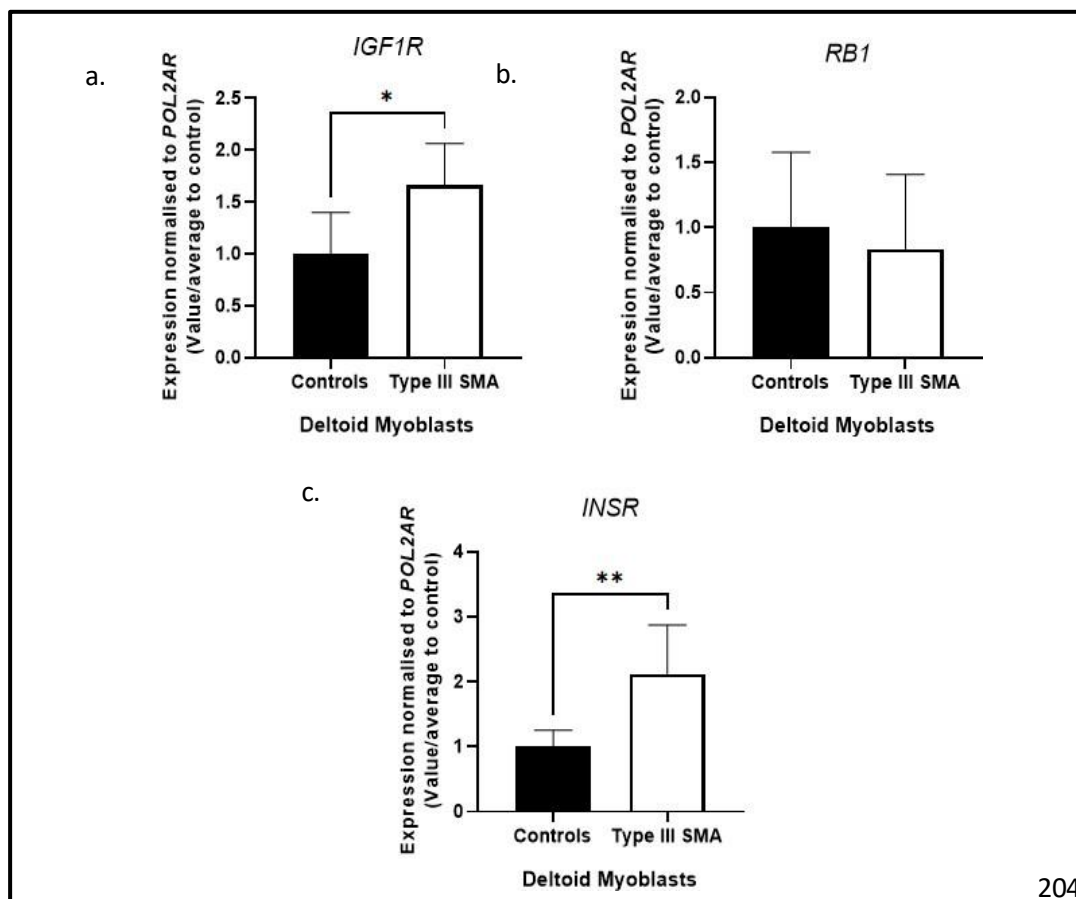


Figure 5. 4 The insulin target gene, IGF1R and INSR, significantly upregulated in Type III SMA deltoid myoblasts.

The mRNA expressions were performed by qPCR. The expression level of a. The expression level of *Igf1R*, b. *Rb1* and c. *InsR* in primary myoblast from deltoid muscle biopsies from healthy controls and Type III SMA patients (N=6). Each round dot represents a healthy person and each black square dot represents Type III SMA patient; error bars represent +/- SEM; unpaired t-test, ns= not significant, *p<0.05, **p<0.01, ***p<0.001, ****p<0.0001.

5.3.4 The level of *Igf1R* increased in both D0 *Smn*-KD-C2C12 and D7 *Smn*-KD- C2C12

The *Smn* gene knockdown was implemented at two key stages of muscle development. Initially, proliferating *Smn*-KD-C2C12s cells shown in figure 5.5.a while, *Smn*-KD- D7-C2C12s cells depicted in figure 5.5.b. For comparative purposes, un-transfected C2C12s cells are illustrated with black bars, while cells treated with scrambled siRNA, serving as a non-specific transfection control, are shown with white bars. Cells where *Smn* was specifically knocked down are represented with grey bars (*Smn*-siRNA). Our findings indicated a significant downregulation in *Igf1R* in both myoblast and myotube cells, due to lower *Smn* gene expression. Consequently, it seems that SMN protein deficiency can cause the dysregulation of the *Igfr1* gene in D0 & D7 C2C12s. Thus, the level of *Igf1R* in C2C12 myoblasts and myotubes rises in correlation with SMN deficiency.

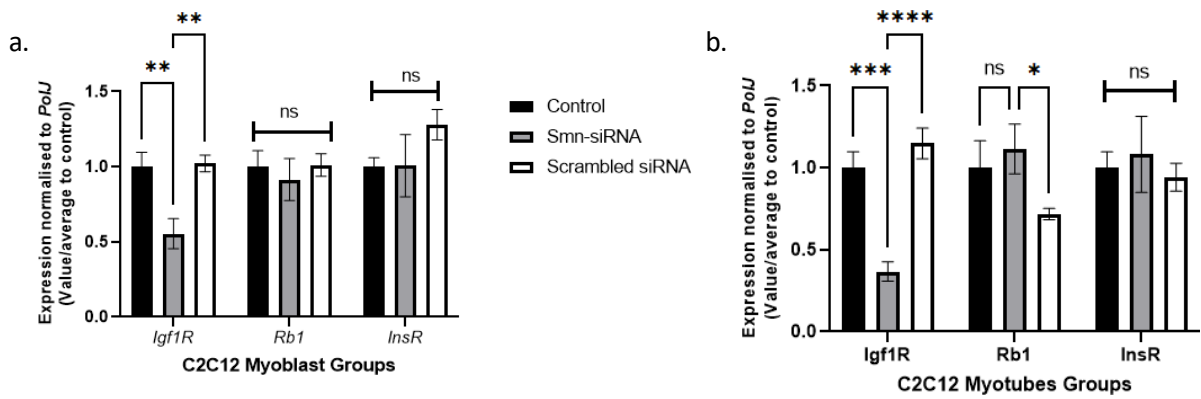


Figure 5.5 The mRNA expression of predicted *Igf1R* gene is increased in both Smn-KD proliferating and differentiated C2C12s model.

The mRNA expressions were performed by qPCR. a. The expression level of *Igf1R*, *Rb1* and *InsR* in Smn-KD myoblast form of C2C12s b. The pattern of target genes shows in D7 Smn-depleted C2C12S. Black represent positive control, grey represent Smn-KD form of C2C12s, white show scrambled-SiRNA in C2C12s. Data represent N=4 samples per group across two-independent experiments; error bars represent +/- SEM; Two-way ANOVA with post-hoc uncorrected Fishers LSD test, ns=not significant, * $p < 0.05$, ** $p < 0.01$, *** $p < 0.001$, **** $p < 0.0001$.

5.3.5 Canonical atrophy did not result in alterations of *Igf1R*, *Rb1* and *InsR* genes in C2C12 cells

When comparing the expression levels of target genes, *Igf1R*, *Rb1* and *InsR*, in the serum-starved C2C12 cells (depicted as white bars in figure 5.6) to those in the control group (shown as black bars in the same figure), we observed no significant differences.

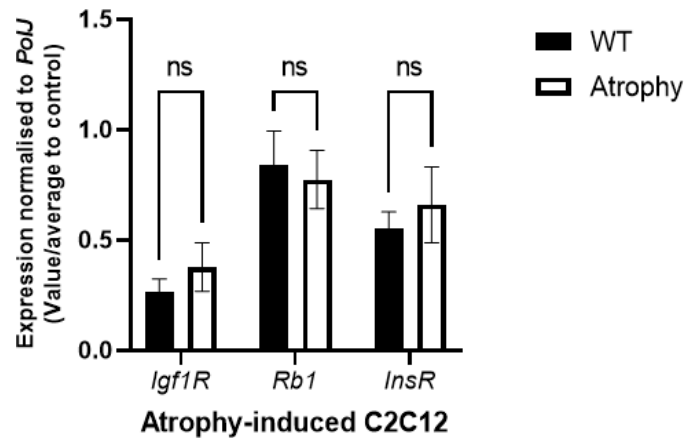


Figure 5. 6 Canonical atrophy does not lead to any changes in the level of insulin targeted genes in the serum-starvation-induced atrophy C2C12s.

The mRNA expressions were performed by qPCR. a. The target genes levels are in atrophy induced C2C12s. Black represents positive control, white shows serum-starvation-induced atrophy C2C12s model. Data represent N=4 samples per group across two-independent experiments; error bars represent +/- SEM; Two-way ANOVA with post-hoc uncorrected Fishers LSD test, ns=not significant. *p<0.05, **p<0.01, ***p<0.001, ****p<0.0001.

5.3.6 Upon administering 100nM insulin, an elevation in the expression of the *Rb1* target gene was noted in myotubes.

In the forthcoming phase of our study, our focus shifts to understanding how insulin affects certain genes in C2C12 cells, specifically *Igf1r*, *Rb1*, and *InsR*. To thoroughly investigate this, we exposed C2C12 cells to different insulin concentrations, specifically 1 nM, 10 nM, and 100 nM, maintaining the treatment for a duration of 24 hours. This approach allowed us to observe the gene responses across a range of insulin levels.

A particularly interesting observation emerged when we examined the *Rb1* gene. After administering 100 nM of insulin, there was a noticeable increase in the expression of the *Rb1* gene in myotubes. This result, which is clearly depicted on the right side of figure 5.7.b, highlights the sensitivity and responsiveness of the *Rb1* gene (figure5.7.b.). There was no change in expression of *Igf1R* and *InsR* in both myoblast and myotubes C2C12s (figure5.7.a; b.).

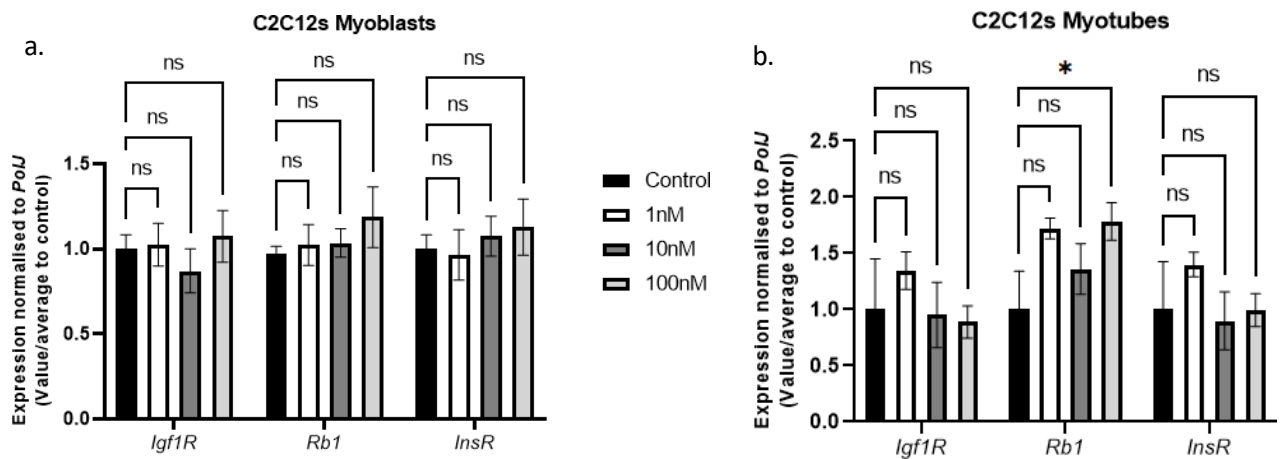


Figure 5.7 Following 100nM insulin treatment, an upregulation was observed in the predicted candidate *Rb1* target gene in myotubes.

The mRNA expression of insulin target genes *Igf1R*, *Rb1* and *InsR* were performed via qPCR. a. myoblast and b. myotubes form of C2C12s were treated for 24-hours by 1nM (white), 10nM (dark grey) and 100nM (light grey) and without any treatment/control (black). Data represent N=4 samples per group across two-independent experiments; error bars represent +/- SEM; Two-way ANOVA with post-hoc uncorrected Fishers LSD test, ns= not significant, *p<0.05, **p<0.01, ***p<0.001, ****p<0.0001.

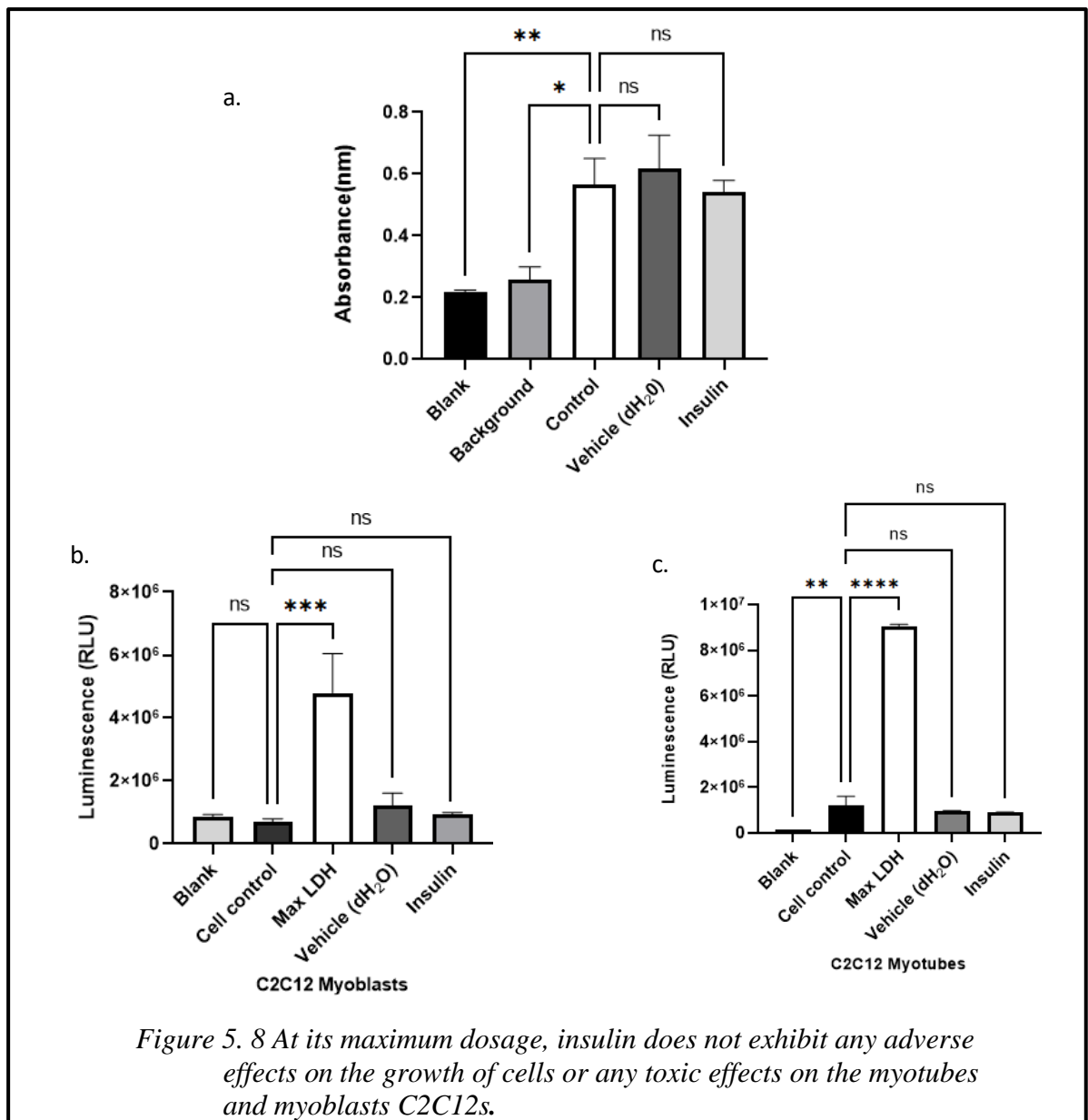
5.3.7 At the highest dosage insulin demonstrated neither a negative effect on proliferation nor any toxic impact on the formation of myotubes and myoblasts.

In our subsequent investigation, we assessed if insulin influences the proliferation of C2C12s cells, using BrdU labelling for tracking.

The graph provided illustrates different conditions: the blank control (black bar) shows the media components alone, without cells. The background control (medium grey bar) displays the cell environment sans BrdU labelling (as seen in figure 5.8.a). The standard control with cells labelled with BrdU is represented by white bars (also in figure 5.8.a). Cells treated with the highest insulin dose are marked with light grey bars, and a corresponding amount of vehicle control (dH₂O) is shown in dark grey (figure 5.8.a).

This experiment indicated that insulin at this concentration does not hinder cell proliferation.

The next phase involves determining if insulin is toxic to C2C12 cells through an LDH assay (shown in figure 5.8.b; c). For the LDH assay, various controls were utilized: the background control, which measures the signal from the reagents alone without cells; the cell control, providing a baseline LDH level from healthy cells (shown as a black bar); and the negative control (white bar), created by killing most cells with 0.1% Triton-X. Additionally, we included a vehicle control (dark grey bar) and investigated the effects of the highest insulin concentration (light grey bar). Our results showed that neither the highest concentration of insulin nor an equivalent volume of the vehicle (dH₂O) caused toxicity in either the D0 or D7 C2C12s cells.



We measured the absorbance wavelengths (nm) for various conditions: blank (media only), background (cell presence), and C2C12s myoblasts treated with either an anti- BrDU antibody, vehicle (dH₂O), or 100 nM insulin for 24 hours. The results of the BrDU assay are presented in panel a. For the toxicity, LDH assay was performed. Absorbance is readed from lactate dehydrogenase (LDH) level in cell culture supernatant from b. proliferating C2C12s and c. differentiated C2C12s. Black is untreated, white is negative control (1% Triton-X), dark grey is vehicle (dH₂O) control and light grey represent 100 nM insulin treatment. Data were obtained from four samples per group, spanning two independent experiments. Error bars represent the standard error of the mean (SEM). Statistical analysis was performed using one-way ANOVA, followed by Dunnett's post-hoc test. Notations for statistical significance are as follows: ns = not significant, *p<0.05, **p<0.01, ***p<0.001, ****p<0.0001.

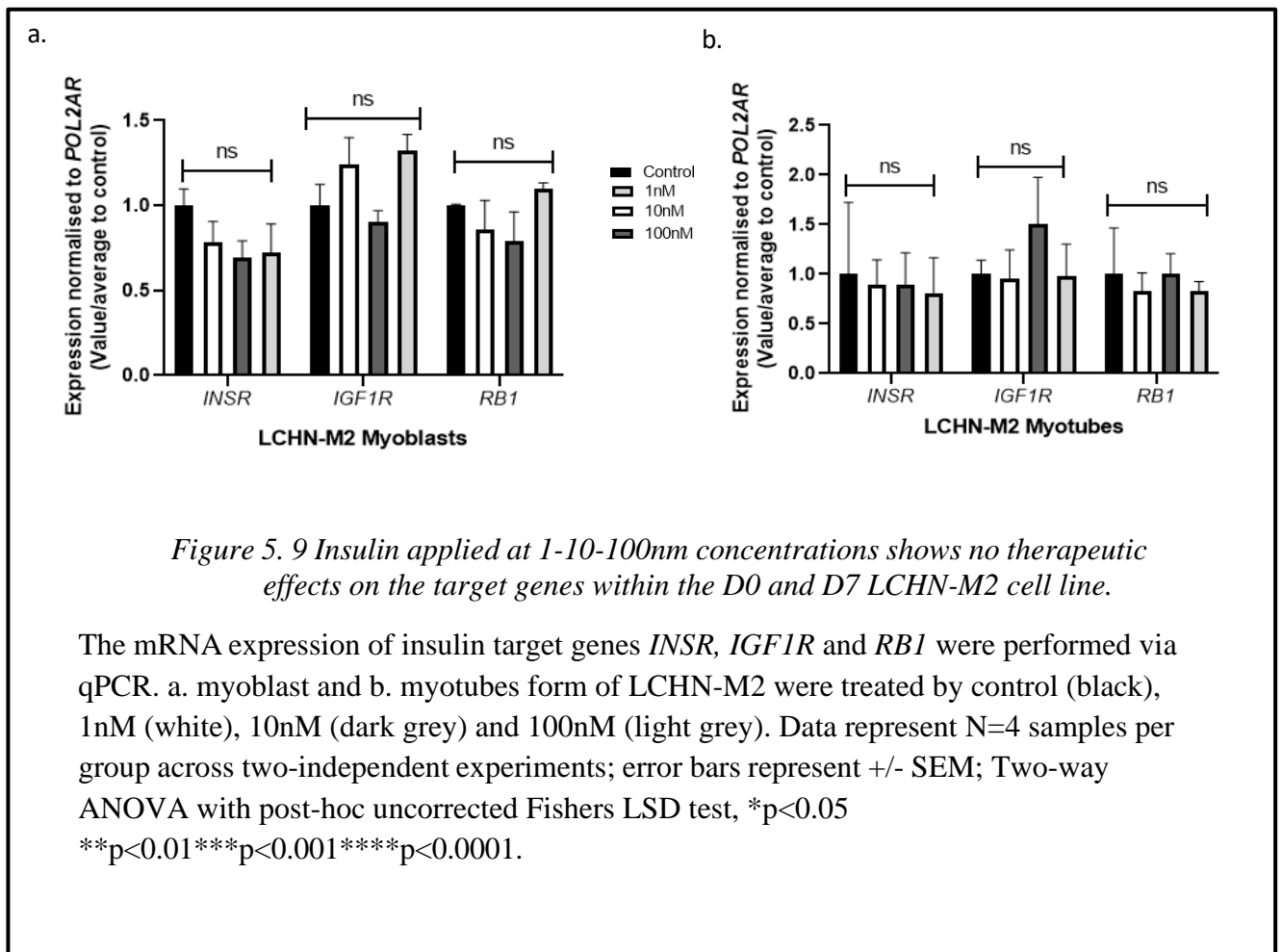
Table 5.1 Summary of insulin effect on SMA model

	Model	Tissue/sub-model	Significant difference comparing controls
Validation of <i>in-silico</i> data	<i>Smn</i> ^{-/-} ;SMN2	Triceps Skeletal muscle	Level of <i>Igf1R</i> , <i>Rb1</i> and <i>InsR</i> increased
	<i>Smn</i> ^{2B/-} Mice		<i>Rb1</i> increased; no change in <i>Igf1R</i> and <i>InsR</i>
	Type III SMA patients	Deltoid myoblasts	<i>IGF1R</i> and <i>INSR</i> increased; no change <i>RB1</i>
	Proliferating C2C12s	Smn-KD with <i>Smn</i> -siRNA transfection	<i>Igf1R</i> decreased There is no SMN-dependent changes in <i>Rb1</i> and <i>InsR</i>
	Differentiated-C2C12s		<i>Igf1R</i> decreased There is no SMN-dependent changes in <i>Rb1</i> and <i>InsR</i>
	Differentiated-C2C12s	Atrophy-induced	No change
Insulin impact	C2C12s	Myoblast	No alteration
		Myotubes	<i>Rb1</i> increased (10nM insulin treatment)

The provided table, as shown in the figure, systematically summarizes from left to right: the objective of the study plan, the chosen model, the targeted tissue/sub-model, the statistically different results result examined. This table allows us to view the models used and their results during the validation process. Following this, the effect of insulin on the expression of target genes was studied in C2C12s, following insulin application. This approach provides a comprehensive overview of the influence of insulin on gene expression in these specific model systems.

5.3.8 The application of insulin at concentrations of 1-10-100nM did not display any effect on predicted insulin target genes in the D0 and D7 LCHN-M2 cell line.

Another area of study focuses on examining how insulin affects the expression of *INSR*, *IGF1R*, and *RBI* in human muscle cells. To begin, we treated LCHN-M2 cells in their growth phase with different insulin concentrations for 24 hours. These included 1 nM μ M (indicated by white bars), 10 nM (dark grey bars), and 100 nM (light grey bars). After that, we applied the same insulin levels to mature LCHN-M2 cells for an identical time period. The outcome revealed no variation in the expression of the specified genes in both growing and mature human muscle cells in response to insulin treatment, as illustrated in figure 5.9.



5.3.9 Even at the highest dose, insulin did not adversely affect the growth of cells or cause any toxicity in the formation of LCHN-M2 myotubes and myoblasts.

In our further study, we examined how insulin influences the proliferation of LCHN- M2 cells, utilizing BrdU labeling for monitoring. The chart demonstrates different scenarios: a blank control (black bar) representing just media components without cells, and a background control (medium grey bar) showing cells without BrdU labeling (referenced in figure 5.10.a). The normal control with BrdU-labeled cells is denoted by white bars (also in figure 5.10.a), while cells treated with the highest insulin dose are indicated by light grey bars, with an equivalent volume of vehicle control (dH₂O) shown in dark grey (figure 5.10.a). This experiment revealed that high insulin concentrations do not restrict cell growth.

The next step was to evaluate insulin's toxicity on LCHN-M2 cells through an LDH assay (illustrated in figure 5.10.b; c). Various controls were used here: a background control for just the reagent signal without cells, a cell control for standard LDH levels from healthy cells (black bar), and a negative control (white bar) created by killing most cells with 0.1% Triton-X. We also included a vehicle control (dark grey bar) and examined the impact of the highest insulin concentration (light grey bar). Our results indicated that neither the highest concentration of insulin nor the equivalent volume of the vehicle (dH₂O) led to toxicity in either the D0 or D7 LCHN-M2 cells.

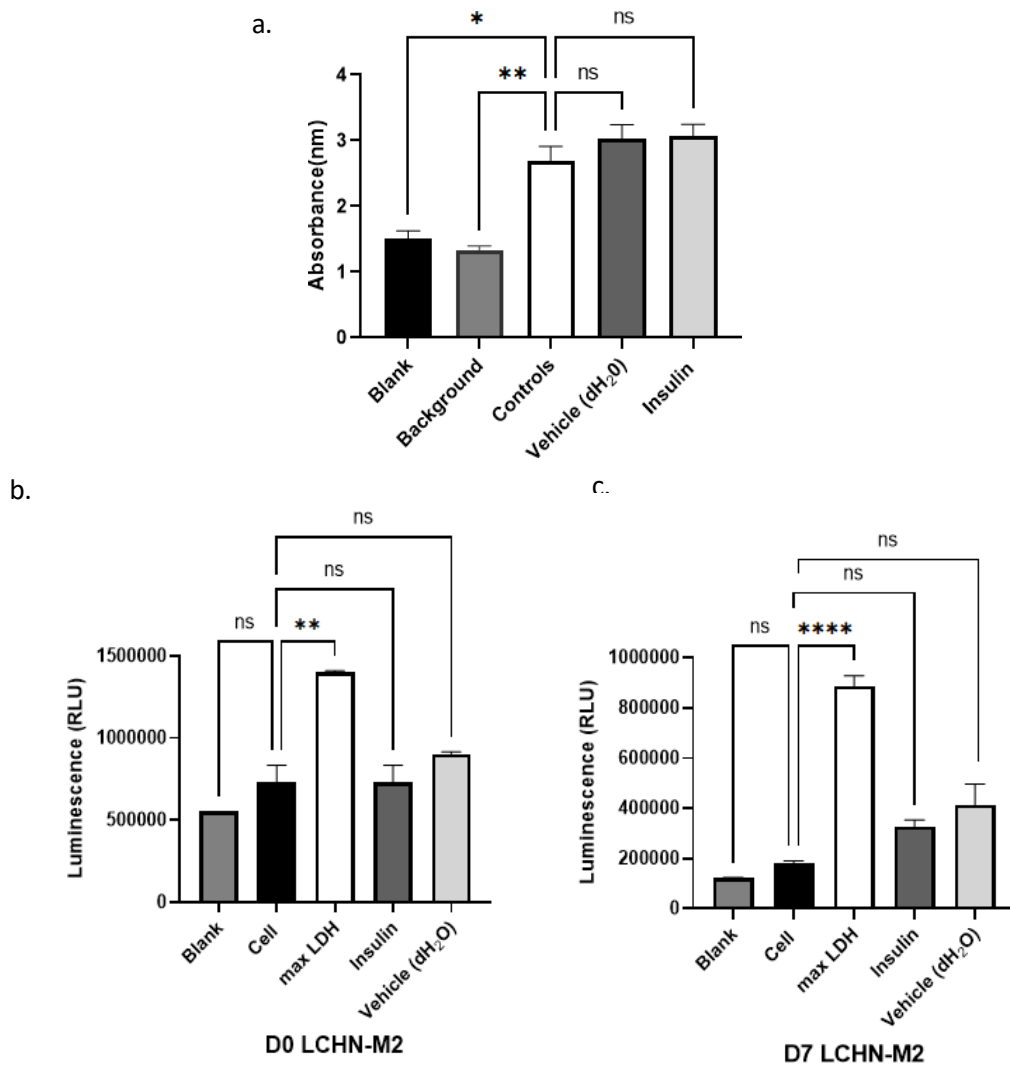


Figure 5. 10 When administered at its highest dose, insulin neither hampers the growth of cells nor leads to any toxic effects in the creation of LCHN-M2 myotubes and myoblasts.

We measured the absorbance wavelengths (nm) for various conditions: blank (media only), background (cell presence), and LCHN-M2 myoblasts treated with either an anti- BrDU antibody, vehicle (dH₂O), or 100 nM insulin for 24 hours. The results of the BrDU assay are presented in panel a. For the toxicity, LDH assay was performed.

Absorbance is readed from lactate dehydrogenase (LDH) level in cell culture supernatant from b. proliferating LCHN-M2 and c. differentiated LCHN-M2. Black is untreated, white is negative control (1% Triton-X), dark grey is vehicle (dH₂O) control and light grey represent 100 nM insulin treatment. Data were obtained from four samples per group, spanning two independent experiments. Error bars represent the standard error of the mean (SEM). Statistical analysis was performed using one-way ANOVA, followed by Dunnett's post-hoc test. Notations for statistical significance are as follows: ns = not significant, *p<0.05, **p<0.01, ***p<0.001, ****p<0.0001.

Altogether, while insulin demonstrates a safe profile for LCHN-M2 within a 1- 100nm dosage range, it does not have any effect on the expression of the estimated target genes in either the myoblast or myotube forms of LCHN-M2.

5.3.10 Increasing doses of subcutaneous insulin injections resulted in a body weight increase in *Smn*^{2B/-} mice.

Following combined *in-silico* analyses, which identified specific target genes (*Igf1R*, *InsR*, *Rb1*) dysregulated in SMA pathology, these findings were confirmed *in vitro* and *in vivo* SMA models. Notably, insulin was observed to regulate the expression pattern of the *Rb1* gene, a target in the C2C12 line, and exhibited a safety profile. Consequently, this led to the initiation of *in vivo* insulin applications.

Our initial step involved conducting animal trials to determine the optimal dosage and regimen for insulin. Utilizing the *Smn*^{2B/-} mouse model, we investigated two different initiation periods—P5 and P8. A variety of dosages were evaluated, starting from 0.1U and incrementally increasing by 0.5U every 5 days, with doses including 0.15U, 0.2U, and 0.25U.

Following the dosage refinement phase, our results indicated that the most effective treatment protocol involved starting with a 0.2U dosage initiated on day 8 via subcutaneous injection, increasing by 0.5U every 5 days and maintained up to the humane endpoint. This approach was favored due to the notable improvements observed in the weight trends of the mice, as detailed in table 5.1.

Table 5.2 Administering 0.2U via subcutaneous injection is the most effective treatment method.

Initiating dose of insulin	Treatment Starting Day	Effect on Survival	Effect on Weight
0.1 U	P8	no change	no change
0.15 U	P5	no change	no change
0.2 U	P5	no change	no change
0.2 U	P8	no change	increase
0.25 U	P8	Toxicity observed	

This table outlines the dosage and schedule of insulin administration in mouse experiments. To determine the best treatment strategy, SMA mice were exposed to different dosages of insulin. We then evaluated melatonin's efficacy based on weight and survival trends. In an extensive study, we examined the effects of administering insulin on *Smn*^{2B/-} mouse models. This dosage was compared against untreated control groups.

Interestingly, mice receiving insulin injections showed a significant increase in body weight from the 13th postnatal day onwards. This trend of weight gain continued up to the twentieth postnatal day, demonstrating a steady and prolonged positive impact of melatonin on physical development (figure 5.11.a.). Similarly, following insulin administration, weight gain patterns observed on days 14 and 19 were also noted in the control group (figure 5.11.b.). However, there was no change in the lifespan (figure 5.11.c.) or RR (figure 5.11.d.) of SMA mice due to the insulin application.

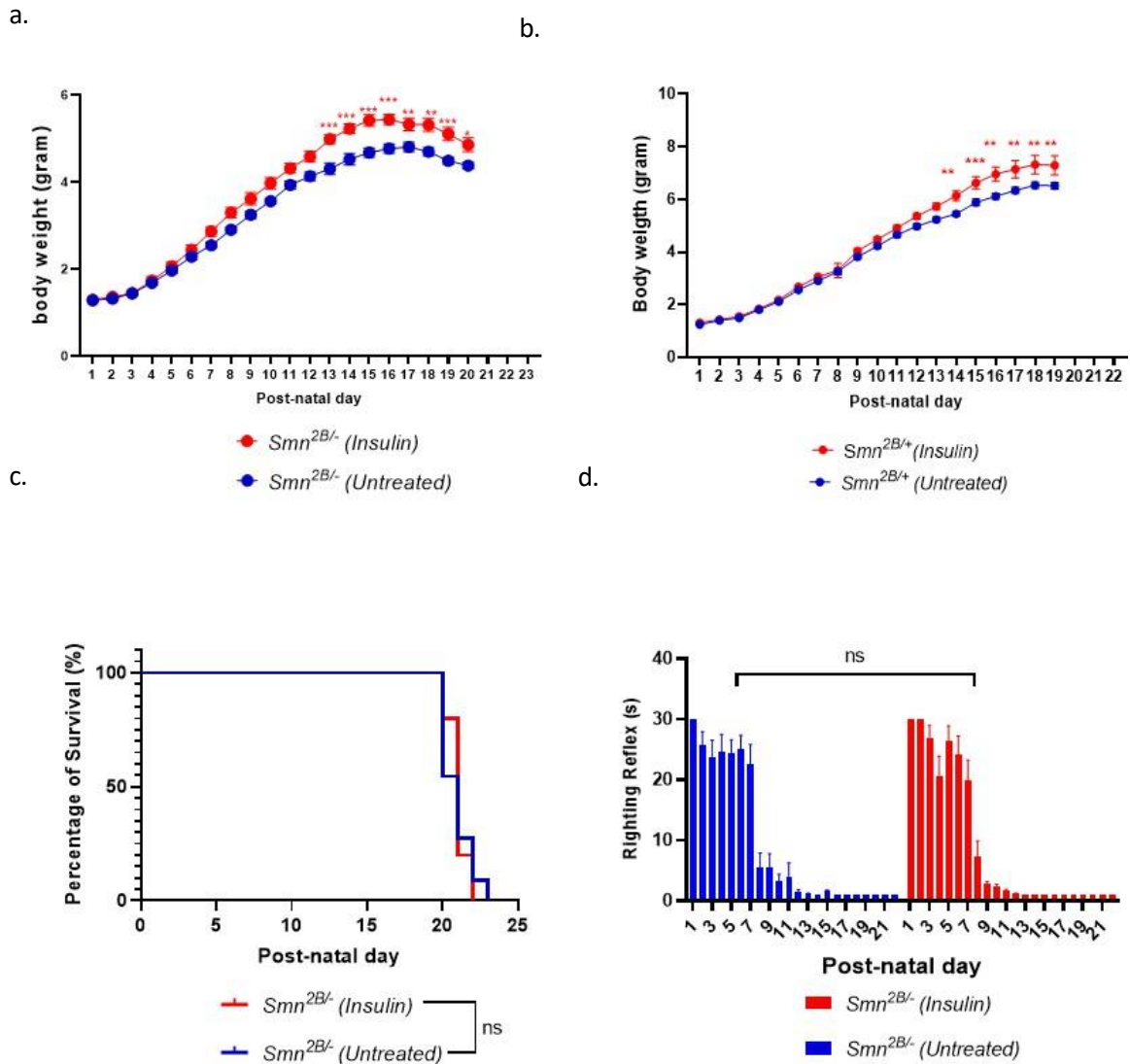


Figure 5. 11 Elevating the doses of subcutaneous insulin injections leads to a rise in body weight in *Smn*^{2B/-} mice.

a. Daily weights of insulin-treated (red, n=10), untreated (blue, n=15) on *Smn*^{2B/-}_{SMA} mice. Error bars represent +/- SEM; Two-way ANOVA with post-hoc Sidak's multiple comparisons test between untreated (blue) and 50 mg/kg/day oral melatonin (red). ns= not significant, *p<0.05, **p<0.01, ***p<0.001, ****p<0.0001. b. Daily weights of insulin-treated (red, n=10), untreated (blue, n=15) on *Smn*^{2B/+}_{SMA} mice. Error bars represent +/- SEM; Two-way ANOVA with post-hoc Sidak's multiple comparisons test between untreated (blue) and 50 mg/kg/day oral melatonin (red). ns= not significant, *p<0.05, **p<0.01, ***p<0.001, ****p<0.0001. c. Kaplan-Meier survival curves for n=15 untreated (blue, median survival:20 days) and n=16 insulin-treated (red, n=10), (red, median survival:21 days) on *Smn*^{2B/-}_{SMA} mice, Long-rank (Mantel-Cox) test, **p<0.01, ns= n significant. d. Daily righting reflex test up to a 30 second max time point of drug-treated (red, n=10) and untreated (blue, n=15) on *Smn*^{2B/-}_{SMA} mice.

Data represents mean and +/- SD error bars, One-way ANOVA with post-hoc Turkey's multiple comparisons test. ns= not significant, *p<0.05, **p<0.01, ***p<0.001, ****p<0.0001.

5.4 Discussion

Combined in silico analyses predicted that in symptomatic severe SMA mouse models' skeletal muscle, genes *Igfr1*, *Rb1*, and *InsR* are elevated. These genes are expected to decrease upon insulin treatment, showing a similar effect as seen with prednisolone application (Hoolachan *et al.*, 2023). This suggests a potential therapeutic pathway for SMA treatment involving insulin regulation to counteract specific gene alterations.

The study confirmed that certain target genes, which become dysregulated under SMA conditions, were validated in SMA Type III deltoid muscle samples and SMA mouse models. In the C2C12 cell line, the effect of insulin on the expression of these target genes was observed. Significantly, in the *Smn*^{2B/-} mouse model, post-insulin application, an increase in weight patterns was noted. Importantly, we observed an increase in weight in control groups of mice following the application of insulin. These observations allow us to assert that the effects of insulin are independent of the canonical SMA pathology. This aligns with findings in the literature regarding *Smn*^{+/-} mice, which demonstrate that even a slight deficiency in SMN protein can independently contribute to extra metabolic stress, separate from the NMD pathology typically associated with SMA (Bowerman *et al.*, 2014).

Firstly, our research revealed that in symptomatic *Smn*^{-/-}; *SMN2* mice, the mRNA level of *Igf1R* in skeletal muscle decreased. Interestingly, this gene remained unchanged in *Smn*^{2B/-} mice, possibly indicating a link to the severity of the condition. This is supported by findings that in human skeletal muscle samples from SMA type I and III patients, *IGF1* levels increased in type I but decreased in type III, suggesting that IGF1's expression patterns may vary depending on the severity of SMA (Millino *et al.*, 2009). This study proposed that muscle samples from SMA type III patients exhibited a hypertrophic phenotype in relation to the upregulation of mTOR (Millino *et al.*, 2009). In a muscle-specific mTOR-null mouse line, severe myopathy was observed (Risson *et al.*, 2009), and another study found that downstream of *Igf1*, factors such as *Foxo* and *mTOR*, which play roles in muscle development, were identified (Florini *et al.*, 1996).

Consequently, the impact of *Igf1* on muscle development is complex and warrants detailed investigation in future studies.

In the C2C12s cell model, both in its proliferating and differentiated states with *Smn*-KD, an increased mRNA expression of the *Igf1R* gene was found. We propose that *Igf1r* is dysregulated in a manner dependent on the SMN protein, both in vitro and in vivo models, playing a key role in the pathology of SMA. Literature review shows that *Igf1* activates satellite cells to promote myoblast growth, triggering their differentiation into muscle cells and increasing muscle cell size (Shavlakadze et al., 2010). Parallel, in the *SMNΔ7* mouse model, mice overexpressing muscle-specific isoform *Igf-1* (mIGF1) had more developed muscle fibers (Bosch-Marcé et al., 2011) and a 40% longer median lifespan than those without this overexpression (Bosch-Marcé et al., 2011). These observations suggest that enhancing *Igf-1* in muscles could alter SMA mice characteristics and offer new avenues for SMA progression through therapies targeting muscle development. In addition to its role in muscle development, *Igf1* is also associated with glucose metabolism in muscle (O'Neill et al., 2015). This has been demonstrated in studies using mouse models with knockdowns of *Glut4* and *Igf1*, highlighting the *Igf1* facilitates the movement of glucose receptors to the cell surface, thereby promoting increasing membrane localized glucose transporters and glucose uptake (O'Neill et al., 2015). This indicates that an increase in *Igf1* levels in skeletal muscle can enhance the muscle's utilization of glucose, contributing to the tissue's metabolism and growth in SMA.

Drawing attention to the potential impact of certain pathways involved in the downregulation of *Igf1* on muscle development and metabolism, future studies are suggested to include the examination of these pathways' patterns following insulin application (as an *Igf1* agonist). On the other hand, *Igf1* operates several pathways located in its downstream, activating or inactivating them. One such pathway is PI3K- AKT-FOXO, where an increase in *IGF1R* leads to the activation of *Foxo*, which can inhibit muscle atrophic factors like *atrogin* (Puig et al., 2003). Another pathway influenced by *Igf1* is PI3K-AKT-MTOR-4EBP1. In this pathway, increased expression of *Igf1* decreases the level of *4EBP1*, regulating protein synthesis (Yang et al., 2010). The final pathway to consider is Ras-Raf-MEK-ERK-MNK (Menu et al., 2004). Here, heightened *Igf1* levels lead to increased ERK activity, which reduces MNK expression, playing a role in the regulation of protein synthesis. *Igf1R* is a critical trigger factor

involved in various metabolic and atrophic pathways, and its impact on muscle growth, muscle atrophy, and muscle metabolism through these pathways warrants detailed investigation in future studies. This thorough exploration of *Igf1R*'s role in these pathways will provide deeper insights into its multifaceted influence on muscle physiology.

In both *Smn*^{-/-}; *SMN2* and *Smn*^{2B/-} mice models, a significant increase in *Rb1* expression was observed. Furthermore, the study highlights that temporarily inhibiting protein phosphatase 1 activity, leading to a transient inactivation of p*Rb* in satellite cells, might serve as an innovative therapeutic approach against muscle atrophy (Hosoyama et al., 2011). This method aims to promote a short-term increase in muscle stem cells and myoblast populations, offering a new strategy for managing muscle wasting conditions (Hosoyama et al., 2011).

In both *Smn*^{-/-}; *SMN2* and *Smn*^{2B/-} mice models, there was a notable increase in *Rb1* gene expression. When these myotubes were treated with 100nM of insulin, an enhancement in the expression of *Rb1* target genes was observed. In muscle stem cell researches, *Rb1* has been reported to have time-course-specific effects and to play a role in muscle atrophy pathology (Hosoyama et al., 2011). Similarly, in Pax7CreER- *Rb1*- KD mice, the inactivation of *Rb1* significantly increased satellite cell and myoblast numbers (Hosoyama et al., 2011). The contradiction arises from the fact that sustained *Rb1* inactivation diminishes terminal differentiation, leading to muscle fiber formation deficits (Hosoyama et al., 2011). In summary, the positive effect of *Rb1* on muscle atrophy is emphasized to be dependent on the short-term expose downregulated-*Rb1* expression especially during myoblast phase of muscle development.

On the other hand, in studies conducted on ischemic muscles, it has been found that the inhibition of *Rb1* regulates the AMPK α 2/NLRP3 inflammasome signaling pathway, which enhances muscle repair (Wang et al., 2021). Abnormalities in peripheral immune organs and T-cell maturation dysfunction have been observed in SMA (Cappellano et al., 2013)

Overall, these findings provide a deeper understanding of the molecular mechanisms underlying metabolism of SMA and open new possibilities for targeted treatments that address both muscle and systemic aspects of this debilitating condition.

6 General Discussion

Three gene therapies approved by the FDA for Spinal Muscular Atrophy (SMA) are nusinersen (Spinraza), onasemnogene (Zolgensma), and risdiplam (Evrysdi) (Hoolachan et al., 2019). While these therapies offer significant, potentially life-changing benefits (Ogbonmide et al., n.d.), they also have limitations, such as high costs limiting accessibility, reduced benefits in older SMA patients, and variable impacts on CNS and muscle pathologies (Day et al., 2022). To address these drawbacks, developing combinatorial approaches that target both the CNS and peripheral systems is crucial. This is because SMA pathophysiology extends beyond the neuromuscular system, necessitating a comprehensive, whole-lifespan approach to therapy, incorporating both SMN-dependent and SMN-independent strategies (Hamilton and Gillingwater, 2013).

Our goal is to develop second-generation combinatorial treatments for SMA, targeting delayed symptoms and ongoing needs for maintaining whole-body metabolic homeostasis post-initial gene therapy. Recognizing developmental and metabolic pathologies in peripheral tissues, including muscle, liver, pancreas, and adipose tissues, we used RNA sequencing on skeletal muscle from symptomatic Taiwanese *Smn*^{-/-}; *SMN2* mice and WT animals. Through databases like KEGG-DRUG, iPathwayGuide, and the Drug-Gene Interaction database, we identified commercially available drugs predicted to restore differentially expressed genes in SMA muscle. The key pharmacological candidates identified are pioglitazone, melatonin, and insulin, marking a significant step in repurposing existing drugs for comprehensive SMA treatment. In the first phase, we confirmed *in silico* data with *in vivo* and *in vitro* SMA models. In the second phase, we observed the dose- and stage-dependent effects of potential compounds on C2C12s and LCHN-M2 cell lines and established a safe profile of three compounds. The effects of candidate molecules on the SMA phenotype were assessed in the *Smn*^{2B/-} mouse model over weight, survival, and RR. Both pioglitazone and melatonin were observed to increase weight patterns and extend lifespans of *Smn*^{2B/-}. The next step aimed to understand these phenotypic improvements through genes involved in metabolic pathways. This approach was directed towards a comprehensive analysis of multisystemic pathology and treatment strategies, highlighting the importance of considering systemic factors alongside SMA's central pathologies.

Initially, the effects of targeted compounds on peripheral tissues were investigated through genes involved in mitochondrial development and function. Pioglitazone increased the expression of the *Ide* gene, linked to the preprotein processing mechanism in skeletal muscle of *Smn^{2B/-}* mice. Moreover, melatonin administration enhanced the expression of *Sirt1*, involved in mitochondrial biogenesis, in triceps and WAT tissues. Intriguingly, it was suggested that melatonin could redirect the energy function of WAT tissue towards ATP production by increasing *Ucp1* expression. Melatonin's mitochondrial targets overlap with the mitochondrial defects observed in SMA pathology. These include reduced mtDNA numbers in mitochondria from murine SMA muscles (Houdebine et al., 2019c), decreased mitochondrial respiration and OXPHOS in human SMA myoblasts (Hellbach et al., 2018), a decline in the enzymatic activity of complexes I, II, and IV of the ETC in SMA mouse muscles (Houdebine et al., 2019c), and an increase in lipogenesis (Harpey et al., 1990).

Moderate exercise has emerged as a viable and beneficial therapeutic strategy to enhance mitochondrial function in muscle fibers (Memme et al., 2021). This approach is particularly advantageous for SMA patients, as exercise therapy has been shown to significantly improve their muscular strength and size, by activating the AMPK–p38–PGC-1 α signaling pathway in *Smn^{2B/-}* mouse model (Ng et al., 2019). These leads to increased oxygen consumption in skeletal muscles and a consequent reduction in lipogenesis in *Smn^{2B/-}* mouse model (Ng et al., 2019). Similarly, the pharmacological activation of the AMPK-p38 pathway using celecoxib, a COX-2 inhibitor, has been observed to improve lifespan and motor abilities in SMA mice (Farooq et al., 2013).

These insights suggest that targeting mitochondrial abnormalities specific to muscles can help in addressing not only muscular weakness but also related systemic issues such as hyperglycaemia, hyperglucagonemia, glucose resistance, and dyslipidaemia, which are often seen in SMA patients (Deguise et al., 2021a). Therefore, the effects of melatonin and pioglitazone on mitochondrial function and biogenesis, as well as their potential contribution to interconnected metabolic pathways, should be more thoroughly examined in SMA mouse models.

It has been observed that melatonin has tissue-specific metabolic and circadian effects. In a detailed examination, when evaluating tissue-specific daily gene patterns, skeletal muscle, liver, and adipose tissue showed the same patterns in all diurnal genes. This coordination indicates the need for these tissues to work

synchronously due to their shared roles in energy metabolism (Pickel and Sung, 2020). The study catabolism in the *Smn*^{2B/-} mouse model, demonstrates the crosstalk among peripheral tissues in SMA pathology, particularly focusing on the liver-pancreas-skeletal muscle-adipose tissue axis and its shift towards catabolism (Deguise et al., 2021c). The ability of compounds like melatonin and pioglitazone to target multiple tissues strengthens the possibility of their effectiveness in the multisystemic pathology of SMA, which is based on this peripheric crosstalk.

On the other hand, gluconeogenesis is another factor that impacts glucose metabolism. Investigations into melatonin's effect on gluconeogenesis have been conducted through in situ liver perfusion experiments, which have shown that melatonin suppresses hepatic gluconeogenesis (Faria *et al.*, 2013). To further understand melatonin's role in this mechanism within the SMA mouse model, it is considered beneficial to examine the liver's levels of gluconeogenic enzymes and glucose-6-phosphatase post-melatonin treatment (Lelli et al., 2016). Interestingly, in the SMA mouse model, SMN protein deficiency is associated with an increase in p-CREB phosphorylation and activity, leading to enhanced gluconeogenesis (Deguise *et al.*, 2019). Furthermore, p-CREB/ CREB can be considered an important protein target for the treatment of SMA; since the protein involves the pathologies which has already related to SMA disease such as gluconeogenesis (Bowerman *et al.*, 2014), anti- apoptosis (Kong et al., 2008) and muscle development (Berdeaux and Hutchins, 2019). In another study that reinforces the potential significance of p-CREB in SMA pathogenesis, the most potent activator of PGC-1alpha is TORC 1, a coactivator of CREB (Wu et al., 2006). This finding highlights the critical role of CREB and its coactivators in mitochondrial function and energy metabolism, pertinent to SMA pathology. This observation indicates that melatonin might play a role in counteracting the elevated glucose production driven by p-CREB, and it is suggested that the contribution of p-CREB-dependent gluconeogenesis in the SMA mouse model warrants further investigation.

In the application of pioglitazone and melatonin, a shared mechanism of action can be the IRS-PI3K-AKT pathway. The role on glucose and lipid metabolism of this pathway is well-known role (Choi et al., 2018). For example, the activation of IRS- PI3K causes a decrease in insulin resistance and oxidative stress depending on hyperglycaemia (Horii et al., 2020). Moreover, in the downregulation of this pathway, the anti-apoptotic protein BCL2 (Mardilovich et al., 2009) is a target of melatonin. Additionally, it is noteworthy that PPAR- α/β are involved in the downregulation of this pathway (Bao et al., 2020), with

pioglitazone being one of their targets. Another crucial aspect of the AKT/mTORC1 pathway is its role as a fundamental mechanism regulating protein anabolism (i.e., protein synthesis) in muscle cells (Goodman, 2014). The suppression of AKT/mTORC1 activation can lead to a decrease in protein synthesis, contributing to muscle atrophy (Bodine, 2022). In cases of high-dose GC administration, this suppression of the AKT/mTORC1 pathway has been observed in dogs (Yoshida et al., 2022). In our study, we started with the hypothesis that melatonin and pioglitazone, at lower doses compared to prednisolone (Lisa M. Walter et al., 2018), might exhibit similar effects in supporting muscle phenotype. In the study involving the SMN Δ 7 SMA mouse model, SMA patient fibroblasts, and SMN- knockdown NSC-34 cell line, Loganin, a botanical extract known for its anti-diabetic and antioxidant properties, has shown to increase SMN protein levels and enhance muscle development and strength in gastrocnemius muscle of SMA mice by elevating p-AKT levels (Tseng et al., 2016). The activity of Loganin in induced the Akt pathway and its identification as an anti-diabetic agent are reminiscent of pioglitazone (Zhao et al., 2021) and melatonin (Kong et al., 2008). A detailed examination of the AKT/mTORC1 pathway could not only elucidate the dose-dependent effects of prednisolone but might also reveal potential common mechanisms and novel protein targets shared by melatonin, pioglitazone, and prednisolone. This could be a significant step in understanding these drugs' interactions and their collective impact on muscle health.

On the other hand, following the application of both pioglitazone and melatonin, a decrease in *Fas* and *Pmaip-1* levels was observed in symptomatic SC tissues from *Smn*^{2B/-}, indicating an progress in SC survival. To elaborate further, when examining whether pioglitazone and melatonin share a common pathway in their neuroprotective effects, their activation of the GABA neurotransmitter system emerges as a significant overlap (Pourhanifeh et al., 2020). In detail, in STZ-induced diabetic rats, it was found that melatonin inhibits the oxidative stress-induced, by normalizing the levels of neurotransmitters such as GABA and glutamate (Pourhanifeh et al., 2020). Similarly, pioglitazone has demonstrated neuroprotective effects by restoring the number of active GABA-A receptors in rats made anxious and depressed due to prolonged hypokinesia.

It achieves this through the reduction of microglial activation, mitochondrial dysfunction, and the expression of various inflammatory mediators (Amin et al., 2017). Importantly, SMA *C. elegans* model shows structural and functional abnormalities in GABAergic at NMJs, which is related to locomotor dysfunction. Remarkably, it was found that solely enhancing GABAergic neurotransmission could correct this locomotor dysfunction (Wu et al., 2018). Altogether, it is recommended to examine the effects of pioglitazone and melatonin on GABA levels to gain a clearer understanding of their neuroprotective effects in SMA for future experiments.

Regarding *Igf1R*, a target of insulin, in the *Smn*-KD-C2C12s cell model, both in its proliferating and differentiated states, there was an increase in *Igf1R* mRNA expression. This suggests that *Igf1R* is dysregulated depending on the SMN protein deficiency, suggesting a crucial role for *Igf1R* in SMA pathology (Murdocca et al., 2012). This dysregulation may be related to muscle atrophy and metabolism in SMA. Supportively, in the SMN Δ 7 mouse model, overexpression of muscle-specific *Igf-1* (*mIgf1*) led to more developed muscle fibers and a 40% longer lifespan (Bosch-Marcé et al., 2011). Moreover, *Igf1* plays a crucial role in facilitating the movement of glucose receptors to the cell surface in skeletal muscle (O'Neill et al., 2015). This action enhances the presence of membrane-localized glucose transporters and promotes glucose uptake (O'Neill et al., 2015). Elevating *Igf1* levels in skeletal muscle can positively impact muscle metabolism and growth, making it a viable therapeutic target for SMA. This approach highlights the potential of targeting muscle-specific pathways to improve SMA outcomes.

In conclusion, our comprehensive study underscores the significant potential of melatonin, pioglitazone, and insulin in addressing the complexities of SMA. The evidence gathered from our research reveals that these compounds can significantly impact the genes associated with mitochondrial function, glucose metabolism, and muscle development. The potential of melatonin, pioglitazone, and insulin in SMA treatment. These compounds offer a comprehensive approach to addressing the multifaceted challenges of SMA. This integrative treatment strategy, which considers both central and peripheral pathologies, represents a significant advancement in SMA therapy, aiming to improve overall patient outcomes and quality of life.

7 Reference

- Aartsma-Rus, A., 2017. FDA Approval of Nusinersen for Spinal Muscular Atrophy Makes 2016 the Year of Splice Modulating Oligonucleotides. *Nucleic Acid Ther.* 27, 67–69. <https://doi.org/10.1089/nat.2017.0665>
- Abdulwahab, D.A., El-Missiry, M.A., Shabana, S., Othman, A.I., Amer, M.E., 2021. Melatonin protects the heart and pancreas by improving glucose homeostasis, oxidative stress, inflammation and apoptosis in T2DM-induced rats. *Heliyon* 7, e06474. <https://doi.org/10.1016/j.heliyon.2021.e06474>
- Ameshima, S., Golpon, H., Cool, C.D., Chan, D., Vandivier, R.W., Gardai, S.J., Wick, M., Nemenoff, R.A., Geraci, M.W., Voelkel, N.F., 2003. Peroxisome Proliferator-Activated Receptor Gamma (PPAR γ) Expression Is Decreased in Pulmonary Hypertension and Affects Endothelial Cell Growth. *Circ. Res.* 92, 1162–1169. <https://doi.org/10.1161/01.RES.0000073585.50092.14>
- Bachand, F., Boisvert, F.-M., Côté, J., Richard, S., Autexier, C., 2002. The product of the survival of motor neuron (SMN) gene is a human telomerase-associated protein. *Mol. Biol. Cell* 13, 3192–3202. <https://doi.org/10.1091/mbc.e02-04-0216>
- Bai, J., Xia, M., Xue, Y., Ma, F., Cui, A., Sun, Y., Han, Y., Xu, X., Zhang, F., Hu, Z., Liu, Z., Liu, Y., Cai, G., Su, W., Sun, X., Wu, H., Yan, H., Chang, X., Hu, X., Bian, H., Xia, P., Gao, J., Li, Y., Gao, X., 2020. Thrombospondin 1 improves hepatic steatosis in diet-induced insulin-resistant mice and is associated with hepatic fat content in humans. *eBioMedicine* 57. <https://doi.org/10.1016/j.ebiom.2020.102849>
- Bald, E.M., Nance, C.S., Schultz, J.L., 2021. Melatonin may slow disease progression in amyotrophic lateral sclerosis: Findings from the Pooled Resource Open- Access ALS Clinic Trials database. *Muscle Nerve* 63, 572–576. <https://doi.org/10.1002/mus.27168>
- Bao, S., Wu, Y.-L., Wang, X., Han, S., Cho, S., Ao, W., Nan, J.-X., 2020. Agriophyllum oligosaccharides ameliorate hepatic injury in type 2 diabetic db/db mice targeting INS-R/IRS-2/PI3K/AKT/PPAR- γ /Glut4 signal pathway. *J. Ethnopharmacol.* 257, 112863. <https://doi.org/10.1016/j.jep.2020.112863>
- Bäumer, D., Lee, S., Nicholson, G., Davies, J.L., Parkinson, N.J., Murray, L.M., Gillingwater, T.H., Ansorge, O., Davies, K.E., Talbot, K., 2009. Alternative splicing events are a late feature of pathology in a mouse model of spinal muscular atrophy. *PLoS Genet.* 5, e1000773. <https://doi.org/10.1371/journal.pgen.1000773>
- Beker, M.C., Caglayan, B., Caglayan, A.B., Kelestemur, T., Yalcin, E., Caglayan, A., Kilic, U., Baykal, A.T., Reiter, R.J., Kilic, E., 2019. Interaction of melatonin and Bmal1 in the regulation of PI3K/AKT pathway components and cellular survival. *Sci. Rep.* 9, 19082. <https://doi.org/10.1038/s41598-019-55663-0>
- Bentzinger, C.F., Wang, Y.X., Rudnicki, M.A., 2012. Building Muscle: Molecular Regulation of Myogenesis. *Cold Spring Harb. Perspect. Biol.* 4, a008342. <https://doi.org/10.1101/cshperspect.a008342>
- Berciano, M.T., Puente-Bedia, A., Medina-Samamé, A., Rodríguez-Rey, J.C., Calderó, J., Lafarga, M., Tapia, O., 2020. Nusinersen ameliorates motor function and prevents motoneuron Cajal body disassembly and abnormal poly(A) RNA distribution in a SMA mouse model. *Sci. Rep.* 10, 10738. <https://doi.org/10.1038/s41598-020-67569-3>

- Berdeaux, R., Hutchins, C., 2019. Anabolic and Pro-metabolic Functions of CREB- CRTC in Skeletal Muscle: Advantages and Obstacles for Type 2 Diabetes and Cancer Cachexia. *Front. Endocrinol.* 10, 535. <https://doi.org/10.3389/fendo.2019.00535>
- Berger, M., Kemmer, F.W., Becker, K., Herberg, L., Schwenen, M., Gjinavci, A., Berchtold, P., 1979. Effect of physical training on glucose tolerance and on glucose metabolism of skeletal muscle in anaesthetized normal rats. *Diabetologia* 16, 179–184. <https://doi.org/10.1007/BF01219795>
- Bersanini, C., Khirani, S., Ramirez, A., Lofaso, F., Aubertin, G., Beydon, N., Mayer, M., Maincent, K., Boulé, M., Fauroux, B., 2012. Nocturnal hypoxaemia and hypercapnia in children with neuromuscular disorders. *Eur. Respir. J.* 39, 1206– 1212. <https://doi.org/10.1183/09031936.00087511>
- Bertram, R., Gram Pedersen, M., Luciani, D.S., Sherman, A., 2006. A simplified model for mitochondrial ATP production. *J. Theor. Biol.* 243, 575–586. <https://doi.org/10.1016/j.jtbi.2006.07.019>
- Biondi, O., Branchu, J., Salah, A.B., Houdebine, L., Bertin, L., Chali, F., Desseille, C., Weill, L., Sanchez, G., Lancelin, C., Aïd, S., Lopes, P., Pariset, C., Lécolle, S., Côté, J., Holzenberger, M., Chanoine, C., Massaad, C., Charbonnier, F., 2015. IGF-1R Reduction Triggers Neuroprotective Signaling Pathways in Spinal Muscular Atrophy Mice. *J. Neurosci.* 35, 12063–12079. <https://doi.org/10.1523/JNEUROSCI.0608-15.2015>
- Biral, D., Scarpini, E., Angelini, C., Salviati, G., Margreth, A., 1989. Myosin heavy chain composition of muscle fibers in spinal muscular atrophy. *Muscle Nerve* 12, 43–51. <https://doi.org/10.1002/mus.880120109>
- Bodine, S.C., 2022. The role of mTORC1 in the regulation of skeletal muscle mass. *Fac. Rev.* 11, 32. <https://doi.org/10.12703/r/11-32>
- Bogacka, I., Xie, H., Bray, G.A., Smith, S.R., 2004. The Effect of Pioglitazone on Peroxisome Proliferator-Activated Receptor- γ Target Genes Related to Lipid Storage In Vivo. *Diabetes Care* 27, 1660–1667. <https://doi.org/10.2337/diacare.27.7.1660>
- Bosch-Marcé, M., Wee, C.D., Martinez, T.L., Lipkes, C.E., Choe, D.W., Kong, L., Van Meerbeke, J.P., Musarò, A., Sumner, C.J., 2011. Increased IGF-1 in muscle modulates the phenotype of severe SMA mice. *Hum. Mol. Genet.* 20, 1844– 1853. <https://doi.org/10.1093/hmg/ddr067>
- Bowerman, M., Becker, C.G., Yáñez-Muñoz, R.J., Ning, K., Wood, M.J.A., Gillingwater, T.H., Talbot, K., The UK SMA Research Consortium, 2017. Therapeutic strategies for spinal muscular atrophy: SMN and beyond. *Dis. Model. Mech.* 10, 943–954. <https://doi.org/10.1242/dmm.030148>
- Bowerman, M., Michalski, J.-P., Beauvais, A., Murray, L.M., DeRepentigny, Y., Kothary, R., 2014. Defects in pancreatic development and glucose metabolism in SMN-depleted mice independent of canonical spinal muscular atrophy neuromuscular pathology. *Hum. Mol. Genet.* 23, 3432–3444. <https://doi.org/10.1093/hmg/ddu052>
- Bowerman, M., Murray, L.M., Scamps, F., Schneider, B.L., Kothary, R., Raoul, C., 2018. Pathogenic commonalities between spinal muscular atrophy and amyotrophic lateral sclerosis: Converging roads to therapeutic development. *Eur. J. Med. Genet.* 61, 685–698. <https://doi.org/10.1016/j.ejmg.2017.12.001>
- Bowerman, M., Swoboda, K.J., Michalski, J.-P., Wang, G.-S., Reeks, C., Beauvais, A., Murphy, K., Woulfe, J., Sreaton, R.A., Scott, F.W., Kothary, R., 2012a.

- Glucose Metabolism and Pancreatic Defects in Spinal Muscular Atrophy. *Ann. Neurol.* 72, 256–268. <https://doi.org/10.1002/ana.23582>
- Bowerman, M., Swoboda, K.J., Michalski, J.-P., Wang, G.-S., Reeks, C., Beauvais, A., Murphy, K., Woulfe, J., Sreaton, R.A., Scott, F.W., Kothary, R., 2012b. Glucose metabolism and pancreatic defects in spinal muscular atrophy. *Ann. Neurol.* 72, 256–268. <https://doi.org/10.1002/ana.23582>
- Boyer, J., Ferrier, A., Kothary, R., 2013. More than a bystander: the contributions of intrinsic skeletal muscle defects in motor neuron diseases. *Front. Physiol.* 4.
- Boyer, J.G., Deguise, M.-O., Murray, L.M., Yazdani, A., De Repentigny, Y., Boudreau-Larivière, C., Kothary, R., 2014. Myogenic program dysregulation is contributory to disease pathogenesis in spinal muscular atrophy. *Hum. Mol. Genet.* 23, 4249–4259. <https://doi.org/10.1093/hmg/ddu142>
- Boyer, J.G., Murray, L.M., Scott, K., De Repentigny, Y., Renaud, J.-M., Kothary, R., 2013. Early onset muscle weakness and disruption of muscle proteins in mouse models of spinal muscular atrophy. *Skelet. Muscle* 3, 24. <https://doi.org/10.1186/2044-5040-3-24>
- Bryda, E.C., 2013. The Mighty Mouse: The Impact of Rodents on Advances in Biomedical Research. *Mo. Med.* 110, 207–211.
- Bürglen, L., Lefebvre, S., Clermont, O., Burlet, P., Viollet, L., Cruaud, C., Munnich, A., Melki, J., 1996. Structure and Organization of the Human Survival Motor Neurone (SMN) Gene. *Genomics* 32, 479–482. <https://doi.org/10.1006/geno.1996.0147>
- Caballero, B., Vega-Naredo, I., Sierra, V., Huidobro-Fernández, C., Soria-Valles, C., De Gonzalo-Calvo, D., Tolivia, D., Gutierrez-Cuesta, J., Pallas, M., Camins, A., Rodríguez-Colunga, M.J., Coto-Montes, A., 2008. Favorable effects of a prolonged treatment with melatonin on the level of oxidative damage and neurodegeneration in senescence-accelerated mice. *J. Pineal Res.* 45, 302–311. <https://doi.org/10.1111/j.1600-079X.2008.00591.x>
- Cappellano, G., Carecchio, M., Fleetwood, T., Magistrelli, L., Cantello, R., Dianzani, U., Comi, C., 2013. Immunity and inflammation in neurodegenerative diseases. *Am. J. Neurodegener. Dis.* 2, 89–107.
- Carrasco, C., Rodriguez, A.B., Pariente, J.A., 2014. Effects of melatonin on the oxidative damage and pancreatic antioxidant defenses in cerulein-induced acute pancreatitis in rats. *Hepatobiliary Pancreat. Dis. Int. HBPD INT* 13, 442–446. [https://doi.org/10.1016/s1499-3872\(14\)60271-x](https://doi.org/10.1016/s1499-3872(14)60271-x)
- Carvalho, T., Almeida, F., Calapez, A., Lafarga, M., Berciano, M.T., Carmo-Fonseca, M., 1999. The spinal muscular atrophy disease gene product, SMN: A link between snRNP biogenesis and the Cajal (coiled) body. *J. Cell Biol.* 147, 715–728. <https://doi.org/10.1083/jcb.147.4.715>
- Cerf, M.E., 2013. Beta Cell Dysfunction and Insulin Resistance. *Front. Endocrinol.* 4, 37. <https://doi.org/10.3389/fendo.2013.00037>
- Chan, K., Wong, F.S., Pearson, J.A., 2022. Circadian rhythms and pancreas physiology: A review. *Front. Endocrinol.* 13, 920261. <https://doi.org/10.3389/fendo.2022.920261>
- Chemello, F., Pozzobon, M., Tsansizi, L.I., Varanita, T., Quintana-Cabrera, R., Bonesso, D., Piccoli, M., Lanfranchi, G., Giacomello, M., Scorrano, L., Bean, C., 2023a. Dysfunctional mitochondria accumulate in a skeletal muscle knockout model of *Smn1*, the causal gene of spinal muscular atrophy. *Cell Death Dis.* 14, 1–13. <https://doi.org/10.1038/s41419-023-05573-x>

- Chemello, F., Pozzobon, M., Tsansizi, L.I., Varanita, T., Quintana-Cabrera, R., Bonesso, D., Piccoli, M., Lanfranchi, G., Giacomello, M., Scorrano, L., Bean, C., 2023b. Dysfunctional mitochondria accumulate in a skeletal muscle knockout model of *Smn1*, the causal gene of spinal muscular atrophy. *Cell Death Dis.* 14, 1–13. <https://doi.org/10.1038/s41419-023-05573-x>
- Choi, J., Kim, K.-J., Koh, E.-J., Lee, B.-Y., 2018. Gelidium elegans Extract Ameliorates Type 2 Diabetes via Regulation of MAPK and PI3K/Akt Signaling. *Nutrients* 10, 51. <https://doi.org/10.3390/nu10010051>
- Cooper, G.M., 2000. Mitochondria, in: *The Cell: A Molecular Approach*. 2nd Edition. Sinauer Associates.
- Coovert, D. D., Le, T.T., McAndrew, P.E., Strasswimmer, J., Crawford, T.O., Mendell, J.R., Coulson, S.E., Androphy, E.J., Prior, T.W., Burghes, A.H., 1997. The survival motor neuron protein in spinal muscular atrophy. *Hum. Mol. Genet.* 6, 1205–1214. <https://doi.org/10.1093/hmg/6.8.1205>
- Coovert, Daniel D., Le, T.T., McAndrew, P.E., Strasswimmer, J., Crawford, T.O., Mendell, J.R., Coulson, S.E., Androphy, E.J., Prior, T.W., Burghes, A.H.M., 1997. The Survival Motor Neuron Protein in Spinal Muscular Atrophy. *Hum. Mol. Genet.* 6, 1205–1214. <https://doi.org/10.1093/hmg/6.8.1205>
- Czech, M.P., 2020. Mechanisms of insulin resistance related to white, beige, and brown adipocytes. *Mol. Metab.* 34, 27–42. <https://doi.org/10.1016/j.molmet.2019.12.014>
- D, S., Jg, B., K, B., R, K., 2010. Identification of novel interacting protein partners of SMN using tandem affinity purification. *J. Proteome Res.* 9. <https://doi.org/10.1021/pr9006987>
- Da Cruz, S., Parone, P.A., Lopes, V.S., Lillo, C., McAlonis-Downes, M., Lee, S.K., Vetto, A.P., Petrosyan, S., Marsala, M., Murphy, A.N., Williams, D.S., Spiegelman, B.M., Cleveland, D.W., 2012. Elevated PGC-1 α activity sustains mitochondrial biogenesis and muscle function without extending survival in a mouse model of inherited ALS. *Cell Metab.* 15, 778–786. <https://doi.org/10.1016/j.cmet.2012.03.019>
- Da Silva, J.S., Medina, M., Zuliani, C., Di Nardo, A., Witke, W., Dotti, C.G., 2003. RhoA/ROCK regulation of neuritogenesis via profilin IIa-mediated control of actin stability. *J. Cell Biol.* 162, 1267–1279. <https://doi.org/10.1083/jcb.200304021>
- Dale, J.M., Shen, H., Barry, D.M., Garcia, V.B., Rose, F.F., Lorson, C.L., Garcia, M.L., 2011. The spinal muscular atrophy mouse model, SMA Δ 7, displays altered axonal transport without global neurofilament alterations. *Acta Neuropathol. (Berl.)* 122, 331–341. <https://doi.org/10.1007/s00401-011-0848-5>
- D’Antona, G., Ragni, M., Cardile, A., Tedesco, L., Dossena, M., Bruttini, F., Caliaro, F., Corsetti, G., Bottinelli, R., Carruba, M.O., Valerio, A., Nisoli, E., 2010. Branched-chain amino acid supplementation promotes survival and supports cardiac and skeletal muscle mitochondrial biogenesis in middle-aged mice. *Cell Metab.* 12, 362–372. <https://doi.org/10.1016/j.cmet.2010.08.016>
- Das, N., Mandala, A., Naaz, S., Giri, S., Jain, M., Bandyopadhyay, D., Reiter, R.J., Roy, S.S., 2017. Melatonin protects against lipid-induced mitochondrial dysfunction in hepatocytes and inhibits stellate cell activation during hepatic fibrosis in mice. *J. Pineal Res.* 62. <https://doi.org/10.1111/jpi.12404>
- Dathan-Stumpf, A., Vogel, M., Hiemisch, A., Thiery, J., Burkhardt, R., Kratzsch,

- J., Kiess, W., 2016. Pediatric reference data of serum lipids and prevalence of dyslipidemia: Results from a population-based cohort in Germany. *Clin. Biochem.* 49, 740–749.
<https://doi.org/10.1016/j.clinbiochem.2016.02.010>
- Davis, R.L., Weintraub, H., Lassar, A.B., 1987. Expression of a single transfected cDNA converts fibroblasts to myoblasts. *Cell* 51, 987–1000. [https://doi.org/10.1016/0092-8674\(87\)90585-x](https://doi.org/10.1016/0092-8674(87)90585-x)
- Day, J.W., Howell, K., Place, A., Long, K., Rossello, J., Kertesz, N., Nomikos, G., 2022. Advances and limitations for the treatment of spinal muscular atrophy. *BMC Pediatr.* 22, 632. <https://doi.org/10.1186/s12887-022-03671-x>
- de Luxán-Delgado, B., Potes, Y., Rubio-González, A., Caballero, B., Solano, J.J., Fernández-Fernández, M., Bermúdez, M., Rodrigues Moreira Guimarães, M., Vega-Naredo, I., Boga, J.A., Coto-Montes, A., 2016. Melatonin reduces endoplasmic reticulum stress and autophagy in liver of leptin-deficient mice. *J. Pineal Res.* 61, 108–123.
<https://doi.org/10.1111/jpi.12333>
- De Vivo, D.C., Bertini, E., Swoboda, K.J., Hwu, W.-L., Crawford, T.O., Finkel, R.S., Kirschner, J., Kuntz, N.L., Parsons, J.A., Ryan, M.M., Butterfield, R.J., Topaloglu, H., Ben-Omran, T., Sansone, V.A., Jong, Y.-J., Shu, F., Staropoli, J.F., Kerr, D., Sandrock, A.W., Stebbins, C., Petrillo, M., Braley, G., Johnson, K., Foster, R., Gheuens, S., Bhan, I., Reyna, S.P., Fradette, S., Farwell, W., NURTURE Study Group, 2019. Nusinersen initiated in infants during the presymptomatic stage of spinal muscular atrophy: Interim efficacy and safety results from the Phase 2 NURTURE study. *Neuromuscul. Disord.* NMD 29, 842–856.
<https://doi.org/10.1016/j.nmd.2019.09.007>
- Deguisse, M.-O., Baranello, G., Mastella, C., Beauvais, A., Michaud, J., Leone, A., De Amicis, R., Battezzati, A., Dunham, C., Selby, K., Warman Chardon, J., McMillan, H.J., Huang, Y.-T., Courtney, N.L., Mole, A.J., Kubinski, S., Claus, P., Murray, L.M., Bowerman, M., Gillingwater, T.H., Bertoli, S., Parson, S.H., Kothary, R., 2019b. Abnormal fatty acid metabolism is a core component of spinal muscular atrophy. *Ann. Clin. Transl. Neurol.* 6, 1519–1532. <https://doi.org/10.1002/acn3.50855>
- Deguisse, M.-O., Boyer, J.G., McFall, E.R., Yazdani, A., De Repentigny, Y., Kothary, R., 2016. Differential induction of muscle atrophy pathways in two mouse models of spinal muscular atrophy. *Sci. Rep.* 6, 28846.
<https://doi.org/10.1038/srep28846>
- Deguisse, M.-O., Chehade, L., Kothary, R., 2021a. Metabolic Dysfunction in Spinal Muscular Atrophy. *Int. J. Mol. Sci.* 22, 5913.
<https://doi.org/10.3390/ijms22115913>
- Deguisse, M.-O., Pileggi, C., De Repentigny, Y., Beauvais, A., Tierney, A., Chehade, L., Michaud, J., Llaverro-Hurtado, M., Lamont, D., Atrih, A., Wishart, T.M., Gillingwater, T.H., Schneider, B.L., Harper, M.-E., Parson, S.H., Kothary, R., 2021b. SMN Depleted Mice Offer a Robust and Rapid Onset Model of Nonalcoholic Fatty Liver Disease. *Cell. Mol. Gastroenterol. Hepatol.* 12, 354–377.e3.
<https://doi.org/10.1016/j.jcmgh.2021.01.019>
- Deymeer, F., Serdaroglu, P., Poda, M., Gulsen-Parman, Y., Ozcelik, T., Ozdemir, C., 1997. Segmental distribution of muscle weakness in SMA III: implications for deterioration in muscle strength with time. This work was presented at the New Challenges in Neuromuscular Disorders, 25–27 September 1996, London, UK. *Neuromuscul. Disord.* 7, 521–528.
<https://doi.org/10.1016/S0960->

- Di Donfrancesco, A., Berlingieri, C., Giacomello, M., Frascarelli, C., Magalhaes Rebelo, A.P., Bindoff, L.A., Reeve, S., Renbaum, P., Santorelli, F.M., Massaro, G., Viscomi, C., Zeviani, M., Ghezzi, D., Bottani, E., Brunetti, D., 2023. PPAR- γ agonist pioglitazone recovers mitochondrial quality control in fibroblasts from PITRM1-deficient patients. *Front. Pharmacol.* 14, 1220620. <https://doi.org/10.3389/fphar.2023.1220620>
- Farooq, F., Abadía-Molina, F., MacKenzie, D., Hadwen, J., Shamim, F., O'Reilly, S., Holcik, M., MacKenzie, A., 2013. Celecoxib increases SMN and survival in a severe spinal muscular atrophy mouse model via p38 pathway activation. *Hum. Mol. Genet.* 22, 3415–3424. <https://doi.org/10.1093/hmg/ddt191>
- Feng, Y., Cui, Y., Jin, J., Huang, S., Wei, J., Yao, M., Zhou, D., Mao, S., 2023. The Alterations of Gut Microbiome and Lipid Metabolism in Patients with Spinal Muscular Atrophy. *Neurol. Ther.* 12, 961–976. <https://doi.org/10.1007/s40120-023-00477-6>
- Fischer, T.W., Kleszczyński, K., Hardkop, L.H., Kruse, N., Zillikens, D., 2013. Melatonin enhances antioxidative enzyme gene expression (CAT, GPx, SOD), prevents their UVR-induced depletion, and protects against the formation of DNA damage (8-hydroxy-2'-deoxyguanosine) in ex vivo human skin. *J. Pineal Res.* 54, 303–312. <https://doi.org/10.1111/jpi.12018>
- Fischer, U., Liu, Q., Dreyfuss, G., 1997. The SMN-SIP1 complex has an essential role in spliceosomal snRNP biogenesis. *Cell* 90, 1023–1029. [https://doi.org/10.1016/s0092-8674\(00\)80368-2](https://doi.org/10.1016/s0092-8674(00)80368-2)
- Florini, J.R., Ewton, D.Z., Coolican, S.A., 1996. Growth hormone and the insulin-like growth factor system in myogenesis. *Endocr. Rev.* 17, 481–517. <https://doi.org/10.1210/edrv-17-5-481>
- Ford, E.S., Li, C., Zhao, G., Mokdad, A.H., 2009. Concentrations of Low-Density Lipoprotein Cholesterol and Total Cholesterol Among Children and Adolescents in the United States. *Circulation* 119, 1108–1115. <https://doi.org/10.1161/CIRCULATIONAHA.108.816769>
- Fridén, J., Lieber, R.L., 2001. Quantitative evaluation of the posterior deltoid to triceps tendon transfer based on muscle architectural properties. *J. Hand Surg.* 26, 147–155. <https://doi.org/10.1053/jhsu.2001.20161>
- Gabanella, F., Butchbach, M.E.R., Saieva, L., Carissimi, C., Burghes, A.H.M., Pellizzoni, L., 2007. Ribonucleoprotein assembly defects correlate with spinal muscular atrophy severity and preferentially affect a subset of spliceosomal snRNPs. *PloS One* 2, e921. <https://doi.org/10.1371/journal.pone.0000921>
- Ganassi, M., Badodi, S., Ortuste Quiroga, H.P., Zammit, P.S., Hinitz, Y., Hughes, S.M., 2018. Myogenin promotes myocyte fusion to balance fibre number and size. *Nat. Commun.* 9, 4232. <https://doi.org/10.1038/s41467-018-06583-6>
- Gao, C., Wang, A.-Y., 2009. Significance of Increased Apoptosis and Bax Expression in Human Small Intestinal Adenocarcinoma. *J. Histochem. Cytochem.* 57, 1139–1148. <https://doi.org/10.1369/jhc.2009.954446>
- Gastaldelli, A., Casolaro, A., Ciociaro, D., Frascerra, S., Nannipieri, M., Buzzigoli, E., Ferrannini, E., 2009. Decreased whole body lipolysis as a mechanism of the lipid-lowering effect of pioglitazone in type 2 diabetic patients. *Am. J. Physiol.- Endocrinol. Metab.* 297, E225–E230. <https://doi.org/10.1152/ajpendo.90960.2008>
- Girard, J.P., Lehtonen, H., Caizergues-Ferrer, M., Amalric, F., Tollervey, D., Lapeyre, B., 1992. GAR1 is an essential small nucleolar RNP protein

- required for pre-rRNA processing in yeast. *EMBO J.* 11, 673–682.
<https://doi.org/10.1002/j.1460-2075.1992.tb05099.x>
- Goodman, C.A., 2014. The role of mTORC1 in regulating protein synthesis and skeletal muscle mass in response to various mechanical stimuli. *Rev. Physiol. Biochem. Pharmacol.* 166, 43–95.
https://doi.org/10.1007/112_2013_17
- Greene, L.A., Tischler, A.S., 1976. Establishment of a noradrenergic clonal line of rat adrenal pheochromocytoma cells which respond to nerve growth factor. *Proc. Natl. Acad. Sci. U. S. A.* 73, 2424–2428.
<https://doi.org/10.1073/pnas.73.7.2424>
- Hahnen, E., Schönling, J., Rudnik-Schöneborn, S., Raschke, H., Zerres, K., Wirth, B., 1997. Missense Mutations in Exon 6 of the Survival Motor Neuron Gene in Patients with Spinal Muscular Atrophy (SMA). *Hum. Mol. Genet.* 6, 821–825. <https://doi.org/10.1093/hmg/6.5.821>
- Hamilton, G., Gillingwater, T.H., 2013. Spinal muscular atrophy: going beyond the motor neuron. *Trends Mol. Med.* 19, 40–50.
<https://doi.org/10.1016/j.molmed.2012.11.002>
- Han, H.-S., Kang, G., Kim, J.S., Choi, B.H., Koo, S.-H., 2016. Regulation of glucose metabolism from a liver-centric perspective. *Exp. Mol. Med.* 48, e218–e218. <https://doi.org/10.1038/emm.2015.122>
- Hardeland, R., Pandi-Perumal, S.R., Cardinali, D.P., 2006. Melatonin. *Int. J. Biochem. Cell Biol.* 38, 313–316. <https://doi.org/10.1016/j.biocel.2005.08.020>
- Hasty, P., Bradley, A., Morris, J.H., Edmondson, D.G., Venuti, J.M., Olson, E.N., Klein, W.H., 1993. Muscle deficiency and neonatal death in mice with a targeted mutation in the myogenin gene. *Nature* 364, 501–506. <https://doi.org/10.1038/364501a0>
- Holt, R.I.G., Simpson, H.L., Sönksen, P.H., 2003. The role of the growth hormone- insulin-like growth factor axis in glucose homeostasis. *Diabet. Med. J. Br. Diabet. Assoc.* 20, 3–15.
<https://doi.org/10.1046/j.1464-5491.2003.00827.x>
- Hong, Y., Tak, H., Kim, C., Kang, H., Ji, E., Ahn, S., Jung, M., Kim, H.L., Lee, J.-H., Kim, W., Lee, E.K., 2020. RNA binding protein HuD contributes to β -cell dysfunction by impairing mitochondria dynamics. *Cell Death Differ.* 27, 1633–1643. <https://doi.org/10.1038/s41418-019-0447-x>
- Hoolachan, J.M., McCallion, E., Sutton, E.R., Çetin, Ö., Pacheco-Torres, P., Dimitriadi, M., Sari, S., Miller, G.J., Okoh, M., Walter, L.M., Claus, P., Wood, M.J.A., Tonge, D.P., Bowerman, M., 2023a. A transcriptomics-based drug repositioning approach to identify drugs with similar activities for the treatment of muscle pathologies in spinal muscular atrophy (SMA) models. *Hum. Mol. Genet.* ddad192. <https://doi.org/10.1093/hmg/ddad192>
- Hoolachan, J.M., McCallion, E., Sutton, E.R., Çetin, Ö., Pacheco-Torres, P., Dimitriadi, M., Sari, S., Miller, G.J., Okoh, M., Walter, L.M., Claus, P., Wood, M.J.A., Tonge, D.P., Bowerman, M., 2023b. A transcriptomics-based drug repositioning approach to identify drugs with similar activities for the treatment of muscle pathologies in spinal muscular atrophy (SMA) models. *Hum. Mol. Genet.* ddad192. <https://doi.org/10.1093/hmg/ddad192>
- Hoolachan, J.M., Sutton, E.R., Bowerman, M., 2019. Teaching an old drug new tricks: repositioning strategies for spinal muscular atrophy. *Future Neurol.* 14, FNL25. <https://doi.org/10.2217/fnl-2019-0006>
- HOPCROFT, D.W., MASON, D.R., SCOTT, R.S., 1985. Structure-Function Relationships in Pancreatic Islets: Support for Intra-islet Modulation of Insulin Secretion*. *Endocrinology* 117, 2073–2080.
<https://doi.org/10.1210/endo-117->

- Horii, N., Hasegawa, N., Fujie, S., Uchida, M., Iemitsu, M., 2020. Resistance exercise- induced increase in muscle 5 α -dihydrotestosterone contributes to the activation of muscle Akt/mTOR/p70S6K- and Akt/AS160/GLUT4-signaling pathways in type 2 diabetic rats. *FASEB J. Off. Publ. Fed. Am. Soc. Exp. Biol.* 34, 11047– 11057.
<https://doi.org/10.1096/fj.201903223RR>
- Hosoyama, T., Nishijo, K., Prajapati, S.I., Li, G., Keller, C., 2011. Rb1 Gene Inactivation Expands Satellite Cell and Postnatal Myoblast Pools *. *J. Biol. Chem.* 286, 19556–19564. <https://doi.org/10.1074/jbc.M111.229542>
- Houdebine, L., D'Amico, D., Bastin, J., Chali, F., Desseille, C., Rumeau, V., Soukkari, J., Oudot, C., Rouquet, T., Bariohay, B., Roux, J., Sapaly, D., Weill, L., Lopes, P., Djouadi, F., Bezier, C., Charbonnier, F., Biondi, O., 2019. Low-Intensity Running and High-Intensity Swimming Exercises Differentially Improve Energy Metabolism in Mice With Mild Spinal Muscular Atrophy. *Front. Physiol.* 10, 1258. <https://doi.org/10.3389/fphys.2019.01258>
- Hsieh-Li, H.M., Chang, J.G., Jong, Y.J., Wu, M.H., Wang, N.M., Tsai, C.H., Li, H., 2000. A mouse model for spinal muscular atrophy. *Nat. Genet.* 24, 66–70. <https://doi.org/10.1038/71709>
- Hubers, L., Valderrama-Carvajal, H., Laframboise, J., Timbers, J., Sanchez, G., Côté, J., 2011. HuD interacts with survival motor neuron protein and can rescue spinal muscular atrophy-like neuronal defects. *Hum. Mol. Genet.* 20, 553–579. <https://doi.org/10.1093/hmg/ddq500>
- Insulin human [WWW Document], n.d. URL <https://go.drugbank.com/drugs/DB00030> (accessed 11.28.23).
- Iyer, C.C., McGovern, V.L., Wise, D.O., Glass, D.J., Burghes, A.H.M., 2014. Deletion of atrophy enhancing genes fails to ameliorate the phenotype in a mouse model of spinal muscular atrophy. *Neuromuscul. Disord.* 24, 436–444. <https://doi.org/10.1016/j.nmd.2014.02.007>
- Jablonka, S., Schrank, B., Kralewski, M., Rossoll, W., Sendtner, M., 2000. Reduced survival motor neuron (Snm) gene dose in mice leads to motor neuron degeneration: an animal model for spinal muscular atrophy type III. *Hum. Mol. Genet.* 9, 341–346. <https://doi.org/10.1093/hmg/9.3.341>
- James, R., Chaytow, H., Ledahawsky, L.M., Gillingwater, T.H., 2021. Revisiting the role of mitochondria in spinal muscular atrophy. *Cell. Mol. Life Sci. CMLS* 78, 4785–4804. <https://doi.org/10.1007/s00018-021-03819-5>
- Jang, Y.-N., 2013. JAK-STAT pathway and myogenic differentiation. *JAK-STAT* 2, e23282. <https://doi.org/10.4161/jkst.23282>
- Jespersen, N.Z., Larsen, T.J., Peijs, L., Daugaard, S., Homøe, P., Loft, A., de Jong, J., Mathur, N., Cannon, B., Nedergaard, J., Pedersen, B.K., Møller, K., Scheele, C., 2013. A Classical Brown Adipose Tissue mRNA Signature Partly Overlaps with Brite in the Supraclavicular Region of Adult Humans. *Cell Metab.* 17, 798–805. <https://doi.org/10.1016/j.cmet.2013.04.011>
- Jonckheere, A.I., Smeitink, J.A.M., Rodenburg, R.J.T., 2012. Mitochondrial ATP synthase: architecture, function and pathology. *J. Inherit. Metab. Dis.* 35, 211–225. <https://doi.org/10.1007/s10545-011-9382-9>
- Justice, M.J., Dhillon, P., 2016. Using the mouse to model human disease: increasing validity and reproducibility. *Dis. Model. Mech.* 9, 101–103. <https://doi.org/10.1242/dmm.024547>
- Kambach, C., Walke, S., Young, R., Avis, J.M., Fortelle, E. de la, Raker, V.A., Lührmann, R., Li, J., Nagai, K., 1999. Crystal Structures of Two Sm Protein Complexes and Their Implications for the Assembly of the

- Spliceosomal snRNPs. *Cell* 96, 375–387. [https://doi.org/10.1016/S0092-8674\(00\)80550-4](https://doi.org/10.1016/S0092-8674(00)80550-4)
- Keller, N., Paketci, C., Altmueller, J., Fuhrmann, N., Wunderlich, G., Schrank, B., Unver, O., Yilmaz, S., Boostani, R., Karimiani, E.G., Motameny, S., Thiele, H., Nürnberg, P., Maroofian, R., Yis, U., Wirth, B., Karakaya, M., 2021. Genomic variants causing mitochondrial dysfunction are common in hereditary lower motor neuron disease. *Hum. Mutat.* 42, 460–472. <https://doi.org/10.1002/humu.24181>
- Kim, C.H., Kim, K.H., Yoo, Y.-M., 2011. Melatonin protects against apoptotic and autophagic cell death in C2C12 murine myoblast cells. *J. Pineal Res.* 50, 241–249. <https://doi.org/10.1111/j.1600-079X.2010.00833.x>
- Kim, J.-K., Jha, N.N., Feng, Z., Faleiro, M.R., Chiriboga, C.A., Wei-Lapierre, L., Dirksen, R.T., Ko, C.-P., Monani, U.R., 2020. Muscle-specific SMN reduction reveals motor neuron-independent disease in spinal muscular atrophy models. *J. Clin. Invest.* 130, 1271–1287. <https://doi.org/10.1172/JCI131989>
- Kim, T.W., Jeong, J.-H., Hong, S.-C., 2015. The impact of sleep and circadian disturbance on hormones and metabolism. *Int. J. Endocrinol.* 2015, 591729. <https://doi.org/10.1155/2015/591729>
- Kolb, S.J., Battle, D.J., Dreyfuss, G., 2007. Molecular Functions of the SMN Complex. *J. Child Neurol.* 22, 990–994. <https://doi.org/10.1177/0883073807305666>
- Kong, P.-J., Byun, J.-S., Lim, S.-Y., Lee, J.-J., Hong, S.-J., Kwon, K.-J., Kim, S.-S., 2008. Melatonin Induces Akt Phosphorylation through Melatonin Receptor- and PI3K-Dependent Pathways in Primary Astrocytes. *Korean J. Physiol. Pharmacol.* 12, 37–41. <https://doi.org/10.4196/kjpp.2008.12.2.37>
- Kosmalksi, M., Ziółkowska, S., Czarny, P., Szemraj, J., Pietras, T., 2022. The Coexistence of Nonalcoholic Fatty Liver Disease and Type 2 Diabetes Mellitus. *J. Clin. Med.* 11, 1375. <https://doi.org/10.3390/jcm11051375>
- Kröger, S., Pfister, H., 2009. Agrin in the nervous system: synaptogenesis and beyond. *Future Neurol.* 4, 67–86. <https://doi.org/10.2217/14796708.4.1.67>
- Lee, D., Goldberg, A.L., 2013. SIRT1 Protein, by Blocking the Activities of Transcription Factors FoxO1 and FoxO3, Inhibits Muscle Atrophy and Promotes Muscle Growth *. *J. Biol. Chem.* 288, 30515–30526. <https://doi.org/10.1074/jbc.M113.489716>
- Lee, E.Y., Sakurai, K., Zhang, X., Toda, C., Tanaka, T., Jiang, M., Shirasawa, T., Tachibana, K., Yokote, K., Vidal-Puig, A., Minokoshi, Y., Miki, T., 2015. Unsuppressed lipolysis in adipocytes is linked with enhanced gluconeogenesis and altered bile acid physiology in *InsrP1195L/+* mice fed high-fat-diet. *Sci. Rep.* 5, 17565. <https://doi.org/10.1038/srep17565>
- Lefebvre, S., Bürglen, L., Reboullet, S., Clermont, O., Burlet, P., Viollet, L., Benichou, B., Cruaud, C., Millasseau, P., Zeviani, M., Le Paslier, D., Frézal, J., Cohen, D., Weissenbach, J., Munnich, A., Melki, J., 1995. Identification and characterization of a spinal muscular atrophy-determining gene. *Cell* 80, 155–165. [https://doi.org/10.1016/0092-8674\(95\)90460-3](https://doi.org/10.1016/0092-8674(95)90460-3)
- Lefebvre, S., Burlet, P., Liu, Q., Bertrand, S., Clermont, O., Munnich, A., Dreyfuss, G., Melki, J., 1997. Correlation between severity and SMN protein level in spinal muscular atrophy. *Nat. Genet.* 16, 265–269. <https://doi.org/10.1038/ng0797-265>

- Lelli, S.M., Mazzetti, M.B., San Martín de Viale, L.C., 2016. Melatonin modulates drug-induced acute porphyria. *Toxicol. Rep.* 3, 141–147. <https://doi.org/10.1016/j.toxrep.2015.12.010>
- Liu, Q., Fischer, U., Wang, F., Dreyfuss, G., 1997. The spinal muscular atrophy disease gene product, SMN, and its associated protein SIP1 are in a complex with spliceosomal snRNP proteins. *Cell* 90, 1013–1021. [https://doi.org/10.1016/s0092-8674\(00\)80367-0](https://doi.org/10.1016/s0092-8674(00)80367-0)
- Lorson, C.L., Androphy, E.J., 1998. The domain encoded by exon 2 of the survival motor neuron protein mediates nucleic acid binding. *Hum. Mol. Genet.* 7, 1269–1275. <https://doi.org/10.1093/hmg/7.8.1269>
- Mardilovich, K., Pankratz, S.L., Shaw, L.M., 2009. Expression and function of the insulin receptor substrate proteins in cancer. *Cell Commun. Signal. CCS* 7, 14. <https://doi.org/10.1186/1478-811X-7-14>
- Martin, L.J., Chen, K., Liu, Z., 2005. Adult Motor Neuron Apoptosis Is Mediated by Nitric Oxide and Fas Death Receptor Linked by DNA Damage and p53 Activation. *J. Neurosci.* 25, 6449–6459. <https://doi.org/10.1523/JNEUROSCI.0911-05.2005>
- Martínez-Hernández, R., Bernal, S., Alias, L., Tizzano, E.F., 2014. Abnormalities in early markers of muscle involvement support a delay in myogenesis in spinal muscular atrophy. *J. Neuropathol. Exp. Neurol.* 73, 559–567. <https://doi.org/10.1097/NEN.0000000000000078>
- Massenet, S., Pellizzoni, L., Paushkin, S., Mattaj, I.W., Dreyfuss, G., 2002. The SMN Complex Is Associated with snRNPs throughout Their Cytoplasmic Assembly Pathway. *Mol. Cell. Biol.* 22, 6533–6541. <https://doi.org/10.1128/MCB.22.18.6533-6541.2002>
- Mastroiannopoulos, N.P., Nicolaou, P., Anayasa, M., Uney, J.B., Phylactou, L.A., 2012. Down-Regulation of Myogenin Can Reverse Terminal Muscle Cell Differentiation. *PLoS ONE* 7, e29896. <https://doi.org/10.1371/journal.pone.0029896>
- McElhinny, A.S., Kakinuma, K., Sorimachi, H., Labeit, S., Gregorio, C.C., 2002. Muscle-specific RING finger-1 interacts with titin to regulate sarcomeric M-line and thick filament structure and may have nuclear functions via its interaction with glucocorticoid modulatory element binding protein-1. *J. Cell Biol.* 157, 125–136. <https://doi.org/10.1083/jcb.200108089>
- McTigue, D.M., Tripathi, R., Wei, P., Lash, A.T., 2007. The PPAR gamma agonist Pioglitazone improves anatomical and locomotor recovery after rodent spinal cord injury. *Exp. Neurol.* 205, 396–406. <https://doi.org/10.1016/j.expneurol.2007.02.009>
- Meijboom, K.E., Sutton, E.R., McCallion, E., McFall, E., Anthony, D., Edwards, B., Kubinski, S., Tapken, I., Bünermann, I., Hazell, G., Ahlskog, N., Claus, P., Davies, K.E., Kothary, R., Wood, M.J.A., Bowerman, M., 2022. Dysregulation of Tweak and Fn14 in skeletal muscle of spinal muscular atrophy mice. *Skelet. Muscle* 12, 18. <https://doi.org/10.1186/s13395-022-00301-z>
- Melhuish Beaupre, L.M., Brown, G.M., Gonçalves, V.F., Kennedy, J.L., 2021. Melatonin's neuroprotective role in mitochondria and its potential as a biomarker in aging, cognition and psychiatric disorders. *Transl. Psychiatry* 11, 1–10. <https://doi.org/10.1038/s41398-021-01464-x>
- Memme, J.M., Erlich, A.T., Phukan, G., Hood, D.A., 2021. Exercise and mitochondrial health. *J. Physiol.* 599, 803–817. <https://doi.org/10.1113/JP278853>
- Menu, E., Kooijman, R., Valckenborgh, E.V., Asosingh, K., Bakkus, M., Camp, B.V., Vanderkerken, K., 2004. Specific roles for the PI3K and the MEK–ERK pathway in IGF-1-stimulated chemotaxis, VEGF secretion and

- proliferation of multiple myeloma cells: study in the 5T33MM model. *Br. J. Cancer* 90, 1076–1083. <https://doi.org/10.1038/sj.bjc.6601613>
- Millino, C., Fanin, M., Vettori, A., Laveder, P., Mostacciolo, M.L., Angelini, C., Lanfranchi, G., 2009a. Different atrophy-hypertrophy transcription pathways in muscles affected by severe and mild spinal muscular atrophy. *BMC Med.* 7, 14. <https://doi.org/10.1186/1741-7015-7-14>
- Minokoshi, Y., Toda, C., Okamoto, S., 2012. Regulatory role of leptin in glucose and lipid metabolism in skeletal muscle. *Indian J. Endocrinol. Metab.* 16, S562. <https://doi.org/10.4103/2230-8210.105573>
- Monani, U.R., 2005. Spinal Muscular Atrophy: A Deficiency in a Ubiquitous Protein; a Motor Neuron-Specific Disease. *Neuron* 48, 885–895. <https://doi.org/10.1016/j.neuron.2005.12.001>
- Monani, U.R., Sendtner, M., Coover, D.D., Parsons, D.W., Andreassi, C., Le, T.T., Jablonka, S., Schrank, B., Rossoll, W., Prior, T.W., Morris, G.E., Burghes, A.H., 2000. The human centromeric survival motor neuron gene (SMN2) rescues embryonic lethality in *Smn(-/-)* mice and results in a mouse with spinal muscular atrophy. *Hum. Mol. Genet.* 9, 333–339. <https://doi.org/10.1093/hmg/9.3.333>
- Muramatsu, H., Kuramochi, T., Katada, H., Ueyama, A., Ruike, Y., Ohmine, K., Shida-Kawazoe, M., Miyano-Nishizawa, R., Shimizu, Y., Okuda, M., Hori, Y., Hayashi, M., Haraya, K., Ban, N., Nonaka, T., Honda, M., Kitamura, H., Hattori, K., Kitazawa, T., Igawa, T., Kawabe, Y., Nezu, J., 2021. Novel myostatin-specific antibody enhances muscle strength in muscle disease models. *Sci. Rep.* 11, 2160. <https://doi.org/10.1038/s41598-021-81669-8>
- Murdocca, M., Malgieri, A., Luchetti, A., Saieva, L., Dobrowolny, G., de Leonibus, E., Filareto, A., Quitadamo, M.C., Novelli, G., Musarò, A., Sanguolo, F., 2012. IPLEX administration improves motor neuron survival and ameliorates motor functions in a severe mouse model of spinal muscular atrophy. *Mol. Med. Camb. Mass* 18, 1076–1085. <https://doi.org/10.2119/molmed.2012.00056>
- Murray, L.M., Beauvais, A., Gibeault, S., Courtney, N.L., Kothary, R., 2015a. Transcriptional profiling of differentially vulnerable motor neurons at pre-symptomatic stage in the *Smn2b(-)*-mouse model of spinal muscular atrophy. *Acta Neuropathol. Commun.* 3, 55. <https://doi.org/10.1186/s40478-015-0231-1>
- Nakrani, M.N., Wineland, R.H., Anjum, F., 2023. Physiology, Glucose Metabolism, in: *StatPearls*. StatPearls Publishing, Treasure Island (FL).
- Narayanan, U., Ospina, J.K., Frey, M.R., Hebert, M.D., Matera, A.G., 2002. SMN, the spinal muscular atrophy protein, forms a pre-import snRNP complex with snurportin1 and importin beta. *Hum. Mol. Genet.* 11, 1785–1795. <https://doi.org/10.1093/hmg/11.15.1785>
- Ng, S.Y., Mikhail, A., Ljubicic, V., 2019. Mechanisms of exercise-induced survival motor neuron expression in the skeletal muscle of spinal muscular atrophy-like mice. *J. Physiol.* 597, 4757–4778. <https://doi.org/10.1113/JP278454>
- Norris, A.W., Chen, L., Fisher, S.J., Szanto, I., Ristow, M., Jozsi, A.C., Hirshman, M.F., Rosen, E.D., Goodyear, L.J., Gonzalez, F.J., Spiegelman, B.M., Kahn, C.R., 2003. Muscle-specific PPARgamma-deficient mice develop increased adiposity and insulin resistance but respond to thiazolidinediones. *J. Clin. Invest.* 112, 608–618. <https://doi.org/10.1172/JCI17305>

- O'Connor, G., Edel, L., Raquq, S., Bowerman, M., Szmurlo, A., Simpson, Z., Hardy, I., Fewtrell, M., Baranello, G., 2023. Open-labelled study to monitor the effect of an amino acid formula on symptom management in children with spinal muscular atrophy type I: The SMAAF pilot study. *Nutr. Clin. Pract. Off. Publ. Am. Soc. Parenter. Enter. Nutr.* 38, 871–880. <https://doi.org/10.1002/ncp.10940>
- Ogawa, C., Usui, K., Ito, F., Itoh, M., Hayashizaki, Y., Suzuki, H., 2009. Role of survival motor neuron complex components in small nuclear ribonucleoprotein assembly. *J. Biol. Chem.* 284, 14609–14617. <https://doi.org/10.1074/jbc.M809031200>
- Ogbonmide, T., Rathore, R., Rangrej, S.B., Hutchinson, S., Lewis, M., Ojilere, S., Carvalho, V., Kelly, I., n.d. Gene Therapy for Spinal Muscular Atrophy (SMA): A Review of Current Challenges and Safety Considerations for Onasemnogene Asepargovec (Zolgensma). *Cureus* 15, e36197. <https://doi.org/10.7759/cureus.36197>
- Ohtaki, E., 1990. Secondarily reduced cytochrome c oxidase activity in various neuromuscular disorders. *Brain Dev.* 12, 326–333. [https://doi.org/10.1016/s0387-7604\(12\)80315-9](https://doi.org/10.1016/s0387-7604(12)80315-9)
- O'Neill, B.T., Lauritzen, H.P.M.M., Hirshman, M.F., Smyth, G., Goodyear, L.J., Kahn, C.R., 2015. Differential Role of Insulin/IGF-1 Receptor Signaling in Muscle Growth and Glucose Homeostasis. *Cell Rep.* 11, 1220–1235. <https://doi.org/10.1016/j.celrep.2015.04.037>
- Orasanu, G., Ziouzenkova, O., Devchand, P.R., Nehra, V., Hamdy, O., Horton, E.S., Plutzky, J., 2008. The PPAR γ Agonist Pioglitazone Represses Inflammation In A PPAR α -Dependent Manner In Vitro and In Vivo In Mice. *J. Am. Coll. Cardiol.* 52, 869–881. <https://doi.org/10.1016/j.jacc.2008.04.055>
- Ottesen, E.W., 2017. ISS-N1 makes the First FDA-approved Drug for Spinal Muscular Atrophy. *Transl. Neurosci.* 8, 1–6. <https://doi.org/10.1515/tnsci-2017-0001>
- Ou, T.-H., Tung, Y.-T., Yang, T.-H., Chien, Y.-W., 2019. Melatonin Improves Fatty Liver Syndrome by Inhibiting the Lipogenesis Pathway in Hamsters with High-Fat Diet-Induced Hyperlipidemia. *Nutrients* 11, 748. <https://doi.org/10.3390/nu11040748>
- Palladino, A., Passamano, L., Taglia, A., D'Ambrosio, P., Scutifero, M., Rosaria Cecio, M., Picillo, E., Viggiano, E., Torre, V., De Luca, F., Nigro, G., Politano, L., 2011. Cardiac involvement in patients with Spinal Muscular Atrophies. *Acta Myol.* 30, 175–178.
- Papadimitriou, D., Le Verche, V., Jacquier, A., Ikiz, B., Przedborski, S., Re, D.B., 2010. Inflammation in ALS and SMA: sorting out the good from the evil. *Neurobiol. Dis.* 37, 493–502. <https://doi.org/10.1016/j.nbd.2009.10.005>
- Pasmans, K., Adriaens, M.E., Olinga, P., Langen, R., Rensen, S.S., Schaap, F.G., Olde Damink, S.W.M., Caiment, F., van Loon, L.J.C., Blaak, E.E., Meex, R.C.R., 2021. Hepatic Steatosis Contributes to the Development of Muscle Atrophy via Inter-Organ Crosstalk. *Front. Endocrinol.* 12.
- Passini, M.A., Bu, J., Richards, A.M., Kinnecom, C., Sardi, S.P., Stanek, L.M., Hua, Y., Rigo, F., Matson, J., Hung, G., Kaye, E.M., Shihabuddin, L.S., Krainer, A.R., Bennett, C.F., Cheng, S.H., 2011. Antisense oligonucleotides delivered to the mouse CNS ameliorate symptoms of severe spinal muscular atrophy. *Sci. Transl. Med.* 3, 72ra18. <https://doi.org/10.1126/scitranslmed.3001777>
- Patitucci, T.N., Ebert, A.D., 2016. SMN deficiency does not induce oxidative stress in

- SMA iPSC-derived astrocytes or motor neurons. *Hum. Mol. Genet.* 25, 514–523. <https://doi.org/10.1093/hmg/ddv489>
- Pellizzoni, L., 2007. Chaperoning ribonucleoprotein biogenesis in health and disease. *EMBO Rep.* 8, 340–345. <https://doi.org/10.1038/sj.embor.7400941>
- Pellizzoni, L., Charroux, B., Rappsilber, J., Mann, M., Dreyfuss, G., 2001. A functional interaction between the survival motor neuron complex and RNA polymerase II. *J. Cell Biol.* 152, 75–85. <https://doi.org/10.1083/jcb.152.1.75>
- Pellizzoni, L., Yong, J., Dreyfuss, G., 2002. Essential role for the SMN complex in the specificity of snRNP assembly. *Science* 298, 1775–1779. <https://doi.org/10.1126/science.1074962>
- Pera, M.C., Romeo, D.M., Graziano, A., Palermo, C., Messina, S., Baranello, G., Coratti, G., Massaro, M., Sivo, S., Arnoldi, M.T., Mazzone, E.S., Antonaci, L., Lapenta, L., Albamonte, E., Fanelli, L., de Sanctis, R., Vita, G.L., Sframeli, M., Pane, M., Mercuri, E., 2017. Sleep disorders in spinal muscular atrophy. *Sleep Med.* 30, 160–163. <https://doi.org/10.1016/j.sleep.2016.11.012>
- Pérez, M.J., Quintanilla, R.A., 2017. Development or disease: duality of the mitochondrial permeability transition pore. *Dev. Biol.* 426, 1–7. <https://doi.org/10.1016/j.ydbio.2017.04.018>
- Perlman, R.L., 2016. Mouse models of human disease: An evolutionary perspective. *Evol. Med. Public Health* 2016, 170–176. <https://doi.org/10.1093/emph/eow014>
- Pickel, L., Sung, H.-K., 2020. Feeding Rhythms and the Circadian Regulation of Metabolism. *Front. Nutr.* 7, 39. <https://doi.org/10.3389/fnut.2020.00039>
- Plessel, G., Lührmann, R., Kastner, B., 1997. Electron microscopy of assembly intermediates of the snRNP core: morphological similarities between the RNA-free (E.F.G) protein heteromer and the intact snRNP core1 Edited by A. Klug. *J. Mol. Biol.* 265, 87–94. <https://doi.org/10.1006/jmbi.1996.0713>
- Pons, R., Andreatta, F., Wang, C.H., Vu, T.H., Bonilla, E., DiMauro, S., De Vivo, D.C., 1996. Mitochondrial myopathy simulating spinal muscular atrophy. *Pediatr. Neurol.* 15, 153–158. [https://doi.org/10.1016/0887-8994\(96\)00118-x](https://doi.org/10.1016/0887-8994(96)00118-x)
- Pourhanifeh, M.H., Hosseinzadeh, A., Dehdashtian, E., Hemati, K., Mehrzadi, S., 2020. Melatonin: new insights on its therapeutic properties in diabetic complications. *Diabetol. Metab. Syndr.* 12, 30. <https://doi.org/10.1186/s13098-020-00537-z>
- Puig, O., Marr, M.T., Ruhf, M.L., Tjian, R., 2003. Control of cell number by *Drosophila* FOXO: downstream and feedback regulation of the insulin receptor pathway. *Genes Dev.* 17, 2006–2020. <https://doi.org/10.1101/gad.1098703>
- Pun, S., Sigrist, M., Santos, A.F., Ruegg, M.A., Sanes, J.R., Jessell, T.M., Arber, S., Caroni, P., 2002. An intrinsic distinction in neuromuscular junction assembly and maintenance in different skeletal muscles. *Neuron* 34, 357–370. [https://doi.org/10.1016/s0896-6273\(02\)00670-0](https://doi.org/10.1016/s0896-6273(02)00670-0)
- Putman, C.T., Xu, X., Gillies, E., MacLean, I.M., Bell, G.J., 2004. Effects of strength, endurance and combined training on myosin heavy chain content and fibre-type distribution in humans. *Eur. J. Appl. Physiol.* 92, 376–384. <https://doi.org/10.1007/s00421-004-1104-7>
- Rajendra, T.K., Gonsalvez, G.B., Walker, M.P., Shpargel, K.B., Salz, H.K., Matera, A.G., 2007. A *Drosophila melanogaster* model of spinal muscular atrophy reveals a function for SMN in striated muscle. *J. Cell Biol.* 176,

- 831–841. <https://doi.org/10.1083/jcb.200610053>
- Ramis, M.R., Esteban, S., Miralles, A., Tan, D.-X., Reiter, R.J., 2015. Protective Effects of Melatonin and Mitochondria-targeted Antioxidants Against Oxidative Stress: A Review. *Curr. Med. Chem.* 22, 2690–2711. <https://doi.org/10.2174/0929867322666150619104143>
- Richter, E.A., Hargreaves, M., 2013. Exercise, GLUT4, and Skeletal Muscle Glucose Uptake. *Physiol. Rev.* 93, 993–1017. <https://doi.org/10.1152/physrev.00038.2012>
- Ripolone, M., Ronchi, D., Violano, R., Vallejo, D., Fagiolari, G., Barca, E., Lucchini, V., Colombo, I., Villa, L., Berardinelli, A., Balottin, U., Morandi, L., Mora, M., Bordoni, A., Fortunato, F., Corti, S., Parisi, D., Toscano, A., Sciacco, M., DiMauro, S., Comi, G.P., Moggio, M., 2015a. Impaired Muscle Mitochondrial Biogenesis and Myogenesis in Spinal Muscular Atrophy. *JAMA Neurol.* 72, 666–675. <https://doi.org/10.1001/jamaneurol.2015.0178>
- Ripolone, M., Ronchi, D., Violano, R., Vallejo, D., Fagiolari, G., Barca, E., Lucchini, V., Colombo, I., Villa, L., Berardinelli, A., Balottin, U., Morandi, L., Mora, M., Bordoni, A., Fortunato, F., Corti, S., Parisi, D., Toscano, A., Sciacco, M., DiMauro, S., Comi, G.P., Moggio, M., 2015b. Impaired Muscle Mitochondrial Biogenesis and Myogenesis in Spinal Muscular Atrophy. *JAMA Neurol.* 72, 666–675. <https://doi.org/10.1001/jamaneurol.2015.0178>
- Risson, V., Mazelin, L., Roceri, M., Sanchez, H., Moncollin, V., Corneloup, C., Richard-Bulteau, H., Vignaud, A., Baas, D., Defour, A., Freyssenet, D., Tanti, J.-F., Le-Marchand-Brustel, Y., Ferrier, B., Conjard-Duplany, A., Romanino, K., Bauché, S., Hantäi, D., Mueller, M., Kozma, S.C., Thomas, G., Rüegg, M.A., Ferry, A., Pende, M., Bigard, X., Koulmann, N., Schaeffer, L., Gangloff, Y.-G., 2009. Muscle inactivation of mTOR causes metabolic and dystrophin defects leading to severe myopathy. *J. Cell Biol.* 187, 859–874. <https://doi.org/10.1083/jcb.200903131>
- Samanta, S., 2022. Physiological and pharmacological perspectives of melatonin. *Arch. Physiol. Biochem.* 128, 1346–1367. <https://doi.org/10.1080/13813455.2020.1770799>
- Sato, K., Meng, F., Francis, H., Wu, N., Chen, L., Kennedy, L., Zhou, T., Franchitto, A., Onori, P., Gaudio, E., Glaser, S., Alpini, G., 2020. Melatonin and circadian rhythms in liver diseases: Functional roles and potential therapies. *J. Pineal Res.* 68, e12639. <https://doi.org/10.1111/jpi.12639>
- Saukkonen, T., Shojaee-Moradie, F., Williams, R.M., Amin, R., Yuen, K.C., Watts, A., Acerini, C.L., Umpleby, A.M., Dunger, D.B., 2006. Effects of Recombinant Human IGF-I/IGF-Binding Protein-3 Complex on Glucose and Glycerol Metabolism in Type 1 Diabetes. *Diabetes* 55, 2365–2370. <https://doi.org/10.2337/db05-1646>
- Schiaffino, S., Rossi, A.C., Smerdu, V., Leinwand, L.A., Reggiani, C., 2015. Developmental myosins: expression patterns and functional significance. *Skelet. Muscle* 5, 22. <https://doi.org/10.1186/s13395-015-0046-6>
- Seo, J., Singh, N.N., Ottesen, E.W., Sivanesan, S., Shishimorova, M., Singh, R.N., 2016. Oxidative Stress Triggers Body-Wide Skipping of Multiple Exons of the Spinal Muscular Atrophy Gene. *PLOS ONE* 11, e0154390. <https://doi.org/10.1371/journal.pone.0154390>
- Shababi, M., Habibi, J., Ma, L., Glascock, J.J., Sowers, J.R., Lorson, C.L., 2012. Partial restoration of cardio-vascular defects in a rescued severe model of spinal muscular atrophy. *J. Mol. Cell. Cardiol.* 52, 1074–1082.

- <https://doi.org/10.1016/j.yjmcc.2012.01.005>
- Shahid, S.M., Nawab, S.N., Shaikh, R., Mahboob, T., 2012. Glycemic control, dyslipidemia and endothelial dysfunction in coexisted diabetes, hypertension and nephropathy. *Pak J Pharm Sci.*
- Shang, W., Yang, Y., Zhou, L., Jiang, B., Jin, H., Chen, M., 2008. Ginsenoside Rb1 stimulates glucose uptake through insulin-like signaling pathway in 3T3-L1 adipocytes. *J. Endocrinol.* 198, 561–569.
<https://doi.org/10.1677/JOE-08-0104>
- She, M., Deng, X., Guo, Z., Laudon, M., Hu, Z., Liao, D., Hu, X., Luo, Y., Shen, Q., Su, Z., Yin, W., 2009. NEU-P11, a novel melatonin agonist, inhibits weight gain and improves insulin sensitivity in high-fat/high-sucrose-fed rats. *Pharmacol. Res.* 59, 248–253. <https://doi.org/10.1016/j.phrs.2009.01.005>
- Singh, G., Can, A.S., Correa, R., 2023. Pioglitazone, in: StatPearls. StatPearls Publishing, Treasure Island (FL).
- Sintusek, P., Catapano, F., Angkathunkayul, N., Marrosu, E., Parson, S.H., Morgan, J.E., Muntoni, F., Zhou, H., 2016. Histopathological Defects in Intestine in Severe Spinal Muscular Atrophy Mice Are Improved by Systemic Antisense Oligonucleotide Treatment. *PLoS ONE* 11, e0155032. <https://doi.org/10.1371/journal.pone.0155032>
- Sproule, D.M., Montes, J., Montgomery, M., Battista, V., Koenigsberger, D., Shen, W., Punyanitya, M., De Vivo, D.C., Kaufmann, P., 2009. Increased fat mass and high incidence of overweight despite low body mass index in patients with Spinal Muscular Atrophy. *Neuromuscul. Disord.* 19, 391–396. <https://doi.org/10.1016/j.nmd.2009.03.009>
- SRK-015 - Therapy for Spinal Muscular Atrophy (SMA) [WWW Document], n.d. . Sch. Rock. URL <https://scholarrock.com/our-pipeline/spinal-muscular-atrophy/> (accessed 9.7.23).
- Suetterlin, K.J., Männikkö, R., Matthews, E., Greensmith, L., Hanna, M.G., Bostock, H., Tan, S.V., 2022. Excitability properties of mouse and human skeletal muscle fibres compared by muscle velocity recovery cycles. *Neuromuscul. Disord.* 32, 347–357.
<https://doi.org/10.1016/j.nmd.2022.02.011>
- Suliman, H.B., Piantadosi, C.A., 2014. Mitochondrial Biogenesis: Regulation By Endogenous Gases during Inflammation and Organ Stress. *Curr. Pharm. Des.* 20, 5653–5662.
- Talbot, J., Maves, L., 2016. Skeletal muscle fiber type: using insights from muscle developmental biology to dissect targets for susceptibility and resistance to muscle disease. *Wiley Interdiscip. Rev. Dev. Biol.* 5, 518–534.
<https://doi.org/10.1002/wdev.230>
- Tordjman, S., Chokron, S., Delorme, R., Charrier, A., Bellissant, E., Jaafari, N., Fougere, C., 2017. Melatonin: Pharmacology, Functions and Therapeutic Benefits. *Curr. Neuropharmacol.* 15, 434–443.
<https://doi.org/10.2174/1570159X14666161228122115>
- Tseng, Y.-T., Chen, C.-S., Jong, Y.-J., Chang, F.-R., Lo, Y.-C., 2016. Loganiin possesses neuroprotective properties, restores SMN protein and activates protein synthesis positive regulator Akt/mTOR in experimental models of spinal muscular atrophy. *Pharmacol. Res.* 111, 58–75.
<https://doi.org/10.1016/j.phrs.2016.05.023>
- Turcotte, L.P., Fisher, J.S., 2008. Skeletal Muscle Insulin Resistance: Roles of Fatty Acid Metabolism and Exercise. *Phys. Ther.* 88, 1279–1296.
<https://doi.org/10.2522/ptj.20080018>
- Tyc, K., Steitz, J.A., 1989. U3, U8 and U13 comprise a new class of mammalian snRNPs localized in the cell nucleolus. *EMBO J.* 8,

- 3113–3119. <https://doi.org/10.1002/j.1460-2075.1989.tb08463.x>
- Update on Genentech/Roche Initiation of MANATEE Clinical Study - Cure SMA, n.d. . <https://www.curesma.org/>. URL <https://www.curesma.org/update-on-genentech-roche-initiation-of-manatee-clinical-study/> (accessed 12.6.23).
- Ussar, S., Lee, K.Y., Dankel, S.N., Boucher, J., Haering, M.-F., Kleinridders, A., Thomou, T., Xue, R., Macotella, Y., Cypess, A.M., Tseng, Y.-H., Mellgren, G., Kahn, C.R., 2014. Asc-1, PAT2 and P2RX5 are novel cell surface markers for white, beige and brown adipocytes. *Sci. Transl. Med.* 6, 247ra103. <https://doi.org/10.1126/scitranslmed.3008490>
- Valerio, A., D'Antona, G., Nisoli, E., 2011. Branched-chain amino acids, mitochondrial biogenesis, and healthspan: an evolutionary perspective. *Aging* 3, 464–478.
- Vandenbon, A., Nakai, K., 2010. Modeling tissue-specific structural patterns in human and mouse promoters. *Nucleic Acids Res.* 38, 17–25. <https://doi.org/10.1093/nar/gkp866>
- Verrillo, E., Bruni, O., Pavone, M., Ferri, R., Caldarelli, V., Novelli, L., Testa, M.B.C., Cutrera, R., 2014. Sleep architecture in infants with spinal muscular atrophy type 1. *Sleep Med.* 15, 1246–1250. <https://doi.org/10.1016/j.sleep.2014.05.029>
- Waisman, A., Norris, A.M., Elías Costa, M., Kopinke, D., 2021. Automatic and unbiased segmentation and quantification of myofibers in skeletal muscle. *Sci. Rep.* 11, 11793. <https://doi.org/10.1038/s41598-021-91191-6>
- Walker, M.P., Rajendra, T.K., Saieva, L., Fuentes, J.L., Pellizzoni, L., Matera, A.G., 2008. SMN complex localizes to the sarcomeric Z-disc and is a proteolytic target of calpain. *Hum. Mol. Genet.* 17, 3399–3410. <https://doi.org/10.1093/hmg/ddn234>
- Walter, Lisa M., Deguise, M.-O., Meijboom, K.E., Betts, C.A., Ahlskog, N., Westering, T.L.E. van, Hazell, G., McFall, E., Kordala, A., Hammond, S.M., Abendroth, F., Murray, L.M., Shorrock, H.K., Prosdocimo, D.A., Haldar, S.M., Jain, M.K., Gillingwater, T.H., Claus, P., Kothary, R., Wood, M.J.A., Bowerman, M., 2018. Interventions Targeting Glucocorticoid-Krüppel-like Factor 15-Branched-Chain Amino Acid Signaling Improve Disease Phenotypes in Spinal Muscular Atrophy Mice. *eBioMedicine* 31, 226–242. <https://doi.org/10.1016/j.ebiom.2018.04.024>
- Walter, Lisa M, Koch, C.E., Betts, C.A., Ahlskog, N., Meijboom, K.E., van Westering, T.L.E., Hazell, G., Bhomra, A., Claus, P., Oster, H., Wood, M.J.A., Bowerman, M., 2018. Light modulation ameliorates expression of circadian genes and disease progression in spinal muscular atrophy mice. *Hum. Mol. Genet.* 27, 3582–3597. <https://doi.org/10.1093/hmg/ddy249>
- Wang, Y., Xie, W., Liu, B., Huang, H., Luo, W., Zhang, Y., Pan, X., Yu, X.-Y., Shen, Z., Li, Y., 2021. Stem cell-derived exosomes repair ischemic muscle injury by inhibiting the tumor suppressor Rb1-mediated NLRP3 inflammasome pathway. *Signal Transduct. Target. Ther.* 6, 1–3. <https://doi.org/10.1038/s41392-021-00520-8>
- Weishaupt, J.H., Bartels, C., Pölking, E., Dietrich, J., Rohde, G., Poeggeler, B., Mertens, N., Sperling, S., Bohn, M., Hüther, G., Schneider, A., Bach, A., Sirén, A.-L., Hardeland, R., Bähr, M., Nave, K.-A., Ehrenreich, H., 2006. Reduced oxidative damage in ALS by high-dose enteral melatonin treatment. *J. Pineal Res.* 41, 313–323. <https://doi.org/10.1111/j.1600-079X.2006.00377.x>
- Why are mice considered excellent models for humans? [WWW Document], n.d. . Jackson Lab. URL <https://www.jax.org/why-the-mouse/excellent-models> (accessed 9.15.23).
- Wilcox, G., 2005. Insulin and Insulin Resistance. *Clin. Biochem. Rev.* 26, 19–39.
- Winkler, C., Eggert, C., Gradl, D., Meister, G., Giegerich, M., Wedlich, D.,

- Laggerbauer, B., Fischer, U., 2005. Reduced U snRNP assembly causes motor axon degeneration in an animal model for spinal muscular atrophy. *Genes Dev.* 19, 2320–2330. <https://doi.org/10.1101/gad.342005>
- Wolff, L., Strathmann, E.A., Müller, I., Mählich, D., Veltman, C., Niehoff, A., Wirth, B., 2021. Plastin 3 in health and disease: a matter of balance. *Cell. Mol. Life Sci. CMLS* 78, 5275–5301. <https://doi.org/10.1007/s00018-021-03843-5>
- Wu, C.-Y., Gagnon, D.A., Sardin, J.S., Barot, U., Telenson, A., Arratia, P.E., Kalb, R.G., 2018. Enhancing GABAergic Transmission Improves Locomotion in a *Caenorhabditis elegans* Model of Spinal Muscular Atrophy. *eNeuro* 5. <https://doi.org/10.1523/ENEURO.0289-18.2018>
- Wu, Z., Huang, X., Feng, Yajun, Handschin, C., Feng, Yan, Gullicksen, P.S., Bare, O., Labow, M., Spiegelman, B., Stevenson, S.C., 2006. Transducer of regulated CREB-binding proteins (TORCs) induce PGC-1alpha transcription and mitochondrial biogenesis in muscle cells. *Proc. Natl. Acad. Sci. U. S. A.* 103, 14379–14384. <https://doi.org/10.1073/pnas.0606714103>
- Xiong, Ye, Shen, L., Liu, K.J., Tso, P., Xiong, Yuqing, Wang, G., Woods, S.C., Liu, M., 2010. Antiobesity and antihyperglycemic effects of ginsenoside Rb1 in rats. *Diabetes* 59, 2505–2512. <https://doi.org/10.2337/db10-0315>
- Xu, C.-C., Denton, K.R., Wang, Z.-B., Zhang, X., Li, X.-J., 2016. Abnormal mitochondrial transport and morphology as early pathological changes in human models of spinal muscular atrophy. *Dis. Model. Mech.* 9, 39–49. <https://doi.org/10.1242/dmm.021766>
- Xu, Z., You, W., Liu, J., Wang, Y., Shan, T., 2020. Elucidating the Regulatory Role of Melatonin in Brown, White, and Beige Adipocytes. *Adv. Nutr.* 11, 447–460. <https://doi.org/10.1093/advances/nmz070>
- Yang, Y., Zhou, X., Xiao, M., Hong, Z., Gong, Q., Jiang, L., Zhou, J., 2010. Discovery of chrysoeriol, a PI3K-AKT-mTOR pathway inhibitor with potent antitumor activity against human multiple myeloma cells in vitro. *J. Huazhong Univ. Sci. Technol. Med. Sci.* 30, 734–740. <https://doi.org/10.1007/s11596-010-0649-4>
- Yoo, S.-H., Yamazaki, S., Lowrey, P.L., Shimomura, K., Ko, C.H., Buhr, E.D., Siepk, S.M., Hong, H.-K., Oh, W.J., Yoo, O.J., Menaker, M., Takahashi, J.S., 2004. PERIOD2::LUCIFERASE real-time reporting of circadian dynamics reveals persistent circadian oscillations in mouse peripheral tissues. *Proc. Natl. Acad. Sci.* 101, 5339–5346. <https://doi.org/10.1073/pnas.0308709101>
- Yoshida, K., Matsuoka, T., Kobatake, Y., Takashima, S., Nishii, N., 2022. Quantitative assessment of muscle mass and gene expression analysis in dogs with glucocorticoid-induced muscle atrophy. *J. Vet. Med. Sci.* 84, 275–281. <https://doi.org/10.1292/jvms.21-0325>
- Young, P.J., Man, N. thi, Lorson, C.L., Le, T.T., Androphy, E.J., Burghes, A.H.M., Morris, G.E., 2000. The exon 2b region of the spinal muscular atrophy protein, SMN, is involved in self-association and SIP1 binding. *Hum. Mol. Genet.* 9, 2869–2877. <https://doi.org/10.1093/hmg/9.19.2869>
- Yuan, Y., Cruzat, V.F., Newsholme, P., Cheng, J., Chen, Y., Lu, Y., 2016. Regulation of SIRT1 in aging: Roles in mitochondrial function and biogenesis. *Mech. Ageing Dev.* 155, 10–21. <https://doi.org/10.1016/j.mad.2016.02.003>
- Zammit, P.S., 2017. Function of the myogenic regulatory factors Myf5, MyoD, Myogenin and MRF4 in skeletal muscle, satellite cells and regenerative myogenesis. *Semin. Cell Dev. Biol.* 72, 19–32.

<https://doi.org/10.1016/j.semcd.2017.11.011>

Zanuto, R., Siqueira-Filho, M.A., Caperuto, L.C., Bacurau, R.F.P., Hirata, E., Peliciari- Garcia, R.A., do Amaral, F.G., Marçal, A.C., Ribeiro, L.M., Camporez, J.P.G., Carpinelli, A.R., Bordin, S., Cipolla-Neto, J., Carvalho, C.R.O., 2013.

Melatonin improves insulin sensitivity independently of weight loss in old obese rats. *J. Pineal Res.* 55, 156–165. <https://doi.org/10.1111/jpi.12056>

Zhao, Y., Lützen, U., Gohlke, P., Jiang, P., Herdegen, T., Culman, J., 2021.

Neuroprotective and antioxidative effects of pioglitazone in brain tissue adjacent to the ischemic core are mediated by PI3K/Akt and Nrf2/ARE pathways. *J. Mol. Med.* 99, 1073–1083. <https://doi.org/10.1007/s00109-021-02065-3>

Zhou, P., Xie, W., He, S., Sun, Y., Meng, X., Sun, G., Sun, X., 2019. Ginsenoside Rb1 as an Anti-Diabetic Agent and Its Underlying Mechanism Analysis. *Cells* 8,

204. <https://doi.org/10.3390/cells8030204>

Zhou, Y., Wang, S., Li, Y., Yu, S., Zhao, Y., 2018. SIRT1/PGC-1 α Signaling Promotes Mitochondrial Functional Recovery and Reduces Apoptosis after Intracerebral Hemorrhage in Rats. *Front. Mol. Neurosci.* 10, 443. <https://doi.org/10.3389/fnmol.2017.00443>



PERSONAL LICENCE

Ozge Cetin

A personal licence on its own does not authorise you to perform regulated procedures on protected animals. You apply regulated procedures of the category or categories specified below to animals of the species or groups specified below at places specified in authorised project licences subject to the restrictions and provisions contained in the Act and the conditions and restrictions below.

You are required to keep a record of all regulated procedures that you have carried out, and to make this record available to the Home Office upon request. If you cease to work at the establishment given as the primary availability on your licence, or it ceases to be the place where you wish your licence to be primarily available, you must notify the Home Office.

This licence shall be in force until it is revoked by the Home Office and shall be subject to periodic review.

Primary establishment

Keele University

Keele University Keele Staffordshire ST5 5BG

Handling instructions: Contains personal sensitive information, subject to confidentiality requirements under the Data Protection Act. This should only be circulated in accordance with ASPA Guidance. All government information may be subject to an FOI request and subsequent assessment.

Downloaded: 1:33pm, 28 Nov 2023

Page 1 of 5

Animals (Scientific Procedures) Act, 1986 Universities' Training Group

No: 47080

This is to certify that

Özge çetin

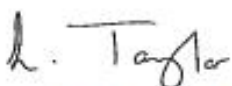
*has successfully completed the following programme of training, as required
under the UK and EU training framework and approved by
the Universities' Accreditation Scheme
at the University of Oxford*

Personal Licence Category B Training Course

UK Modules	EU Modules*	Species Specific
L	(Module 1)	no
E1	(Module 2)	no
PIL A (theory)	(Modules 3.1, 4, 5, 7)	yes
PIL A (skills)	(Modules 3.2, 8)	yes
K (theory)	(Module 6.1)	no
K (skills)	(Module 6.2)	yes
PIL B	(Module 20)	no

Species: --- Mouse---

These modules satisfy the training requirements for Personal Licence category B.

Signed:  for Universities' Training Group
(L. Taylor - Secretary)

Date: 30 March 2021

In the UK, competence in procedures, including euthanasia, using living animals, which could cause pain, suffering, distress or lasting harm, will only be achieved, under supervision, when a person begins their work.

Please note, this Certificate is not a licence to perform regulated procedures under the Animals (Scientific Procedures) Act 1986

EU Modules are described in the common education and training framework to fulfil the requirements under Directive 2010/63/EU; http://ec.europa.eu/environment/chemicals/lab_animals/pdf/Endorsed_E-T.pdf

RESEARCH PROJECTS

- ***Combining Bioinformatic and Drug Repurposing Approaches to Develop Second-Generation Therapies for Spinal Muscular Atrophy***

(Transcriptomics, C2C12s and LCHNM2 Cell Line, *In vitro* and *In vivo* experiments, Behaviour assessment, Drug treatment, RNAi, Immunohistochemistry, Fluorescence Microscope)

- ***Using Deep Neural Networks to Establish a Novel Non-Invasive and Sensitive Motor Skill Assessment Tool for Pre-Clinical Mouse Models of Muscle-Wasting Conditions.***

(Artificial intelligence, Virtual machine, DeepLabcut (GUI), Neural Network-ResNET)

- ***Investigation of Compounds Inducing Alpha Tubulin Acetylation by Drug Repurposing Approach***

(Molecular Docking (AutoDock /SwissDock), NSC34 Cell Line, MTS assay, Drug Treatment, Protein Isolation, Western Blot, Image J, Morphometric Analysis)

- ***Investigation of HDAC inhibitory mechanisms of Quercus Pontica by In vitro and in silico methods.***

(Molecular Docking (AutoDock /SwissDock), Bioinformatics Analysis, NSC34 Cell Line, MTS assay, Drug Treatment, Protein Isolation, Western Blot, Image J)

- ***In Silico toxicological profiling in perfluorinated and polyfluorinated compounds and in Vitro Geno-toxicological assessment of basic targets in the organism.***

(A549 human lung cancer cell culture, compound treatments, human sperm culture, alkaline comet assay)

ORIGINAL PUBLICATIONS

- *Hoolachan JM, McCallion E, Sutton ER, **Çetin Ö**, Pacheco-Torres P, Dimitriadi M, Sari S, Miller GJ, Okoh M, Walter LM, Claus P, Wood MJA, Tonge DP, Bowerman*

M. A transcriptomics-based drug repositioning approach to identify drugs with similar activities for the treatment of muscle pathologies in spinal muscular atrophy (SMA) models. *Hum Mol Genet.* 2023 Nov 8:ddad192. doi: 10.1093/hmg/ddad192. Epub ahead of print. PMID: 37947217.

- *G Renda, S Sevgi; M Šoral; G Bora; S Sari; **Ö Çetin**; P Zobaroğlu-Özer; D Şöhretoğlu. Histone deacetylase inhibitory properties of Quercus pontica K. Koch and its metabolites. Pre-printed stage of Journal of Molecular Structure*

- **Cetin Ö**, Sari S, Erdem-Yurter H, Bora G. Rutin increases alpha-tubulin acetylation via histone deacetylase 6 inhibition. *Drug Dev Res.* 2022 Jun;83(4):993- 1002. doi: 10.1002/ddr.21927. Epub 2022 Mar 9. PMID: 35266183.
- Emerce E, **Cetin Ö**, Genotoxicity assessment of perfluoroalkyl substances on human spermvol 34, 12, 884-890, 2018 (doi.org/10.1177/0748233718799191)

EDUCATION

2021-2023: School of Medicine, Keele University

PhD in Neuropharmacology

Thesis title: Combining Bioinformatic and Drug Repurposing Approaches to Develop Second- Generation Therapies for Spinal Muscular Atrophy.

Supervisor: Dr Melissa Bowerman

2018-2020: School of Medicine, Hacettepe University

Master of Molecular Biology and Genetic

Thesis title: Investigation of Compounds Inducing Alpha Tubulin Acetylation by Drug Repurposing Approach.

Supervisor: Dr Gamze Bora

2012-2017: School of Pharmacy, Gazi University

Bachelor's degree in pharmacy

Thesis title: Genotoxicity Assessment of Perfluoroalkyl Substances on Human Samples.

Supervisor: Dr Esra Emerce

CONFERENCE POSTER PRESENTATIONS

- 2023, 7th -9th of September : 6th Ottawa International Conference on Neuromuscular Disease and Biology, Ottawa, Canada; '' Drug repurposing strategy predicts the therapeutic potential of pioglitazone to ameliorate muscle and metabolic pathologies in spinal muscular atrophy''.
- 2023, 28th -30th of June: 27th Annual SMA Research & Clinical Care Meeting, Orlanda, FL '' Drug repurposing strategy predicts the therapeutic potential of pioglitazone to ameliorate muscle and metabolic pathologies in spinal muscular atrophy''.
- 2022, 13th-15th of September: Oxford-Harrington Rare Disease Centre Symposium poster presentation, "Investigating the therapeutic potential of pioglitazone to treat muscle and metabolic pathologies in SMA".

- 2017, 1st-2nd of June: Anadolu University Faculty of Pharmacy Symposium (ANES), poster presentation "Genotoxicity assessment of perfluoroalkyl substances on human sperm Genotoxicity assessment of perfluoroalkyl substances on human sperm".

CONFERENCE PODIUM PRESENTATIONS

- 2023, 17th November, UK : RJAH, Nerve and Muscle Interest group meeting programme oral presentation, "Investigating the Therapeutic Potential of Melatonin to Treat Muscle and Metabolic Pathologies in Spinal Muscular Atrophy".
 - 2023, 14th of March, UK: Keele University, Postgraduate Students Symposium Day, oral presentation, "Investigating the Therapeutic Potential of Melatonin to Treat Muscle and Metabolic Pathologies in Spinal Muscular Atrophy".
 - 2022, 21st-23rd of October, Spain: 3rd International Scientific Congress on Spinal Muscular Atrophy, oral presentation, "Investigating the Therapeutic Potential of Pioglitazone Treat Muscle and Metabolic Pathologies in SMA".
 - 2022, 28th of April, UK: Faculty of Medicine and Health Sciences Postgraduate Symposium, oral presentation, "Investigating the Therapeutic Potential of Pioglitazone to Treat Muscle and Metabolic Pathologies in SMA".
 - 2021, 25th of March, UK: 14th UK Neuromuscular Translational Research Conference, oral presentation "Investigation of Compounds Inducing Alpha Tubulin Acetylation by Drug Repurposing Approach".
-

TRAINING COURSE

- 2022-present: "Artificial intelligence, Virtual machine, LINUX, DeepLabcut (GUI), Google Colab, Neural Network-ResNET" from Dr. Dmitry Kishkinev
- 2023, 20th-22nd of March: "Muscle stem cells and tissue repair in muscle diseases" muscle workshop from Renoir society
- 2022, 23rd of January: Introduction to Teaching and Demonstrating (ITAD) course
- 2021, 17th of May: Learn R programming skills with online training course.
- 2021, 30th of March: Animals (Scientific Procedures) Act, 1986 Universities' Training Group, Personal Licence Category B Training Course.

- 2019, 5th-6th of December: *I. Molecular Modelling Workshop, Pharmaceutical Chemistry Department, Hacettepe University, training course.*
- 2019, 1st-3rd of July: *Molecular Modelling Workshop, International Multidisciplinary Symposium on Drug Research & Development, training course.*

SUPERVISORY EXPERIENCE

- *2021-present: 7 undergraduates and 2 master students*

Management of final year Undergraduate and master's students, delegating responsibilities and providing support for students in research laboratory etiquette, data analysis and writing.

SKILLS SUMMARY

- *IT Software: Microsoft Office, Literature databases, GraphPad, SPSS, R, AutoDock, DeepLabCut, and Softmouse.*
- *Multitasking: Handling several projects, meeting all assigned deadlines, prioritization*
- *Teamwork: Experienced in working in teams of different sizes and contexts which has strengthened my decision-making and negotiation skills*
- *Planning & Organisation: Laboratory lean processing and self-management of weekly schedule to cover experimental studies, seminar series and conference attendance, teaching responsibilities and collaborative work with internal and external academics.*

AWARDS

- *Doctoral Scholarship, Republic of Turkey National Ministry of Education (2017-...)*

A transcriptomics-based drug repositioning approach to identify drugs with similar activities for the treatment of muscle pathologies in spinal muscular atrophy (SMA) models

Joseph M. Hoolachan¹, Eve McCallion¹, Emma R. Sutton¹, Özge Çetin¹, Paloma Pacheco-Torres², Maria Dimitriadi², Suat Sari^{3,4}, Gavin J. Miller^{4,5}, Magnus Okoh¹, Lisa M. Walter^{6,7}, Peter Claus^{6,7}, Matthew J.A. Wood⁸, Daniel P. Tonge⁹, Melissa Bowerman^{1,10,*}

¹School of Medicine, David Weatherall Building, Keele University, Staffordshire, ST5 5BG, United Kingdom

²School of Life and Medical Sciences, University of Hertfordshire, Hatfield, Hertfordshire, AL9 10 9AB, United Kingdom

³Department of Pharmaceutical Chemistry, Hacettepe University, Ankara, 06100, Turkey

⁴School of Chemical and Physical Sciences, Lennard-Jones Building, Keele University, Staffordshire, ST5 5BG, United Kingdom

⁵Centre for Glycoscience, Keele University, Staffordshire, ST5 5BG, United Kingdom

⁶SMATHERIA gGmbH – Non-Profit Biomedical Research Institute, Feodor-Lynen-Straße 31, 30625, Hannover, Germany

⁷Centre of Systems Neuroscience (ZSN), Hannover Medical School, Bünteweg 2, 30559, Hannover, Germany

⁸Department of Paediatrics, University of Oxford, Level 2, Children's Hospital, John Radcliffe, Headington Oxford, OX3 9DU, United Kingdom

⁹School of Life Sciences, Huxley Building, Keele University, Staffordshire ST5 5BG, United Kingdom

¹⁰Wolfson Centre for Inherited Neuromuscular Disease, RJA Orthopaedic Hospital, Oswestry, SY10 7AG, United Kingdom

*Corresponding author. School of Medicine, David Weatherall Building, Keele University, Staffordshire, ST5 5BG, United Kingdom.
E-mail: m.bowerman@keele.ac.uk

Spinal muscular atrophy (SMA) is a genetic neuromuscular disorder caused by the reduction of survival of motor neuron (SMN) protein levels. Although three SMN-augmentation therapies are clinically approved that significantly slow down disease progression, they are unfortunately not cures. Thus, complementary SMN-independent therapies that can target key SMA pathologies and that can support the clinically approved SMN-dependent drugs are the forefront of therapeutic development. We have previously demonstrated that prednisolone, a synthetic glucocorticoid (GC) improved muscle health and survival in severe *Smn*^{-/-};SMN2 and intermediate *Smn*^{2B/-} SMA mice. However, long-term administration of prednisolone can promote myopathy. We thus wanted to identify genes and pathways targeted by prednisolone in skeletal muscle to discover clinically approved drugs that are predicted to emulate prednisolone's activities. Using an RNA-sequencing, bioinformatics, and drug repositioning pipeline on skeletal muscle from symptomatic prednisolone-treated and untreated *Smn*^{-/-}; SMN2 SMA and *Smn*^{+/-}; SMN2 healthy mice, we identified molecular targets linked to prednisolone's ameliorative effects and a list of 580 drug candidates with similar predicted activities. Two of these candidates, metformin and oxandrolone, were further investigated in SMA cellular and animal models, which highlighted that these compounds do not have the same ameliorative effects on SMA phenotypes as prednisolone; however, a number of other important drug targets remain. Overall, our work further supports the usefulness of prednisolone's potential as a second-generation therapy for SMA, identifies a list of potential SMA drug treatments and highlights improvements for future transcriptomic-based drug repositioning studies in SMA.

Keywords: spinal muscular atrophy; skeletal muscle; transcriptomics; drug repurposing; animal models

Rutin increases alpha-tubulin acetylation via histone deacetylase 6 inhibition

Özge Çetin^{1,2} | Suat Sari³ | Hayat Erdem-Yurter¹ | Gamze Bora¹

¹Department of Medical Biology, Faculty of Medicine, Hacettepe University, Ankara, Turkey

²The Faculty of Health and Medical Sciences, School of Medicine, Keele University, Staffordshire, UK

³Department of Pharmaceutical Chemistry, Faculty of Pharmacy, Hacettepe University, Ankara, Turkey

Correspondence

Gamze Bora, Department of Medical Biology, Faculty of Medicine, Hacettepe University, Ankara 06100, Turkey.
Email: gamzeb@hacettepe.edu.tr

Funding information

Hacettepe University Scientific Research Projects Coordination Unit,
Grant/Award Number: TYL-2020-18598

Abstract

Microtubules are dynamic cytoskeletal filaments composed of alpha- (α) and beta (β)-tubulin proteins. α -tubulin proteins are posttranslationally acetylated, and loss of acetylation is associated with axonal transport defects, a common alteration contributing to the pathomechanisms of several neurodegenerative diseases. Restoring α -tubulin acetylation by pharmacological inhibition of HDAC6, a primary α -tubulin deacetylase, can rescue impaired transport. Therefore, HDAC6 is considered a promising therapeutic target for neurodegenerative diseases, but currently, there is no clinically approved inhibitor for this purpose. In this study, using drug repurposing strategy, we aimed to identify compounds possessing HDAC6 inhibition activity and inducing α -tubulin acetylation. We systematically analyzed the FDA-approved library by utilizing virtual screening and consensus scoring approaches. Inhibition activities of promising compounds were tested using *in vitro* assays. Motor neuron-like NSC34 cells were treated with the candidate compounds, and α -tubulin acetylation levels were determined by Western blot. Our results demonstrated that rutin, a natural flavonoid, inhibits cellular HDAC6 activity without inducing any toxicity, and it significantly increases α -tubulin acetylation level in motor neuron-like cells.

KEYWORDS

drug repurposing, HDAC6, microtubule, neurodegenerative diseases, rutin, α -tubulin acetylation

Genotoxicity assessment of perfluoroalkyl substances on human sperm

Toxicology and Industrial Health
2018, Vol. 34(12) 884–890
© The Author(s) 2018
Article reuse guidelines:
sagepub.com/journals-permissions
DOI: 10.1177/0748233718799191
journals.sagepub.com/home/tih



Esra Emerce¹ and Özge Çetin¹

Abstract

Perfluoroalkyl and polyfluoroalkyl substances (PFAS) are synthetic chemicals that have been used in industry and consumer products. Because the presence of PFAS has been identified in humans and the environment in the last decade, human exposure to PFAS is a current public health concern. It has been shown that some PFAS lead to adverse health effects in the male reproductive system. However, there is no information about probable genotoxic effects of these chemicals on sperm cells. This study aimed to investigate the possible genotoxic damage on human sperm cells exposed to certain major PFAS compounds that were selected considering their extensive usage, high persistence in the environment, and high bioaccumulation in humans. These PFAS are perfluorooctanesulfonic acid (PFOS), perfluorooctanoic acid (PFOA), perfluorononanoic acid (PFNA), and perfluorohexanoic acid (PFHxA). The alkaline comet assay was used to detect the DNA damage to sperm. Sperm cells were treated with 0.1–1 mM of each PFAS at 32°C for 1 h to obtain optimal survival. As a result of the experiments, it was discovered that the exposure to PFOS, PFOA, PFNA, and PFHxA did not cause significant levels of cytotoxicity and did not cause damage to sperm DNA under these conditions. The results suggest that the exposure to these PFAS did not interfere with sperm DNA. Indirect toxicity mechanisms should be taken into account to assess the association between the PFAS exposure and male reproductive toxicity.

Keywords

Perfluoroalkyl substances, PFAS, sperm, genotoxicity, comet assay, DNA damage